ASSESSMENT OF FUTURE TRANSITION IN CLIMATE EXTREMES OVER WESTERN GHATS OF INDIA USING MACHINE LEARNING BASED MULTI-MODEL ENSEMBLE TECHNIQUES

Thesis

Submitted in partial fulfilment of requirements for the degree of

DOCTOR OF PHILOSOPHY

by

SWATHI SHETTY

(Reg. No. 187AM509)

WATER RESOURCES AND OCEAN ENGINEERING DEPARTMENT

NATIONAL INSTITUTE OF TECHNOLOGY KARNATAKA

SURATHKAL - 575025

FEBRUARY 2024

ASSESSMENT OF FUTURE TRANSITION IN CLIMATE EXTREMES OVER WESTERN GHATS OF INDIA USING MACHINE LEARNING BASED MULTI-MODEL ENSEMBLE TECHNIQUES

Thesis

Submitted in partial fulfilment of requirements for the degree of

DOCTOR OF PHILOSOPHY

by

SWATHI SHETTY

(Reg. No. 187AM509)

Under the Guidance of

Dr. PRUTHVIRAJ U

WATER RESOURCES AND OCEAN ENGINEERING DEPARTMENT

NATIONAL INSTITUTE OF TECHNOLOGY KARNATAKA

SURATHKAL - 575025

FEBRUARY 2024

DECLARATION

I hereby declare that the thesis entitled **"Assessment of Future Transition in Climate Extremes over Western Ghats of India using Machine Learning based Multi-Model Ensemble Techniques"** which is being submitted to the **National Institute of Technology Karnataka, Surathkal**, in partial fulfilment of the requirements for the award of Degree of **Doctor of Philosophy** in **Department of Water Resources and Ocean Engineering** is a *bonafide report of the research work carried out by me.* The material contained in this Research Thesis has not been submitted to any other University or Institution for the award of any degree.

Swathi S 28/02/24

(Swathi Shetty)

Water Resources and Ocean Engineering Department
National Institute of Technology Karnataka Surathkal-575025,
Karnataka, India

Place: NITK Surathkal

Date: 28-02-2024

CERTIFICATE

This is to certify that the research thesis entitled **"Assessment of Future Transition in Climate Extremes over Western Ghats of India using Machine Learning based Multi-Model Ensemble Techniques"** submitted by **Swathi Shetty (187AM509)** as a record of the work carried out by her, is accepted as the Research Thesis submission in partial fulfilment of the requirements for the award of the degree of **Doctor of Philosophy**.

Pruthviraj U 24/2/24

Dr. Pruthviraj U

Research Guide

(Signature with Date and Seal)

T. N 28/02/24

Chairman - DRPC

(Signature with Date and Seal)

Department of Water Resources and Ocean Engineering

NITK Surathkal - 575025

Chairman (DRPC)
Dept. of Water Resources & Ocean Engineering

In loving memory of my dear parents, whose unwavering love, wisdom, and sacrifices shaped the foundation of my journey. Though you are no longer with me in the physical realm, your enduring spirit and the lessons you imparted live on every page of this thesis. This work is a tribute to the indelible imprints you left on my heart and intellect. Thank you for instilling the values of resilience, curiosity, and determination. I carry your love in my heart, and I dedicate this achievement to the cherished memory of my beloved parents.

ACKNOWLEDGEMENTS

During the course of my doctoral thesis, I received invaluable guidance and support from a multitude of individuals.

At outset, I would like to express my sincere gratitude to my research guide **Dr. Pruthviraj U**, Water Resources and Ocean Engineering Department, National Institute of Technology Karnataka Surathkal for his whole hearted co-operation, relentless support and valuable suggestions during the research work. **Prof. Amba Shetty** for her infinite love, care, motivation and invaluable guidance throughout my research work. Their expertise, insights, and continuous encouragement have been instrumental in shaping my work. I am eternally grateful for their mentorship and the knowledge they have shared with me.

I also extend my sincere thanks to our Head of the Department **Dr. K. Varija**, our former HoD, **Prof. Dodamani B M**, for their support. I will always be grateful to all faculty members of the Department of Water Resources and Ocean Engineering, for their kind support and encouragement throughout my tenure as a research scholar in the Department.

I am grateful to Research Progress Assessment Committee members, **Dr. B. Manu** Civil Engineering Department and **Dr. Ramesh H** Water Resources and Ocean Engineering Department for their critical evaluation and considerable suggestions during the progress of the work.

My sincere thanks to **Prof. K.V Gangadharan**, Head of Centre for System Design, National Institute of Technology Karnataka, Surathkal for his endearing co-operation throughout the completion of the research work during my tenure as a Senior Research Fellow in the centre. My colleagues and friends, **Mrs. Aishwarya Shetty**, **Mrs. Aishwarya Hegde**, **Mrs. Akshaya**, **Mrs. Anusha**,

Mr. Deepak, **Mrs. Jyothi Prashanth**, **Mrs. Jayashree Arun**, **Mr. Nishan B Shetty**, **Mrs. Shradha Shetty**, **Mrs. Shreshta**, and **Mr. Vishwas A S** for creating a joyful moments during my difficult times and making the PhD journey easier with the constant support and encouragement and the love they offered. A special Thanks to **Mr. Tejas Pethkar** for helping me in the initial stages of python learning. I express my heartfelt thanks to **Dr. Praveen Shenoy** for all the valuable inputs in the initial phase of my research which helped me to navigate in the right direction of the research work.

Whatever I am today is because of the blessings of my mother **Smt. Pushpa Shetty** and father **Sri. Sudhakar Shetty** and my brothers **Mr. Mithun Shetty** and **Mr. Anil Shetty**. This thesis would not have been possible without the amazing support, patience, constant encouragement, care, unfettered belief and prayers of my parents, my brothers and other family members. I am grateful to my better half **Dr. Akshay Shetty**, for his unwavering emotional support, love, and care throughout my research journey. His presence has been a constant source of strength and inspiration. I am also deeply thankful to my in-laws **Mr. Ramesh Shetty** and **Mrs. Shankunthala Shetty** for their limitless support, love, and encouragement during this research work. A special thanks to my loyal companions, Shadow and Maya, their presence brought comfort and joy to the journey of completing this thesis.

Finally, I thank the God Almighty for making all these events happen smoothly and for all the teaching and non-teaching staffs of Water Resources and Ocean Engineering Department, the CSD family members and to every one of them who has encouraged, supported and contributed directly and indirectly to the successful completion of my doctoral research.

Swathi Shetty

ABSTRACT

Better hazard management in the future requires a ramifications of climate change on water resources, with particular emphasis on the regional scale. The rapid urbanization and industrialization, combined with the drastic changes in the land use and land cover of the region over the Western Ghats (WG), have driven regional heterogeneity in the climate. Key factors such as rainfall, temperature, topography, and vegetation are crucial in unraveling the intricate interactions between ecosystems and climate systems. The comprehension of forthcoming variability in these factors holds significant importance for the region owing to its global significance. The future climate projections rely on the Global Circulation Models (GCMs) ; thus, it is crucial to make sure those GCMs are accurate representations of the current climate in the region. Therefore, the study aimed to a) understand the role of topographic structure on rainfall distribution and its association with topo-climatic variables, and the vegetation, b) rank the GCM models and examine the efficacy of advanced machine learning based ensemble techniques to capture the inter-seasonal temporal variability over diverse geo-climatic basins of ghat, c) examine the uncertainties in multi-model ensembles of GCMs to capture the extreme climate indices and their trend d) model the potential occurrence of severe minimum and maximum temperatures, rainfall events, potential evapotranspiration, and historical and projected trends and e) understand the impact of climate change on the future variability in the streamflow.

The dependability of rainfall on the topography and climate of the region is evaluated using the Geographically Weighted Regression method. It is observed that the effect of the terrain is amplified in the broad, gradually sloping intermediate rough mountain located in close proximity to the coast. The maximum amount of rainfall is contingent upon the steepness of a mountain's windward side and the topographic structure resulting in the difference in the elevation of maximum rainfall occurrence. Based on this, the six river basins located in the

diverse-geoclimate of the Western Ghat are used to evaluate the performance of the GCMs and to understand the future variability in climate and the extremes. The top-performing GCMs obtained from Technique for Order Preference by Similarity to an Ideal Solution were ensembled using simple Arithmetic Mean (AM) and seven machine learning-based ensemble methods. Further, its ability to imitate extreme climatic events is analyzed using the indices formulated by the Expert Team on Climate Change Detection and Indices. Then the frequency and trend in the projected extremes of precipitation, minimum and maximum temperature, are obtained for the Shared Socioeconomic Pathways SSP245 and SSP585 for the Near Future (2021–2050) and Far Future (2051–2100) horizon. The streamflow of the river basins is simulated using Long Short Term Memory (LSTM), a deep learning technique to assess the potential impact of climate change on streamflow.

The performance of individual GCM models varies in all the basins; also, the ability to imitate the observation varies with the climatic variables, with notable disparities in the simulation of climate patterns. The ensemble of top-performing models has been proven beneficial in river basin scale by overcoming the constraints of bias correction methods. The Multi-model ensemble (MME) of Extreme Gradient Boosting (XGBR) and Random Forest Regression stand out for their superior performance across all river basins, with exceptional performance over the per-humid basins, while Adaptive Boosting, Support Vector Regression, and the AM underperform. Despite excellent accuracy in predicting daily/monthly rainfall, still, a great deal of variability in calculating climatic indices is noted, with higher relative bias in precipitation indices. Except for the duration-based precipitation indices, the XGBR calculated indices have been shown to be more accurate across all basins.

The anticipated fluctuations in temperature emphasize the onset of increased warming in November, which extends up to June, resulting in a notably warmer winter and an extended summer season. In future decades, warm days and nights increase by 45–65% and 45–70% in Aghanshini and northern river basins, and 45-85%, 60-80% in southern and Netravati river basins receptively, with two fold

warming in the winter season. After the mid-21st century, the warming trends start to slow down with decreasing trends in the pre-monsoon maximum temperature in southern and central river basins and a decrease in the monsoon minimum temperature in the northern river basins. The June and July rainfall will be highly inconsistent in the future decades, with a substantial increase in very wet to extremely wet days and medium to heavy rainfall in northern river basins. The streamflow in the monsoon season decreases substantially, with a decrease in annual streamflow in Chaliyar and Netravati and converse in other river basins. The southern river basins and the Netravati river basins are extremely vulnerable to water scarcity risk in May and June months, which extends to April and July in the high emission scenarios. These findings serve as an indication of the range of anticipated changes in the magnitude of extreme maximum and minimum temperature, rainfall, and geographical pattern over the Western Ghats.

KEYWORDS: Climate Change, Multi-Model Ensemble, TOPSIS, XGBoost Model, LSTM Model, ETCCDI Indices, Western Ghats of India

TABLE OF CONTENTS

LIST OF FIGURES

LIST OF TABLES

LIST OF ABBREVIATIONS

AdaBoost	Adaptive Boosting Regression
AM	Arithmetic Mean
ANN	Artificial Neural Network
ANN-BP	Artificial Neural Network with backpropagation
Cd	Coast Distance
CF	Coastal Flat region
CMIP	Coupled Model Inter-comparison Project
CNN	Convolutional Neural Network
CV	Coefficient of Variation
DEM	Digital Elevation Model
DNN	Deep Neural Network
DP	Deccan Plateau region
DR	Directional Relief
ECMRWF	European Centre for Medium-Range Weather Forecasts
EML	eXtreme Machine Learning
EQM	Empirical Quantile Mapping
ETCCDI	Expert Team on Climate Change Detection and Indices
ETR	Extra Tree Regression

FF	Far Future
GCM	Global Circulation Models
GWR	Geographically Weighted Regression
HBV	Hydrologiska Byråns Vattenbalansavdelning
IMD	India Meteorological Department
InSAR	Interferometric Synthetic Aperture Radar
IPCC	Intergovernmental Panel on Climate Change
KNN	K-nearest neighbor
LC	Land Cover
LK	Leptokurtic Distribution
LSSVR	Least Squares Support Vector Regression
LST	Land Surface Temperature
LSTM	Long Short Term Memory
LU	Land Use
MARs	Multivariate Adaptive Regression
MCDM	Multiple Criteria Decision Making Technique
ML	Machine Learning
MLP	Multi-layer perceptron neural network
MLR/LR	Multiple Linear Regression
MME	Multi-Model Ensemble
MODIS	Moderate Resolution Imaging Spectroradiometer

NCIWRD	National Commission for Integrated Water Resources Development
NDVI	Normalized Differential Vegetation Index
NF	Near Future
NRMSE	Normalized Root Means Square Rrror
NSE	Nash-Sutcliffe Efficiency
PK	Platykurtic Distribution
RCP	Representative Concentration Pathway
Rd	Ridge Distance
RF	Random Forest
RFR	Random Forest Regression
RMSE	Root Mean Square Error
RNN	Reccurent Neural Network
RSLK	Right Skewed Leptokurtic Distribution
RTA	Relative Terrain Aspect
RVM	Relevance Vector Machine
SEH	SE Facing Hilly region
SRTM	Shuttle Radar Topography Mission
SSP	Shared Socio-economic Pathway
SVM	Support Vector Machine
SVR	Support Vector Regression
SWAT	Soil & Water Assessment Tool

SWH	SW Facing Hilly region
TOPSIS	Technique for Order Preference by Similarity to an Ideal Solution
TRI	Terrain Ruggedness Index
VIC	Variable Infiltration Capacity
WG	Western Ghats
WMO	World Meteorological Organization
XGBoost	eXtreme Gradient Boosting
XGBR	eXtreme Gradient Boosting Regression

CHAPTER 1

INTRODUCTION

1.1 BACKGROUND

The uptake in Greenhouse gases and Carbon dioxide due to human anthropogenic activities has imbalanced the climate system. These combined activities have actuated the global and local changes on the environmental ecosystem, water resources, hydrological extremes, land productivity, agriculture, food security, water quantity/quality, and also on human lives (Parry *et al.*, 2007). Precipitation intensity, distribution patterns, and dry/wet extremes are all influenced by changes in land use and land cover, as well as increased emission of greenhouse gases, which have a profound effect on atmospheric water vapor, circulation patterns, and moisture availability (Christensen *et al.*, 2004; Safeeq and Fares, 2012). These changes have posed attention to monitoring of water resources, especially on the mountain water resources, as the mountains and plateaus are more sensitive to climate change than low lying areas (Beniston, 2003). Further, the topographical features and local mountain climatic regimes instigate the spatiotemporal variability of hydrologic factors in the hostile mountainous terrain (Church, 2015). The general consensus is that there has been an increase in disaster frequency, severity, and risk, particularly with regard to food, droughts, and floods (Sugar *et al.*, 2013; Alamgir *et al.*, 2019; Verma *et al.*, 2022). Employing short-to long-term adaptation strategies is essential for dealing with the effects of climate change to lessen the harm or take advantage of favourable chances by changing natural or social systems. Therefore, accurate climate prediction to quantify the potential variability and trend in the climate extremes under the changing climate is essential for effective climate risk management and adaptation strategies.

1.2 CAUSES AND IMPACT OF CLIMATE CHANGE

Six-fold increase in human population in 20^{th} century has amplified the socio-economic growth of India (Richards and Flint, 1994). The combustion of fossil fuels for energy and changes in land use during the Industrial Revolution has significantly boosted emissions of carbon dioxide (CO_2) and other greenhouse gases (GHGs). The 60% of the portend amount of carbon dioxide in the atmosphere is stored alone in the forest systems (Winjum *et al.*, 1992). CO_2 is re-emitted into the atmosphere as a result of deforestation, resulting in an increase in greenhouse gas concentrations. The increase of CO_2 and other GHGs in the atmosphere enhances the "greenhouse effect" and leads to a rise in temperature. The warming climate and the drastic rate of change in land cover and land use have led to unprecedented changes in regional climate heterogeneity in recent decades. These have strengthened the extreme climatic events in the Asian countries, which are more exposed to tropical cyclones and climate disasters (Singh *et al.*, 2014; Roxy *et al.*, 2017; Pradhan *et al.*, 2019; Dubey *et al.*, 2022). In India, meteorological extremes have tripled since 1950 (Roxy *et al.*, 2017), central India, western India and the northeastern part of India has experienced increased meteorological events in the monsoon season (Goswami *et al.*, 2006).

1.3 IMPACT OF CLIMATE CHANGE IN WESTERN GHATS OF INDIA

The changes in the climate have a significant impact on modifying the hydrological cycle and, thereby, the extreme weather. The Western Ghat (WG) is the "Water Tower" for all the rivers in peninsular India, and its inhabitants rely on these rivers for survival (Ramachandra *et al.*, 2016). The region below the Ghats is a coastal region that is highly populated and experiencing rapid industrialization, and the regions near the valley are used for agriculture and plantations. Though the region is accustomed to heavy rainfall, a vast variability in rainfall has been observed in recent decades, with frequent extremes (Mudbhatkal *et al.*, 2017; Nan-

ditha *et al.*, 2020). Also, the increase in non-seasonal temperatures, along with the high humidity, has become precarious for the health and lifestyle of the people and their livestock. In the future, the growth in population and rapid industrialization will increase the water demand for irrigation and industries with warming climate risks. This changing trend in meteorological extremes is projected to significantly impact the global ecosystem and exacerbate existing difficulties in regional river basins (Sharma *et al.*, 2018). Therefore, investigating the historical and projected future temperature and rainfall can assist us in comprehending the variations in the climate extremes at a regional scale for the formulation of better climate risk planning and adaptation strategies.

1.4 ASSESSMENT AND MODELING OF CLIMATE CHANGE

The variation in the southwest monsoon rainfall in India has an impact on the agrarian economy of the country as it solely accounts for 75% - 90% of the total annual rainfall of the country (Mooley *et al.*, 1981). In addition to changing climate, regional topographic heterogeneity and local climatic regimes exacerbate the spatial-temporal variability of hydrologic factors. These have made comprehending the spatiotemporal distribution of rainfall difficult for scientists.(Church, 2015). The changes in the earth's thermodynamics and circulation pattern due to the orography of the mountain and varying temperatures have a more significant influence on the spatial variability of rainfall (Collins *et al.*, 2013). There have been plenty of ongoing research on water resource models and climate models at a regional scale that needs prior knowledge of the sensitivity of the rainfall distribution to the topography and the local climate of the region. But the sparse and uneven distribution of climate monitoring networks in the steep, hostile terrain impedes the understanding of the spatiotemporal variability of the hydro-climatic variables (Prudhomme and Reed, 1998). However, understanding rainfall variability in the complex mountainous terrain is essential, as rainfall is an important input in hydro-geological applications like agriculture, irrigation, erosion studies, flood mapping, watershed management, and many other climate change impact

studies. The advancement in satellite observation of rainfall has given a new platform for these studies and has been proven to be a reliable source for monitoring of water resources (Mu *et al.*, 2007; Lettenmaier *et al.*, 2015). In recent days, the high-resolution Digital Elevation Models (DEM) and the hydrological data have promoted a more detailed insight into the influence of topography on rainfall.

Further, the future projection of climatic variables is important to quantify the climate change impact on water resources and climate extremes; the historical and projected future is essential for effective climate risk management and adaptation strategies. The Global Circulation Models (GCMs) simulated climatic variables are the most progressive and reliable data types used to investigate the future climate (Ahmed *et al.*, 2019*b*; Sonali and Nagesh Kumar, 2020). Climate change scenarios flourish a way the future might unfold. The principles of radiative heat transfer, thermodynamics, and fluid dynamics form the basis for these three-dimensional numerical models. The GCM simulates the global climate system, including the land surface, ocean, atmosphere, and cryosphere, to assess how the climate would change in the face of rising greenhouse gas concentrations.

First, the Intergovernmental Panel on Climate Change (IPCC FAR) in 1990 discussed a scenario with a fixed CO_2 concentration, which is called an "equilibrium Scenario"; the next scenario showed a fixed percentage increase in CO_2 concentration every year. The third scenario is a new Scientific Assessment Emission Scenario (SA90) which is based on the projected population. The later developed projections encompass a wide variety of transient scenarios that project population, energy resources, development in technology, global emissions, atmospheric concentrations, radiative forcings, and global temperature over time. The sets of standard scenarios developed by the Integrated Assessment Modeling community have become more comprehensive with each new generation, as the SA90 scenario was replaced by the IS92 emission scenarios in 1990, which led to the Special Report on Emission Scenario 2000 (SRES). This scenario considered demographics, the flow of information and technology, international trade, and global socio-economic characteristics.

Later, the IPCC's fifth assessment report replaced the SRES with a new scenario called Representative Concentration Pathways (RCPs). RCPs primarily focus on the evolution of greenhouse gas concentrations in the atmosphere. It introduced four new pathways and formed the basis for modeling experiments on a near to long-term basis. RCPs are radiative forcing scenarios; each scenario in it is tied to a value of the change in radiative forcings at the tropopause by the year 2100 relative to pre-industrial levels. The +2.6, +4.5, +6.0, and +8.5 Watts per square meter (W/m^2) refer to the change in radiative forcings by 2100. They provide different pathways for future emissions of greenhouse gases and other radiatively important substances, without specifying the underlying socioeconomic or policy factors driving those emissions. The new updated version of Coupled Model Inter-comparison Project is the CMIP6 includes a wide range of models with a higher horizontal resolution and release scenarios to meet the growing demand of the climate research community (Eyring *et al.*, 2016; Stouffer *et al.*, 2017; Abbasian *et al.*, 2019; Gusain *et al.*, 2020). The Shared Socio-economic Pathways (SSPs) scenarios are the most intricate ones created so far as they focus on the socioeconomic and policy narratives that drive greenhouse gas emissions and other aspects of environmental change. These narratives span a wide spectrum, ranging from highly ambitious emission reduction efforts to sustained emission growth.

The SSPs encompass essential socio-economic factors such as population dynamics, economic expansion, educational trends, urbanization rates, and the pace of technological advancements within their modeling frameworks. They delineate hypothetical future scenarios that deviate based on the degree of barriers posed to adaptation and mitigation efforts. These new scenarios, namely SSP1-2.6 (SSP126), SSP3-7.0 (SSP370), SSP2-4.5 (SSP245), SSP4-6.0 (SSP460), and SSP5-8.5 (SSP585), each produce radiative forcing levels in 2100 that are comparable to those of their predecessors in AR5. In Figure 1.1 each quadrant of the SSP framework represents a distinct road, characterized by either high or low barriers to adaptation and mitigation. Additionally, a fifth pathway is included to depict a scenario with moderate challenges to both adaptation and

mitigation. SSP126 depicts a future marked by minimal challenges in adaptation and mitigation, emphasizing sustainability and environmental conservation. In contrast, SSP245 presents intermediate challenges for both mitigation and adaptation. SSP370 centers on high regional competition and fragmentation, posing high risks for both adaptation and mitigation. SSP460 is characterized by high social and economic inequality, indicating low challenges for mitigation but high challenges for adaptation. Lastly, SSP585 signals the extreme scenario of continued fossil fuel dominance, presenting a high challenge for mitigation and a low challenge for adaptation.

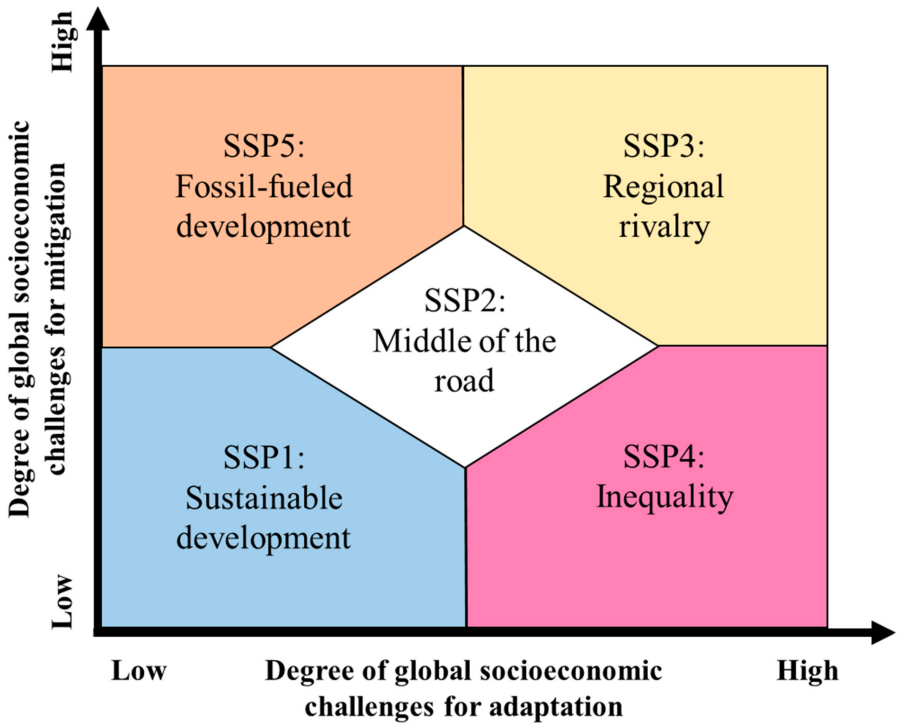

Fig. 1.1: Shared Socioeconomic Pathway adaptation and mitigation axes (Sellers and Ebi, 2018)

1.5 PROBLEM STATEMENT

Better hazard management in the future requires a detailed analysis on the impact of climate change on water resources, especially at the local level. Climate change affects the hydrosphere at the catchment scale, altering hydrological and

hydrodynamical processes at the river reach scale. The Western Ghats (WG), a tropical mountain forest located perpendicular to the Indian summer monsoon circulation, play a pivotal role in persuading heavy rainfall over the west coast of Peninsular India. The WG is anticipated to have a variation in rainfall, an increase in temperature, and extreme events. Under the changing climate, the Western Ghat might witness calamities such as lower moisture content and increased fire incidences. Changes in evapotranspiration rates will inevitably result from an increase in temperature and variations in the intensity and magnitude of precipitation, thereby influencing streamflow.

The northern and central regions of the Western Ghats are more susceptible to climate change, as the rate of temperature increase is anticipated to outpace precipitation increase. The increase in non-seasonal temperatures, along with the high humidity, has become precarious for the health and lifestyle of the people and their livestock. In the future, the increase in population along with rapid industrialization will increase the water demand for irrigation and industries with warming climate risks. Even the land use/land cover (LU/LC) are changing over the region (Gopalakrishnan *et al.*, 2011). The rate of deforestation in WG has been 0.57% annually during the period of 1920–1990 (Menon and Bawa, 1998), satellite remote sensing estimated a high degree of deforestation in the WG (Jha *et al.*, 2000), Kerala region has experienced an annual decline of 0.9% in between 1961 and 1988 (Prasad *et al.*, 1998). The drastic rate of change in LU/LC phenomenal changes in regional heterogeneity in recent years in the Indian monsoon has driven unprecedented changes in the environment and ecosystem at a regional scale (Niyogi *et al.*, 2010). Rainfall, temperature, topography, and vegetation are critical factors in understanding the interactions between ecosystems and climate systems on a regional scale. A comprehensive understanding of these interactions is essential to the research community. This motivates the present study to investigate the interdependency of climate variables, and the variability in the long term association, especially rainfall, with the topography in the mountainous terrain of WG.

For the management of the water resources and related hydro-infrastructure, which are designed based on the assumption of stationarity in the climate, the trend of the hydrological cycle component is essential. The changes to rainfall and temperature due to climate and LU/LC change tend to influence evapotranspiration and stream flow patterns. The frequency and trend of historical and projected future temperature and rainfall, along with their extremes, play a crucial role in understanding the impact of climate change in a specific location. Analyzing these patterns can assist in comprehending the impact of climate change for the formulation of better climate risk planning and adaptation strategies. The study relies on future climate projections from a group of GCMs; thus, it is crucial to make sure those GCMs are accurate representations of the current climate in the region. Over the complex mountainous terrain of WG, Konda and Vissa (2023) have highlighted the under performance of recent CMIP6 GCM models and the variation in the performance of the GCMs over different geo-climatic regions and between coastal areas and inland regions (Ojha *et al.*, 2014). There is a need to improve the performance of the GCM models in the region, especially due to their global importance. Additionally, it is important to determine the variation in ensembled GCM models performance across a variety of geo-climatic zones and its performance in the estimation of the extreme climate indices. Keeping this in view, the following objectives are framed.

1.6 RESEARCH OBJECTIVES

- To study the effect of mountain topography on rainfall distribution and to model the relationship between rainfall, topo-climatic variables, and vegetation in the Western Ghats of India.

- To rank the GCM model and investigate the effectiveness of multi-model ensemble (MME) by seven advanced machine learning (ML)-based ensemble techniques to capture the inter-seasonal temporal variability over diverse geo-climatic basins of WG.

- To examine the uncertainties in MMEs to capture the extreme climate indices and their trend over diverse geo-climatic basins of WG.

- To model the potential occurrence of severe minimum and maximum temperatures, rainfall events, potential evapotranspiration, and historical and projected trends in the diverse geo-climate basins.

- To understand the impact of climate change on streamflow variability in the diverse climate basins.

1.7 ORGANIZATION OF THE THESIS

The thesis report comprises of eight chapters, following this introduction chapter, remaining chapters are organized as follows:

Chapter 2 deals with a critical review of the literature and is divided into four themes. First, the studies on the association of rainfall with the topographical and meteorological parameters in mountainous terrain on a global to regional scale are explained. The climate change studies carried out in the past and the uncertainties associated with the climate projection models are explained based on the previous works. Finally, literature related to streamflow modelling using physically distributed models and data-driven empirical models in the projection of streamflow is discussed.

Chapter 3 describes the study area, the data products used, and the methodology followed to fulfil each objective of this study.

Chapter 4 explains the detailed methodology and the interdependence between the rainfall, topo-climate of the region using the Geographically Weighted Regression (GWR) technique. Also, the role of three peculiar mountain structures in the distribution of rainfall is explained.

Chapter 5 the raking of the GCMs over the six river basins and the performance of nine MMEs in imitating the historical climate is explained.

Chapter 6 explains the uncertainties in the MMES in the estimation of extreme climate indices. Also, the variability and trend in the rainfall, minimum and max-

imum temperature, their extremes, and the potential evapotranspiration over the projected future are explained.

Chapter 7 presents the modelling of the streamflow by using the deep-learning method and the variability in streamflow with the rainfall, and the water scarcity risk in the future decades.

Chapter 8 presents the summary and conclusions, and other related information of the research.

In order to arrive at the objective of research, literatures were focused on selected themes and review of the same is presented in the following chapter.

CHAPTER 2

LITERATURE REVIEW

This chapter deals with a review of relevant literature to bring out the studies undertaken in the selected research area. The four major themes organized are namely;

- Association of rainfall with topographical and meteorological parameters
- Uncertainties associated with the projection of hydro-climatic parameters
- Climate change studies in the past
- The rainfall-runoff models

Survey of literatures carried out under these themes is presented in the sections to follows.

2.1 ASSOCIATION OF RAINFALL WITH TOPOGRAPHICAL AND METEOROLOGICAL PARAMETERS

The variation in the southwest monsoon rainfall in India has an impact on crop production and, thus, on the agrarian economy of the country, as it solely accounts for 75% - 90% of the total annual rainfall of the country (Mooley *et al.*, 1981). The regional heterogeneity in topography and local climatic regimes instigate the spatiotemporal variability of hydrologic factors (Church, 2015). The sparse and uneven distribution of climate monitoring networks in the steep, hostile terrain impedes the understanding of the spatiotemporal variability of the hydro-climatic variables, especially the rainfall (Prudhomme and Reed, 1998). The changes in the earth's thermodynamics and circulation pattern due to the orography of the mountain and varying temperatures have a more significant influence on the spatial variability of rainfall (Collins *et al.*, 2013). However, understanding rainfall variability in the complex mountainous terrain is essential, as rainfall is an important

input in hydro-geological applications like agriculture, irrigation, erosion studies, flood mapping, watershed management, and many other climate change impact studies. The advancement in satellite observation of rainfall has given a new platform for these studies and has been proven to be a reliable source for monitoring of water resources (Lettenmaier *et al.*, 2015). In recent days, the high-resolution Digital Elevation Models (DEM) and the hydrological data have promoted a more detailed insight into the influence of topography on rainfall. Although it is difficult to articulate the physical mechanisms that link climate to topographical and geographical features, basic statistical score-based methods can be employed to assess the relationship (Feidas *et al.*, 2014). The relationship between rainfall, topographical, and geographical features is explored at various time scales using univariate and multivariate regression techniques and geostatistical methods (Goovaerts, 2000; Al-Ahmadi and Al-Ahmadi, 2014; Kumari *et al.*, 2017*a*). The model must alter over space to reflect the spatial heterogeneity of rainfall over the undulating mountainous terrain. This spatial heterogeneity could be better explained by the Local Regression Models. The Geographically Weighted Regression model can better explain this relationship with the inclusion of topographic and climatic factors (Kumari *et al.*, 2017*a*).

Multiple studies have made an attempt to assess the association between the distribution of rainfall with the elevation, location, slope, and aspect (Puvaneswaran and Smithson, 1991; Hayward and Clarke, 1996; Sevruk, 1997; Goovaerts, 2000; Diodato, 2005; Oettli and Camberlin, 2005; Buytaert *et al.*, 2006; Al-Ahmadi and Al-Ahmadi, 2014; Tawde and Singh, 2015; Kumari *et al.*, 2017*a*; Ruiz-Ortiz *et al.*, 2022), distance from moisture sources (Hayward and Clarke, 1996; Weisse and Bois, 2001; Johansson and Chen, 2003; Ruiz-Ortiz *et al.*, 2022), with geographical and meteorological factors (Johansson and Chen, 2003; Ruiz-Ortiz *et al.*, 2022), environmental factors (Adler *et al.*, 2008; Cong and Brady, 2012), and with the changes in land-use and land-covers (Chamaille-Jammes *et al.*, 2006; Ruiz-Ortiz *et al.*, 2022) in a global and regional scales. Basist *et al.* (1994) studied the interaction between rainfall and six topographic variables, namely elevation, slope,

orientation, exposure, and the product of slope and orientation, and elevation and exposure, using linear bivariate and multivariate analysis. The study revealed that exposure and the interaction of elevation and exposure are the best predictors of annual precipitation, with varying topographic influences in convective and non-convective environments. Hayward and Clarke (1996) noted the similar variability in the magnitude of rainfall with the distance from the sea on both sea-facing and stations in the rain shadow region of the mountain, with a pronounced influence of altitude on the sea-facing stations during the monsoon on the Freetown Peninsula of Sierra Leone. Rainfall in the monsoon months increased with altitude, but the relationships between monthly rainfall and altitude were more marked for rain-shadow gauges than for ocean-facing gauges. Frei and Schär (1998) a study over the European Alps noted the amplification of rainfall along the foothills of the Alps and the shielding of the inner-Alpine valleys. A straightforward relationship between precipitation and altitude cannot be established as the topographic influence is associated with slope and shielding rather than height effects (Frei and Schär, 1998). The effect of wind speed on the mountain's windward and leeward sides is highlighted in Johansson and Chen (2003), with a greater effect of the slope near the coast and a diminishing influence in mountain valleys with upwind barriers. The exposure and the slope of the area (Oettli and Camberlin, 2005), and the geographical location along with the topographical parameters have the ability to explain the interaction between rainfall and topography more adequately (Buytaert *et al.*, 2006). These effects are more pronounced in the seasonal variability of rainfall, especially if the region is near the mountain/sea in the semi-arid climate (Al-Ahmadi and Al-Ahmadi, 2014) and in the arid climate (Jemai *et al.*, 2022).

Buttafuoco and Lucà (2020) showed a linear relationship between the orographic influence of distance from the coast on precipitation over the Mediterranean climate of the Calabria Region of Italy. Ruiz-Ortiz *et al.* (2022) explained the role of physiographic variables and rainfall using a physiographic-based multilinear regression model over the Iberian Peninsula, dominated by a Mediterranean

climate. The wet and dry periods have different controlling variables; elevation and distance to the coast explain a substantial part of rainfall depth with an inverse relationship between rainfall and the distance to the coast, and in the dry period, location (longitude) and elevation are the influencing factors of rainfall variability. The association of rainfall with latitude is seasonally variable; the elevation and distance from the sea are important driving factors for the precipitation regime, along with Normalized Differential Vegetation Index (NDVI) (Feidas *et al.*, 2014). Akbas (2023) revealed the interaction of topography with tracks of weather systems intensifies the extreme rainfall. Some of the studies carried out in the Indian mountains are reviewed in the sub section.

2.1.1 Related Studies in Indian Mountains

Over the Himalayan range, rainfall follows an exponentially decreasing trend with altitude, and maximum rainfall occurs in the middle Himalayan range (Singh and Kumar, 1997). Bookhagen and Burbank (2006) study in the Himalayas to determine the relationships between topography, terrain relief, and rainfall locations discovered two distinct rainfall maxima along the mountain's strike. The extreme rainfall intensity and frequency negatively correlates with the altitude, experiencing heavy extremes in the plains and foothills of the northwest Himalaya (Bharti *et al.*, 2016). Shrestha *et al.* (2012) highlighted the two rainfall peaks during the monsoon season at 500-700 m above MSL and the latter 2000-2200 m above MSL leading to frequent rainfall. In the WG of India, some high-elevated regions on the windward side of the WG in Kerala receive below-normal rainfall (Simon and Mohankumar, 2004). Raj and Azeez (2010) studied the rainfall variability with the height in the Palakkad gap in the WG near Kerala and claimed that the altitude, valley, and hillock features give higher rainfall. Sijikumar *et al.* (2013) proved that the absence of the WG barrier suppresses rainfall over the west coast of India without any variation in the rainfall over the Arabian Sea. (Tawde and Singh, 2015) revealed the influence of topography, slope steepness on the windward side, and mountain altitude on the amount of orographic precipitation using

satellite rainfall data. Rainfall over the WG is greater before the mountain's peak and is restricted to an altitude of 800 meters. A study by Mudbhatkal and Amai (2018) also revealed that the maximum precipitation occurs at a distance on the windward side from the crest of the Ghat and at the crest on the leeward side of the Ghat.

2.2 UNCERTAINTIES ASSOCIATED WITH THE PROJECTION OF HYDRO-CLIMATIC PARAMETERS

The eco-hydrological processes at many river basins have seen significant alterations in recent decades as a result of climate change and many unregulated human activities. The general consensus is that there has been an increase in disaster frequency, severity, and risk, particularly with regard to food, droughts, and floods (Sugar *et al.*, 2013; Alamgir *et al.*, 2019; Verma *et al.*, 2022). Employing short to long-term adaptation strategies is essential for dealing with the effects of climate change to lessen the harm or take advantage of favourable chances by changing natural or social systems. Therefore, accurate climate prediction is vital in planning and management.

The General Circulation Models (GCMs) simulated climatic variables aid as a reliable source to evaluate the future climate; still, there remains a substantial degree of uncertainty associated with the GCMs. The different GCMs lead to contrasting outputs of the future under the same forcing due to the uncertainties resulting from insufficient understanding of the atmospheric process, approximations during numerical modeling, and the various conditions used to force the numerical models. The advancement in the understanding of possible uncertainties and their respective solutions has also significantly progressed through the years, greatly improving the recent version of GCMs (Raju and Kumar, 2020). The Coupled Model Intercomparison Project (CMIP) 5-GCM simulations show substantial improvements over its predecessor CMIP3-GCMs, with improved representation of aerosols, land-ice boundary interactions, stratosphere–troposphere interactions, the carbon cycle, and interactions between ecosystems and other processes (Car-

valho *et al.*, 2022). The newest, updated general circulation model, CMIP6, has a remarkable improvement over CMIP5 and can better predict climatic variables (Gusain *et al.*, 2020; Tokarska *et al.*, 2020). This made GCMs a reliable source for past and future climatic variables, especially on a global scale. But the GCMs are incapable of capturing climate variability at a finer scale. Therefore in order to bridge the gap between the local phenomenon and the coarse resolution GCM outputs, they are often down-scaled to represent the local heterogeneity in the climate and topography using statistical or dynamical down-scaling techniques. The dynamical down-scaling techniques employ high-resolution Regional Climate Models (RCMs) nested within GCMs to produce the fine-resolution data of local climatic variables (Chen *et al.*, 2010). The implications of dynamical downscaling methods are limited by the higher computational effort required to run the models at a finer spatiotemporal resolution. In contrast, statistical downscaling techniques use empirical evidence to connect local climatic variables with large-scale GCM outputs. However, in both raw and down-scaled simulations of GCMs, there remains a considerable bias, which need to be rectified using the proper bias correction techniques (Wang *et al.*, 2016; Chokkavarapu and Mandla, 2019; Suman *et al.*, 2022). The performance of linear scaling, variance scaling, local intensity scaling, power transformation, distribution mapping, and the delta-change approach has been verified by Teutschbein and Seibert (2012); Shrestha *et al.* (2017); Mudbhatkal and Mahesha (2018), with distribution mapping performing best in the Swedish catchments, delta change approach in the catchments of WG of India in streamflow modeling, and no significant difference in linear scaling and quantile mapping methods over the catchment in Nepal (Shrestha *et al.*, 2017).

Various studies analyzed the efficacy of bias correction techniques and their capability to accurately represent regional climate and emphasized the need for evaluating the performance of various bias correction methods due to the variability in the performance on different GCMs, and geo-climatic condition (Minville *et al.*, 2008; Ojha *et al.*, 2014; Mudbhatkal and Mahesha, 2018; Mohan and Bhaskaran, 2019; Suman *et al.*, 2022). Still, the bias correction is only effective at resolving

a subset of the systematic GCM biases and is limited in its ability to address non-stationary biases and inter-GCM uncertainty (Wang *et al.*, 2018). Another strategy used for reducing the uncertainties associated with GCMs is through the appropriate selection of GCM/GCMs. Mohan and Bhaskaran (2019); Suman *et al.* (2022) highlighted that the competency of GCMs at the local scale can be improved through the careful selection of GCMs and the down-scaling/bias correction procedures, which together lower the uncertainty associated with the projection of past and future climate. Different approaches are followed to select the best GCM or an ensemble of GCMs. The aggregation of multiple GCMs compensates for the weakness of individual models, increases the skill, reliability, and consistency of model forecasts, and ultimately achieves the best climate projection (Lutz *et al.*, 2016; Ahmed *et al.*, 2020; Shiru *et al.*, 2020). (Raju and Kumar, 2015) stressed the need for the usage of ensembles of multiple models from a pool of GCMs to assess GCM performance to boost confidence in future climate projections (Zhao *et al.*, 2020). Such analyses play a significant role in developing effective adaptation and mitigation strategies against the risks and effects of climate change.

The multi-model ensemble (MME) mean methods have advanced from simple arithmetic mean to complex machine learning-based approaches. The arithmetic mean (AM) is one of the widely used straightforward ensemble methods (Knutti *et al.*, 2010; Sanderson *et al.*, 2015). Statistical methods such as Bayesian or weighted averages consider both simulation skills and model interdependence. These methods rely on the concept of linear regression based on some specific relationships or indices, potentially neglecting useful information (Knutti *et al.*, 2010; Brunner *et al.*, 2020). Recent years have seen an uptick in the popularity of using cutting-edge machine learning (ML) methods to solve a wide range of climate change research and prediction issues. The ML versatility, ability to explore nonlinearity, high dimensionality, and hierarchical complex interactions between the predictors and the response have made it more popular than other methods (Acharya *et al.*, 2014; Shortridge *et al.*, 2016; Sachindra *et al.*, 2018; Crawford *et al.*, 2019; Ahmed *et al.*, 2020). The most commonly used models are

the Support Vector Machine (SVM), Random Forest (RF), and Artificial Neural Networks (ANNs), K-nearest neighbor (KNN), Relevance Vector Machine (RVM), which can model complex, often nonlinear relationships in climate data. Multiple studies have accounted for the machine learning approach for the ensemble of precipitation, temperature, and evaporation (Wang *et al.*, 2018; Ahmed *et al.*, 2020; Dey *et al.*, 2022; Jose *et al.*, 2022; Kadkhodazadeh *et al.*, 2022), and found the best performance of RF and SVM in most of the studies over Southwest Asia, Australia (Wang *et al.*, 2018), KNN and RVM over SVM and ANN in Pakistan (Ahmed *et al.*, 2020), RF over decision tree, adaptive boosting, and linear regression for China (Li *et al.*, 2021; Yang *et al.*, 2022). Also, the studies have endorsed the best performance of RF and SVM over ANN and AM methods in a tropical monsoon climate in eastern India (Dey *et al.*, 2022), and RF over the per-humid river basin in south India (Jose *et al.*, 2022). Konda and Vissa (2023) have highlighted the underperformance of ten CMIP6 models ensembled by using the AM over the WG of India. This highlights the need for enhancing the performance of the GCMs at the basin level using uncertainty reduction/ advanced ensemble techniques. The following section describes climate change studies in the global to regional.

2.3 CLIMATE CHANGE STUDIES IN THE PAST

Several studies investigated the impact of climate change on the primary drivers of the hydrological cycle. The World Meteorological Organization noted the rise of 0.7 ^{o}C in the global average surface temperature since the 20th century. The global average temperature has seen a sharp rise since the 1970s, and the 2000s was warmer than the decade spanning the 1990s (Organization, 2009). Much of the warming during the last four decades is attributable to the increasing atmospheric greenhouse gas (GHG) levels due to human activities. The rising greenhouse gas emission enhances the atmosphere's ability to hold water vapor. This intensifies the global water cycle, causing more evaporation from oceans and land, leading to increased atmospheric moisture. The warming also alters atmospheric circulation

patterns, affecting wind, pressure systems, and jet streams. These changes result in shifts in weather systems, impacting precipitation patterns and the frequency of extreme weather events. Altered circulation affects the distribution of moisture, leading to changes in weather patterns and influencing local and regional climates. Some areas may experience more precipitation, while others may face reduced moisture supply, contributing to drought conditions (Safeeq and Fares, 2012; Diksha *et al.*, 2022; Lal *et al.*, 2023).

2.3.1 Rainfall, Temperature, and their Extremes

Past studies have tried to address the important problem of trends in rainfall and temperature in India since the 20^{th} century. Some previous studies have found that there is no consistent pattern of the average annual rainfall over India either rising or declining (Lal *et al.*, 2001; Krishnakumar *et al.*, 2009; Kumar *et al.*, 2010). Although no study obtained a long-term trend in the monsoon rainfall across India, significant long-term changes have been recognized (Dash *et al.*, 2007; Kumar *et al.*, 2010; Joshi and Pandey, 2011). Kumar *et al.* (1992) reports that monsoon rainfall over the west coast, central peninsular, and northwest India has increased by 10–12% of the normal rainfall during a span of 100 years. Krishnakumar *et al.* (2009) observed decreasing trend of rainfall during the southwest monsoon and is reversed during post-monsoon rainfall in southernmost India. Rajeevan *et al.* (2008) examined the variability and long-term trends of extreme rainfall events over Central India for 104 years and found a 6% increase per decade is associated with the increasing trend of sea surface temperature and surface latent heat flux over the tropical Indian Ocean. Roy and Balling (2004) recognized the rise in the amount of heavy rainfall in India over the last ten decades. The rise in extreme events is strongest in regions stretching from the northwest of the Himalayas through most of the Deccan Plateau in the southern peninsular region of India and decreases in the eastern part of the Gangetic Plain and parts of Uttaranchal. Guhathakurta *et al.* (2011) also found an increase in the frequency of heavy rainfall events in peninsular, east, and northeast India and decreasing in parts of

central and north India. The extremely high and extremely low rainfall increased from the year 1930 to 2013 by 2-fold and 4-fold with high variation, particularly in the early 2000s (Jun *et al.*, 2015). India has a rising trend in minimum, mean, and maximum temperature and is severe in non-monsoon seasons in southern and northern India (Arora *et al.*, 2005; Jain *et al.*, 2013). The increase in summer precipitation over northwest and west-south peninsular India and reduction over northeast and north-central India is projected over the next 3 to 6 decades (Woo *et al.*, 2019).

It has been accepted that the occurrence of enormous climate extremes is entwined with the global mean temperature. The frequency of both the temperature and precipitation extremes have noticeably increased in the past decades more than the mean and seasonal, and this trend is likely to continue as the climate warms (Dong *et al.*, 2018; Mukherjee *et al.*, 2018; Nanditha *et al.*, 2020). The recurrent and intense extremes have a threatening role on the freshwater sources, human health, agrarian economy of the country, and stability of infrastructure, especially in the rapidly developing countries (AghaKouchak *et al.*, 2020; Singh *et al.*, 2021). The global climate models simulated climatic variables are the most progressive and reliable data types used to investigate the future climate (Ahmed *et al.*, 2019*b*; Sonali and Nagesh Kumar, 2020). The new updated version of Coupled Model Inter-comparison Project is the CMIP6 includes a wide range of models with a higher horizontal resolution and release scenarios to meet the growing demand of the climate research community (Eyring *et al.*, 2016; Abbasian *et al.*, 2019; Gusain *et al.*, 2020).

Several studies have examined the performance of various CMIP models models namely CMIP3, CMIP5, CMIP6 in projecting future climate variability (Ahmed *et al.*, 2019*b*; Sonali and Nagesh Kumar, 2020; Chhetri *et al.*, 2021; Zhu *et al.*, 2021; Kumar *et al.*, 2023) and noted an upsurge in climate variability at global to regional scale (Shrestha *et al.*, 2020; Chhetri *et al.*, 2021; Zhu *et al.*, 2021; Shafeeque and Luo, 2021; Tan *et al.*, 2021; Jose and Dwarakish, 2021; Kumar *et al.*, 2023). The change in the temperature is a primary cause for the increase

in the intensity and frequency of the extreme precipitation events and dry spell length as the warmer air can hold and carry more water vapor (Sippel *et al.*, 2017; Sharma and Goyal, 2020; Kumar *et al.*, 2021) and this becomes a critical issue in the late 21st century (Singh and Goyal, 2016; Shiferaw *et al.*, 2018; Sharma and Goyal, 2020; Kumar *et al.*, 2021, 2023; Rao *et al.*, 2023). The variation in the climate extremes in the projected future is evaluated over the Indian scale by many researchers (Nanditha *et al.*, 2020; Varghese *et al.*, 2020; Kumar *et al.*, 2021; Shafeeque and Luo, 2021; Sarkar and Maity, 2022; Rao *et al.*, 2023). The long-term trend in historical extreme rainfall events over the majority of India is increasing (Lal *et al.*, 2022) and is bound with the increase in the sea surface temperature and surface latent heat flux over the Indian ocean (Rajeevan *et al.*, 2008); meanwhile, the light and moderate precipitation events have decreased (Mishra *et al.*, 2018*a*), and the change in the frequency of extremes dominate over the intensity in the future (Sarkar and Maity, 2022). Past studies predicted the intensification of monsoon rainfall from the climate model simulations over South Asia (Lal *et al.*, 2000; Meehl *et al.*, 2003; Kumar *et al.*, 2006). However, accurate assessments of future changes in the regional monsoon rainfall have remained unclear due to extensive deviations among the model projections (Annamalai *et al.*, 2007; Kripalani *et al.*, 2007; Kumar *et al.*, 2010). Kripalani *et al.* (2003); Krishnan *et al.* (2013) justified that the rainfall response to global warming by climate models is accompanied by a weakening of the large-scale southwest monsoon flow. The potential of CMIP6 models to capture the spatio-temporal distribution of monsoon rainfall over India, especially in the complex topography of tropical Western Ghat mountains and in the North-East foothills of the Himalayas, where the local climatic regimes play an imperative role in the distribution of rainfall have been highlighted in Goswami *et al.* (2018); Gusain *et al.* (2020); Kumar *et al.* (2021). Also, Singh and Goyal (2016) noted that the high elevated mountain regions and low elevated regions have disparate endurance to extreme rainfall events.

2.3.2 Evapotranspiration, River Runoff, and Water Availability

As a consequence of climate change, the vulnerability of communities to floods has increased in most parts of the world, including Southeast Asia (Supharatid *et al.*, 2022). Proper management of flood in a changing climate needs study at the local level as climate change affects the hydrosphere at the catchment scale, altering hydrological processes, which in turn impact hydrodynamics at the river reach scale. Hengade and Eldho (2016) reported that a slight decrease in rainfall causes a higher percentage decrease in the surface runoff of the basin. The change in LU/LC is the second most important driver of runoff change after climate change (Gerten *et al.*, 2008). The shorter growing periods, lower rooting depths, and lower interception losses due to deforestation augment the streamflow (Gerten *et al.*, 2008). The slight decrease in the annual precipitation amount will lead to a significant decrease in streamflow volumes in a river basin of Israel (Givati *et al.*, 2019). A study in the Yellow River basin of China by Liu and Cui (2011) concluded that the streamflow responds differently to precipitation and potential evaporation change in wet and dry locations. Over the Nile river basin of Ethiopia, the increase in potential evapotranspiration (PET) is observed with the increase in temperature, increased dry season rainfall, and decreased rainy season rainfall, along with corresponding increase and decrease in streamflow is observed.

The Central India has experienced an increase in the reference evapotranspiration with the increase in temperature and decrease in rainfall (Kundu *et al.*, 2017). The increase in the precipitation and streamflow with a decrease in actual evapotranspiration has to be endured in the future decades in Thungabhadra basin (Meenu *et al.*, 2013). Mishra and Lilhare (2016) noted an increase in the evapotranspiration with an increase of up to 40% in the monsoon streamflow using CMIP5 GCMs, and highlighted the sensitivity of streamflow to monsoon rainfall variation over the Ganges and Godavari river basin. The Nepal's Bheri basin observed the increase in annual runoff, decrease in July and August and increase during the dry season (Mishra *et al.*, 2018*b*).

2.3.3 Related Studies in the Western Ghats

Many studies have been carried out in the river basins of the WG. The study carried out by Mudbhatkal *et al.* (2017) on the river basins of WG indicated the reduction in streamflow, and a decrease in southwest monsoon contribution to annual rainfall with the increase in non-monsoon rainfall and temperature. Especially, the rivers in the southern portion of the Western Ghats of India are highly vulnerable to changing climate followed by the central portion. Sharannya *et al.* (2018) assessed the hydrological consequences of climate change on rainfall, temperature, and streamflow in a basin situated in the Central WG and found a declining trend in rainfall for both historical and projected medium emission scenario with a increase in temperature. (Sinha *et al.*, 2020) over the basin in the southern WG, the mean surface runoff declines in the future decades with increase in the winter and summer season, and the worst decline occurs in the extreme emission scenario. The reduction in forest area, and large scale conversion to agricultural land in the future in most of the regions of WG of India, increases the river streamflow (Brown *et al.*, 2005; Sinha *et al.*, 2020; Sharannya *et al.*, 2021; Visweshwaran *et al.*, 2022). The mixed pattern in the variation of Evapotranspiration is noted over the WG; increase in the future decades is highlighted by Nilawar and Waikar (2019); Visweshwaran *et al.* (2022) and decrease over few catchments of WG by Sinha *et al.* (2022). The temperature, precipitation and streamflow increases in Purna basin (Nilawar and Waikar, 2019), Upper Sind River Basin (Narsimlu *et al.*, 2013), Bharathapuzha river basin (Visweshwaran *et al.*, 2022), conversely, streamflow decreases in Kalada river basin (Sinha *et al.*, 2022), due to the regional climate hetereogenity.

2.4 THE RAINFALL-RUNOFF MODELS

The increasing population in India and the associated developmental activity have a threatening role on freshwater sources. The assessment made by the National Commission for Integrated Water Resources Development (NCIWRD) report that the Indian subcontinent is expected to be stressed in the light of cli-

mate change. Annually as much as 45% of river runoff flows into the sea (GoI 2007), several schemes are proposed and under construction to minimize the loss of available runoff. But, the successful implementation of these water resource plans on the rivers and agro-climatic regions is possible only with the understanding of spatiotemporal variability in the runoff in light of climate change. Because of its connection to stochastic and nonlinear phenomena including evapotranspiration, precipitation, temperature, and watershed features, streamflow forecasting is highly intricate (Yuan *et al.*, 2018). The streamflow under different LU/LC and climate conditions has been projected using physical based semi-distributed models such as Soil & Water Assessment Tool (SWAT) (Babar and Ramesh, 2015; Sharannya *et al.*, 2018; Visweshwaran *et al.*, 2022), Variable Infiltration Capacity (VIC) (Kim *et al.*, 2022), Hydrologiska Byråns Vattenbalansavdelning (HBV) (Bizuneh *et al.*, 2021; Tibangayuka *et al.*, 2022), and HEC-HMS (Khoi, 2016; Sanjay Shekar and Vinay, 2021; Tibangayuka *et al.*, 2022). These physical based-models function by representing physical processes and boundary conditions and solving the complex mathematical equations underlying them. This model, however, calls for a great deal of space and time information as well as model parameters that can be elusive to anticipate (Makwana and Tiwari, 2014). The accuracy of the output depends on the precision of the input data and the accuracy of the model parameters (Babar and Ramesh, 2015). Furthermore, the calibration and validation processes are time consuming and complicated due to the huge number of parameters, broad range of values, and their intricate interconnections (Rezaeianzadeh *et al.*, 2014).

Recently, machine learning methods have shown great potential in runoff simulation and forecasting. These data driven models imitate physical norms derived from historical data to establish a functional relationship between inputs and outputs. Unlike many other models, which necessitate the use of equations and assumptions based on physical processes in order to function, machine learning models can be used to simulate natural systems with great success (Yaseen *et al.*, 2018). These new modeling approaches can capture the highly nonlinear

relationship of catchment properties with runoff generations at different spatial scales and thus, open a new horizon of runoff modeling. Many studies have compared the performances of different ML methods to reveal their applicability in streamflow simulation and forecasting in different catchments (Meehl *et al.*, 2003; Shortridge *et al.*, 2016). Several machine learning models are used to predict streamflow, including Artificial Neural Networks (Noori and Kalin, 2016; Jimeno-Sáez *et al.*, 2018), Multivariate Adaptive Regression (MARs) (Adnan *et al.*, 2019; Yaseen *et al.*, 2016; Sharma *et al.*, 2023) ,Multiple Linear Regression (MLR) (Rasouli *et al.*, 2012; Tyralis *et al.*, 2021; Rahimzad *et al.*, 2021), Random Forest (Papacharalampous and Tyralis, 2018; Sharma *et al.*, 2023), Extreme Learning Machine(ELM) (Goudarzi *et al.*, 2021), Multi-layer perceptron (MLP) (Rahimzad *et al.*, 2021; Rahman *et al.*, 2022), Support Vector Regression (SVR) (Rasouli *et al.*, 2012; Rahimzad *et al.*, 2021), Gradient Boosted Regression Trees (GBRT) (Erdal and Karakurt, 2013), LSTM (Cheng *et al.*, 2020; Thapa *et al.*, 2020; Rahimzad *et al.*, 2021; Sharma *et al.*, 2023). It is claimed that the data-driven model has surpassed the physical models in terms of prediction accuracy in many hydrological applications, despite the inherent limits in the physical interpretability of the processes (Shortridge *et al.*, 2016; Adnan *et al.*, 2019; Yang *et al.*, 2019; Kabir *et al.*, 2020; Herath *et al.*, 2021; Mohammadi *et al.*, 2021; Yuan and Forshay, 2021).

The semi-distributed models are coupled with data driven models such as Artificial Neural Networks for predicting daily streamflow in unmonitored watersheds (Noori and Kalin, 2016; Jimeno-Sáez *et al.*, 2018). The combination improves the modeling environment by eliminating the need for calibration and sensitivity analysis to fine-tune model parameters and by reducing the number of inputs to ANN (Noori and Kalin, 2016). SWAT has the ability to simulate low flows, and ANN can better simulate high flows (Jimeno-Sáez *et al.*, 2018). The conjuction of SWAT and multi-layer perceptron improved the prediction accuracy, and the MLP alone performed outstandingly in the peak streamflow prediction over the upper Indus basin (Rahman *et al.*, 2022). Goudarzi *et al.* (2021) compared the SWAT model

output to the Extreme Machine Learning, the Support Vector Regression, and the Least Squares Support Vector Regression (LSSVR) over a watershed in Iran and highlighted the performance of LSSVR. Parisouj *et al.* (2020) predicted the streamflow by ML models; SVR, Artificial Neural Network with backpropagation (ANN-BP) and ELM in the snow-melt dominated basin indicated the appreciable performance of SVR. Thapa *et al.* (2020) highlights the performance of a shallow long short-term memory (LSTM) model with a hidden layer over the snow melt region of the Himalayas. The deep learning-based deep neural network (DNN), convolutional neural network (CNN), and LSTM models have recently seen an increase in the number of streamflow prediction applications due to their capacity to handle complex stochastic datasets and abstract the underlying physical mechanism (Fu *et al.*, 2020; Ghobadi and Kang, 2022). The majority of the studies indicated that the LSTM as a robust data-driven technique to characterize the time series behaviors in hydrological modeling applications (Kratzert *et al.*, 2018; Apaydin *et al.*, 2020; Rahimzad *et al.*, 2021).

There are very few global studies in which these models were used to predict the long-term streamflow for future periods in light of climate change (Das and Nanduri, 2018; Thapa *et al.*, 2021; Adib and Harun, 2022). This may be due to the difficulties associated with data assimilation posed by the use of coarse-resolution scenario data derived from general circulation models, that restricts their direct implementation in regional impact assessment (Adib and Harun, 2022). Das and Nanduri (2018) compared the RVM and SVM models, and predicted the monthly monsoon streamflow of future decade using CMIP5 GCMs across the Wainganga basin (India) for monsoon season. Adib and Harun (2022) coupled RF and SVR to analyze the variations in the monthly streamflow pattern of the Kurau River of Malaysia using CMIP6 GCMs. Zareian and Salem (2022) used CNN to project the monthly streamflow for the next four decades using CMIP6 GCMs. CNN, LSTM runoff prediction presents a higher reproducibility than that of the SWAT model in simulating runoff variation according to time-series changes (Lee *et al.*, 2020; Zareian and Salem, 2022). Singh *et al.* (2023) Predicted declines in the streamflow

of Sutlej River of western Himalaya during the pre-monsoon and winter season seasons using the RF method.

2.5 LITERATURE SUMMARY

Impact studies of climate change are fraught with uncertainty. The advancement in the understanding of possible uncertainties and their respective solutions has uncovered the various factors which were ignored earlier. The researchers have demonstrated novel approaches in uncertainty quantification, which substantially improves future predictions and, consequently, climate adaptation options. Few studies have used advanced uncertainty quantification methods and have demonstrated the efficacy of the GCM models in regional scale studies. These are particularly important in the assessment of climate changes impact on the climate extremes. The increased temperature and change in intensity and magnitude of precipitation are bound to bring about changes in evapotranspiration rates, thereby affecting river runoff. Higher variability in the impact of climate change is noted over the globe to the regional scale of WG. The ghat plays a pivotal role in persuading heavy rainfall over the West Coast of India. Due to its climatic heterogeneity and geographical complexity, many of the studies have focused on the regional scale variability analysis, which further highlights the complexity of understanding the climate change impact on rainfall and other hydrological parameters (ET, runoff, Water Availability). The modification in the regional level of the mountain terrain, LU/LC is expected to have a higher impact on these variables, further making it complicated. Several studies have shed light on the spatiotemporal variability in the rainfall with the mountain terrain of WG and highlighted the importance of regional heterogeneity of the mountain. Which is an important factor playing a pivotal role in the converse trend of hydro-meteorological parameters. Further, its latitudinal variation in the geo-climatic variables are highlighted in the past studies. Based on the studies reviewed following key points are emphasized.

2.6 LITERATURE GAP

1. Though there are studies that explain the spatial variability of rainfall in mountainous terrain, limited studies have focused on understanding spatial variability concerning all the topographical parameters and the climate of the region.

2. The uncertainty in the GCMs/RCMs varies with the geography and the climate of the region, therefore it is important to rank the down-scaled/bias corrected GCM models at regional scale to account for the uncertainty reduction. Which is highlighted by poor performance of CMIP6 GCM models over the WG.

3. CMIP6 models being the recent version and the most updated models of climate change assessment, studies needs to be focused to improve the performance using the up to date uncertainty reduction methodologies.

4. The performance of advanced ensemble methods such as AdaBoost and XGBoost over the most widely used RF and SVM has not been explored in the ensemble of the GCMs for the projection of climate variables. Additionally, it is important to determine the variation in GCM-MME performance across a variety of geo-climatic zones.

5. The future is expected to have enormous climate extremes, though the GCMs simulated the daily/monthly rainfall and temperatures with close agreement to the observation, the analysis of its ability to estimate the extreme climatic events are important. The studies have gave importance to the uncertainty reduction in the daily/ monthly scale, but have not studied its capacity to simulate the extreme climate.

6. The change in frequency of extreme rainfall events and their trend has to be given importance in WG as this region receives extreme events of rainfall all along the west coast of India.

7. The relationship with the rainfall and the streamflow in the future decades are important for the water resource planning and management. The empirical models have been proved to be perform better than the physical based semi-distributed hydrological models with limited data availability. Which is not explored in the basins of complex mountainous terrain of WG.

Inferences drawn from the literature survey guides the objectives of this research. Formulated objectives address few important aspects related to climate change impact over WG of India. The description of area under investigation and materials used are outlined in the next chapter.

CHAPTER 3

MATERIALS AND METHODOLOGY

3.1 INTRODUCTION

This chapter includes the description of

1. Geographical location and characteristics of the study region,
2. Data products used in this study,
3. Overall methodology adopted for the study,

3.2 DESCRIPTION OF THE STUDY AREA

The Western Ghats is a tropical forest mountain range situated between the Arabian Sea on the west and the Eastern Ghats on the east. The WG stretch to 1600 km parallel to the Arabian Sea, 100 km in the East-West direction. The WG rises from north to south with a maximum elevation of 2685 meters above mean sea level and an average elevation of 900 meters (Shetty *et al.*, 2022). The Ghats form the catchment area for complex riverine drainage systems and are called as the "Water Tower of South Indian Rivers" (Ramachandra *et al.*, 2016). The Indian summer monsoon circulation passing through the Arabian Sea is blocked by the mountains of the WG, which run perpendicular to monsoon winds passing through the sea. The monsoon circulation gets modulated due to the orographic influence of the Ghat. The moisture-laden wind in the Ghat cools to saturation, and then it condenses due to the high amount of water vapour collected from the Indian Ocean and the Arabian Sea. This enhances the convective rainfall over the west coast of India and the orographic stratified rainfall over the WG hills (Zhang and Smith, 2018). After crossing the peak of the WG, the air sinks and get heated up, causing a decrease in the rainfall over the leeward side of the mountain (Venkatesh and Jose, 2007). The West Coast area receives an average annual rainfall of 3,000

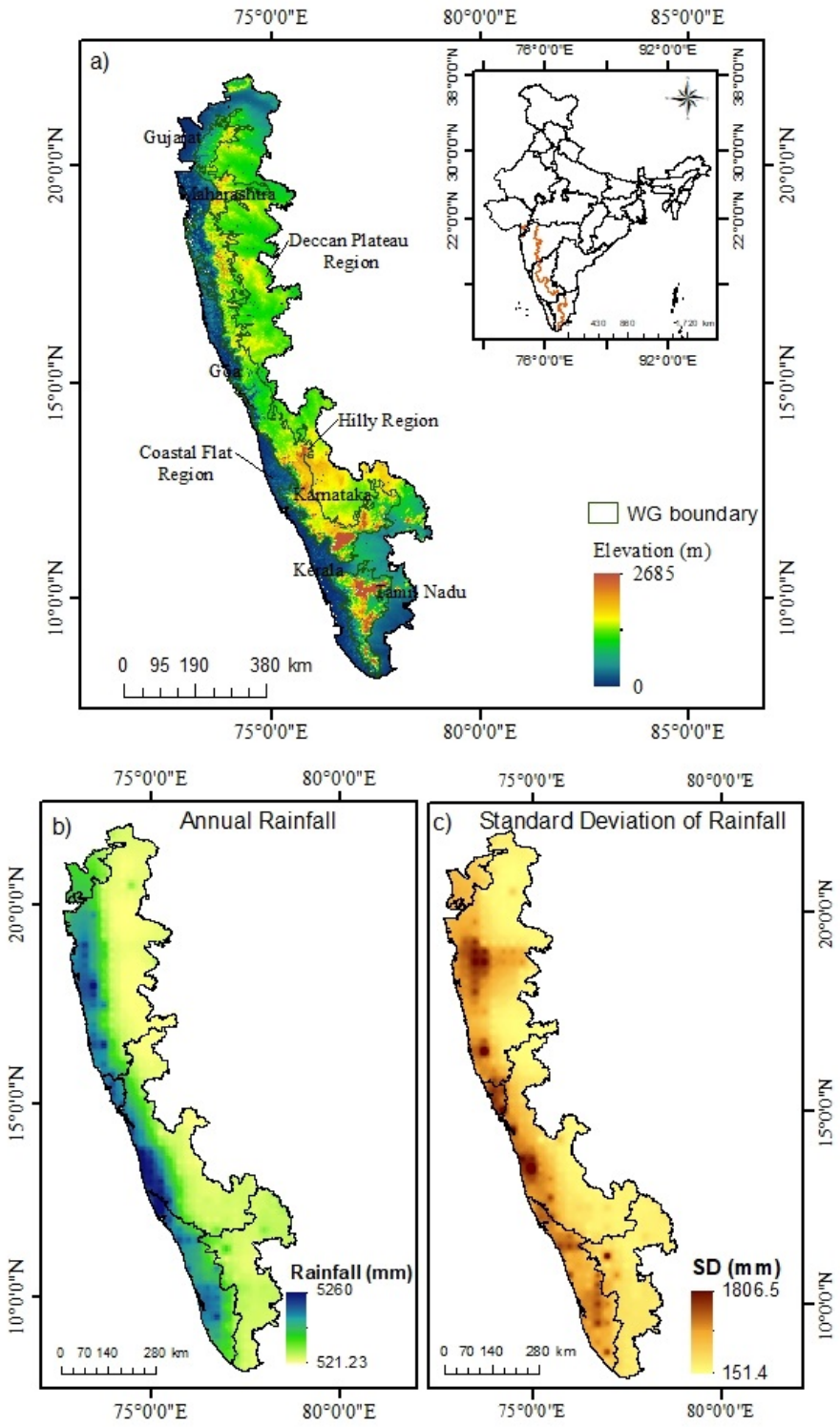

Fig. 3.1: The spatial variation in a) elevation b) annual rainfall and c) standard deviation in annual rainfall over the study area

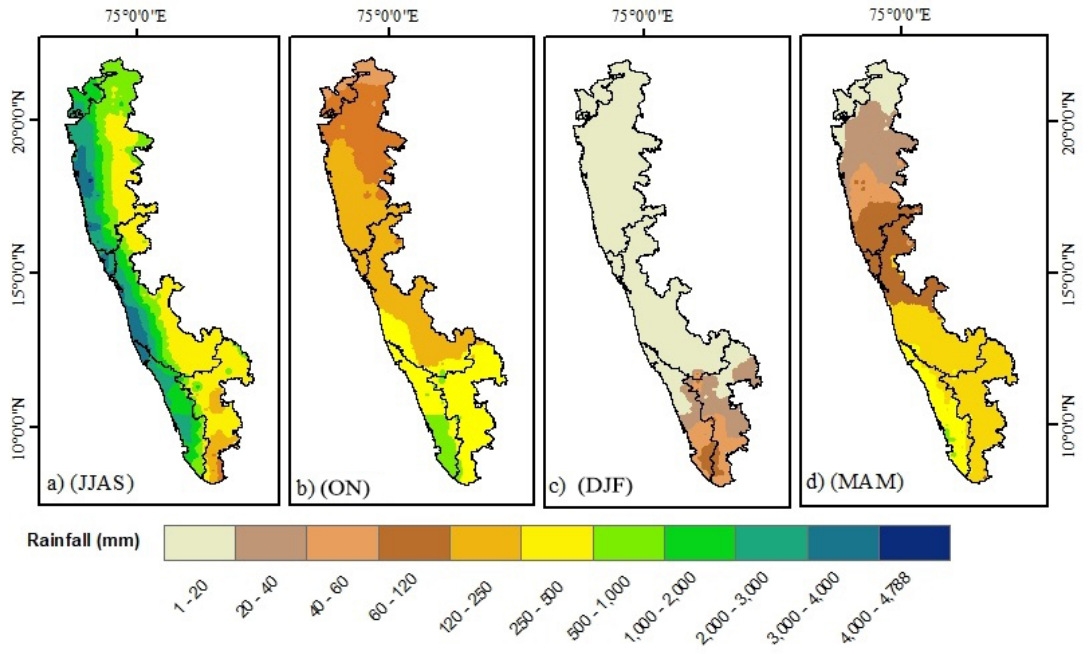

Fig. 3.2: The spatial distribution of seasonal rainfall

mm and approximately 6,000 mm near the hill, with maximum rainfall varying up to 7,000 mm in a few locations. The eastern part of the mountain receives an average annual rainfall of around 1800 mm, and the plateau region receives about 700 mm of rainfall. These tropical upper mountain rainforests are rich in flora and fauna and are characterized by conical, broad, and flat-topped hills with stunted evergreen trees. The diverse topography and precipitation patterns have given rise to a vast range of plant life, including shrub vegetation on the east side, dry deciduous vegetation at higher elevations, and evergreen forests on the west side. The Western Ghats mountain forests are more attractive to researchers because of their vast eco-biodiversity, and continuous and complex mountainous terrain with more rainfall variability than the Eastern Ghats of India. The overall study area covers approximately 3,16,000 km^2 area, including all the districts through which WG passes. Figure 3.1 explains the elevation of the region with the spatial distribution of rainfall and standard deviation (SD). The SD of rainfall is higher in the coastal area and lower in the eastern part of the mountain, which follows a similar distribution of the rainfall amount received. The seasonal variability in the rainfall is shown in Figure 3.2.

Further, six west-flowing river basins originating in the Ghat, which are at four different climate zones according to the revised Thornthwaite-type global climate classification system, are considered for the study. Figure 3.3 shows the location details of the six river basins, namely Vamanapuram, Chaliyar, Netravati, Aghanashini, Ulhas, and Purna river basins in the WG of India. The revised Thornthwaite-type global climate classification method classifies the climate based on Moisture Index (I_m); i.e., I_m>100 as per-humid (A), which represents the wettest climate, I_m between 20-100 as humid (80-100 as Humid (B4) and 60-80 as Humid (B3)), I_m from -20 to 0 represents dry sub-humid climate (C2) (Feddema, 2005). The characteristics of the six river basins are represented in Table 3.1.

The Vamanapuram and Chaliyar basins are the major rivers of Kerala and are the southernmost river basins in the study. Netravati and Aghanashini rivers flows through Karnataka and are located in the central WG. River Ulhas flows through Maharashtra, Purna river originates in Maharashtra and flows through Maharashtra and Gujarat. The rivers Vamanapuram, Chaliyar, Netravati, and Ulhas are steep in the initial reaches and have long flat plains (Figure 3.3). The area of the basins ranges between 541 km^2 to 3351 km^2, representing small to mesoscale river basins in the WG. The LU/LC of the basins and the changes observed in the 15 years are shown in Figures 3.4, 3.5, 3.6. The southern basins are dominated by evergreen to deciduous forests (around 52-72.5%) and the plantation (23-38%). In the past 15 years, when the region has seen rapid development, though the forest area has not seen a decrease in the area, the fallow or wastelands has significantly decreased with an increase in the built-up area. The built-up area has seen almost five times increase (0.4% in 2005 to 2.06% in 2020) in the 15 years in the Chaliyar basin. The central river basins have experienced an increase in the crop land with a decrease in the fallow land, and the increase in built-up area is doubled in both river basins. The fallow land in the northern river basins has converted to crop land. The basins have lesser development in the built-up area compared to other basins.

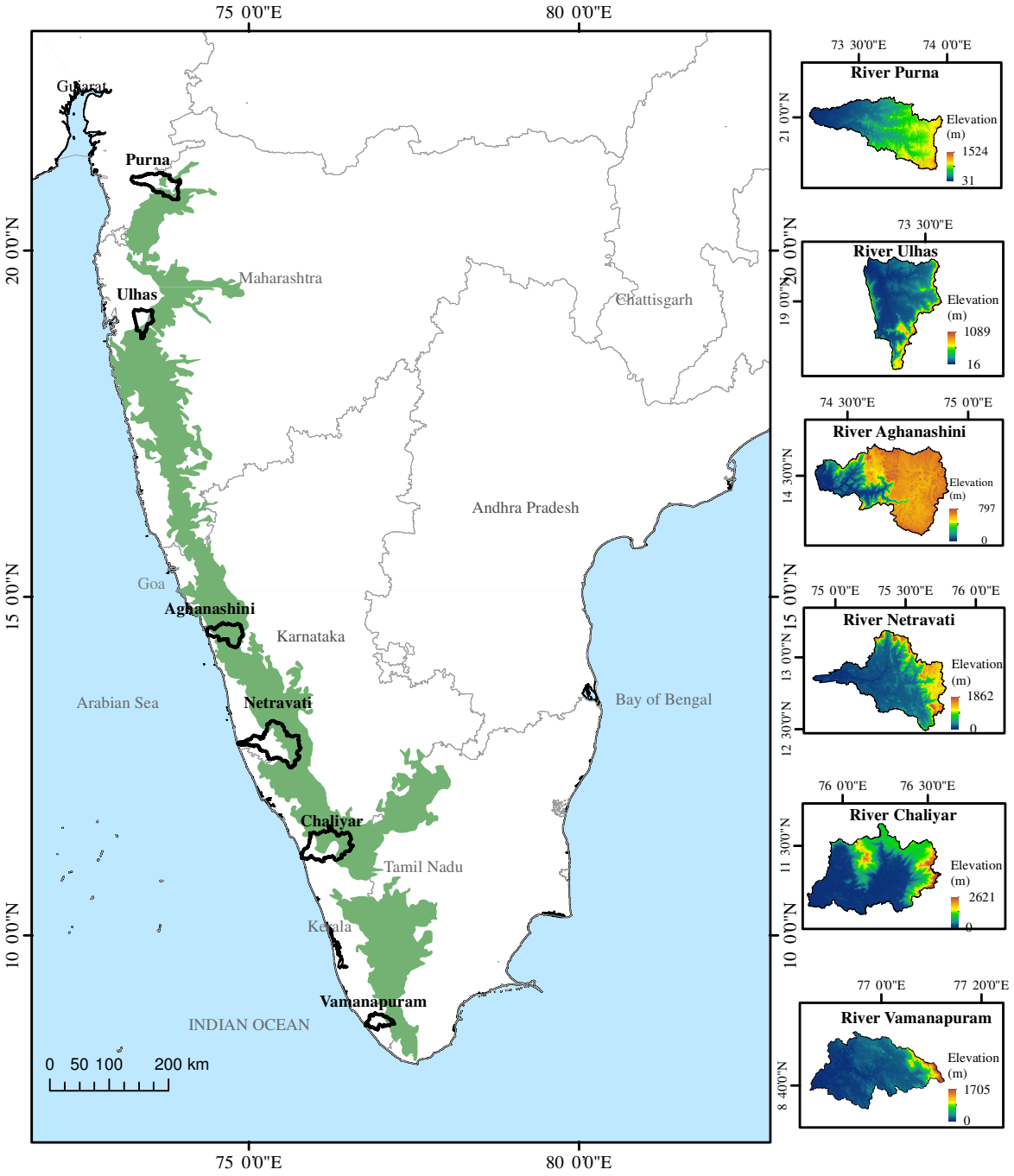

Fig. 3.3: Location details of the six river basins with the elevation

Table 3.1: Descriptions of river basins and their features

State	River	Climate Zone	Area of Catchment (km^2)	Average Annual Rainfall (mm)	Maximum Temperature (°C)	Minimum Temperature (°C)
Kerala	Vamanapuram	Humid (B3)	541	1800	31.8	23.2
Kerala	Chaliyar	Dry sub-humid (C1)	2923	2700	29.1	19.4
Karnataka	Netravati	Per humid (A)	3351	3700	28.7	19.7
Karnataka	Aghanashini	Per humid (A)	1295	3550	28.8	19.6
Maharashtra	Ulhas	Humid (B4)	886	2866	32.6	21.0
Gujarat	Purna	Dry sub-humid (C1)	1655	1360	32.6	20.6

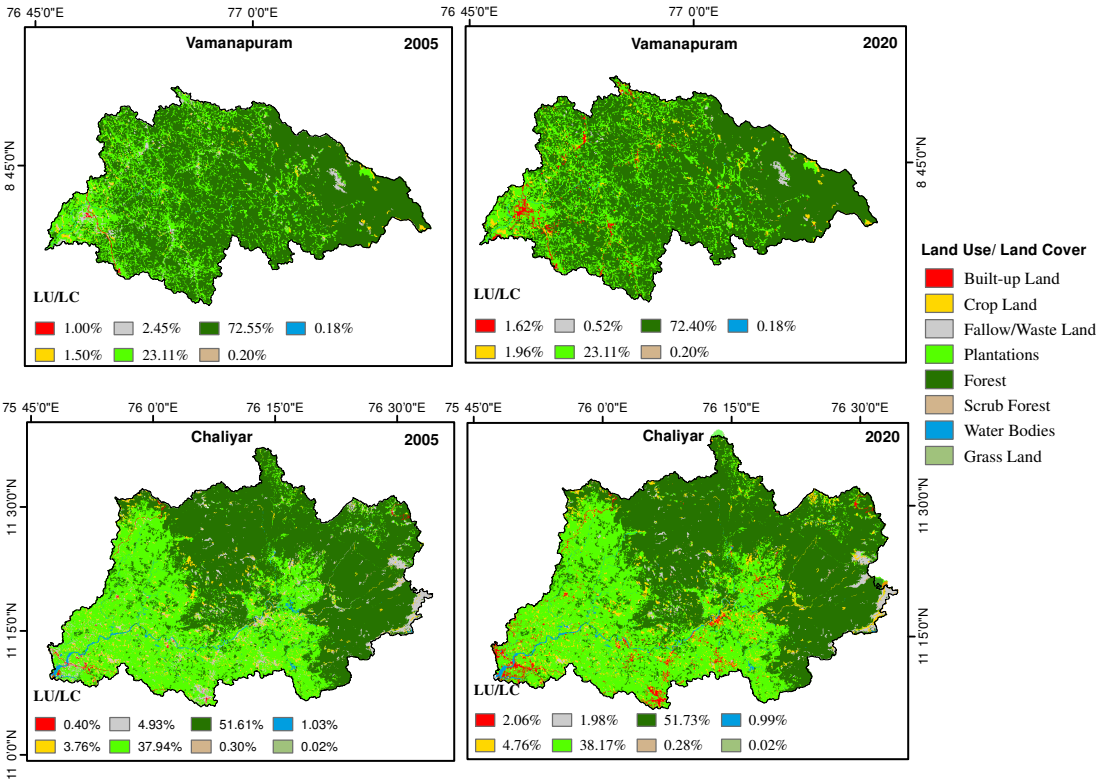

Fig. 3.4: LU/LC of southern river basins

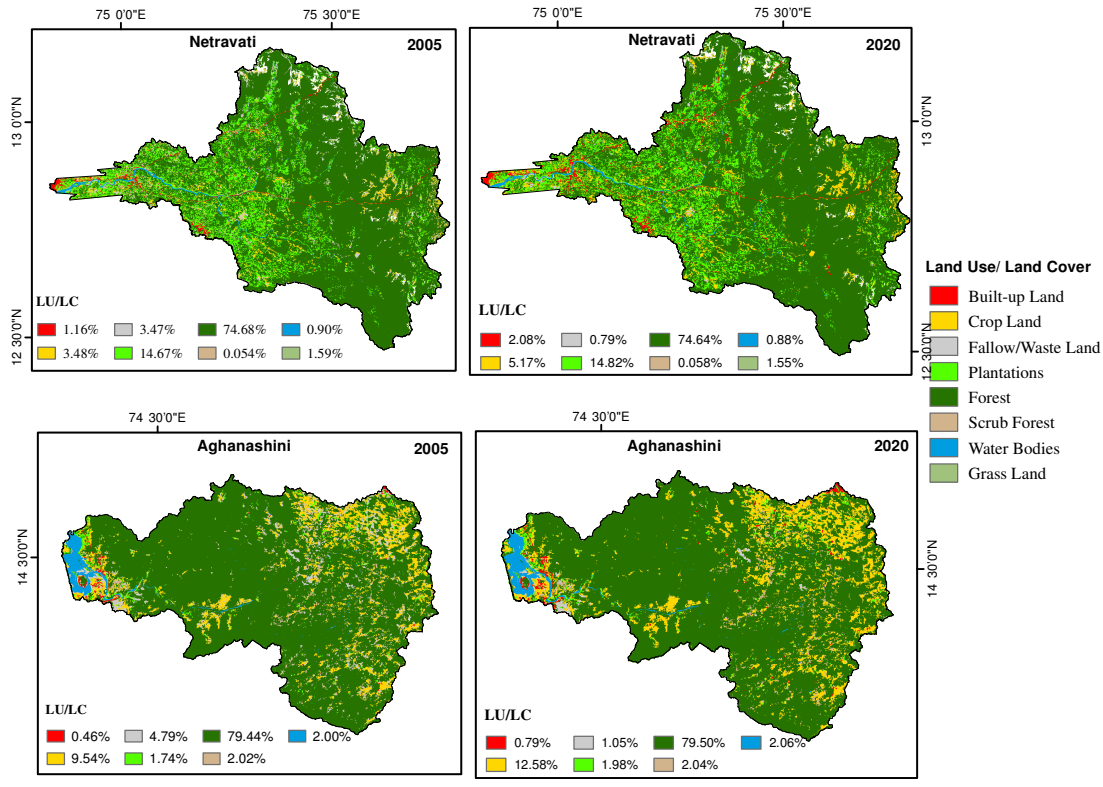

Fig. 3.5: LU/LC of central river basins

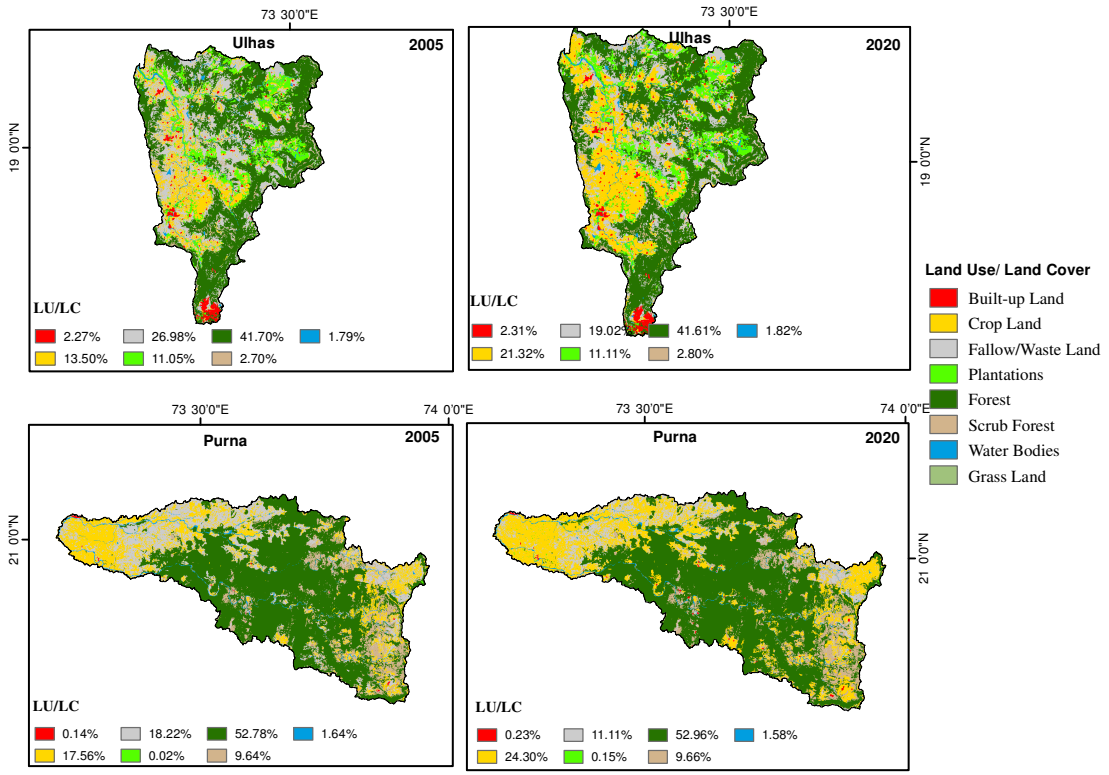

Fig. 3.6: LU/LC of northern river basins

3.3 DATA PRODUCTS USED

The long-term daily precipitation data of 0.25° × 0.25° spatial resolution from the India Meteorological Department (IMD) is used as ground truth data for the evaluation of the MMEs of GCM. To generate the gridded IMD precipitation data for India, data from 6955 rain gauge stations were interpolated using Shepard's method. The daily maximum and minimum temperature data from more than 350 stations across India are interpolated using a variant of Shepard's angular distance weighting algorithm. The long-term temperature data is available at a spatial resolution of 1° × 1°. More details of the gridded data development of precipitation and temperature and the quality control procedures are explained in (Srivastava *et al.*, 2009; Pai *et al.*, 2014). The high resolution and increased station density are employed to represent a more practical distribution of precipitation, even in the challenging hilly terrains (Pai *et al.*, 2014; Prakash *et al.*, 2015).

Shuttle Radar Topography Mission (SRTM) of the 30 m Digital Elevation

Model (DEM) is used to visualize the elevation and topographic structure of the study area owing to its acceptable accuracy compared to other freely available DEM sources (Shetty *et al.*, 2021). SRTM extracts 80% of earth's landmass elevation with two antennas separated by a 60m long mast using C-band (5.6 cm wavelength) and X-band (3.1 cm wavelength) Interferometric Synthetic Aperture Radar (InSAR) (Zebker and Goldstein, 1986). This SRTM data is downloaded from the United States Geological Survey (`https://earthexplorer.usgs.gov/`) website. The slope, Terrain Ruggedness Index (TRI), Directional Relief (DR), Relative Terrain Aspect (RTA), Distance to coast and ridge of the mountain are derived from this product.

The Day and Night Land Surface Temperature (LSTmax and LSTmin) and the Normalized Differential Vegetation Index (NDVI) data are extracted from the Moderate Resolution Imaging Spectroradiometer (MODIS) instruments on-board Terra and Aqua NASA satellite at a resolution of 1 km. MODIS Aqua satellite data are mostly preferred to extract maximum and minimum daily temperatures as it descends at 1:30 PM and ascends at 1:30 AM at the equator. Terra passes the equator at 10:30 PM and 10:30 AM in the opposite direction (Justice *et al.*, 2002). The MODIS LST is derived from two thermal infra-red bands, i.e., 31 (10.78–11.28 lm) and 32 (11.77–12.27 lm), using the split-window algorithm. The MODIS Land Surface Temperature and Emissivity monthly product portrays the local difference in temperature due to meteorological and environmental conditions in greater detail across the world from 2003 to 2019 (Wan, 2008; Hengl *et al.*, 2012; Wan, 2014).

The NDVI data products from MODIS offer an excellent opportunity to study land-cover/land-use change because of their high temporal and spatial resolution characteristics, improved spectral resolution, and enhanced atmospheric calibration (Zhang *et al.*, 2003). A total of 294 MODIS NDVI tiles cover the globe, and the MODIS data are obtained through the online Data Pool at the NASA Land Processes Distributed Active Archive Center (NASA LP DAAC) (`https://e4ftl01.cr.usgs.gov/`). The NDVI value ranges from -1 to 1, indicates the

amount of green vegetation in the area, and is strongly related to the radiation absorbed by actively growing plants (Davenport and Nicholson, 1993; Onema and Taigbenu, 2009). The surface wind data is obtained from ERA5 reanalysis data produced by European Centre for Medium-Range Weather Forecasts (ECMWF) (`https://cds.climate.copernicus.eu/`). The ERA5 is created by merging a numerical weather prediction model with satellite and ground-based observational data. It computes atmospheric variables at 137 pressure levels with a spatial resolution of 0.25^0 and temporal resolution of 1 hour (Hersbach *et al.*, 2020).

The LU/LC of the WG has been obtained from National Remote Sensing Centre at a resolution of 54 m for a period 2004-2005, and 2019-2020. The change in the land cover and land use of the study area in the span of 15 years is shown in Figure 3.4 for southern river basins, Figure 3.5 for central river basins, Figure 3.4 for northern river basins. The hydrological data of the river basin is obtained from Central Water Commission, India (`http://www.indiawris.nrsc.gov.in/`). The river gauging data for Vamanapuram basin is at Ayilam (1979–2013), Chaliyar basin at Kuniyil (1980–2013), Netravati basin at Bantwal (1970–2013), Aghanashini basin at Santeguli (1988–2013), Ulhas basin at Badlapur (2003–2020), and Purna basin at Mahuva station (1971–2013).

The newest, updated General Circulation Model, Coupled Model Inter-comparison Project-6 of the IPCC, includes a wide range of experiments to meet the growing demand of the climate research community and address the shortcomings of CMIP5 (Eyring *et al.*, 2016; Stouffer *et al.*, 2017; Gusain *et al.*, 2020). This study utilized 13 GCM models; the specifications of the models are given in Table 3.2. The daily precipitation, maximum temperature, and minimum temperature of the 13 GCM models of CMIP6 are bias-corrected using Empirical Quantile Mapping (EQM) for South Asia (Mishra *et al.*, 2020). The data set comprises projections for the four scenarios (SSP126, SSP245, SSP370, SSP585) for the historical (1951-2013) and projected (2014-2100) time periods and is available at a spatial resolution of $0.25^o \times 0.25^o$. The technical validation of this bias-corrected data set against the observations for mean and intense precipitation events, as well as

maximum and minimum temperatures over India, has been carried out by Mishra *et al.* (2020).

3.4 OVERALL METHODOLOGY

The combined methodology adopted in this study is given in Figure 3.7. The detailed methodology followed to achieve the objectives is explained in the next chapters. The present study can be divided into four sub-studies which answers the five objective of the study. In first objective, the dependability of the rainfall with topo-climate (elevation, slope, Terrain Ruggedness Index (TRI), Directional Relief (DR), Relative Terrain Aspect (RTA), distance from the coast (Cd), and distance from the ridge (Rd), Land Surface Temperature (LST) and Normalized Differential Vegetation Index (NDVI), Wind speed) of the WG, its long-term spatio-temporal variation in the association, the role of topographic structure on the rainfall distribution is studied. This study is explained in Chapter 4. In the second objective, the performance of the individual GCM models are assessed and ranked based on its performance, further the top performing GCMs are ensembled using a simple arithmetic mean and the seven machine learning based methods. The effectiveness of these ensemble models over the diverse-climate basins of the WG is studied. This objective is explained in Chapter 5. These ensemble models performance in the estimation of extreme climatic indices are evaluated for the river basins in Objective 3, the top performing ensemble model is used to project the future climatic variables and the extreme indices. The assessing the future variability in these variables and their trend in the historical and future horizon under two future scenarios is of Objective 4. These two objectives are explained in Chapter 6. In the last objective the streamflow is modelled by a deep-learning LSTM technique and annual percentage variability in the future decades, and the water scarcity risk assessment is carried out, and is explained in the Chapter 7.

Table 3.2: Details of CMIP-6 GCM models

Model Name	Country	Modelling Agency	Resolution	Reference
ACCESS-CM2	Australia	Australia Commonwealth Scientific and Industrial Research Organisation (CSIRO), Australian Research Council Centre of Excellence for Climate System Science (ARCC)	$1.25^o \times 1.875^o$	Bi *et al.* (2020)
ACCESS-ESM1-5	Australia	Australian Community Climate and Earth System Simulator	$1.25^o \times 1.875^o$	Ziehn *et al.* (2020)
BCC-CSM2-MR	China	Beijing Climate Center Climate System Model	$1.1215^o \times 1.125^o$	Wu *et al.* (2019*b*)
CanESM5	Canada	Canadian Earth System Model Version 5	$2.7906^o \times 2.8125^o$	Swart *et al.* (2019)
INM-CM4-8	Russia	Institute for Numerical Mathematics, Russian Academy of Science, Russia	$1.5^o \times 2^o$	Wyser *et al.* (2020)
INM-CM5	Russia	Institute for Numerical Mathematics	$1.5^o \times 2^o$	Volodin and Gritsun (2018)
EC-Earth3	Europe	EC-Earth Consortium	$0.7018^o \times 0.7031^o$	Döscher *et al.* (2021)
EC-Earth3-Veg	Europe	EC-Earth Consortium	$0.7018^o \times 0.7031^o$	Döscher *et al.* (2021)
MRI-ESM2-0	Japan	Meteorological Research Institute	$1.1215^o \times 1.125^o$	Yukimoto *et al.* (2019)
MPI-ESM1-2-HR	Germany	Max Planck Institute, Germany	$0.9351^o \times 0.9375^o$	Mauritsen *et al.* (2019)
MPI-ESM1-2-LR	Germany	Max Planck Institute, Germany	$1.8653^o \times 1.875^o$	Gutjahr *et al.* (2019)
NorESM2-LM	Norway	Norwegian Climate Center Earth System Model Version 2.0	$1.8947^o \times 2.5^o$	Seland *et al.* (2020)
NorESM2-MM	Norway	Norwegian Climate Center Earth System Model Version 2.0	$0.9424^o \times 1.25^o$	Seland *et al.* (2020)

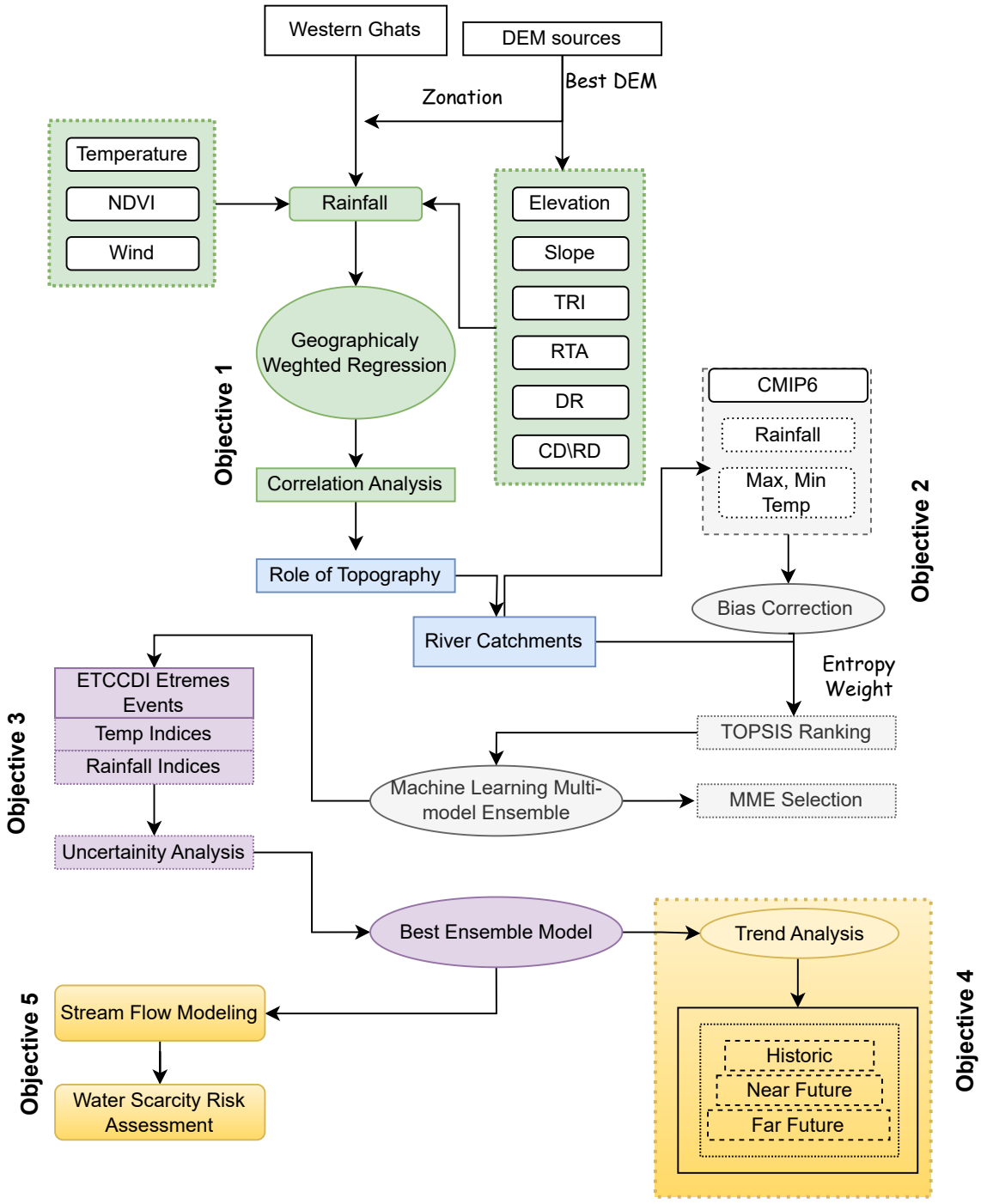

Fig. 3.7: The broad methodology formed to achieve the objectives

CHAPTER 4

DEPENDABILITY OF RAINFALL TO TOPOGRAPHY AND CLIMATE

4.1 BACKGROUND

There is a wide choice of techniques for understanding the interaction between rainfall, temperature, topography, and vegetation, but the model must alter over the space to reflect the spatial heterogeneity of rainfall especially over the undulating mountainous terrain. This spatial heterogeneity could be better explained by the Local Regression Models (Hengl, 2009; Kumari *et al.*, 2017*b*). The Geographically Weighted Regression (GWR) model can better explain this relationship with the inclusion of topographic and climatic factors (Kumari *et al.*, 2017*a*). The GWR is a robust method to describe spatial heterogeneity on a regional scale. It establishes a relationship between primary and secondary variables by fitting a local regression model specific to a location using the sub-sampled data from the nearest neighbouring observations (Barry, 1992; Li *et al.*, 2010). The use of global models masks the widespread local variation, but these local models improve the prediction accuracy and quantify the spatial drift of the regression parameters (Li *et al.*, 2010).

4.2 METHODOLOGY

4.2.1 Zonation of the Western Ghats

The study area has a coastal belt in the western stretch, followed by a complex ascending mountain topography (SW facing) that receives orographic rainfall. This is followed by the descending mountain terrain (SE facing). This is the rainshdow region of the WG to the SW monsoon, the region forms an arid and semi-arid climate with scanty rainfall. Which is followed by an undulating region with flat to complex topography in the eastern stretch. The region receives varying rainfall

in each of the zones due to the complex topographic structure. In climatological studies, it is often needed to cluster variables into homogeneous groups (DeGaetano, 2001) and identify patterns (Burrough, 2001) to enhance the understanding of atmospheric phenomena like rainfall. Based on this, the WG is divided into four zones, 0-400 m on the coast side as a coastal flat region (CF) counting 118 grid points, 401-2685 m as SW facing hilly region (SWH) counting 48 grid points, 401-2685 m as SE facing hilly region (SEH) counting 140 grid points, and 400-1200 m in the foot of mountain areas as Deccan plateau region (DP) counting 124 grid points.

4.2.2 Rainfall, Land Surface Temperature, NDVI, and Wind Speed

Historical daily rainfall values are accumulated to get the annual rainfall (January-December) and seasonal rainfall (Winter: December-February, Pre-Monsoon: March-May, Monsoon: June-September, and Post-Monsoon: October-November) in accordance with the seasons of India as specified by the India Meteorological Department (IMD). The NDVI from the Moderate Resolution Imaging Spectroradiometer monthly product (MOD13) at 1 km and MODIS Land Surface Temperature and Emissivity (MOD11) at 1 km resolution is re-sampled to 25 km resolution, and the values at each grid location are extracted. The NDVI values higher than 0.5 represent dense vegetation. The values between 0.2 to 0.3 correspond to shrubs and grasslands. The values lower than 0.1 correspond to areas with little or no vegetation (rocks, ice, and desert). The wind speed in each of the seasons is computed from the zonal and meridional wind components of ERA5 near the surface. The spatial variation in these are shown in Figure 4.1.

4.2.3 Topographical Parameters

The topographic characteristics of the WG modulate the rainfall, which results in intense rainfall in the coastal plains and on the windward side of the Ghat. Therefore, at every grid location, the elevation, slope, TRI, DR, RTA, distance from the coastline, and distance from the ridgeline are extracted from the SRTM

DEM. The topographical variables computed at a scale of 5 km are used as an optimal resolution for the correlation study (Daly *et al.*, 1994; Kumari *et al.*, 2017*b*). TRI index is a measure of terrain heterogeneity, developed by Riley *et al.* (1999). The TRI determines the Root Mean Square Deviation for each of the cells, considering the eight neighboring cells of the DEM. The distance from the coastline is an indirect measure of the moisture in the air. The distance from the coast and the ridge of the mountain ranges, along with the topography of the mountain, has a significant role in altering the moisture-laden wind over the Western Ghats of India.

The topographic exposure to the wind is derived from the RTA considering the terrain orientation. RTA is an angular measure of the distance between the terrain aspect and the regional wind azimuth, calculated excluding the influence of exposure/sheltering of the location by neighboring landforms and the deflection of wind by the topography (Böhner and Antonić, 2009). The influence of the exposure/sheltering of the location by neighboring landforms is taken into account in the directional relief parameter. DR calculates the relief of terrain in a defined direction. It is an index of the degree to which a location is lower or higher than its adjoining locations. The positive directional relief value indicates that the location is relatively sheltered, whereas the negative directional relief value indicates the location is relatively exposed than its surroundings (Lapen and Martz, 1993). As the monsoon wind is due to the south-west wind circulation and post-monsoon is from the north-east circulation, the average of eight directions from west of N-S is taken for monsoon season and east of N-S for the post-monsoon season, and an average of 16 directions for winter and pre-monsoon season in the calculation of RTA and DR parameters.

4.2.4 Regression Models

The zone-wise spatial and temporal correlation between these independent parameters and rainfall is obtained by the ordinary least square regression (OLS). The regression model has been fit between rainfall (annual and seasonal) and

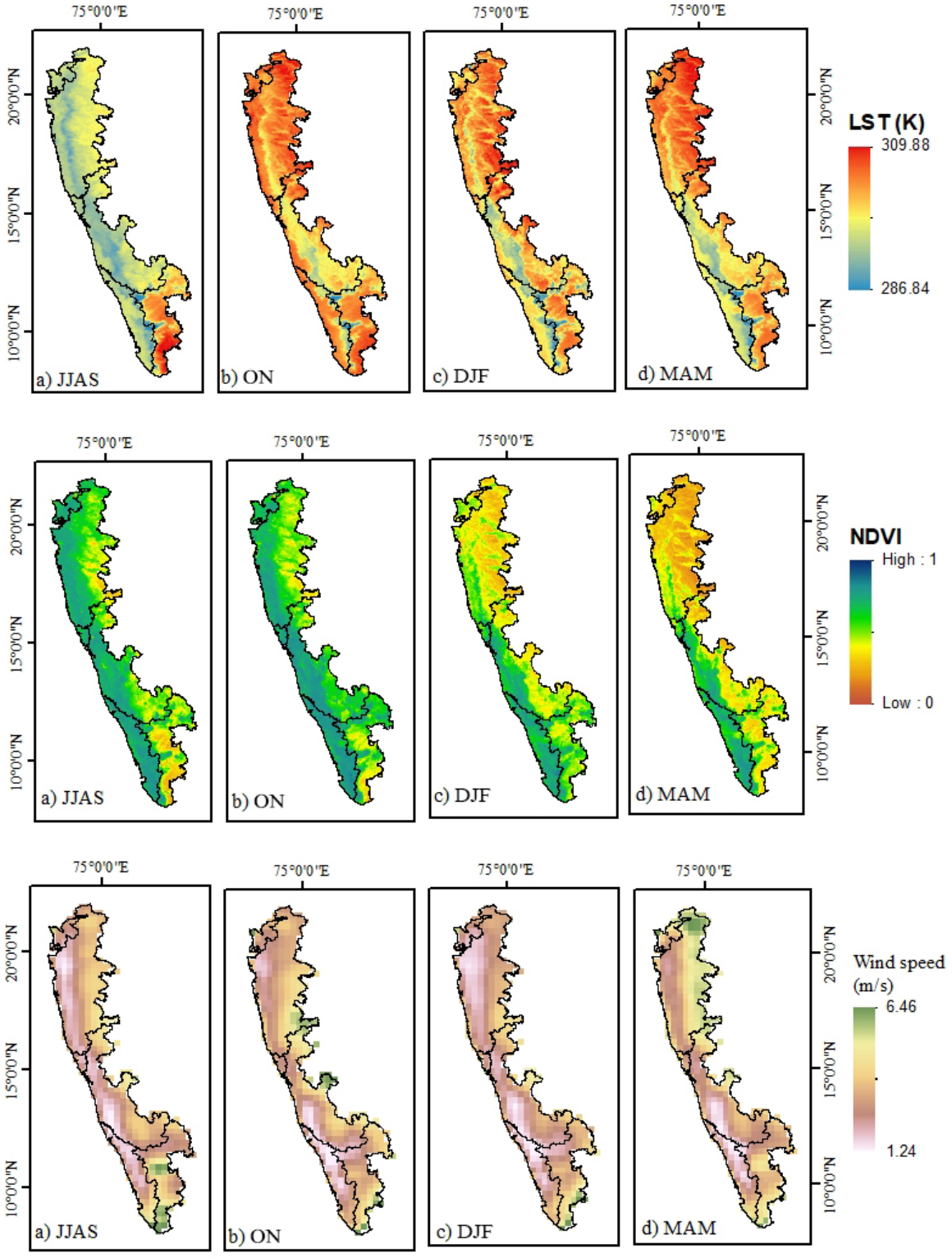

Fig. 4.1: Spatial variation in the LST, NDVI and Wind speed

other topographical variables (elevation, slope, TRI, distance from the coastline, and distance from the ridge line) for a time series of 119 years (1901-2019) and 17 years (2003-2019) for LST and NDVI due to the limited availability of the data. The relationship between topographical parameters and rainfall varies with seasons. The long-term seasonal variation in the correlation between rainfall and other independent parameters discloses the temporal variability under the changing climate.

Though the OLS, a global regression techniques reveal the association between dependent and independent variables, it assumes that the relationship is uniform across the study area, but in the complex terrain of Western Ghats, the rainfall-topographic relationship is non-stationary. This relationship can be better explained by using local regression models to incorporate spatial heterogeneity, like Geographically Weighted Regression Models. GWR builds a relationship between the dependent and independent parameters using location details and the local fit model between the variables. The detailed principle of GWR can be obtained from Brunsdon *et al.* (1999).

$$y_j = P_0\left(u_j, v_j\right) + \sum_{j}^{n} P_k\left(u_j, v_j\right) x_{jk} + \varepsilon_j \tag{4.1}$$

Where, j=1,2,3, ...,m; k=1,2,3, ..., n; y_j, x_{j1}, x_{j2}.....,x_{jk}, are the observation coefficients between the dependent variable y and independent variable x_{jk} at the geographical location (u_j, v_j) as (longitude, latitude) and $P_k(u_j, v_j)$ represents the unknown parameters at that observation site. The regression model is calibrated on all data that lie in a specified kernel around a regression point, and the process continues for all regression points. All the points in regression are weighted by their distance from the regression points; points close to regression points get a higher weight than points with more distance from regression points. For fixed kernel size, the weight of each point is calculated by applying the Gaussian function.

$$w_{jk} = exp\left[-\frac{1}{2}\left(\frac{d_{jk}}{b}\right)\right]^2 \tag{4.2}$$

Where d_{jk} is the distance between k and j, and b is the bandwidth. For large b values, the GWR model yields the same result as Ordinary Least Squares (OLS) regression. In the case of small bandwidth, the parameter estimates depend on the observation in the neighborhood, resulting in increased variance. In order to reduce the bias in an estimate due to inappropriate bandwidth selection, the Bisquare-Adaptive method of weight setting is chosen with 25 neighbor points.

The standard error of the estimate, coefficient of determination (R^2), and Root Mean Square Error (RMSE) is used to determine the goodness of fit of the GWR models. The higher the value of R^2, the better the comprehension of the variables that influence the variability in the dependent variable.

4.3 RESULTS AND DISCUSSION

4.3.1 Exploratory Analysis of Rainfall

The rainfall over the zones of WG is studied using descriptive statistics. These descriptive statistics of all the regions with variability in Coefficient of Variation (CV), Skewness (SK) and Kurtosis (Kurt) within the region are shown in Table 4.1. The distribution pattern in CF is Right Skewed Leptokurtic Distribution in winter, pre-monsoon, annual scale, and has Platykurtic, Right Skewed Distribution during monsoon and post-monsoon season. The mean rainfall over the region is normally distributed in SWH and SEH during post-monsoon and has Right Skewed Leptokurtic distribution during other seasons. Rainfall is normally distributed in the pre-monsoon season and has Right Skewed Leptokurtic Distribution during other seasons in the DP region.

4.3.2 Association between the Rainfall, Topographical Variables, and Distance from the Coast and Ridge of Mountain

4.3.2.1 Association of Rainfall with Elevation

The Figure 3.2 shows the variation in the average seasonal rainfall, the region has spatial variability in the local climate over the WG of India. The WG has a

Table 4.1: Descriptive statistics of rainfall in topographical zones

	Zone	CF	SWH	SEH	DP
Scale	Elevation(m)	1-400	400-2685	800-2695	0-1200
Annual (JD)	CV(%)	18-54	19-48	21-123	29-93
	Skewness (SK)	0-2.3	0.3-4.5	0.2-9.6	0-10
	Kurtosis	-1.3-15.21	-0.24-30.86	-0.93-95	0-96
	Distribution	RSLK	RSLK	RSLK	RSLK
Monsoon (JJAS)	CV(%)	17-77	20-100	18.9-155	24.8-153
	Skewness (SK)	-0.48-2.15	-0.45-5.3	0.03-9.91	-0.17-9.96
	Kurtosis	-1.38-4.94	-0.46-38.8	-1.27-99.94	-0.59-100.75
	Distribution	PK	RSLK	RSLK	RSLK
Post-Monsoon (OND)	CV(%)	30-143	32.9-113	32-91.3	34-138
	Skewness (SK)	0-6.59	0.22-4	0.26-2.54	0.14-2.74
	Kurtosis	-0.74-56	-0.18-24.40	-0.7-12.45	-0.67-9.72
	Distribution	RS	N	N	LK
Winter (JF)	CV(%)	87-452	80-320	85-369	93-409
	SK	0.88-9.12	0.74-9.03	0.92-7.03	1.1-8.57
	Kurtosis	-0.09-88.70	-0.28-87	0.25-55.83	0.58-80.44
	Distribution	RSLK	RSLK	RSLK	RSLK
Pre-Monsoon (MAM)	CV(%)	36.4-185	42-173.5	34-148	34-138
	Skewness (SK)	0.35-4.22	0.72-3.96	0.17-6.51	0.16-2.74
	Kurtosis	0.22-23.08	-0.19-23.53	-0.38-55.42	-0.68-9.72
	Distribution	RSLK	RSLK	RSLK	N

N- Normal Distribution, RSLK- Right Skewed Leptokurtic Distribution, LK- Leptokurtic Distribution, PK- Platykurtic Distribution

clustered pattern of rainfall distribution, in such terrains the linear relationship between rainfall and elevation improves by the topographic zonation based on the mountain structure (Figure 4.2 (a)). In the four zones of the WG, the DP region has greater variation in correlation with rainfall. The SEH region of the mountain

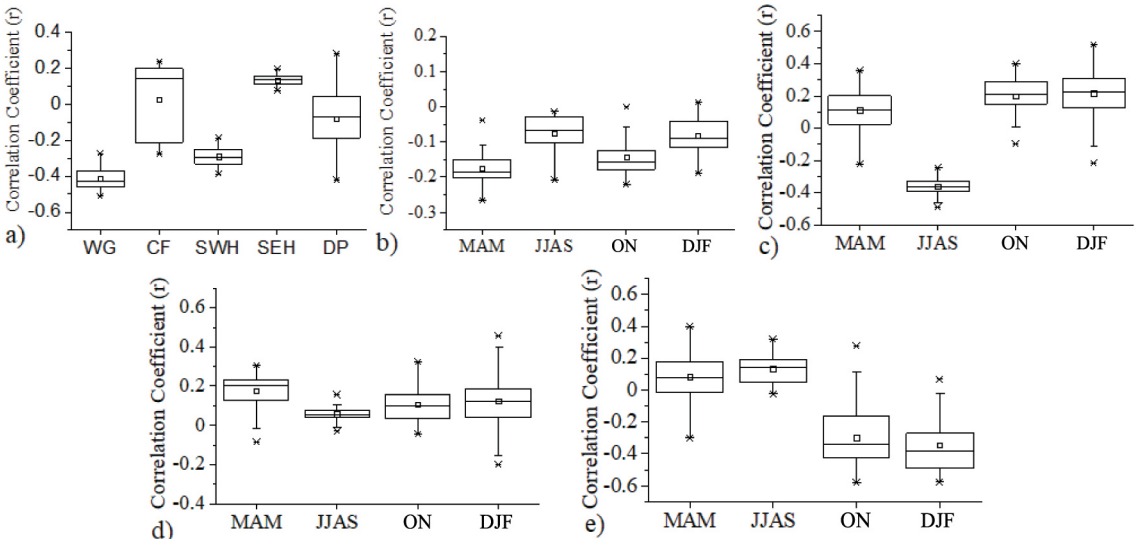

Fig. 4.2: Variation in 119 years correlation between rainfall and elevation in a) Annual b) CF c) SWH d) SEH e) DP

has a positive correlation, and the SWH region has a negative correlation between annual rainfall and elevation. In the CF region, there is no association between rainfall and elevation on the annual and seasonal scale (Figure 4.2 (b)).

The influence of elevation is prominent only during the monsoon season in the SWH region (negative correlation in a range of 0.23-0.51) and has a positive correlation in other seasons. This concludes that in the post-monsoon and winter season, rainfall is more at higher elevation ranges of mountains (Figure 4.2 (c)). In SEH of mountains, there is no good correlation with elevation and rainfall even though it has a highly variable topographic structure (Figure 4.2 (d)). In the DP region, during the pre-monsoon season, the correlation varies from -0.28 to 0.4, and in the post-monsoon and winter season, the correlation ranges from -0.12 to -0.57. It represents the more spatial variation in the distribution of rainfall in these seasons (Figure 4.2 (e)).

In Figure 4.3 the local correlation differs from that of zone wise correlation of rainfall with the elevation, as zone wise correlation averages the local variations. In the CF region, the rainfall is high even though the region is flat; hence it has a high negative association with elevation in most of the regions except the northern coastal part of Maharashtra and the regions near the coastal Kerala-Karnataka

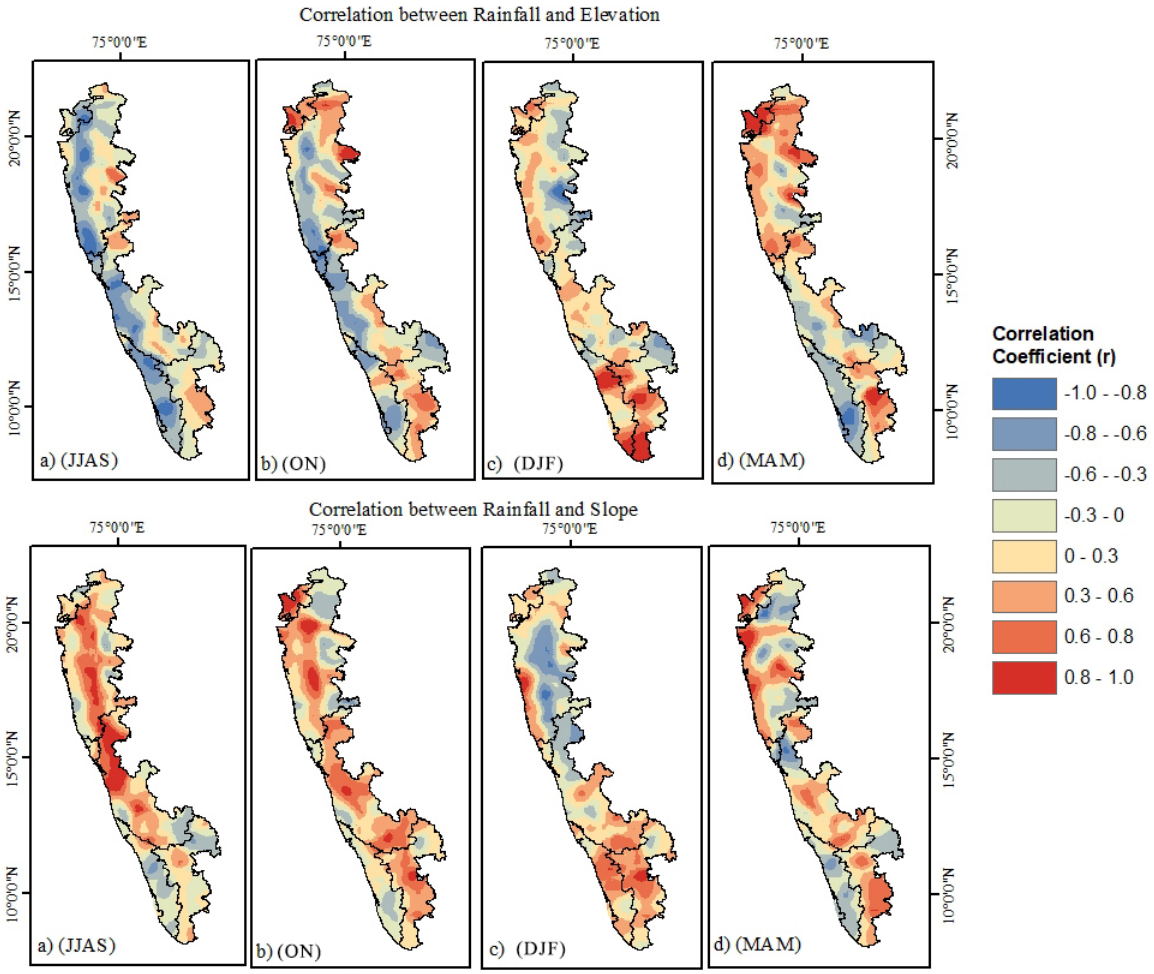

Fig. 4.3: Local correlation between rainfall, elevation and slope

border. In this region, rainfall and elevation have a positive association in all seasons. This positive association is in a very flat region, and as elevation increases in the ghats, the correlation reduces; it conveys that the association of rainfall with elevation is not linear. In the hilly and the DP region, the correlation has more local variability, which is interlinked to the topographic structure of the mountain. The topography of Western Ghats of India has three types of mountain ranges, namely, cascaded narrow mountains in Maharashtra (maximum width around 100 km), cascaded broad mountains in Karnataka (maximum width around 300km), and isolated mountain in Kerala (Tawde and Singh, 2015).

In Karnataka, due to the broad mountain structure, the rain shadow region is more. In contrast, in Kerala and Maharashtra, the width of the rain shadow

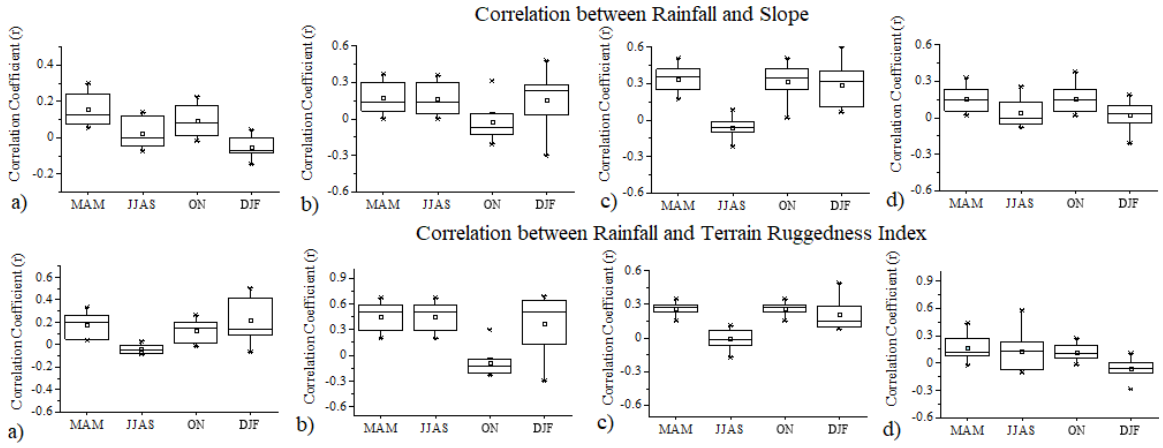

Fig. 4.4: Variation in 119 years correlation between rainfall, slope and TRI in a) CF b) SWH c) SEH d) DP

region is less due to narrower ranges. Therefore, it has more regions with a positive correlation. In the post-monsoon season, as the rainfall is due to North East wind, the SEH and DP region are directly exposed to rainfall; because of this, it shows a strong positive correlation with elevation. There is a positive correlation with elevation in the "Palghat Gap," which is the gap created due to the sudden dip between two elevated mountains; through this gap, the NE rainfall reaches the coast without any obstruction of mountains. The high correlation in mountainous peaks of Kerala explains its high dependency on elevation in winter seasons. In the pre-monsoon season, Maharashtra has more regions with a positive correlation than other regions.

4.3.2.2 Association between Rainfall and Slope of Mountain

Figure 4.4 shows the correlation between rainfall and the slope of the area. The correlation is positive in all four zones, with a mean correlation is near zero. Only in the monsoon season, SEH region has the least negative correlation. Figure 4.3 explains the local correlation in different seasons of the year. In the monsoon season, a negative correlation is observed in the CF and SWH region of Kerala and a positive correlation in the mountain region of Karnataka and Maharashtra. The mountain on the windward side of Karnataka has a gradually increasing slope

compared to the mountains in Maharashtra. In contrast, mountains in Kerala have a steep slope, which can be observed from the strong positive correlation between slope and rainfall over the mountain of Karnataka and the negative correlation in the mountain of Kerala. This gradually increasing slope raises the convective activity in the mountain region by providing a large surface area to the incoming solar radiation. The slope acts as a source of heat to produce convection cells, and the air parcel then converges at the top of the mountain. This fact is confirmed by De and Dutta (2005). A strong positive correlation is noted in the post-monsoon season in the leeward side of the mountain in Kerala and the hilly region of Karnataka and Kerala. In the winter season, a positive association is noted in the southern part of the study area and a negative association in the leeward side of the mountain range in Karnataka and Maharashtra. In the pre-monsoon strong negative correlation is in the CF and SWH region of Kerala; a positive association is noted in the CF and SWH of Karnataka and Maharashtra.

4.3.2.3 Association between Rainfall and Terrain Ruggedness Index

Terrain Ruggedness Index is a measure of terrain heterogeneity. It is the square root of the average of the square of eight elevation differences (Riley *et al.*, 1999). In the study area, the TRI value ranges from 1 to 1032.5. Based on the terrain heterogeneity obtained from TRI, according to Riley *et al.* (1999) the area has all types of terrains, namely, Level (0-80), Nearly Level (81-116), Slightly Rugged (117–161), Intermediately Rugged (162–239), Moderately Rugged (240–497), Highly Rugged (498–958), Extremely Rugged (959–4367). The mountain in Kerala is moderate to highly rugged compared to the mountains in the state of Karnataka and Maharashtra. There is a negative association with TRI and rainfall in the moderate to highly rugged terrain of Kerala and Maharashtra (Figure 4.5). The coastal zone of Kerala and Maharashtra state has nearly level terrain, which is then followed by the rugged mountain terrain. In contrast, the coast of Karnataka has intermediate rugged terrain starting from the coastline, and the ghats are intermediately rugged in the north of the state and moderately

rugged in the south of the state. Therefore the terrain relief of the mountain along with the distance from the moisture source may have a predictable influence on the distribution of rainfall in this area. There is a strong positive correlation in the northern part of the Karnataka state and in the SEH, DP region of Maharashtra state, where the mountain has intermediate ruggedness followed by the level terrain. In the post-monsoon season, the positive correlation is in the DP region of the mountain in the Kerala state. The winter rainfall has shown a positive correlation with the moderate to highly rugged mountain terrain and a negative correlation with the level terrain region. In the pre-monsoon season, the negative correlation is strong in the mountain of Kerala state and positive in the SEH and DP region in the Tamil Nadu state. Also, a positive correlation is observed in the CF and SWH of Maharashtra region.

4.3.2.4 Association between Rainfall and Relative Terrain Aspect

The topography of the mountain affects the wind velocity and direction rather than the altitude of the mountain. Relative Terrain Aspect accounts for the topographic exposure to wind, 0 degrees indicates the windward side, and 180 degrees shows the leeward side of the terrain to the defined wind direction. In the monsoon season (Figure 4.5), the wind circulation is from the southwest direction; the windward side of the mountains in Kerala and Karnataka are completely exposed to the wind flow, whereas the windward side of the mountain in Maharashtra has moderate exposure to the wind. In the leeward side of the ghats, the value of RTA is more than 120 degrees, which indicates the limited exposure of the mountain to southwest wind. The region is having a correlation variation between -0.6 to 0.6 in the majority of the regions. For the north-east monsoon wind, the windward side of the Kerala and Karnataka mountain have limited exposure to wind. In contrast, the Tamil Nadu state and southern Karnataka have strong wind exposure, followed by mountains in Maharashtra. There is a positive correlation in Tamil Nadu state and the southern part of Karnataka in post-monsoon seasons. In the winter and pre-monsoon season, the high-altitude regions have more exposure to

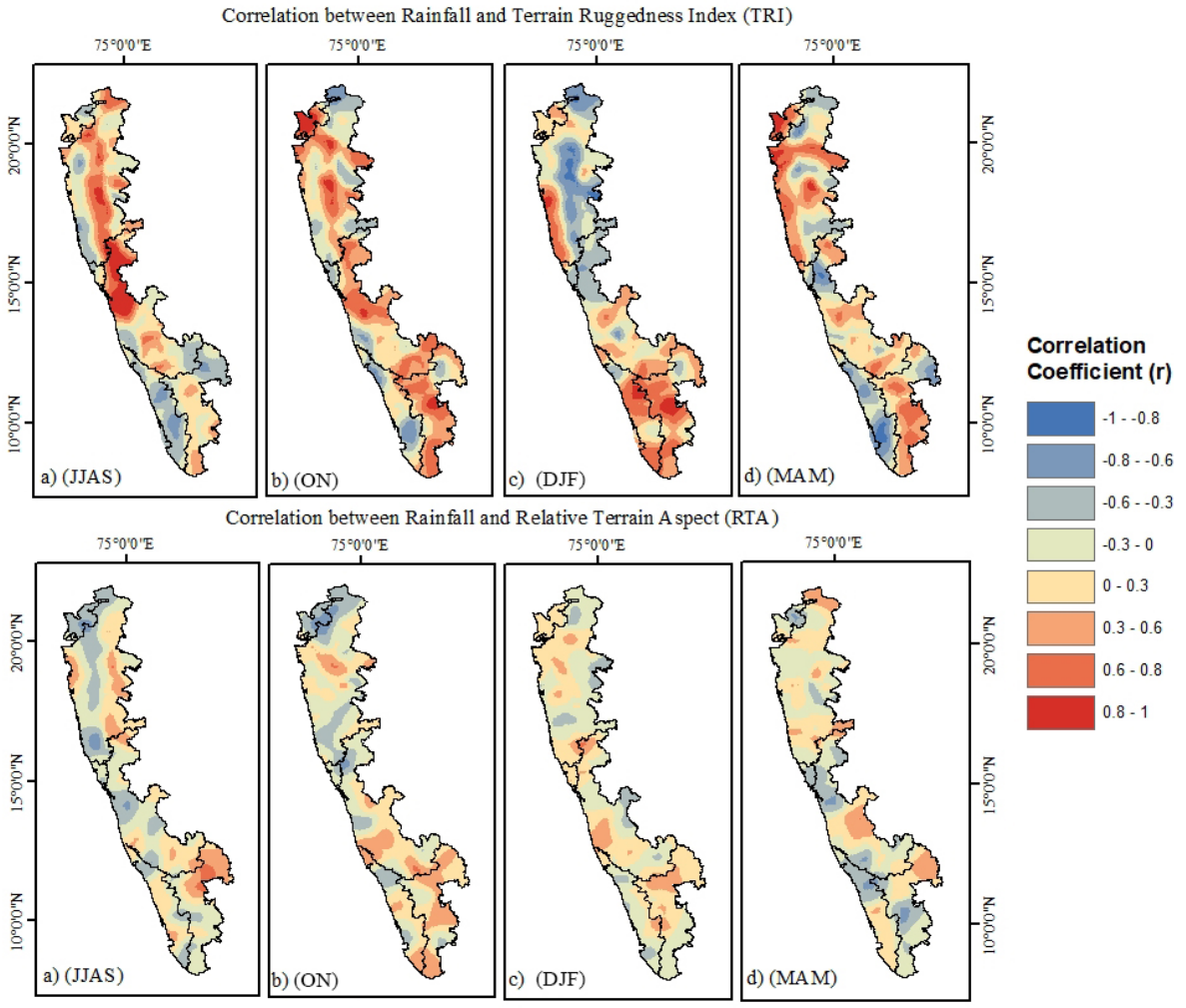

Fig. 4.5: Local correlation between rainfall, TRI and RTA

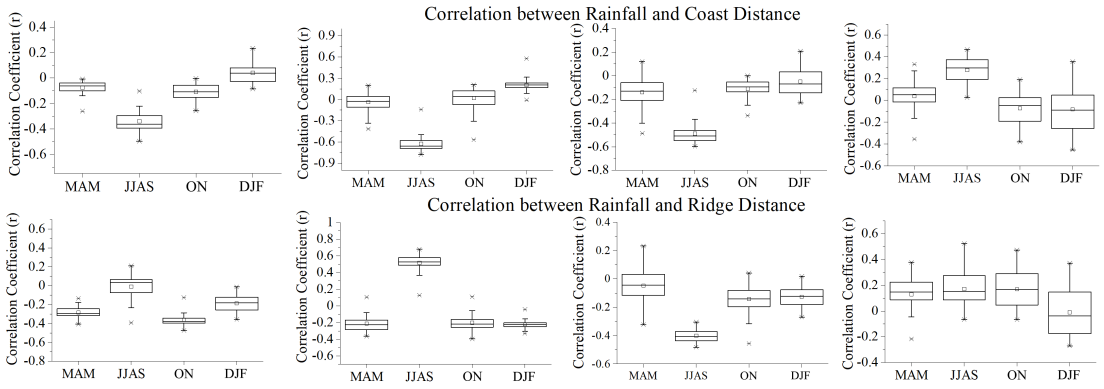

Fig. 4.6: Variation in 119 years correlation between Rainfall, Coast distance and Ridge distance in a) CF b) SWH c) SEH d) DP

the wind. In winter, the easterlies pass through the Palghat Gap to the coast side, and there is a positive correlation noted in this region and the southern Nilgiris peak. The negative correlation is in southern Tamil Nadu and positive in northern Tamil Nadu, and vice-versa is noted in Kerala. The positive correlation is in south Karnataka, where the terrain is more rugged.

4.3.2.5 Association between Rainfall Coast Distance and Ridge Distance

In zone-wise (Figure 4.6), there is no correlation between rainfall and Cd in any season except monsoon in the windward side of the mountain. The average rainfall is more near the coast than the mountain region on the windward side. Therefore, there is a negative correlation with the mean of 0.41 and 0.68 in the CF and SWH region in the monsoon. The association is positive in the winter season in both zones. When the mountain barriers obstruct the flow of moisture-carrying wind, the influence of ridge distance plays a pivotal role than the coast distance on the leeward side of the mountain. The SEH region also has a negative mean correlation of 0.55 in the monsoon season; this is due to the spill-out effect of rain, i.e., the impact of the ridge of the mountain on the moisture-carrying wind. In the DP region, the correlation with the coast distance is positive in the monsoon season and is negative in the post-monsoon seasons. The rainfall

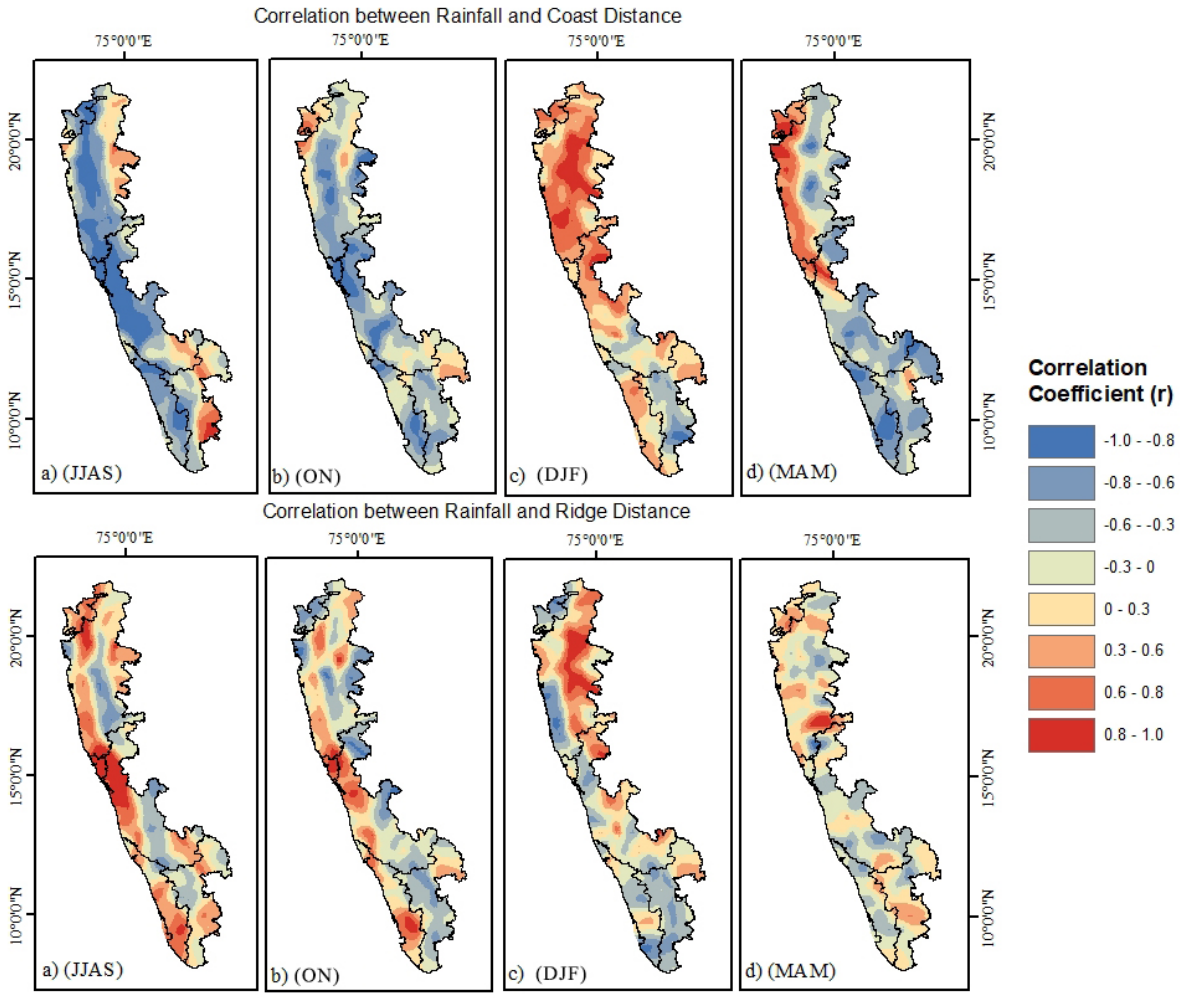

Fig. 4.7: Local correlation between rainfall, Coast Distance and Ridge distance

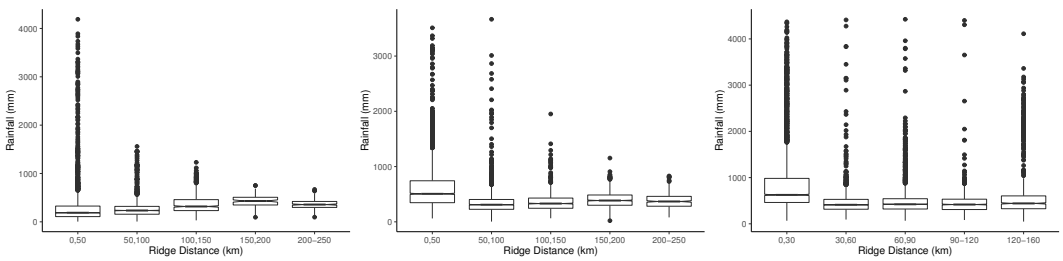

Fig. 4.8: Rainfall variation in the leeward side of the mountain with the ridge distance at 1) Isolated Mountain 2) Cascaded Broad Mountain 3) Cascaded Narrow Mountain

and distance from the ridge of the mountain have no correlation in the CF region and positive correlation in the SWH region in the monsoon season, and negative correlation in the windward side of the mountain in all the seasons. It represents that the monsoon rainfall is not high at the ridge of the mountain. In SEH negative correlation in monsoon is due to the effect of orographic rainfall (Figure 4.6).

At the local level (Figure 4.9), the negative correlation is more common at many locations, and the pattern is almost similar in monsoon, post-monsoon seasons. The DP region in Kerala, the southern part of Karnataka, and Maharashtra showed a positive correlation with the rainfall in post-monsoon seasons as the rainfall increases with the distance from the coast and ridge of the mountain. A high positive correlation is observed in the winter season; in the pre-monsoon season, the CF and SWH of Maharashtra has a positive correlation with Cd.

At the local level, monsoon and post-monsoon has a positive correlation on the windward side of the mountain, leeward side in the winter season, and has a high positive correlation in pre-monsoon in the Kerala region (Figure 4.9). At the peak of the mountain on the leeward side, the rainfall will be more due to the spillover effect, and after a certain distance from the ridge, the rainfall again increases as the rain-bearing wind accumulates moisture as the distance from the ridge increases. The spatial variation of rainfall in the leeward side of the mountain in three mountain ranges is shown in Figure 4.8. The higher rainfall in the leeward side of the mountain is due to the spillover effect; the effect is more on the broad mountain ranges than the isolated mountains of Kerala. In the isolated mountains, the rainfall increases gradually as soon as it passes the ridge of the mountain, Whereas in the broad mountain ranges, the rainfall intensity remains the same up to a distance of approximately 120 km from the mountain ridge, and after that, it increases gradually.

4.3.2.6 Association between Rainfall and Directional Relief

The peak of the mountain regions in the WG are strongly exposed to the summer monsoon winds, and the highly sheltered region is in Tamil Nadu state,

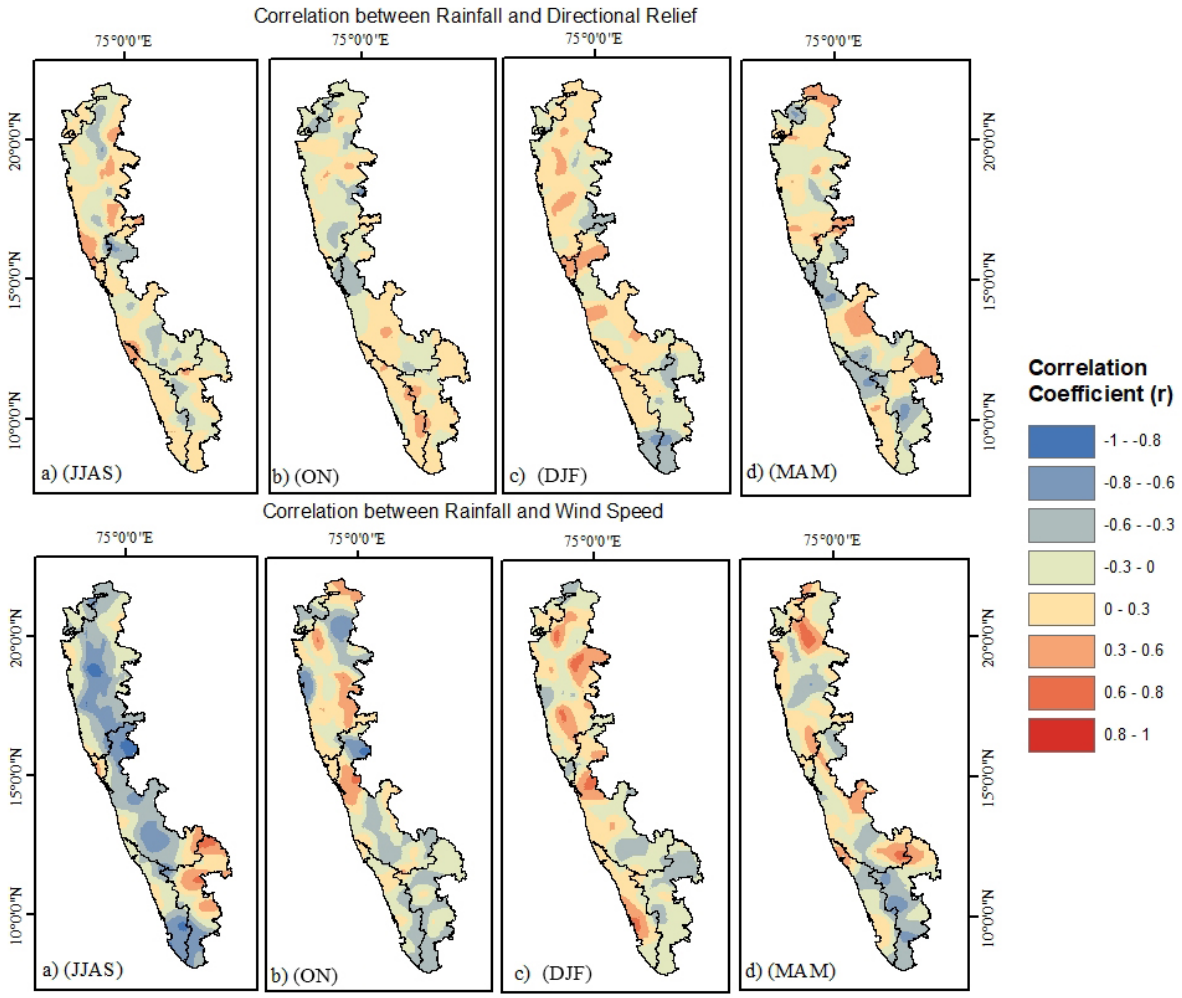

Fig. 4.9: Local correlation between rainfall, Directional Relief and Wind speed

where the isolated peaks in the southern part of the region have sheltered the mountain on the leeward side of the WG. The eastern side of the Nilgiri Mountain has a strong shelter effect to the monsoon winds. Therefore, a positive correlation between the DR and rainfall is noticed in the windward side of the WG in monsoon season, and a negative correlation of 0.57 is noted in the region with a strong sheltering effect. The positive correlation is in the DP region of Maharashtra state. In the post-monsoon season, the region of Tamil Nadu, which experienced shelter effect for monsoon wind, is strongly exposed to the post-monsoon winds. Therefore it has a positive correlation with rainfall. The correlation varies from -0.3 to 0.3 in most of the regions. In the other seasons, only the mountain peaks are strongly exposed to winds. The region at moderate heights below the mountain

peak has sheltering effect in Ghats in Karnataka, Goa, and Maharashtra, and the area surrounding isolated peaks. The southern region has shown a negative correlation with the DR as that is the region with comparable rainfall in the winter season, and most of the region has a positive correlation in the range of 0.23. In the pre-monsoon season, the rainfall has a positive correlation in the southern part of Kerala and a negative correlation in the northern part of Kerala and Karnataka state. A positive correlation is noted in the DP region of Karnataka and Tamil Nadu.

4.3.3 Association between the Rainfall, Wind Speed, NDVI and LST

4.3.3.1 Association between Rainfall and Wind Speed

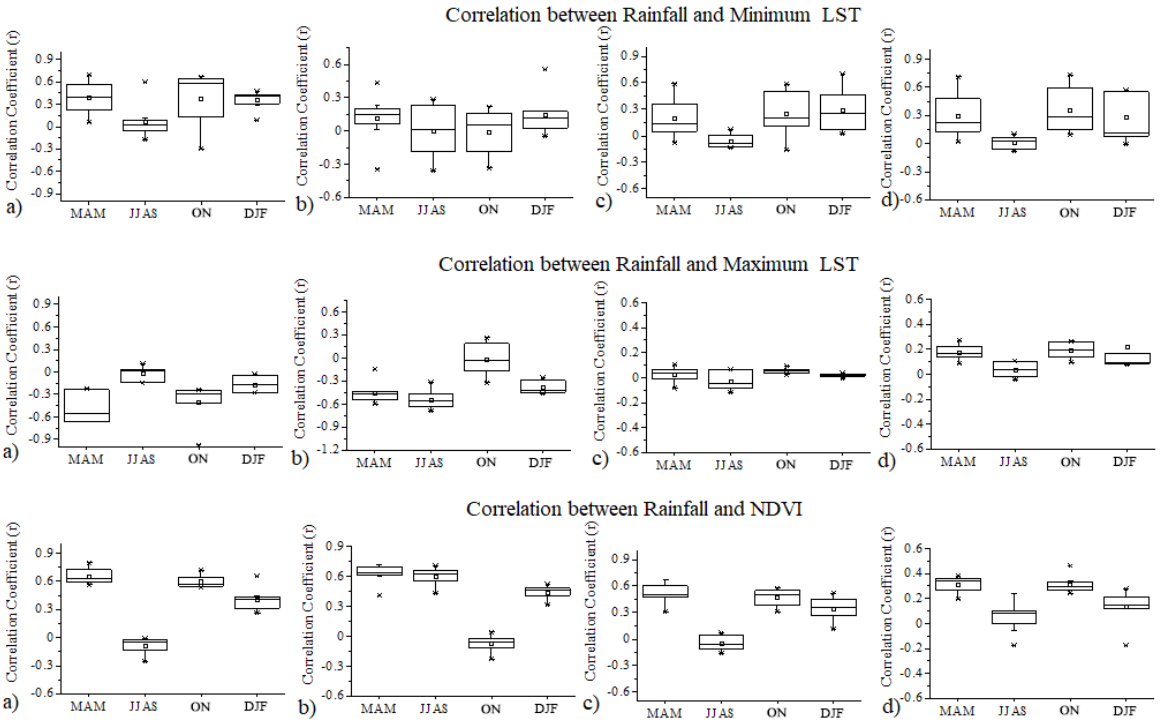

Fig. 4.10: Variation in 17 years correlation between rainfall, maximum and minimum LST and NDVI in a) CF b) SWH c) SEH d) DP

The rate of change in the wind speed varies with the local condition of the terrain, with significant changes in the roughest terrain. The vertical compression of the airflow over the mountain terrain accelerates the wind speed, whereas the

friction effect caused by the obstructions near the earth surface retards the wind speed. The exposed ridges and the isolated peaks experience higher wind speed due to the less frictional effect. The south-west monsoon reaches India through Kerala. The southernmost region has a wind velocity greater than 4 m/sec, and as it enters Kerala, the speed reduces to approximately 2 m/sec. The speed again increases gradually to more than 3 m/sec after crossing the mountain peaks in the broad and cascaded mountains of Karnataka and immediately increases to 4 m/sec in the isolated mountains of Kerala. In the monsoon season, the wind speed and rainfall have a negative association over most regions other than the southern part of Tamil Nadu and in the regions near the coast. The wind speed is lowest during the post-monsoon season than any other season. Except for the southernmost region of Kerala and Tamil Nadu, the wind speed is less than 2 m/sec in the other areas. The north-easterlies bring rainfall during this season; the negative association is in the southern region and positive correlation in the northern part of the study area. During the winter season, the average wind speed over the windward side is less than 2 m/sec, and on the DP and southernmost region is 2.5 m/sec. In the pre-monsoon season, the wind speed is high in the Maharashtra region. In the winter season, the north-easterlies coming through the Bay of Bengal try to cross over the WG near the southern part of Kerala, easterlies pass through the Palghat gap, and north-easterlies through the Arabian Sea gets diverted to the southern side, which then merges with the north easterlies. The variability in the wind speed is more during the pre-monsoon and winter season than during the monsoon and post-monsoon season. In the Tamil Nadu region, both the winter and pre-monsoon rainfall has a negative correlation with the rainfall. The more regions with positive correlation are noticed in the winter and pre-monsoon seasons.

4.3.3.2 Association between Rainfall and LST

The minimum LST and rainfall have a positive correlation in all the seasons in the CF, SEH, and DP region (Figure 4.10). But in the SWH region, though

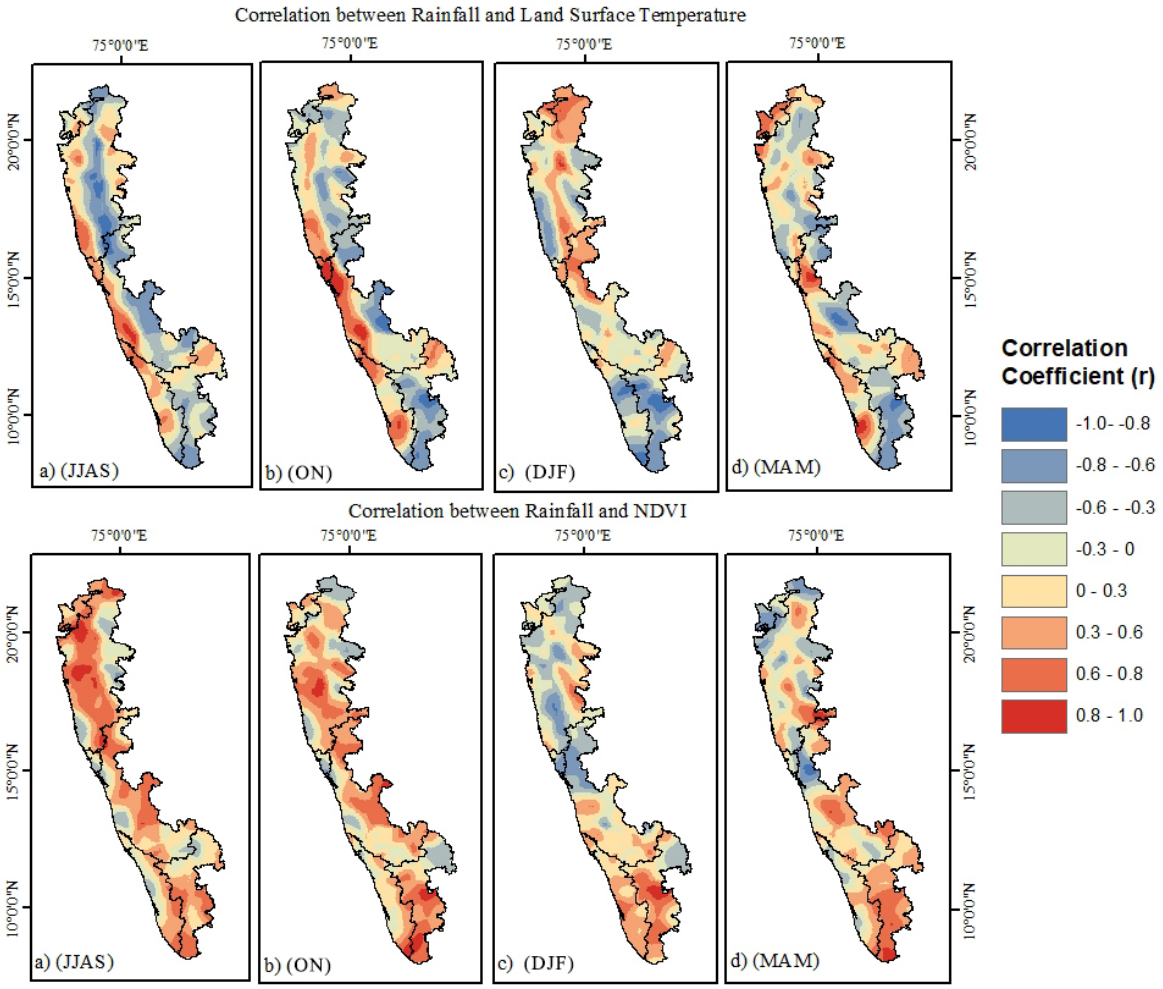

Fig. 4.11: Local correlation between rainfall, mean LST and NDVI

the mean correlation shows no correlation, there is a temporal variation in the correlation varying from -0.22 to 0.19 in pre-monsoon and -0.22 to 0.1 in monsoon seasons. The maximum temperature negatively correlates with rainfall in the CF and SWH region other than the monsoon season. The SEH region has no correlation between the maximum LST and rainfall in any season. Also, the same in the DP region. Figure 4.11 shows the spatial variation in the correlation between mean LST and rainfall. The positive correlation is prominent in the windward side of the mountain in monsoon and post-monsoon seasons. But the inverse correlation is observed in the southern peninsular in all the seasons because of the higher temperature in this region. In the densely vegetated ground, LST is the canopy surface temperature of the vegetation. Therefore, the ghat stretch

shows the least temperature in the study area. The SEH and DP region has a negative correlation between rainfall and LST. In the winter and pre-monsoon season, a negative correlation is more prevalent in the study area.

4.3.3.3 Association between Rainfall and NDVI

There is a positive correlation between rainfall and NDVI in all the zones in pre-monsoon, post-monsoon, and winter season; and, almost no correlation in the monsoon season (Figure 4.10). In the monsoon season, there is a negative correlation between rainfall and NDVI in the coastal region. This might be because of the fact that the vegetation cannot respond to the variation in rainfall as swiftly as the rainfall varies. Also, the rainfall exceeding certain values will adversely affect vegetation growth. Similar results have been reported in Nischitha *et al.* (2014). Revadekar and Preethi (2012) also noted that the NDVI shows an inverse relationship with rainfall during high-intensity rain events. In the coastal belt of Maharashtra and Karnataka, the heavy (64.4 mm $<$ R $\leq$ 124.4 mm) to very heavy rainfall (124.4mm $<$ R $\leq$ 224.4 mm) is frequent during southwest monsoon. The SWH region exhibits the maximum amount of greenness due to the dense humid forest cover. Beyond about 16°N, the dry season is too long for the growth of evergreen forests except in the moist pockets on the hills. This can be visualized in the winter and pre-monsoon season correlations between rainfall and NDVI; beyond 16°N, the negative correlation is more prominent. The post-monsoon greenness is owing to the favourable soil moisture conditions, as the soil stores adequate water from the rainfall throughout the southwest monsoon season. Additionally, other external elements, such as solar radiation, temperature, and wind driven pressure affects the growth and development of the plants and trigger a high amount of greenness during the post-monsoon season (Larcher, 2003). The correlation is always positive in the southernmost region of the study area.

The Figure 4.12 and 4.13 denotes the strength of linear association between rainfall and above explained independent variables. The higher the coefficient of Determination indicates a better understanding of the variables responsible for

the variation in the dependent variable. The standard error and RMSE obtained is more in the monsoon season, than in the other seasons. The maximum error is recorded in the region where the spatial variation in the rainfall is high. The coefficient of determination explains the remarkable performance of the model under all the seasons.

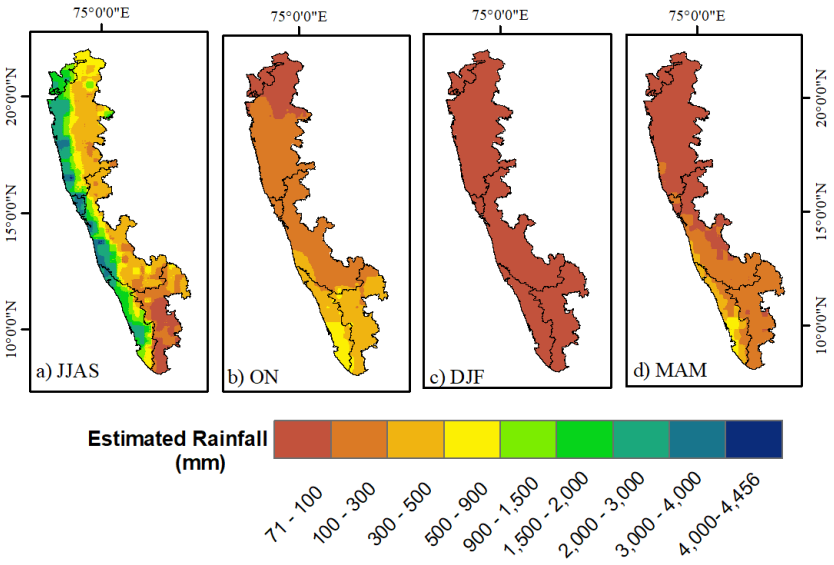

Fig. 4.12: The estimated mean rainfall by GWR model

4.3.4 Role of Mountain Topography on the distribution of Mountain and the Rainfall

The combination of topography and orography can swiftly alter the geographical distribution of precipitation by changing the atmospheric wind circulation pattern . Higher the mountain width provides higher advection time for the moist flow to grow and trigger before crossing the ridge of the mountain (Elliott and Hovind, 1964; Tawde and Singh, 2015). In the mountain forest of Western Ghats, the maximum orographic rainfall occurs at a distance of 50km away from the peak of topographical barriers (Das, 1962; Srinivasan *et al.*, 1972; Tawde and Singh, 2015). This can be observed from Figure 4.14, this may be because falling particles get sufficient depth to grow by collision and coalescence at the foot of the mountain than at the top of the mountain. In the isolated mountain range of Kerala, the

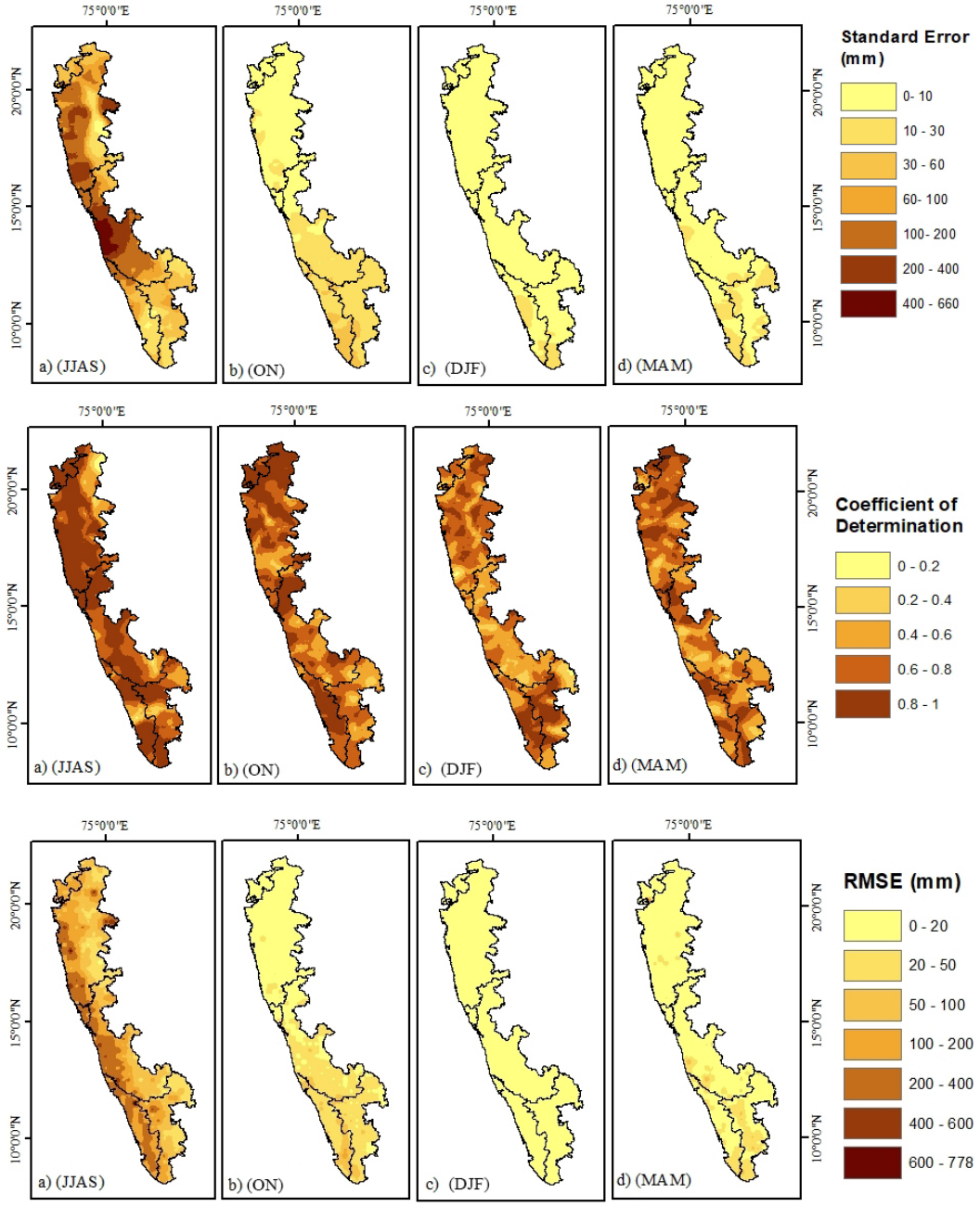

Fig. 4.13: The performance measure of model in terms of Standard Estimation error(top), Coefficient of Determination (middle), and Root Mean Square Error (bottom)

average rainfall on the coast is around 2850 mm. On the windward side, the rainfall is maximum at an elevation of 500-800 m, then an increase in elevation decreases the rainfall up to a height of 1200 m. The moist bearing winds can cross over the mountain through the gaps in the isolated mountains without the

complete triggering of rainfall. Therefore the rainfall rises again after the elevation of 1200 m on the windward side (Figure 4.15). The Cascaded Broad Mountain ranges of Karnataka cater more rainfall near the coast and windward side of the mountain than other mountain ranges. The coastal range receives mean rainfall of 3700 mm; after that, rainfall decreases up to a height of 500 m, and then further increase in elevation; rainfall increases with the highest rainfall in the mountain in the elevation range of around 800-1000 m. The narrow-width mountain ranges of Maharashtra do not provide sufficient advection time for the moist flow to trigger completely. Therefore it allows part of the moist flow to cross over to the leeward side. The coastal range of Maharashtra receives mean rainfall of 3000 mm; after that, rainfall decreases gradually up to a height of 800 m, and then further increase in elevation; rainfall increases with the highest rainfall in the mountain in the elevation range of 800-1000 m. Therefore the control enforced by the elevation of the mountain is limited to a confined to a height. Tawde and Singh (2015) observed that the intense rainfall due to the orography of the WG is confined till the height of 800 m, which may be due to the weak wind speed or presence of temperature

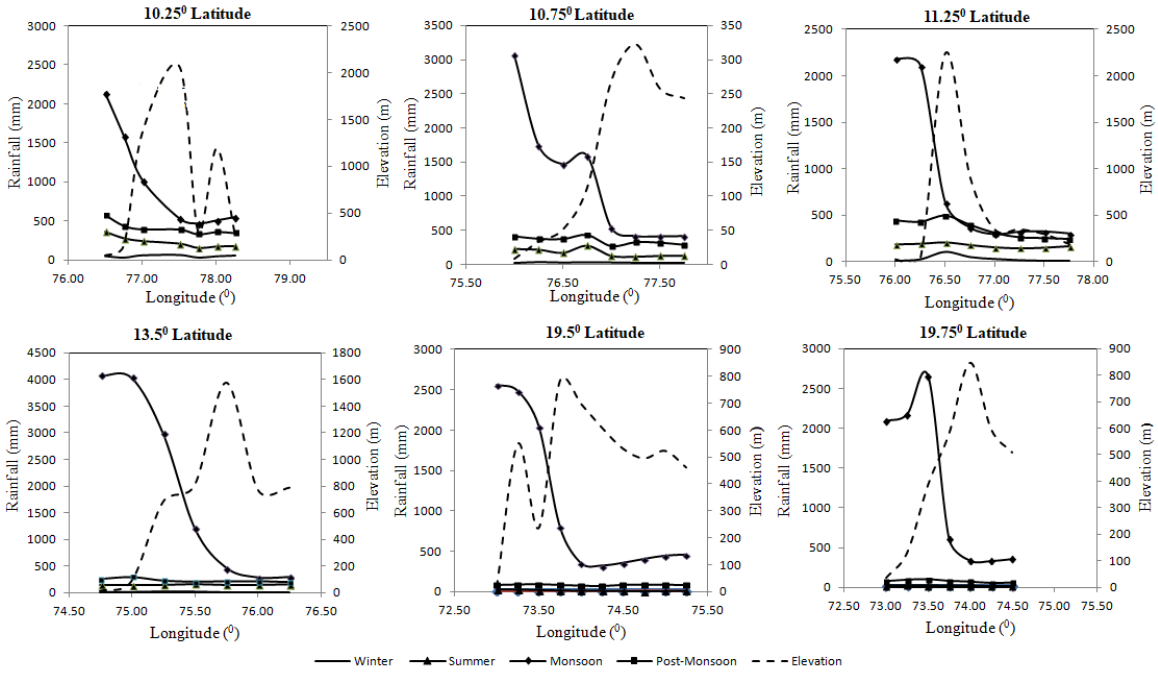

Fig. 4.14: Rainfall variation with elevation at various cross sections of mountain

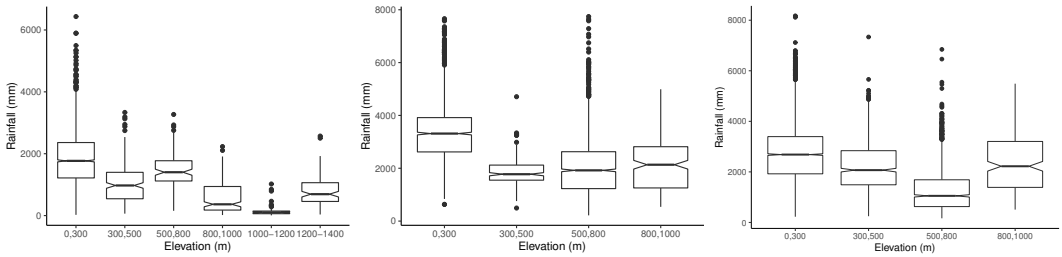

Fig. 4.15: Rainfall variation with elevation at 1) Isolated Mountain 2) Cascaded Broad Mountain 3) Cascaded Narrow Mountain

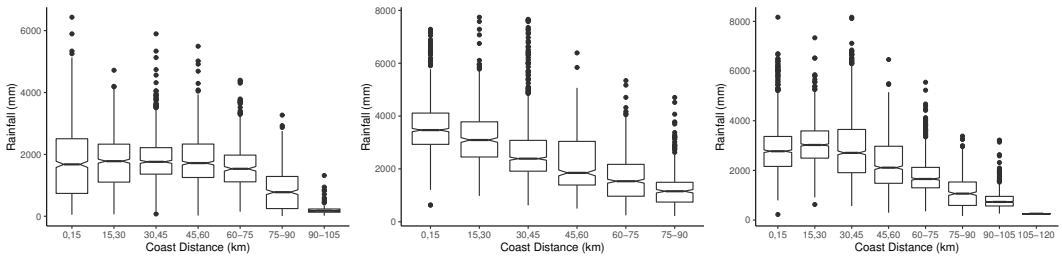

Fig. 4.16: Rainfall variation with coast distance at 1) Isolated Mountain 2) Cascaded Broad Mountain 3) Cascaded Narrow Mountain

inversion layer. Raman *et al.* (1990); Alapaty *et al.* (1994) also found a temperature inversion layer at this height over the AS. The study by Sam *et al.* (2007) observed the coastal atmospheric boundary layer height variation between 700 m to 1,100 m when an off-shore trough was created due to the blocking of currents by the WG. This difference could be due to the complex nature of the land-sea breeze interactions with the topography of the WG mountains. Pant (1978) observed the difference in boundary layer height in the region 10° N from that observed to the south. The effect of the topographic structure of the mountain and its ruggedness is more prominently observed in the present study based on the difference in the maximum rainfall received over the three mountain topographies. The terrain ruggedness is one of the key factors influencing the flow of moist carrying winds in the monsoon seasons. Figure 4.16 highlights the influence of terrain ruggedness along with the distance from the coast. Kerala and Maharashtra, which have isolated to narrow mountain ranges and have level terrain near the coast, receive a maximum rainfall at a distance of 15-30 km, and in Karnataka, where the coastline

starts with intermediate rugged terrain with broad mountain structure, receives maximum rainfall near to the coast. The division of the mountain based on the topographic structure indicates its potential on the distribution of rainfall in the WG of India.

4.4 CONCLUSIONS

The dependability of the rainfall with the topography of the mountain, climate variables are assessed based on the Geographically weighted regression approach. The spatio-temporal variability in the rainfall and the topo-climatic variables over the WG represents the realistic distribution of rainfall. The each variable has varying association with the rainfall, due to the highly complex terrain and local climatic regime of the Ghat. The zonation of the complex mountain is essential in the assessment of climate variability in the WG mountains. The temporal variation in the association of rainfall with the topo-climatic variables over eleven decades does not signify any vigilant changes in rainfall variation over the decades. In the WG, the topographic structure of the mountain in the southern, central and northern portion of the Ghat has a substantial impact on the spatial variability of the rainfall. Here, the effect of the terrain is amplified in the broad, gradually sloping intermediate rough mountain located in close proximity to the coast. The maximum amount of rainfall is contingent upon the steepness of a mountain's windward side and the topographic structure resulting in the difference in the elevation of maximum rainfall occurrence. The topographical variables solely can be used as an influential predictor of rainfall in the Western Ghats of India.

Based on this study, the two river basins located in southern (isolated mountains), central (cascaded broad mountain) and northern part (cascaded narrow mountain) of the WG, representing the diverse climate is considered. To gain insight into the potential fluctuations in precipitation and temperature patterns in the future, this study assesses the efficacy of uncertainty reduction approaches employed in General Circulation Models (GCMs) to enhance the accuracy of future climate projections.

CHAPTER 5

RANKING OF GCM MODELS AND ENSEMBLE BY ADVANCED ML-BASED TECHNIQUES

5.1 BACKGROUND

The competency of GCMs at the local scale can be improved through the careful selection of GCMs (Raju and Kumar, 2015) and the usage of ensembles of multiple models from a pool of GCMs boost confidence in future climate projections (Zhao *et al.*, 2020). Such analyses play a significant role in developing effective adaptation and mitigation strategies against the risks and effects of climate change. The multi-model ensemble methods have advanced from simple arithmetic mean to complex machine learning-based approaches. The versatility of machine learning, its capacity to investigate non-linearity, handle high dimensionality, and capture hierarchical complex interactions between predictors and the response variable, have contributed to its increased popularity relative to other methodologies(Acharya *et al.*, 2014; Shortridge *et al.*, 2016; Crawford *et al.*, 2019; Ahmed *et al.*, 2020). Therefore, the performance of the CMIP6 GCMs in simulating rainfall and temperature. Additionally, the effectiveness of ML-based Multi-Model Ensembles (MMEs) in enhancing the simulation quality across various geo-climatic basins is examined.

5.2 METHODOLOGY

The daily rainfall, maximum temperature, and minimum temperature of the 13 GCM models of CMIP6 are bias-corrected using Empirical Quantile Mapping (EQM) for South Asia (Mishra *et al.*, 2020). The data set comprises projections for the four scenarios (SSP126, SSP245, SSP370, SSP585) for the historical (1951-2014) and projected (2015-2100) time periods and is available at a spatial resolution of $0.25^{o} \times 0.25^{o}$. The technical validation of this bias-corrected data set

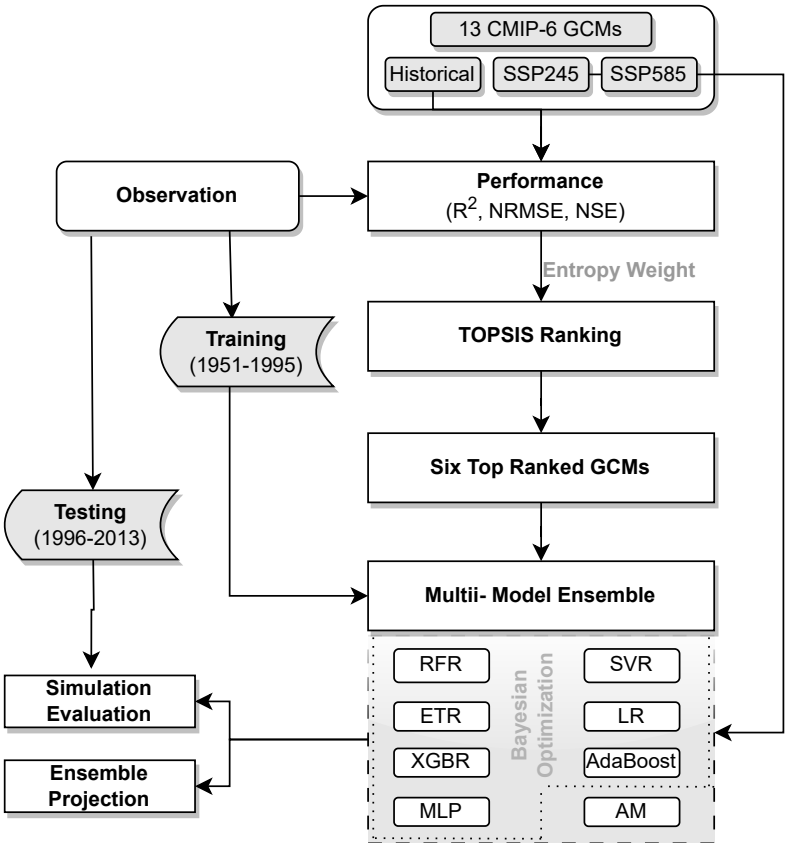

Fig. 5.1: Diagram illustrating the multi-model ensemble simulation design and implementation method

against the observations for mean and intense rainfall events, as well as maximum and minimum temperatures over India, has been carried out (Mishra *et al.*, 2020). For the six river basins, the performance of each individual model is evaluated using periods 1951–1995 as the training period and 1996–2013 as the testing period for validation with the observed rainfall and temperature of the historic period. It is anticipated that the GCMs with the best performance in the historical period will continue to do so in the future (Maxino *et al.*, 2008). The Coefficient of determination (R^2), Normalized Root Means Square Error (NRMSE) and Nash-Sutcliffe Efficiency (NSE) metrics are calculated for the rainfall, mean maximum, and minimum temperature. To select the best-performing GCMs over the basins, the Technique for Order Preference by Similarity to an Ideal Solution (TOPSIS), a multiple-criteria decision-making technique (MCDM), is used. Hwang *et al.* (1981) proposed the TOPSIS approach for ranking alternatives according to the

distance from the ideal and anti-ideal solutions. For the R^2, NRMSE and NSE metrics obtained for each model are weighted based on the entropy method, and the GCMs are assigned with the ranks. Half of the highest-performing GCMs are optimal for a multi-model ensemble (Ahmed *et al.*, 2020). In each basin, the six top-ranked GCMs are selected to form an ensemble. The rainfall, maximum temperature, and minimum temperature of six GCM models are ensembled using the eight multi-model ensemble techniques: simple Arithmetic Mean (AM), machine learning-based Random Forest Regressor (RFR), Support Vector Machine (SVM), Multiple Linear Regression (LR), Adaptive Boosting Regressor (AdaBoost), eXtreme Gradient Boosting Regressor (XGBR), Extra Tree Regressor (ETR) and Multilayer Perceptron neural network (MLP). All the algorithms are implemented in Python using the "sci-kit-learn library" module. To achieve optimal performance, most of the ML algorithm's hyperparameter needs to be tuned. In this study, the Bayesian Optimization method is chosen to tune the hyperparameters. In Bayesian Optimization, Bayesian inference is employed to obtain the distribution of the unknown function based on the prior and sample information (Wu *et al.*, 2019*a*). The search for optimal value is more effective here than with grid search or random search, and the time investment is under control (Du *et al.*, 2022). The performance of MME is verified at the basin level, and the comparison of each ensembling method is carried out using the aforementioned indicators. The schematic representation of the methodology followed is shown in Figure 5.1. The details of the performance metrics employed are described in Sreelatha and Anand Raj (2021). The MME, which obtains the best performance with the observed data, is used to analyse the variation in rainfall, the maximum and minimum temperature in the scenarios SSP245 and SSP585, the former represent moderate challenges for mitigation and adaptation, and the latter represents the extreme scenarios which have a high challenge for mitigation and low for adaptations. The ML MME methods are discussed below.

Random Forest: Random Forest is an ensemble machine learning technique based on the unification of decision trees and statistical learning theory, proposed

by Breiman (Breiman, 2001). RF constructs many independent trees and makes a judegment based on randomization and non-parametric statistical regression (Xu *et al.*, 2019). Multiple classification and regression decision trees (CART) manage input variable types and prevent over-fitting. The decision tree constitutes a root node, sub-node, and leaf node, where the sub-node holds the judgement rule, and the leaf node represents the judgement level. To create a single decision tree, m number of samples are randomly chosen by bagging (bootstrap aggregating), and m number of variables are then randomly chosen at each node as candidates for splitting the node (Xu *et al.*, 2020). To produce a mass regression decision tree, these stages are repeated. The ultimate prediction outcome of the model is the mean of the mass regression decision tree predictions. The most common RF hyperparameters that require tuning are the max depth (the maximum depth of the tree beyond which it is pruned), max features, which is the best feature among the randomly selected maximum feature by each tree, min samples split denotes the least number of samples to split tree nodes, min samples leaf is the least number of samples required at a leaf node, and n estimators is a number of trees in the forest. A detailed description of the model and the parameters can be found from Yin and Li (2022).

Extra Tree Regressor (ETR): ETR is an extension of RF that adds a further level of randomness to the splitting of the trees. ETR trains each tree by utilizing all training data without bootstrapping and randomly selecting a cut point at each node of the decision tree to prevent overfitting Xu *et al.* (2020). Out of the collection of randomly generated splits, the split that yields the highest score is chosen. The parameters n estimators, min samples split, min samples leaf, max features, max depth, and minimum impurity decrease (If the reduction in impurity caused by the split is more than or equal to this value, the node will be split) are optimized for each basin.

Support Vector Machine (SVM): The SVM, a widely used method for classification and regression problems, was introduced by Vapnik in 1998 (Cortes and Vapnik, 1995). Support Vector Regression (SVR) is the SVM that exemplifies the

Table 5.1: Hyper-parameters after Bayesian Optimization for MME of Precipitation

Hyper-parameters (min,max)	Vamanapuram	Chaliyar	Netravati	Aghanashini	Ulhas	Purna
			RFR			
n estimators (100,2000)	1200	1200	1400	1400	1400	1200
Min samples split (1,50)	5	5	5	2	5	5
Min sample leaf (1,50)	2	2	1	2	2	2
Max features	SQRT	SQRT	SQRT	SQRT	SQRT	SQRT
Max depth (1,50)	10	10	10	10	10	10
Bootstrap	TRUE	TRUE	TRUE	TRUE	TRUE	TRUE
			SVR			
C (1,50)	10	100	10	10	10	100
Gamma (0,1)	0.1	0.001	0.001	0.001	0.1	0.01
			AdaBoost			
Learning rate (0,1)	1	1	1	1	1	1
n estimators (100,2000)	1600	2000	600	1000	800	600
n splits	10	10	10	10	10	10
			ETR			
n estimators (100,2000)	250	250	350	450	450	350
Min samples split (1,20)	2	3	2	2	3	2
Min sample leaf (1,20)	10	10	10	10	10	10
Min impurity decrease (0,1)	0.001	0.01	0.01	0.01	0.01	0.01
Max features	0.95	0.95	0.95	0.95	0.95	0.95
Max depth (1,20)	10	10	8	9	8	8
			XGBR			
Learning rate (0,1)	0.01	0.01	0.01	0.01	1	1
n estimators (100,1000)	200	450	300	400	450	200
Min child weight (1,20)	10	12	8	12	12	14
Max depth (1,25)	20	20	6	12	4	10
Subsample (0.3,1)	0.6	0.5	0.5	0.5	0.7	0.5
Colsample bytree (0.3,1)	0.9	0.3	0.3	0.6	0.5	0.6
Gamma (0,1)	0.2	0.1	0.4	0.3	0	0.4
			MLP			
Activation	Tanh	Tanh	ReLU	Tanh	ReLU	ReLU
Solver	Sigmoid	Sigmoid	Sigmoid	Sigmoid	Adam	Adam
Max iteration	2000	2000	2000	2000	2000	2000
Learning rate	Constant	Constant	Adaptive	Adaptive	Adaptive	Adaptive
Hidden layer	(50,100,50)	(50,100,50)	(100,)	(50,50,50)	(100,)	(50,100,50)
Alpha	0.05	0.05	0.05	0.05	0.05	0.05

nonlinear regression problems by employing kernel functions to transform data from a low-dimensional to a high-dimensional feature space. The advantage of SVR is that its computational complexity is unaffected by the dimension of the input space. Furthermore, it has a strong generalization capacity and great prediction accuracy (Awad and Khanna, 2015). The regularisation parameter (C) and the kernel parameter (γ) are two SVM parameters that must be chosen carefully for the optimal performance of the model. More details about SVR can be obtained from Cho and Hoang (2017).

$$f(x) = \sum_{i=1}^{n} (\alpha_i - \alpha_i^*) \, k(x, x_i) + b \tag{5.1}$$

where k(x,x_i) denotes the kernel function, x_i is a vector, x is the independent vector, α_i and α_i* are the Lagrange multipliers, b represents the bias parameter.

Multiple Linear Regression (MLR): Linear regression explains the relationship between the dependent variable and independent variables. It is a common regression analysis method widely utilized for impact assessments and down-scaling in climate studies. In this study, it is further referred to as LR.

$$y = \beta_0 + \beta_1 x_1 + \beta_2 x_{2+.....} + \beta_n x_n + \varepsilon \tag{5.2}$$

where y, x_i represents the dependent and independent variables, β_i are parameters, ε is the error

Adaptive Boosting (AdaBoost): AdaBoost is an iterative augmented regression algorithm. It creates a series of weak classifiers using a single feature as a weak learning algorithm by performing numerous iterations on the same training sample set. The classification effect determines weights, which are used to combine classifiers to generate a strong classifier (Freund and Schapire, 1997). Adjusting the max depth of the base classifier, the learning rate (lr), which establishes the degree to which newly obtained knowledge will supersede previously acquired information, and the number of estimators (number of trees) are the primary tuning knobs in the optimization of the model (Ahmad *et al.*, 2022).

eXtreme Gradient Boosting (XGBoost): The gradient boosting method created by (Chen and Guestrin, 2016) serves as the foundation for the sophisticated machine learning technique known as eXtreme Gradient Boosting (XGBoost). The goal of the XGBoost algorithm is to minimize the objective function, which consists of a loss function and regularisation term. In contrast to traditional trees, which only use first-order derivatives, XGBoost regression (XGBR) innovated by introducing second-order derivatives and regular terms, making the technique effective for training and quick to process. This algorithm uses an ensemble of regression trees and updates the learner based on the previous tree. Through

Table 5.2: Hyper-parameters after Bayesian Optimization for MME of Maximum and Minimum Temperature

Hyper-parameters	Vamanapuram		Chaliyar		Netravati		Aghanashini		Ulhas		Purna	
(min, max)	Tmax	Tmin	Tmax	Tmin	Tmax	Tmin	Tmax	Tmin	Tmax	Tmin	Tmax	Tmin
					RFR							
n estimators (100,2000)	400	1600	1000	1200	2000	1200	400	1400	600	2000	1000	1600
Min samples split (1,50)	2	5	5	5	5	5	10	2	5	5	5	5
Min sample leaf (1,50)	4	2	2	2	1	2	1	1	2	1	4	2
Max features	SQRT	SQRT	SQRT	SQRT	SQRT	SQRT	SQRT	SQRT	SQRT	SQRT	SQRT	SQRT
Max depth (1,50)	10	10	10	10	10	10	10	10	10	10	10	10
Bootstrap	TRUE	TRUE	TRUE	TRUE	TRUE	TRUE	TRUE	TRUE	TRUE	TRUE	TRUE	TRUE
					SVR							
C (0,10)	1	0.1	1	0.1	1	0.1	0.1	0.1	1	1	1	1
Gamma (0,1)	0.002	0.01	0.01	0.01	0.01	0.01	0.01	0.01	0.01	0.001	0.01	0.001
					AdaBoost							
Learning rate (0,1)	0.0001	0.001	0.001	0.001	0.001	0.001	0.001	0.001	0.001	0.1	0.001	0.01
n estimators (100,2000)	200	400	1600	600	400	400	1600	600	600	1000	400	800
					ETR							
n estimators (100,2000)	250	1200	100	500	250	500	500	1200	250	1600	250	600
Min samples split (1,20)	2	7	6	7	2	7	7	7	2	3	6	3
Min sample leaf (1,20)	6	2	10	2	6	2	2	2	10	4	10	4
Min impurity decrease (0,1)	0	0	$1\times e^{-05}$	$1\times e^{-05}$	0	$1\times e^{-05}$	$1\times e^{-05}$	$1\times e^{-05}$	0	0.0001	0	$1\times e^{-05}$
Max depth (1,20)	9	9	10	9	9	9	9	9	10	10	10	10
					XGBR							
Learning rate (0,1)	1	0.1	1	0.1	0.1	1	0.001	0.001	0.0001	1	0.01	1
n estimators (100,1000)	150	200	450	250	250	500	200	100	250	100	50	100
Min child weight (1,20)	10	16	12	16	16	6	4	2	12	10	8	10
Max depth (1,25)	6	12	4	12	2	20	4	20	2	22	12	22
Subsample (0.3,1)	0.4	0.9	0.7	0.7	0.4	0.5	0.9	0.5	0.6	0.3	0.7	0.3
Colsample bytree (0.3,1)	0.4	0.8	0.5	0.9	0.3	0.7	0.4	0.4	0.7	0.6	0.5	0.6
Gamma (0,1)	0	0.01	0.1	0.3	0.4	0.1	0.2	0	0.2	0.3	0.1	0.3
					MLP							
Activation	ReLU	Tanh	ReLU	Tanh	Tanh	ReLU	Relu	ReLU	Relu	Tanh	ReLU	ReLU
Solver	Adam	Adam	Adam	Adam	Sigmoid	Sigmoid	Adam	Sigmoid	Adam	Adam	Adam	Adam
Max iteration	2000	2000	2000	2000	2000	2000	2000	2000	2000	2000	2000	2000
Learning rate	A	C	A	C	C	C	C	C	A	A	C	C
Hidden layer	(50,100,50)	(100,)	(100,)	(100,)	(50,50,50)	(50,100,50)	(100,)	(50,100,50)	(100,)	(50,50,50)	(50,100,50)	(100,)
Alpha	0.05	0.05	0.05	0.05	0.05	0.05	0.05	0.05	0.05	0.05	0.05	0.05

Note : A-Adaptive, C-Constant

model formalization, XGBoost is better able to manage over-fitting (Yu *et al.*, 2020). General, booster, and learning parameters make up the three categories of parameters in the XGBR model. The min child weight (determines the weight of the minimum leaf nodes), max depth, subsample (regulates the distribution of the

random samples of each tree), colsample bytree (control the number of randomly selected columns per tree), gamma (marks the point at which the minimum loss function suffers a reduction in value), and lambda (regular term) are the most crucial booster parameters (Yin and Li, 2022).

Table 5.3: TOPSIS ranking of CMIP6 GCMs for Precipitation

Models	River Basins					
	Vamanapuram	Chaliyar	Netravati	Aghanashini	Ulhas	Purna
ACCESS-ESM1-5	13	11	11	12	11	9
ACCESS-CM2	12	9	7	8	7	10
BCC-CSM2-MR	2	1	1	1	1	1
CanESM5	11	10	8	9	8	12
EC-Earth3	1	5	6	7	6	11
EC-Earth3-Veg	4	6	5	5	5	8
INM-CM4-8	7	13	13	13	13	6
INM-CM5-0	6	12	12	11	12	5
MPI-ESM1-2-HR	5	7	9	6	9	4
MPI-ESM1-2-LR	8	4	4	4	4	3
MRI-ESM2-0	10	8	10	10	10	13
NorESM2-LM	3	2	2	2	2	2
NorESM2-MM	9	3	3	3	3	7

Multilayer Perceptron neural network (MLP): Multiple ANN variants have been developed and effectively implemented in different fields. The association between predictands and predictors in hydro-climatological investigations has been actively determined using a series of ANN-based algorithms (Coulibaly *et al.*, 2005; Ahmed *et al.*, 2015, 2020). Among the series of ANN methods, a MLP is a non-parametric, versatile, and the simplest ANN approach. MLPs have an input layer, a hidden layer (or several hidden layers), and an output layer. MLP inputs come from the input layer (predictor data). The hidden layer uses an activation function to blend weights and bias terms with inputs to generate output. A numerical representation of an MLP with n number of inputs in an input layer ($x = x_1,x_2,..x_n$) and a vector of weights ($w_j=w_{1j},w_{2j},..w_{nj}$) at node j is used to calculate the simulated value y_j at node j is

$$y_j = f(x.w_j - b_j) \tag{5.3}$$

Where, the activation function is denoted by f(), the weight vector is denoted by w_j, and the bias associated with node j is denoted by b_j. The rectified linear activation function (relu) is used in MLP in the present study. Further details on ANN can be found in Haykin and Network (2004).

$$y_k = f_2 \left[\sum_{i=1}^{m} w_{\mathrm{ki}} f_1 \left(\sum_{j=1}^{n} w_{\mathrm{ij}} x_j + b_i \right) + b_k \right] \tag{5.4}$$

Where f_1 and f_2 are the activation functions, i is the hidden layer, j is the input layer, and k refers to the output layer,x_j refers to the inputs to the network, b_i and b_k denotes the bias associated with hidden and output layers, respectively, n and m denote the neurons in the input, and hidden layers, w_{ij} represents the weights between input and w_{ki} hidden layers and represents the weights between hidden and output layers, and y_k is the simulated output of the network. Hereafter, the ANN MLP algorithm used in this study is referred to as MLP. The network structure, activation function for the hidden layer, solver (weight optimization function), and hidden layers indicate the neurons number in the hidden layer, maximum iteration, and learning rate are tuned. More information can be obtained from (Isabona *et al.*, 2022).

5.3 RESULTS AND DISCUSSION

The performances of eight MMEs and the thirteen individual models are evaluated at the six river basins. The ensembled rainfall, maximum temperature, and minimum temperature are evaluated against the measured data of the river basins. The NRMSE, Coefficient of Determination, and NSE are used to assess the performance of the models.

Table 5.4: TOPSIS ranking of CMIP6 GCMs for Maximum and Minimum Temperature

Models	River Basins											
	Vamanapuram		Chaliyar		Netravati		Aghanashini		Ulhas		Purna	
	Tmax	Tmin	Tmax	Tmin	Tmax	Tmin	Tmax	Tmin	Tmax	Tmin	Tmax	Tmin
ACCESS-ESM1-5	10	9	5	4	6	10	8	10	12	10	9	2
ACCESS-CM2	13	10	12	9	9	5	9	8	11	5	10	4
BCC-CSM2-MR	12	7	11	10	5	8	5	6	2	8	8	5
CanESM5	11	11	6	6	10	3	12	5	5	3	11	10
EC-Earth3	5	3	2	8	4	7	4	7	10	7	4	9
EC-Earth3-Veg	6	12	4	12	3	13	1	12	6	12	2	12
INM-CM4-8	3	4	13	3	13	4	13	3	9	4	13	7
INM-CM5-0	2	1	9	1	7	1	6	1	1	1	12	3
MPI-ESM1-2-HR	1	13	1	13	1	12	2	13	4	13	3	13
MPI-ESM1-2-LR	7	5	3	5	2	6	3	4	3	6	1	1
MRI-ESM2-0	8	2	8	2	12	2	10	2	8	2	5	6
NorESM2-LM	4	6	10	7	11	9	11	9	7	9	6	8
NorESM2-MM	9	8	7	11	8	11	7	11	13	11	7	11

5.3.1 Ranking of GCMs

The performance of the individual models for rainfall and temperature on a monthly scale is shown in Figures 5.5, 5.6, 5.7. The NRMSE of rainfall is higher in the Vamanapuram and dry sub-humid basins and is lower for the Ulhas and per-humid river basins. For the individual models, the R^2 of rainfall is negligible for the Vamanapuram, a southernmost basin, and varies in the range of 0.1-0.7 in other basins. In case of maximum temperature, the higher NRMSE is noted in Purna with R^2 ranging from 0.61-0.81, NSE from 0.37-0.61. The NSE and R^2 are lower in the basin Vamanapuram than in other basins in both maximum and minimum temperatures. The ranking of the GCMs in each river basin based on TOPSIS is represented in Table 5.3 for precipitation and Table 5.4 for temperatures. In the case of precipitation, the top three performing GCMs are BCC-CSM2-MR, NorESM2-LM, and NorESM2-MM (EC-Earth3 in Vamanapuram and MPI-ESM1-2-LR in Purna). The GCM MPI-ESM1-2-HR is the first-ranked GCM in case of maximum temperature in basin Vamanapuram, Chaliyar, and Netra-

vati, EC-Earth3-Veg in Aghanashini, INM-CM5-0 in Ulhas and MPI-ESM1-2-LR in Purna. INM-CM4-8 is one of the least-performing GCMs over the per-humid Netravati and Aghanashini and dry sub-humid Purna basins, ACCESS-CM2 in Vamanapuram and NorESM2-MM in Ulhas. The GCM INM-CM5-0 is the best-performing GCM for minimum temperature over the five basins, except for the Purna (MPI-ESM1-2-LR). The GCM MPI-ESM1-2-HR, which is the best-forming GCM for maximum temperature, is one of the least-performing GCMs in the case of minimum temperature over all the basins.

5.3.2 Performance of MMEs in Estimating Daily Precipitation and Temperature

The individual models and performance of MMEs on a daily scale are shown in Figures 5.2, 5.3, 5.4. The performance metrics NRMSE, coefficient of Determination, and NSE of all the models are represented as a heatmap.

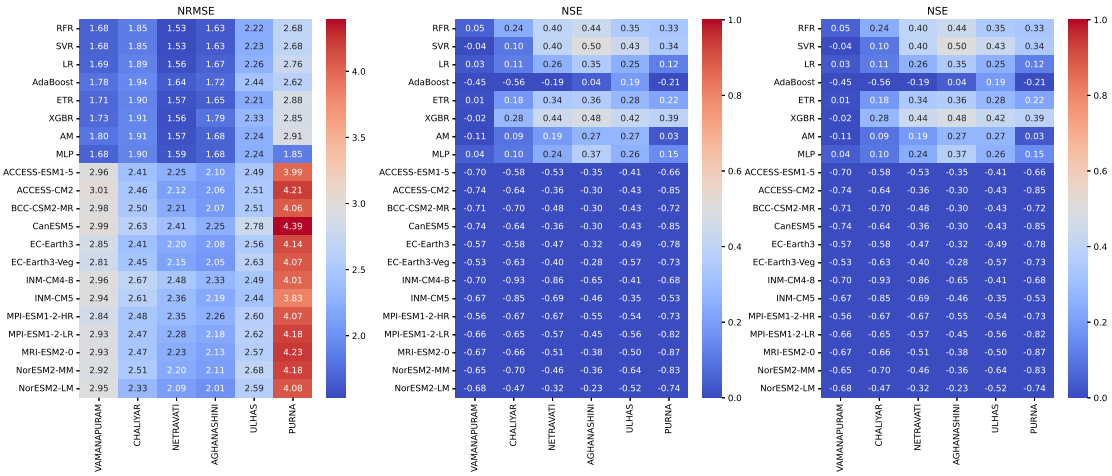

Fig. 5.2: Summary statistics of the predictive quality of daily precipitation by the thirteen individual models and the eight MMEs

a) Precipitation : The NRMSE is higher in the Purna basin and lower in the central river basins. NRMSE has been lowered by about 15–19% after the models were ensembled, primarily in the southern and central basins, and 11-35% in the northern basins. The poor NSE score for the individual models demonstrates the underestimation of the mean when compared to the simulated and observed pre-

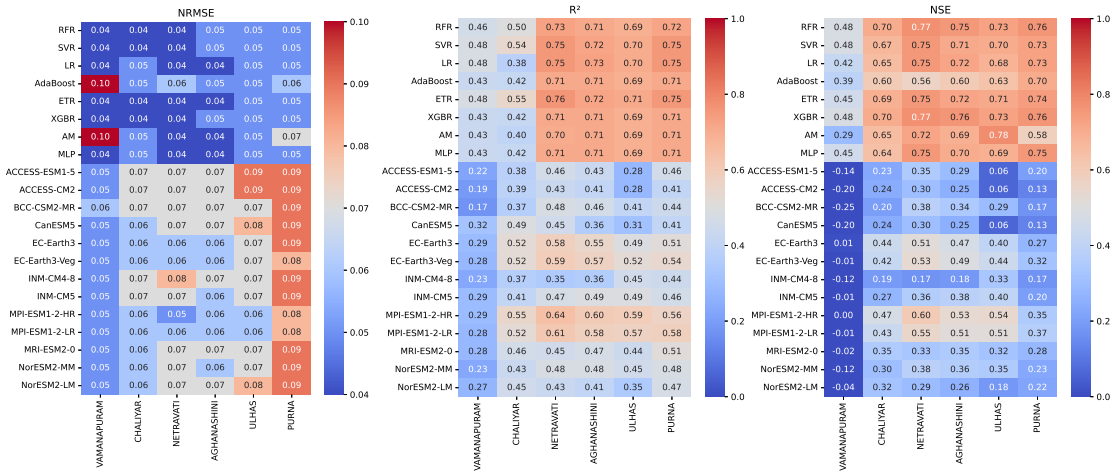

Fig. 5.3: Summary statistics of the predictive quality of daily maximum temperature by the thirteen individual models and the eight MMEs

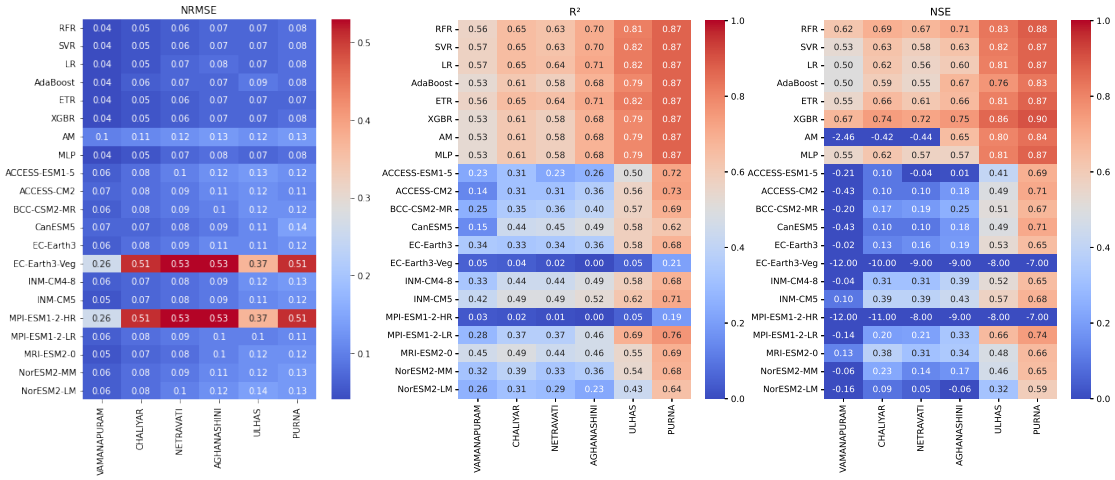

Fig. 5.4: Summary statistics of the predictive quality of daily minimum temperature by the thirteen individual models and the eight MMEs

cipitation. However, while the MMEs have improved NSE to a lesser extent in all basins, the Vamanapuram basin has seen no appreciable change. The AdaBoost being an ML-based MME model delivers a subpar performance with the AM. The straightforward AM approach has better NSE than the AdaBoost, and MLP represents the under performance of these models in case of precipitation. The RFR performed better than any other MMEs in the Netravati, Aghanashini, Purna, and ETR in the Ulhas river basin, with no better prediction in Vamanapuram than any MME model.

b) Maximum Temperature: In the case of maximum temperature, the NRMSE is higher for AM and AdaBoost models in Vamanapuram and Purna. The performance of individual models in terms of NSE and the coefficient of correlation (R) is superior in the central basins. While there has been a noticeable improvement in MME model performance relative to the individual models, the model's remarkable performance in the central and northern basins is the most striking. When compared to standalone models, MME models typically exhibit a 19-29% reduction in NRMSE. It has been found that AM's performance is comparable to that of ML-based MME models in the central river basins with regard to NSE. Despite its low performance in the MME of precipitation, the MLP model holds its own in the MME of maximum temperature. On a daily time scale, the SVR looks to be superior to MME for all of the river basins, followed by ETR, RFR, and XGBR.

.

c) Minimum Temperature: When compared to individual models, MMEs perform far better at predicting the daily minimum temperature. The performance of the ML MME models has substantially improved from the southern basins to the northern river basins after ensembling, with a reduction in NRMSE of about 47-59%. The AM has a negative NSE indicating under performance with the observed minimum temperature. Other ML MMEs models have good performance compared to MME of precipitation, the RFR, and ETR have a better performance, followed by XGBR.

5.3.3 Performance of MMEs in Estimating Precipitation and Temperature

The top six ranked GCMs for each basin are ensembled using seven ML and AM methods, and their improved performance is shown in Figures 5.5, 5.6, 5.7. a) Precipitation: The Baseyian optimized hyper-parameters used in ensembling the selected GCMs are represented in Table 5.1 for each basin. The precipitation distribution in the MME of SVR, AdaBoost, and MLP varies drastically in all six

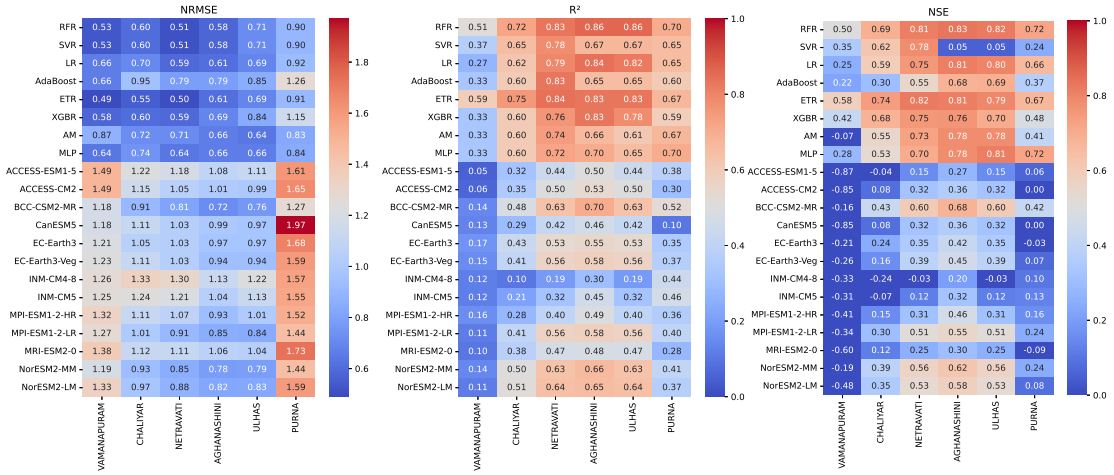

Fig. 5.5: Summary statistics of the predictive quality of monthly precipitation by the thirteen individual models and the eight MMEs.

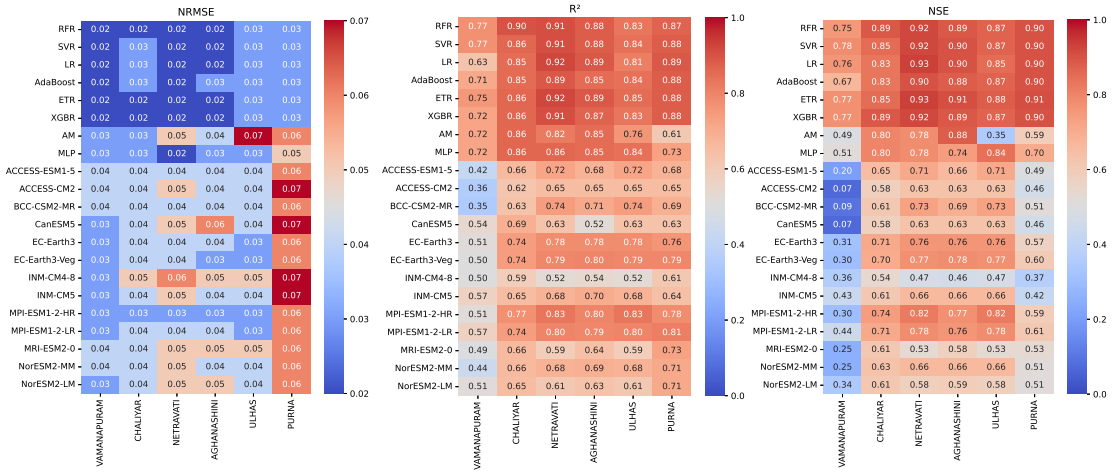

Fig. 5.6: Summary statistics of the predictive quality of monthly maximum temperature by the thirteen individual models and the eight MMEs.

river basins compared to the distribution of other MME models. The MME of SVR and MLP is much less than the observed and other models, representing a severe underestimation of monsoon rainfall, and the AdaBoost overestimates the less intense rainfall, especially the winter and pre-monsoon in all the basins. The MME of the model has reduced the NRMSE by 30-50% in southern basins, 31-34% in central basins, and 25-39% in northern river basins. The R^2 and NSE have been improved by all MMEs. The NRMSE of model AM is lesser than the AdaBoost and XGBR models in central and northern river basins. The RFR and ETR model has

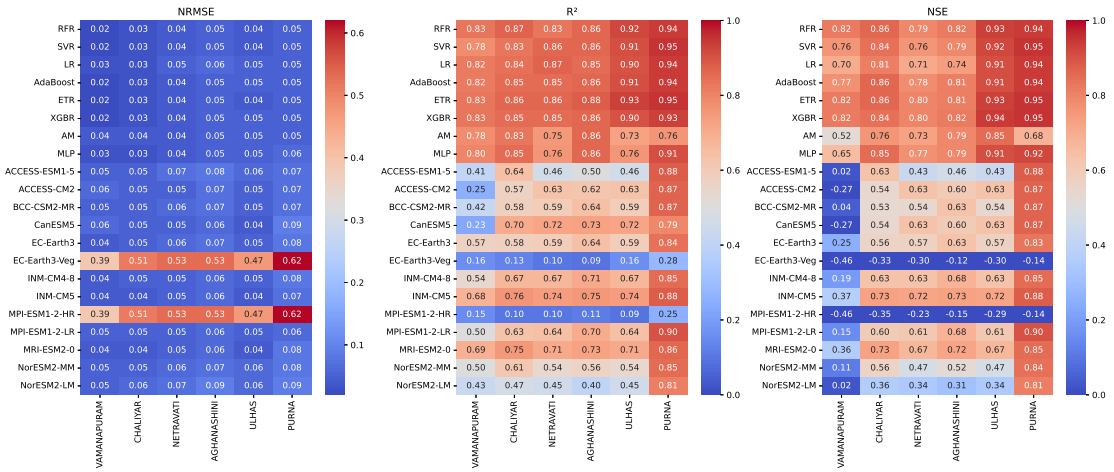

Fig. 5.7: Summary statistics of the predictive quality of monthly minimum temperature by the thirteen individual models and the eight MMEs.

the best performance among the eight MME models, followed by XGBR and SVR models. Figure 5.9 describes the distribution of the seasonal rainfall by eight MME models in the six river basins. Though RFR performs similarly to ETR, there is a significant variation in the distribution of rainfall between these two MMEs. During monsoon season, the distribution of ETR follows the IMD in the southern and northern basins and XGBR in the central river basins with slight variations in the interquartile range. The XGBR has an indistinguishable distribution, mean, and median in post-monsoon and pre-monsoon rainfall. There is a huge variation in the distribution, mean, and median during the winter season prediction by all MME models due to the small rainfall amounts in the Aghanashini and the northern basins. It varies highly in the SVR, LR, and AdaBoost over the southern basins and in the SVR, LR, AdaBoost, and MLP in the central and northern basins.

b) Maximum Temperature: For the maximum and minimum temperature, the optimized parameters for each ML-based MME model are explained in Table 5.2. The MMEs have significantly reduced the NRMSE by approximately 6% to 47% in the six river basins. The performance of the ANN-based machine learning method MLP has higher NRMSE compared to the simple AM method over the Chaliyar basin but has a higher R^2 and NSE over all the basins. All the indi-

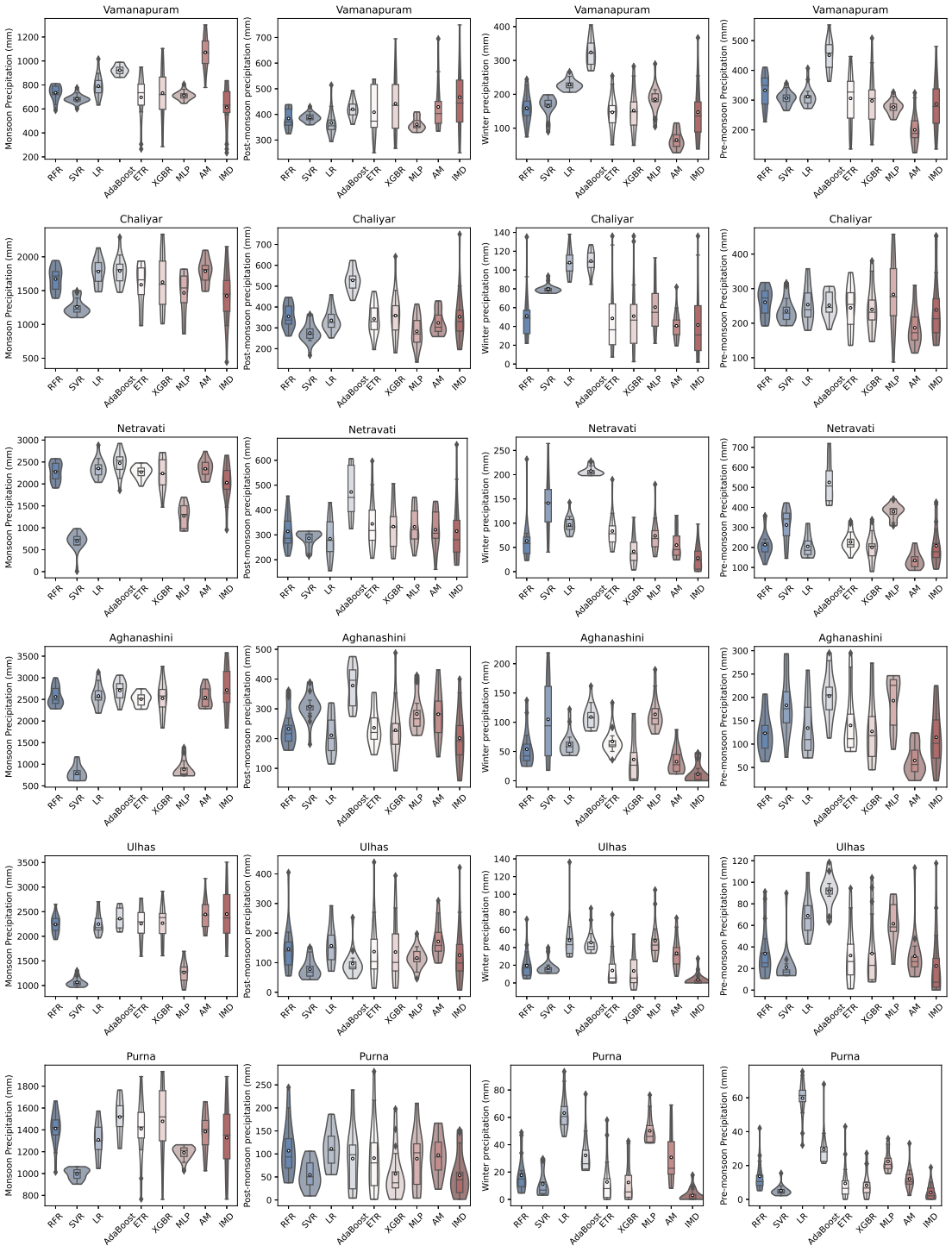

Fig. 5.8: Seasonal distribution of Precipitation from eight MME models with the observation

vidual models agree well with the observed maximum temperature; the MMEs have outperformed in the central and northern river basins with a remarkable R^2

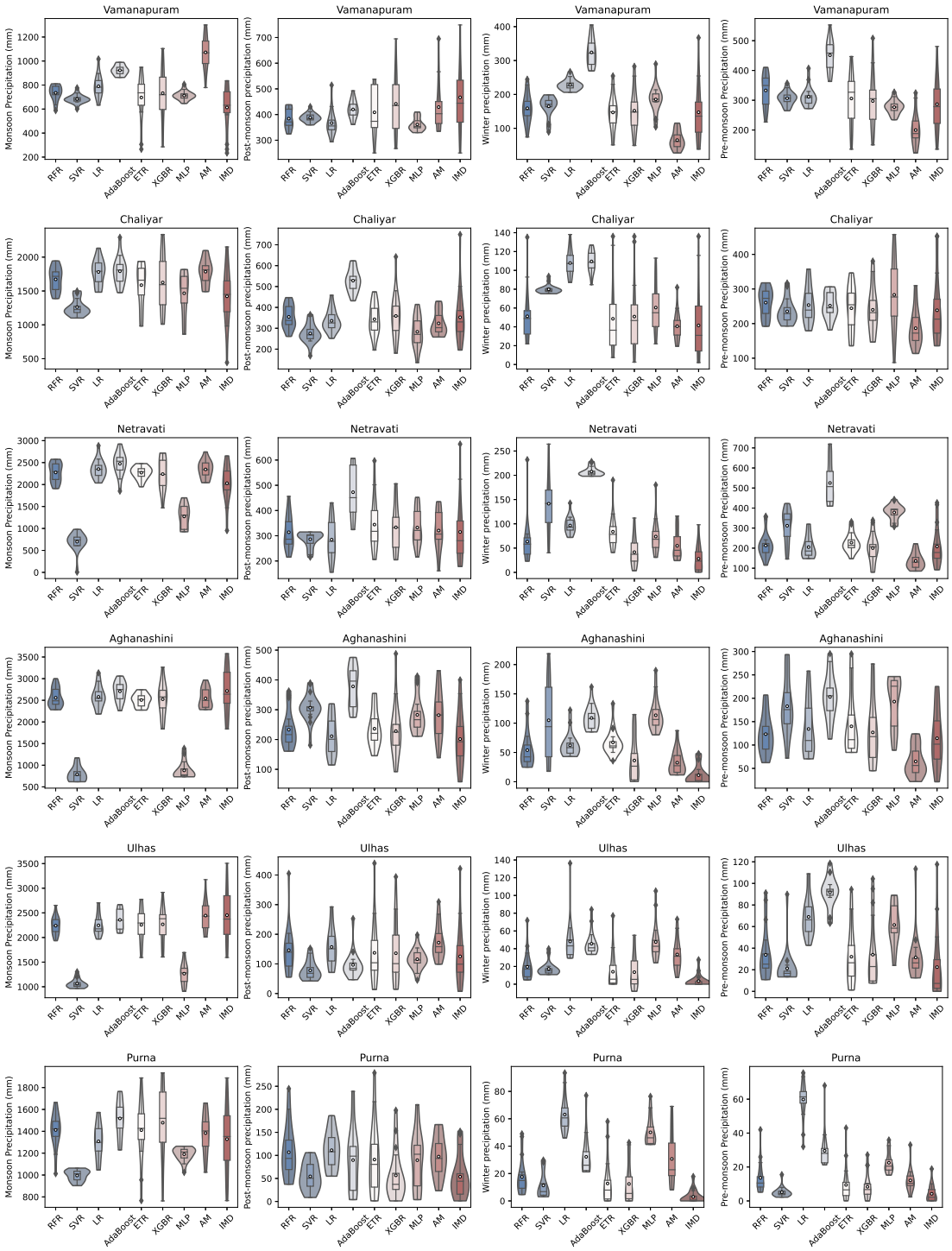

Fig. 5.9: Seasonal distribution of Precipitation from eight MME models with the observation

and NSE. All the MMEs have competitive performance except the AM and MLP. From Figure 5.10, XGBR has a similar distribution as of observed maximum tem-

perature. Although SVR is one of the top-performing MME, it underestimates the mean (approximately 0.55°C) similar to other MME models in Vamanapuram. In Chaliyar, Netravati, Aghanashini, Ulhas, and Purna, XGBR has an identical distribution with the observed temperature in the monsoon. The AM model overestimates the maximum temperature in the central and northern basins with a mean difference of approximately 0.7°C). The RFR model has a similar mean as the IMD but varies in the distribution of predicted temperature. The performance of AdaBoost has improved in the MME of temperature compared to the MME of precipitation. In the pre-monsoon season, XGBR follows the mean, median, and distribution of observed temperature in Vamanapuram, Chaliyar, and Netravati with an underestimation by all the MMEs in Aghanashini and Ulhas basins. The RFR and SVR, the best-performing MMEs, differ in their distribution in all the basins in the monsoon, post-monsoon, and pre-monsoon seasons. During the winter, the MMEs underestimated the maximum temperature in Chaliyar, Netravati, Aghanashini, and Ulhas river basins, with a slight overestimation in the Purna basin. Based on the performance of MMEs in predicting seasonal maximum temperatures, XGBR can be considered the best-performing MME in the ensemble of maximum temperatures.

c) Minimum Temperature: The NRMSE of MME models has improved by approximately 60-75% over six basins. The performance in terms of R^2 is greater than 0.8 in most of the models and basins. The AM model's NSE is lower than any MME model, except in central basins where the LR model underperforms. The RFR, ETR, and XGBR model outperformed other MMEs with an NSE of 0.82 (RFR) in Vamanapuram, 0.86 (RFR, ETR, AdaBoost) in Chaliyar, 0.8 (ETR, XGBR) in Netravati, 0.82 (RFR, XGBR) in Aghanashini, 0.93 (XGBR) in Ulhas and 0.95 (SVR, ETR, XGBR) in Purna river basin. The seasonal variation in the prediction of minimum temperature by the MMEs is shown in Figure 5.11. The monsoon temperature is over predicted by AM model in the southern basins in all the seasons and follows the observed minimum temperature in the other river basins. The SVR under predicted the monsoon minimum temperature and over

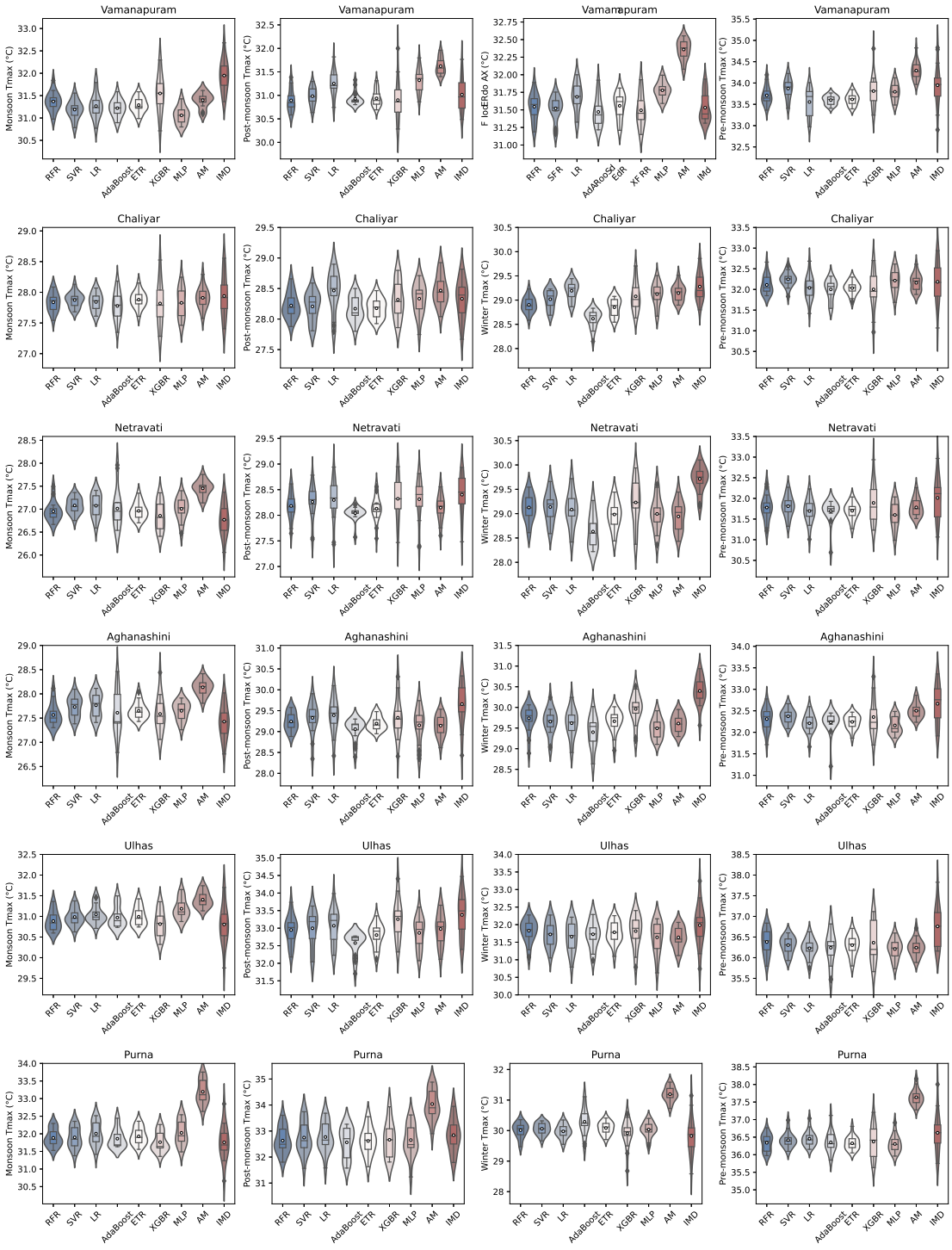

Fig. 5.10: Seasonal distribution of maximum temperature from eight MME models with the observation

predicted the winter temperature. MLP also under predicted in the Chaliyar and Netravati during these two seasons and followed the observed temperature in the

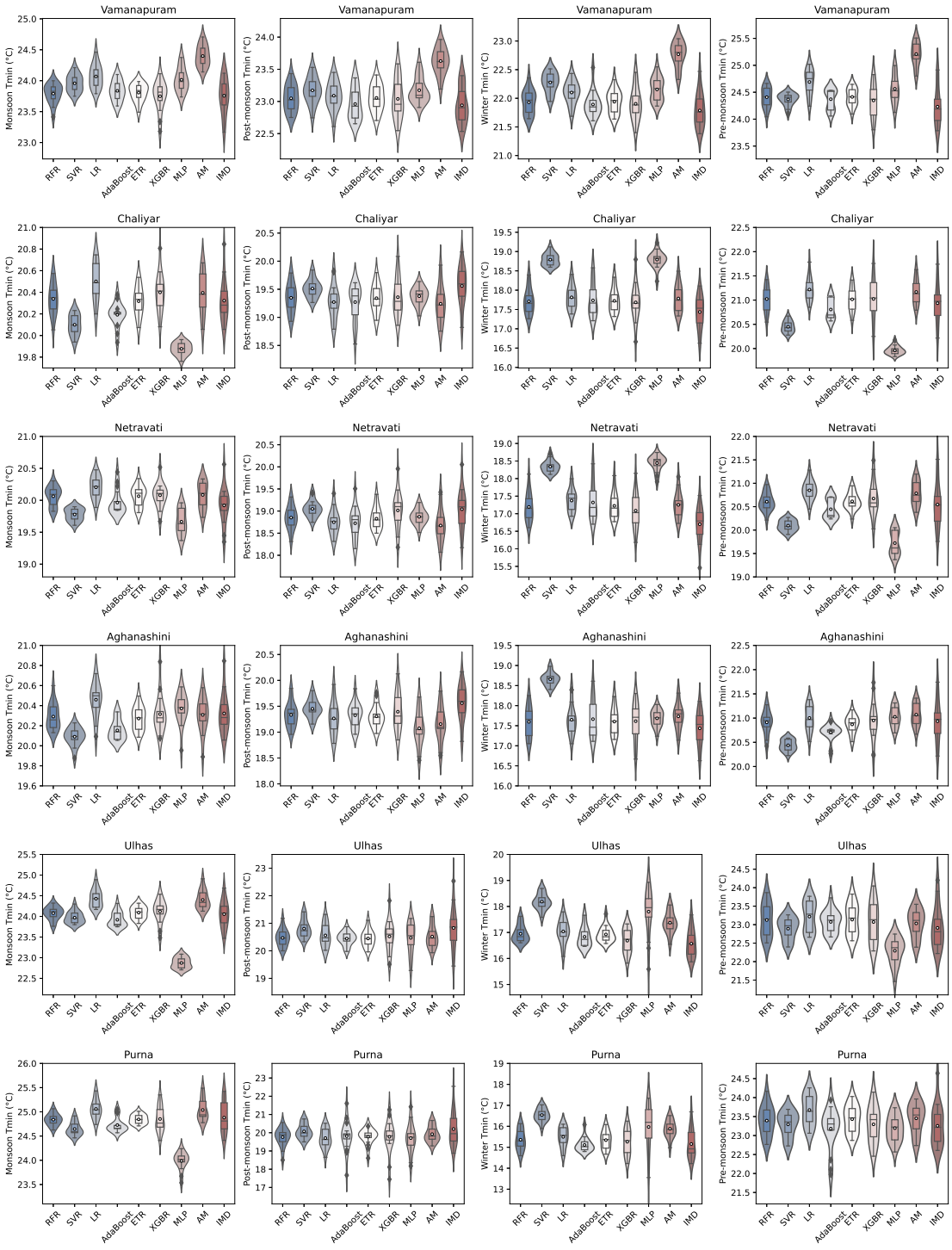

Fig. 5.11: Seasonal distribution of minimum temperature from eight MME models with the observation

other four basins. Though XGBR follows the mean and distribution of observed temperature, the minimum temperature is slightly underestimated in the mon-

soon season. Still, it has well predicted the peak temperature compared to other models. During the winter season, RFR, ETR, and XGBR models predict the minimum temperature at the highest similarity. In predicting pre-monsoon and post-monsoon minimum temperatures, the RFR and ETR differ in distribution with respect to the observed temperature; XGBR is one of the promising MME models which tracks the distribution of the observed values. The LR MME has functioned admirably in the central and northern river basins over the winter, pre-monsoon, and post-monsoon seasons.

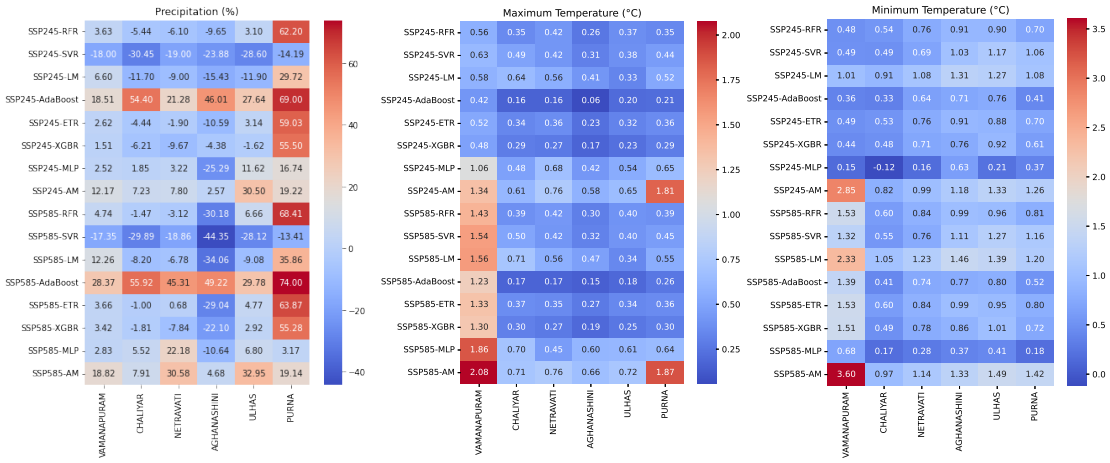

Fig. 5.12: The projected change in mean annual precipitation (in %), mean annual maximum temperature (°C), and minimum temperature (°C) in the near future with respect to historical period

5.3.4 Projected Transition in Precipitation and Temperature

The change in projected future precipitation, maximum, and minimum temperatures by eight MMEs is shown in Figure 5.12 for the near future (2021-2050) and Figure 5.13 in the far future (2051-2100) for SSP245 and SSP585 scenarios. The mean annual rainfall over the southern basins Vamanapuram and Chaliyar is around 1900 mm and 2200 mm, the maximum mean temperature is 31.9 °C, 29.36 °C, and the minimum mean temperature is 23.2 °C, 19.4 °C in the historical period. The temperature in the southern portion of Kerala state tends to be warmer than the temperature in the northern part of Kerala, and vice versa for the annual

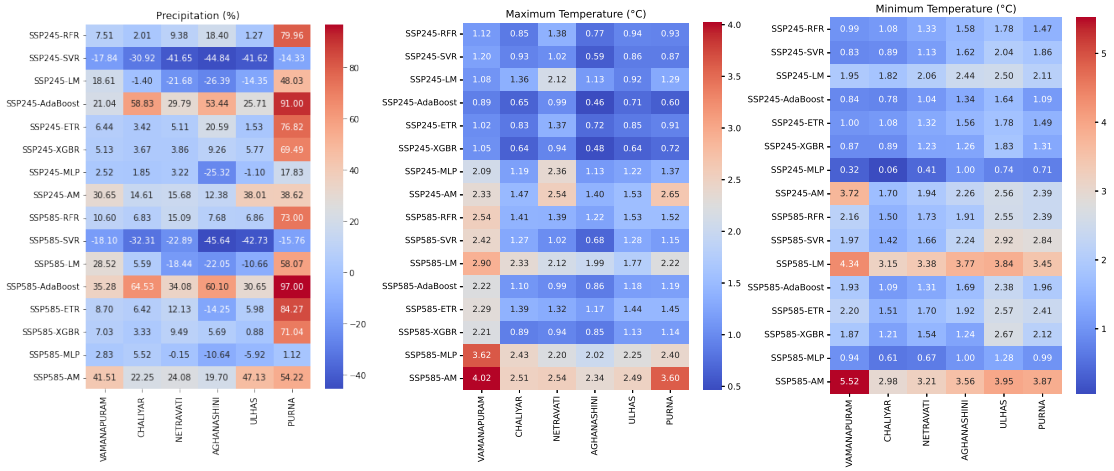

Fig. 5.13: The projected change in mean annual precipitation (in %), mean annual maximum temperature (°C), and minimum temperature (°C) in the far future with respect to the historical period

rainfall in these regions. The central basins, Netravati and Aghanashini, receives higher annual rainfall than the southern and northern basins of WG. These basins receives an annual rainfall of over 3000 mm; the maximum and minimum mean annual temperatures are approximately 29.5 °C and 19.7 °C. Towards the north of the WG, the rainfall decreases with an annual rainfall of 2300 mm in the Ulhas and 1400 mm in the Purna basin. The maximum and minimum annual mean temperatures over the region are 32.7 °C, 21.2 °C approximately. The highest annual rainfall in the central part (Karnataka) of the WG than other parts and decreases in intensity towards the north of the Ghat (Vijay *et al.*, 2021) are intently captured in all the ensemble models. The apprehension of heterogeneity in the distribution of temperature and rainfall by the RFR, XGBR, and ETR ensembles of CMIP6 directs the use of GCMs even at the river basin scale. Undoubtedly, the temperature is expected to increase in the future, and all MMEs show an increase in all the basins in both maximum and minimum temperature. A greater increase may be seen in the AM compared to the other models. In the FF, compared to the RFR, the SVR, and the ETR, the XGBR has shown a lesser increase in temperature. The increase in LR, MLP, and AM MME is more severe than by any of the MME in all the river basins. In FF, the Aghanashini, Ulhas, and Purna

record the highest increase in SSP245, Vamanapuram, Aghanashini, Ulhas, and Purna in the SSP585 scenario. In the precipitation, due to the underestimation of precipitation by SVR, it has shown a decrease in precipitation in both SSPs, and the overestimation by the AdaBoost model has shown an excess increase in precipitation in all the basins in the NF (Figure 5.12). The percentage change in the precipitation in the future horizon shows an increase in Vamanapuram and northern river basins. Whereas mixed variation in the Chaliyar, Netravati and Aghanahini basins by RFR, ETR, and XGBR MMEs; in contrast, AM shows an increase in both SSPs. The increase in the NF precipitation is observed in the SSP585 scenario.

5.3.5 Discussion

The ranking of the GCM models based on the performance of individual GCM offers the best GCM selection. The MME of best-performing GCMs from the pool of GCMs significantly captures the heterogeneity in the climate pattern simulations. The top performing GCMs obtained in this study are in accordance with the observation made by Jose and Dwarakish (2022*b*) over the Netravati river basin based on multiple MCDM techniques. Anil *et al.* (2021) highlighted the performance of EC-Earth3-veg and EC-Earth3 in simulating maximum temperature, MPI-ESM1-2-HR in minimum temperature over the tropical monsoon climate of WG. The daily spatial pattern of precipitation is well simulated by the BCC-CSM2-MR, EC-Earth3, MPI-ESM1-2, and NorESM2 over India (Mitra, 2021). Also, the least ranked GCMs obtained in this study are in consonance with the observation made by Aadhar and Mishra (2020); Mitra (2021). Over the river basin in Eastern India, the MPI-ESM-1-2-HR is found as a top-performing GCM for precipitation, maximum and minimum temperatures (Dey *et al.*, 2022). Though the finding of top-performing models is consistent with the previous studies, there is a wide variability in the performance of the GCMs over the study area. This might be due to the highly elevated rugged mountain terrain, proximity to the coast, and local heterogeneity in the climate over the WG, which offer great

spatiotemporal variability in the climatic variables.

Further, the RFR, ETR, XGBR, and SVR have been proven as the top-performing MMEs in all the basins, with remarkable performance over the per-humid river basins of WG. The Vamanapuram, a southern basin located in peninsular India, has sub-par performance in simulating precipitation; this might be due to the small catchment area, also the difficulty in capturing the ocean land transition during the down-scaling of the coarse resolution GCMs. The ML-based AdaBoost model has a higher error than the simple AM method due to the overestimation of non-monsoon season precipitation, which is improved in the temperature ensemble. This signifies that the increase in the level of complexity does not improve the result. The monsoon precipitation is highly underestimated by the SVR in the southern basins and SVR and MLP in other basins. The winter precipitation in the MME has higher variation in the mean, median, and distribution of all the MMEs. SVR being a top-performing MME of maximum temperature, underestimates the mean, and AM overestimates. The RFR and SVR, the best-performing MMEs, differ in the distribution in all the basins in the monsoon, post-monsoon, and pre-monsoon seasons with indistinguishable mean, median, and distribution by XGBR with the observed maximum temperature. The models which can capture the basic seasonality achieve higher NSE ignoring the inter-annual variability (Legates and McCabe Jr, 1999; Shortridge *et al.*, 2016), which can be observed especially from the SVR MME. Therefore, even with the top performance in terms of NSE, the distribution of these MMEs differs from the observed records. There have been limited studies on AdaBoost and XGBR ML-based ensembles. Most of the previous studies endorse the use of RFR and SVR in the ensemble of precipitation, and temperature Ahmed *et al.* (2019*a*, 2020); Li *et al.* (2021); Dey *et al.* (2022); Jose *et al.* (2022); Yang *et al.* (2022). Asadollah *et al.* (2022) has proved the efficacy of the Gradient Boosting Regression Tree (GBRT) in the downscaling of GCMs over RFR and SVR, XGBR in land degradation study (Saha *et al.*, 2022), and drought-maize yield dynamics study (Muthuvel *et al.*, 2023) using CMIP6 GCMs. Over river basins of the

WG, the XGBR MME has a higher ability to capture the peak temperature and precipitation than other MME models. Further, the anticipated change in maximum and minimum temperature in the SSP245 and SSP585 in the future horizon corroborates the undeniable rise in temperature by all the MMEs compared to the historical mean. The change in the temperature in RFR, ETR, and XGBR in the NF and FF are consistent with one another, with AM showing the most dramatic change. The future precipitation is expected to increase under the climate change, whereas, the WG experience a heterogeneous distribution especially in the NF epoch.

Studies in the past have shown that the upper troposphere warms at a much faster rate than the lower troposphere, and this helps to stabilize the atmosphere over the WG, making it more likely to see less volatility in future precipitation than other places in India (Basha *et al.*, 2017; Varghese *et al.*, 2020). Though the EQM bias-corrected GCMs have been used in climate change studies (Mishra *et al.*, 2020; Yue *et al.*, 2021; Das *et al.*, 2022*a*), the studies have also shown that the quantile mapping-based bias correction technique alters the temporal sequence of the time series; future climate change signals may get distorted with exaggerated or deflated extreme trends (Maraun, 2013; Sachindra *et al.*, 2014). The use of ML MME may significantly reduce the uncertainty in the trend and extreme values due to the consideration of observed data during the training of the model. Future research should pay close attention to how ML-MME affects the persistence of the observed precipitation/temperature relationship and extremes.

5.4 CONCLUSIONS

The performance of each GCM varies in the six basins; also, the ability to imitate the observation varies with the climatic variables with significant unevenness in climate pattern simulation. The TOPSIS ranking of GCMs indicate the top performance of EC-Earth3 in Vamanapuram and BCC-CSM2-MR in other basins in the simulation of precipitation. The MPI-ESM1-2-HR is the first-ranked GCM in case of maximum temperature in basin Vamanapuram, Chaliyar, and

Netravati, EC-Earth3-Veg in Aghanashini, INM-CM5-0 in Ulhas and MPI-ESM1-2-LR in Purna. The GCM INM-CM5-0 is the best-performing GCM for minimum temperature over the five basins, except for the Purna (MPI-ESM1-2-LR). The ACCESS-ESM1-5, CanESM5, INM-CM4-8 in precipitation, ACCESS-CM2, INM-CM4-8 in maximum temperature, EC-Earth3-Veg, MPI-ESM1-2-HR in minimum temperature are the lowest performing GCMs over the river basins of WG. Further, the top six performing GCMs are ensembled using seven machine learning-based RFR, SVR, LR, ETR, AdaBoost, XGBR, MLP, and simple arithmetic mean method tuned by Bayesian optimization for hyper-parameter identification. The ensemble models have been proven beneficial in river basin scale research by overcoming the constraints of bias correction methods, such as nonstationary GCM bias and inter-GCM systematic biases. Also, the potential of ML approaches to explain essential physical and dynamic processes within GCMs further enhances the capability to acquire detailed information. Over river basins of the WG, the XGBR MME has a higher ability to capture the peak temperature and precipitation than other MME models. The anticipated change in maximum and minimum temperature in the SSP245 and SSP585 in the future horizon corroborates the undeniable rise in temperature by all the MMEs compared to the historical mean with a two-time increase in the FF compared to those experienced during the NF epoch. The change in the temperature in RFR, ETR, and XGBR in the NF and FF are consistent with one another, with AM showing the most dramatic change. The precipitation estimation varies widely in these ensemble models in the future epoch. Additionally, we conclude that in regional studies involving complex and diverse mechanisms that drive precipitation, a robust testing and validation approach should be employed in developing ensembles. Though the mean and distribution of the models are in agreement with the observed data, further research on the extremes that the MMEs anticipate is necessary.

The performance of these ensemble models in the estimation of extreme climate indices of temperature and precipitation over the region and the projected trend in future horizon is carried out in the next chapter.

CHAPTER 6

ANTICIPATED IMPACT OF CLIMATE CHANGE ON HYDRO-CLIMATE AND THE EXTREMES

6.1 BACKGROUND

The alteration of the hydrological cycle is a key consequence of changes in the Earth's climate, and it significantly influences the occurrence of extreme weather events (Varghese *et al.*, 2020). The changes due to the warming temperatures in the projected future are evaluated over the Indian scale by many researchers (Nanditha *et al.*, 2020; Varghese *et al.*, 2020; Kumar *et al.*, 2021; Shafeeque and Luo, 2021; Sarkar and Maity, 2022). In India, agriculture and related sectors heavily rely on timely and adequate rainfall. In the future, the growth in the population and rapid industrialization will increase the water demand for irrigation and industries with warming climate risks, and this becomes a critical issue in the late 21st century (Singh and Goyal, 2016; Shiferaw *et al.*, 2018; Sharma and Goyal, 2020; Kumar *et al.*, 2021). Therefore, investigating the historical and projected future temperature and rainfall can assist us in comprehending the variations in the climate and their extremes at a regional scale. Though the studies have improved the daily prediction of precipitation and temperature using ensemble techniques, the effectiveness of the ensemble approaches on extreme values has not been explored much on a regional scale. As a result, this research looks at how ML-MME modifies the persistence of the rainfall and temperature extremes, and the observed trend in the time-series.

6.2 METHODOLOGY

Based on the performance of the ensemble methods, the best performing MME, namely RFR, SVR, ETR, and XGBR, are selected along with the AM. In order to understand the simulation ability of the MMEs to capture extreme climatic

events, nine rainfall indices and nine temperature-based indices, formulated by the Expert Team on Climate Change Detection and Indices (ETCCDI) have been analysed (Zhang *et al.*, 2011), considering the period 1961–1990 as the base period. The temperature intensity-based indices (hottest day (TXx), warmest night (TNx), coldest day (TXn), coldest night (TNn) and frequency-based indices (warm days (TX90p), warm nights (TN90p), cold days (TX10p), cold nights (TN10p), and DTR) are used to evaluate the change in the intensity and frequency of the temperature. To evaluate the characteristics of rainfall, the absolute rainfall indices (R×1day, R×5day), percentile indices (R95p, R99p), threshold-based indices (R10, R30, R65), duration-based indices (CWD, CDD) are used. The potential of the indices has been affirmed based on their applicability by numerous studies across various regions. The multiple investigations from across the globe have confirmed the robustness of the indicators based on their applicability (Ongoma *et al.*, 2018; Babaousmail *et al.*, 2022).

The Modified Mann-Kendall test, Sen's Slope estimator, examines the long-term trend in rainfall, maximum and minimum temperature, and associated extreme indices. A open-source R based "RClimDEX" module developed by WMO CCI/WRCP/JCOMM ETCCDI is used for climate indices calculation. The rainfall and temperature indices used in the study are shown in Table 6.1. Based on the uncertainties assessed in the estimation of climate indices, the best-performing MMEs are used to estimate the future rainfall and temperature indices. The changes in rainfall, humidity, wind speed, temperature, and solar radiation, influence potential evapotranspiration (PET). Vegetation dynamics, particularly the water needs of seasonal agricultural crops, are profoundly impacted by seasonal variation in potential evapotranspiration (Liu *et al.*, 2015). Several methods have been devised to estimate PET, including the Penman-Monteith method (Penman and Monteith, 1965), Hargreaves method (Hargreaves and Samani, 1985), Priestley-Taylor method (Priestley and Taylor, 1972), and the Turc Method (Turc, 1961). Although the Penman-Monteith method is widely used in agricultural research, it necessitates a comprehensive database (Niranjan and Nandagiri, 2021).

In this investigation, therefore, the Hargreaves, a temperature-based method, was used to calculate the potential evapotranspiration. Then the frequency and trend in the projected extremes of precipitation, minimum and maximum temperature, are obtained for the Shared Socioeconomic Pathways SSP245 and SSP585 for the Near Future (NF) (2021–2050) and Far Future (FF) (2051–2100).

Table 6.1: ETCCDI Indices of rainfall and temperature used in the study

Rainfall	**Name (Unit)**	**Temperature**	**Name (Unit)**
R×1day	Max 1-day rainfall amount (mm)	TN10p	Percentage of days when TN<10^{th} percentile of 1961–1991 (%)
R×5day	Max 5-day rainfall amount (mm)	TX10p	Percentage of days when TX<10^{th} percentile of 1961–1991 (%)
R10	Annual count of days when rainfall≥ 10mm (days)	TN90p	Percentage of days when TN>90^{th} percentile of 1961–1991 (%)
R30	Annual count of days when rainfall≥ 30mm (days)	Tx90p	Percentage of days when TX>90^{th} percentile of 1961–1991 (%)
R65	Annual count of days when rainfall≥ 65mm (days)	TXx	Maximum value of maximum temperature in a year (°C)
R95p	Annual total rainfall when annual rainfall≥ 95^{th} percentile of 1961–1990 (mm)	TXn	Minimum value of maximum temperature in a year (°C)
R99p	Annual total rainfall when annual rainfall≥ 99^{th} percentile of 1961–1990 (mm)	TNx	Maximum value of minimum temperature in a year (°C)
CWD	Number of rainy days in a year (with rainfall intensity≥ 2.5 mm/day (days)	TNn	Minimum value of minimum temperature in a year (°C)
CDD	Number of rainy days in a year (with rainfall intensity≤ 1 mm/day) (days)	DTR	Diurnal temperature range (°C)

6.2.1 Modified Mann-Kendal Test

It is a rank based non-parametric test to quantify the significance of monotonic trend in the time series. This is a most widely used trend test as it is flexible to outliers in the time series. The Mann–Kendall test statistic S for a time series, $x_i = x_1, x_2, x_3, \ldots\ldots, x_n$,is calculated as

$$S = \sum_{i=1}^{n-1} sgn\,(x_{j-}x_i) \tag{6.1}$$

$$E(S) = 0 \tag{6.2}$$

where n represents the number of data points, x_j and x_i are the data values in time-series j(j>i) and i respectively, and sgn(x_j-x_i) is the sign function, i.e,

$$sgn(x_{i+1} - x_i) = \begin{cases} +1, & \text{if } x_i - x_j > 0. \\ 0, & \text{if } x_i - x_j = 0. \\ -1, & \text{if } x_i - x_j < 0. \end{cases} \tag{6.3}$$

The variance of the distribution depends on whether all the x's are distinct, or if some are repeated values. If there are no ties, the variance of the sampling distribution is given by

$$var\,(s) = \frac{n\,(n-1)\,(2n+5) - \sum_{j=1}^{j} t_j\,(t_j-1)\,(2t_j+5)}{18} \tag{6.4}$$

Where, j indicates the number of groups of repeated values and t_j is the number of repeated value in a j^{th} group. The test statistics Z_c is computed as

$$Z = \begin{cases} \frac{S-1}{\sqrt{var(S)}}, & \text{if S>0).} \\ 0, & \text{if if S=0.} \\ \frac{S+1}{\sqrt{var(S)}}, & \text{if S<0).} \end{cases} \tag{6.5}$$

Presence of statistically significant trend is evaluated using the Z value and here the statistics z has a normal distribution/ Significance level α is used for testing either an upward or downward monotonic trend (a two tailed test). If Z appears greater than $Z\alpha/2$, then the trend is considered as significant. The value for $Z\alpha/2$ is obtained from the standard normal cumulative distribution.

6.2.2 Sen's Slope Estimator Method

It is a potential non-parametric test to quantify the magnitude of the monotonic trend in the time series. For the time series $X_i = X_1, X_2, X_3, \ldots\ldots, X_n$, with N pairs of data, the slope is calculated as

$$T_j = \frac{X_j - X_k}{j - k} \tag{6.6}$$

For all i=1, 2, 3, 4. . . ..N where X_j and X_k are considered as data values at time j and k(j>k) correspondingly. The Sen's estimator of slope Q_i is obtained from the median of N values of T_i

$$Q_i = \begin{cases} T_{\frac{N+1}{2}}, & \text{if N is odd.} \\ \frac{1}{2}(T_{\frac{N}{2}} + T_{\frac{N+2}{2}}), & \text{if N is even.} \end{cases} \tag{6.7}$$

Q_i values that are positive suggest an upward trend, whereas Q_i values that are negative point to a downward trend in the time series.

6.3 RESULTS AND DISCUSSION

6.3.1 Temporal Variation in Rainfall, Temperature and the Indices during the Historical Period using MMEs

The mean monthly rainfall and monthly temperature captured from the MMEs shown in Figure 6.1, 6.2 indicates the variation in the monthly maximum and minimum temperatures over the basins. In the Vamanapuram basin, there is not much variation in the temperature in different seasons/months; in other basins, the maximum temperature is lowest in the months of July and August (December and January in Purna), and the minimum temperature is lowest during the winter months. The central per-humid basin receives higher annual rainfall, followed by the humid Ulhas basin, Chaliyar, and Vamanapuram, and least in the northern-most dry sub-humid Purna basin. The monsoon rainfall contributes up to 65–80% of the annual rainfall in the Chaliyar, Netravati, and Aghanashini, and more than 80% in the Ulhas and Purna basins (Figure 6.2). The time series plot of the annual rainfall and the absolute rainfall indices are shown in Figure 6.3 represents the temporal variation in the MMEs and IMD observations. SVR consistently underestimates the monsoon rainfall in all years following the temporal pattern in the IMD observation, while RFR and ETR MMEs consistently underestimated the higher values and overestimated the lower values across all basins, and AM has overestimated in all the years and in all basins. Monsoon rainfall has a positive relative bias of 3-60% in southern basins, 1% in Netravati, and 3% in Purna; the

negative bias of 3.80% and 0.25% is noted in Aghanashini and Ulhas basins in the XGBR MME. Except the Vamanapuram, the post-monsoon rainfall has a wet bias in the RFR, ETR, XGBR and AM, dry bias in the SVR. A wet bias of 64 mm noted in the northern basins and 21-49 mm in the southern basins. As the contribution of post-monsoon rainfall to annual rainfall is minimal in the northern basins it induce a higher relative wet bias than in the other basins. In summer, the wet bias is noted in RFR and XGBR, whereas the SVR which consistently underestimates the rainfall has dry bias in the southern and central basins and a wet bias of 9-66% in the northern basins. Winter rainfall has a positive bias ranging from 31-73 mm in all the basins. Though SVR underestimated the higher values, the lowest rainfall in the summer and winter seasons are not overestimated, unlike other MMEs.

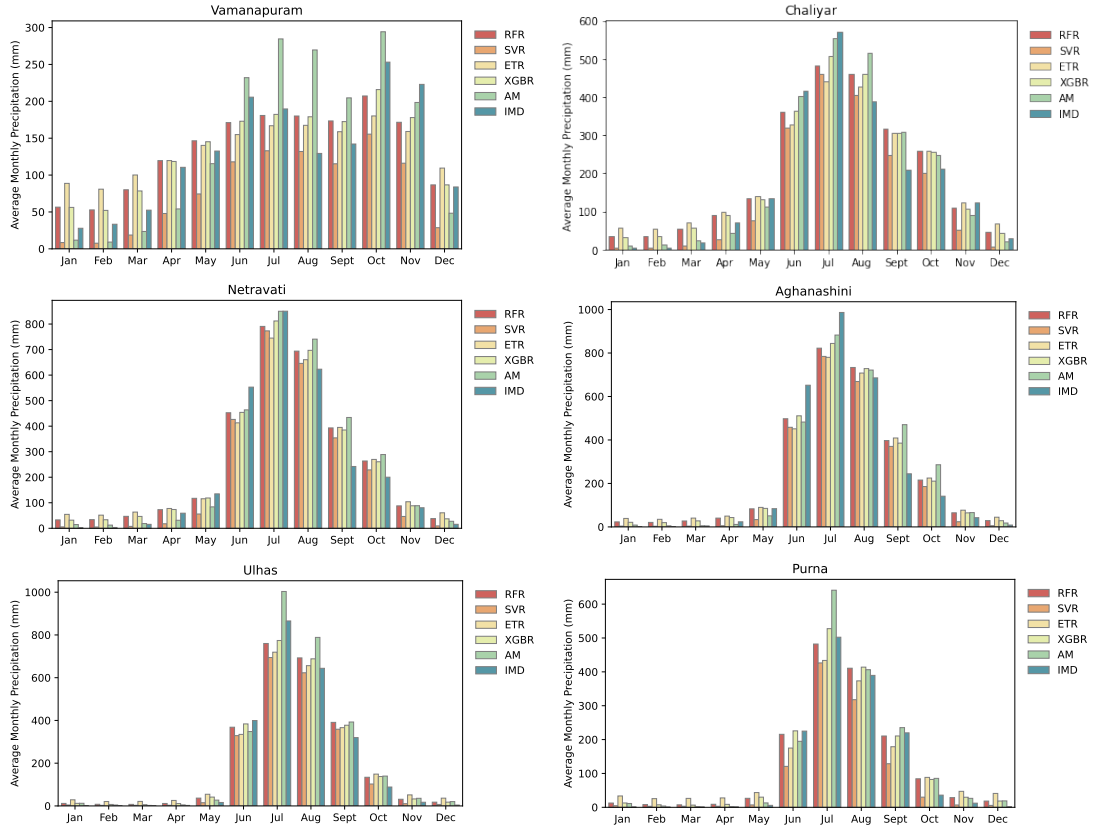

Fig. 6.1: Monthly rainfall captured from five MMEs along with the observation (IMD)

In the mean maximum and minimum temperatures from Figure 6.4, a huge overestimation can be observed, especially in the minimum mean temperature.

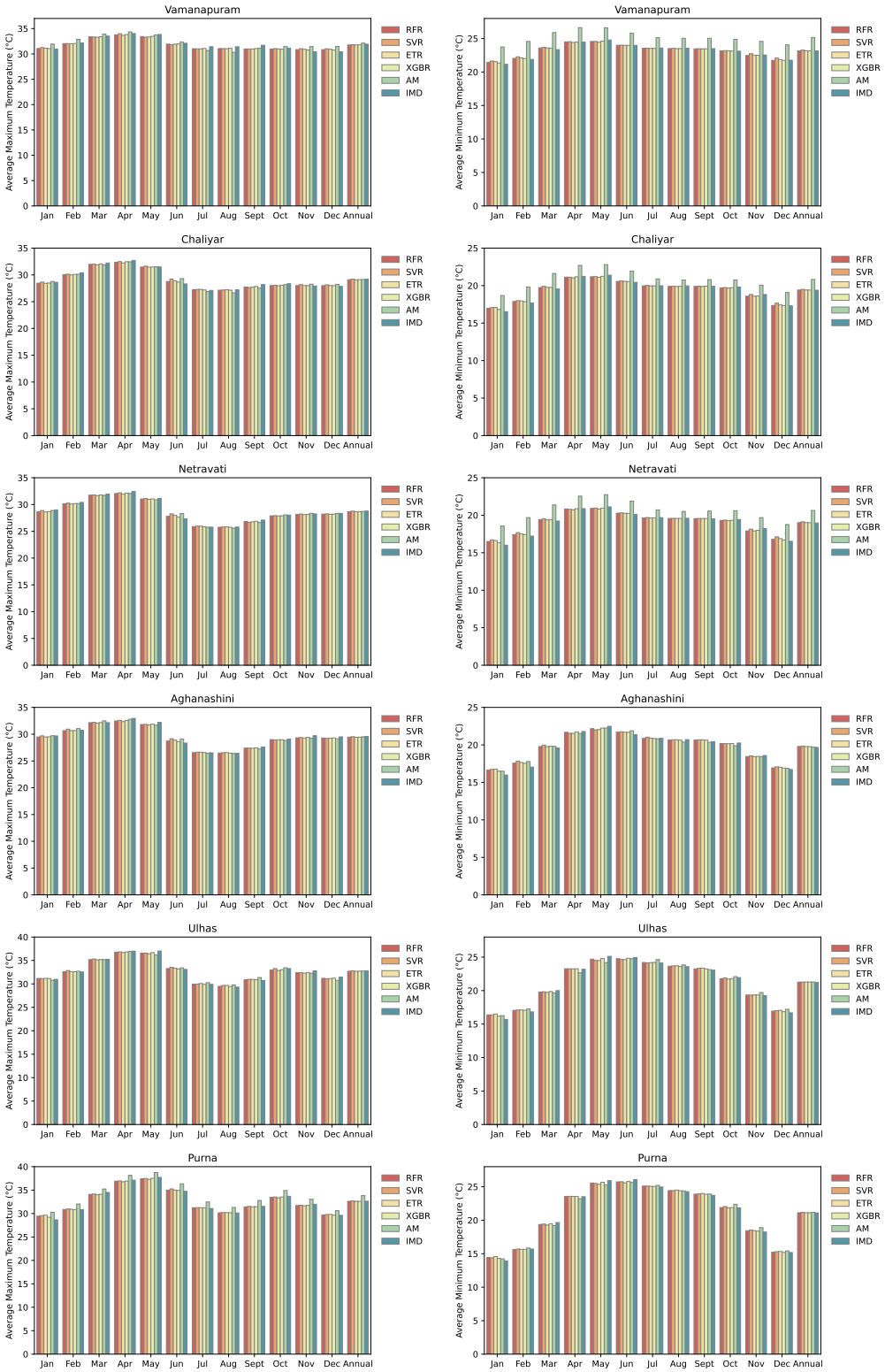

Fig. 6.2: Monthly temperature captured from five MMEs along with the observation (IMD)

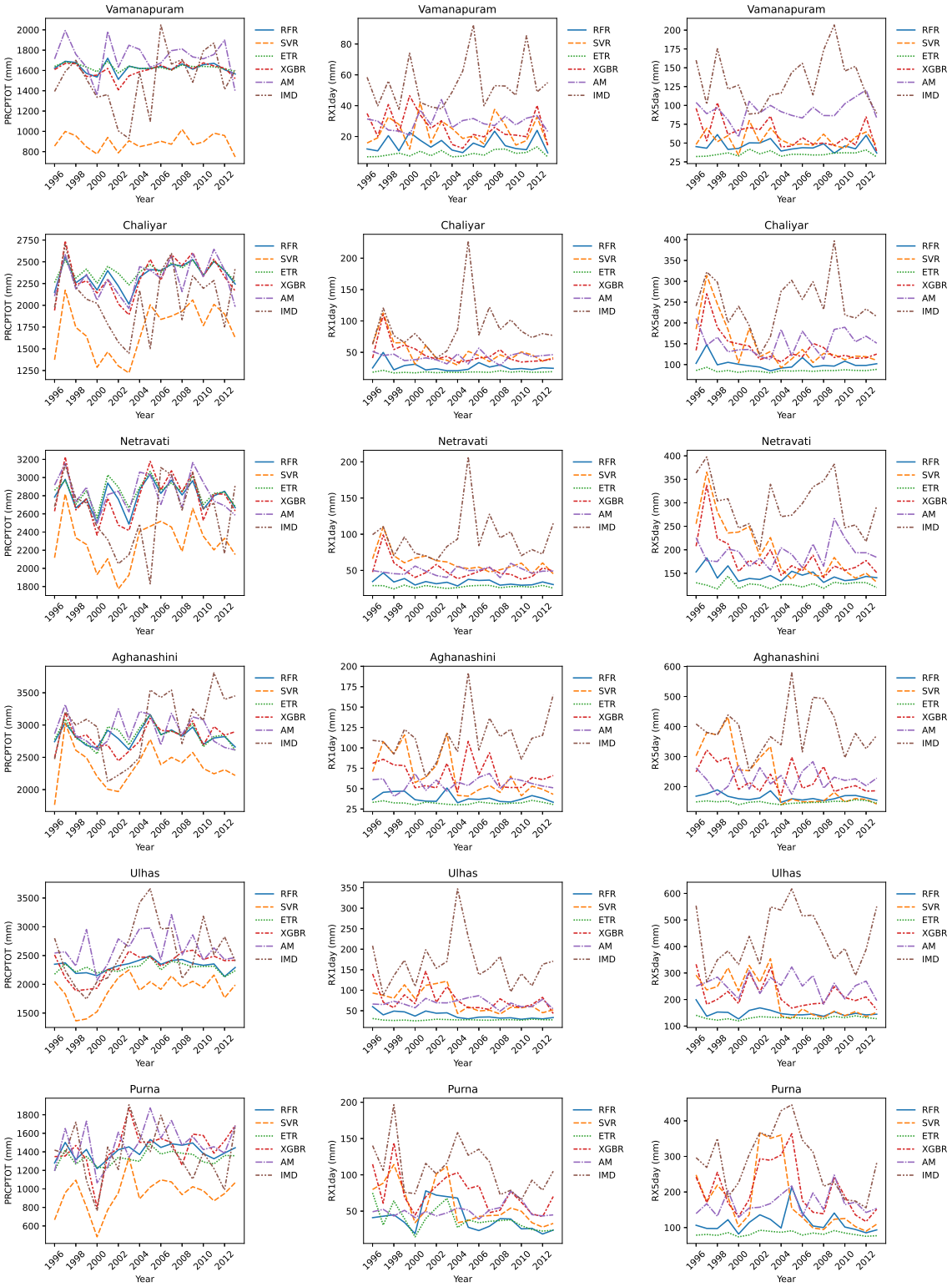

Fig. 6.3: Temporal variation in rainfall and absolute rainfall indices from five MME models

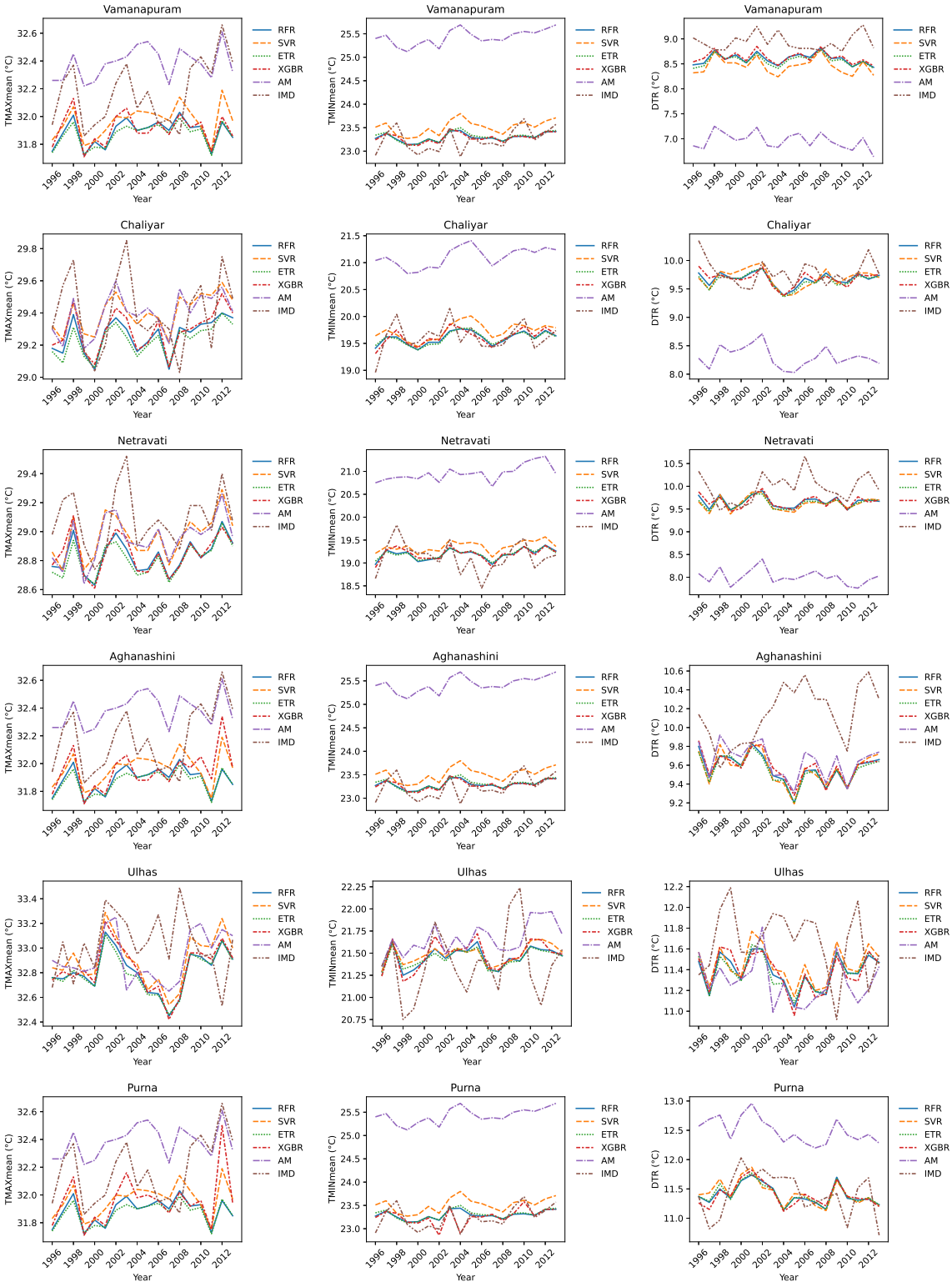

Fig. 6.4: Temporal variation in temperature from five MME models

An overestimation of approximately 2°C in the minimum temperature can be observed in all the basins except the Ulhas basin by AM MME. RFR, ETR, and XGBR have similar estimations, with a slight overestimation by SVR MME. The lowest temperatures have not been captured by the MME models in the Ulhas basin. The maximum temperature is indisputably over-estimated in Vamanapuram, Aghanashini, and the Purna basins. The XGBR MME annual minimum temperature has a mean positive bias < 0.1°C, and annual maximum temperature has a mean negative bias < 0.1°C. In the seasonal temperature simulation, the monsoon and winter minimum temperatures note a warm bias by all the MMEs (except Vamanapuram in the monsoon). A least bias is noted in XGBR , a positive bias $< 0.2\%$ is noted in monsoon minimum temperature, whereas it ranges from 0.4-1% in southern basins, 1.5-2.4% in central basins, and 0.7-1.8% in northern basins in the winter. The minimum summer temperature mean is almost the same as the observed mean, and the post-monsoon minimum temperature has a cold bias of 0.5-0.87% in the per-humid basins, and are less than 0.1% in the humid basins. In the dry sub-humid southern basin, there is a negative bias of 0.75%, positive bias of 0.5% in northern basin in XGBR. In maximum temperature, except for the monsoon temperature, other seasons note a negative relative bias. There is a difference in the performance of the models in Vamanapuram, which can be noticed from the cold bias of 1.1% in the monsoon, and the warm bias of 0.23-0.34% in the post-monsoon and summer seasons. Irrespective of the warm/cold bias, the observed percentage bias are $< 1\%$ in all the seasons in all the MMEs except the AM.

6.3.2 Estimation Accuracy of the Indices

The NRMSE and the coefficient of determination in the time series of intensity-based, frequency-based temperature indices, absolute, percentile, and duration-based rainfall indices calculated from the five MMEs and the observation in the historical period are shown in Figure 6.5 and 6.6. The TN10p, TN90p, TX10p, and TX90p have established a good fit with the observed frequency-based indices. The XGBR model has good R^2 with the IMD in the estimation of the TX10p and

TX90p than the TN10p and TN90p, especially in the southern and central river basins, which is followed by the RFR MME. Though the simulation accuracy of estimating daily temperature is higher in the northern basins, higher correlations in these four indices are noted in the southern and central river basins. In the intensity-based maximum temperature indices, the central per-humid basins have a better correlation than the southern and northern basins. The XGBR MME has a higher correlation than the RFR, ETR, SVR, and AM in both frequency and intensity-based indices.

The RFR and XGBR MMEs perform well in replicating absolute rainfall indices and percentile-based indices, whereas the AM has a poor estimate of all rainfall indices, as indicated by the low correlation between the AM and IMD indices.

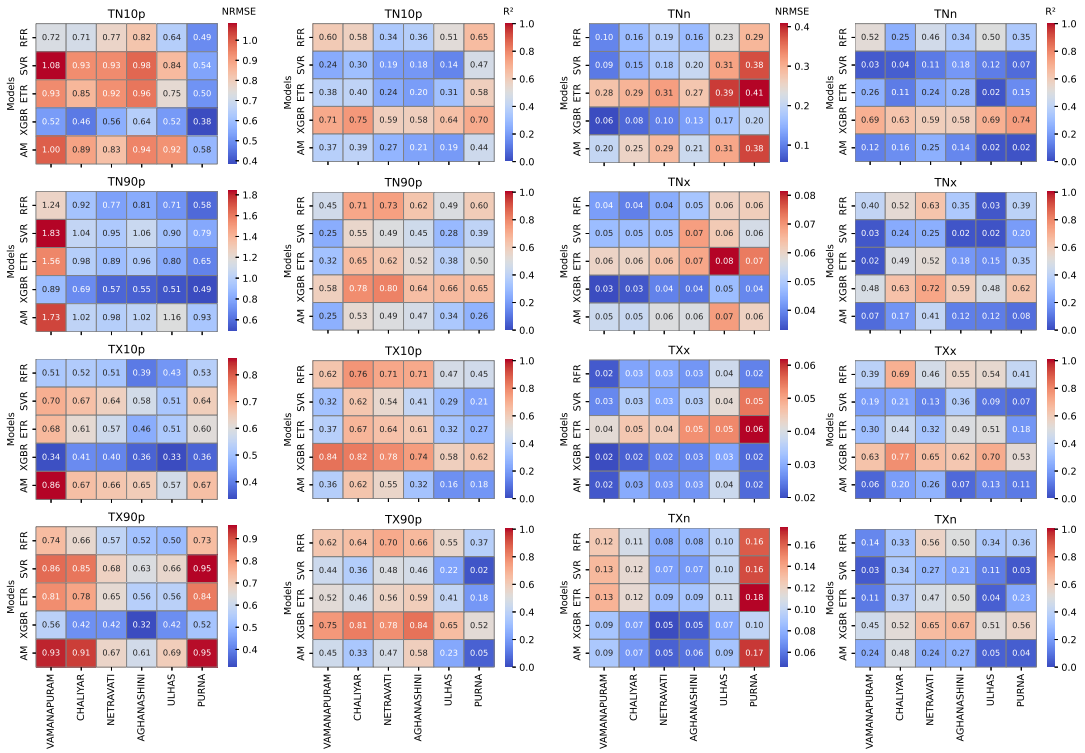

Fig. 6.5: Performance of temperature indices estimated from MMEs and observation

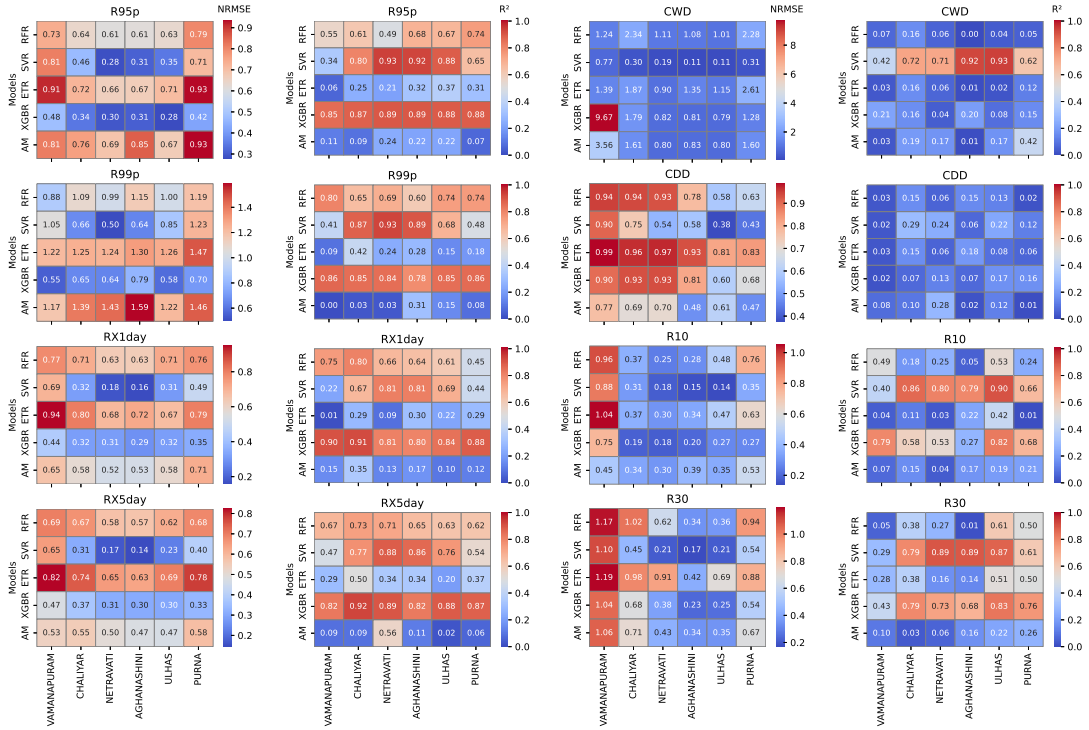

Fig. 6.6: Performance of rainfall indices estimated from MMEs and observation

6.3.3 Precipitation Indices

The RX1day and RX5day rainfall has been understated by all the MMEs in all six river basins. The maximum 1-day and 5-day rainfall have been poorly estimated by ETR with a mean relative bias ranging from 59-75%, followed by RFR (53-64%) and AM (38-55%). Though the annual rainfall is underestimated by SVR, the RX1day and RX5day have better estimations than other methods with a bias range of 18-53% followed by XGBR (29-43%). Figure 6.7 represents the temporal variation in the simulated percentile and absolute rainfall indices with mean and median. The R99p simulated by XGBR follows a similar distribution, mean as of the IMD, with the lowest bias range of 4-41 mm with highest bias in the ETR (31-73 mm). The RFR, ETR, and AM vary in distribution in all the basins. Though SVR underestimates the mean, it has a similar distribution as IMD for R95p, which is followed by XGBR (2-31%) (Figure 6.8). The bias in percentile indices is lowest in the dry sub-humid and per-humid basins than in the humid basins of the Ghat.

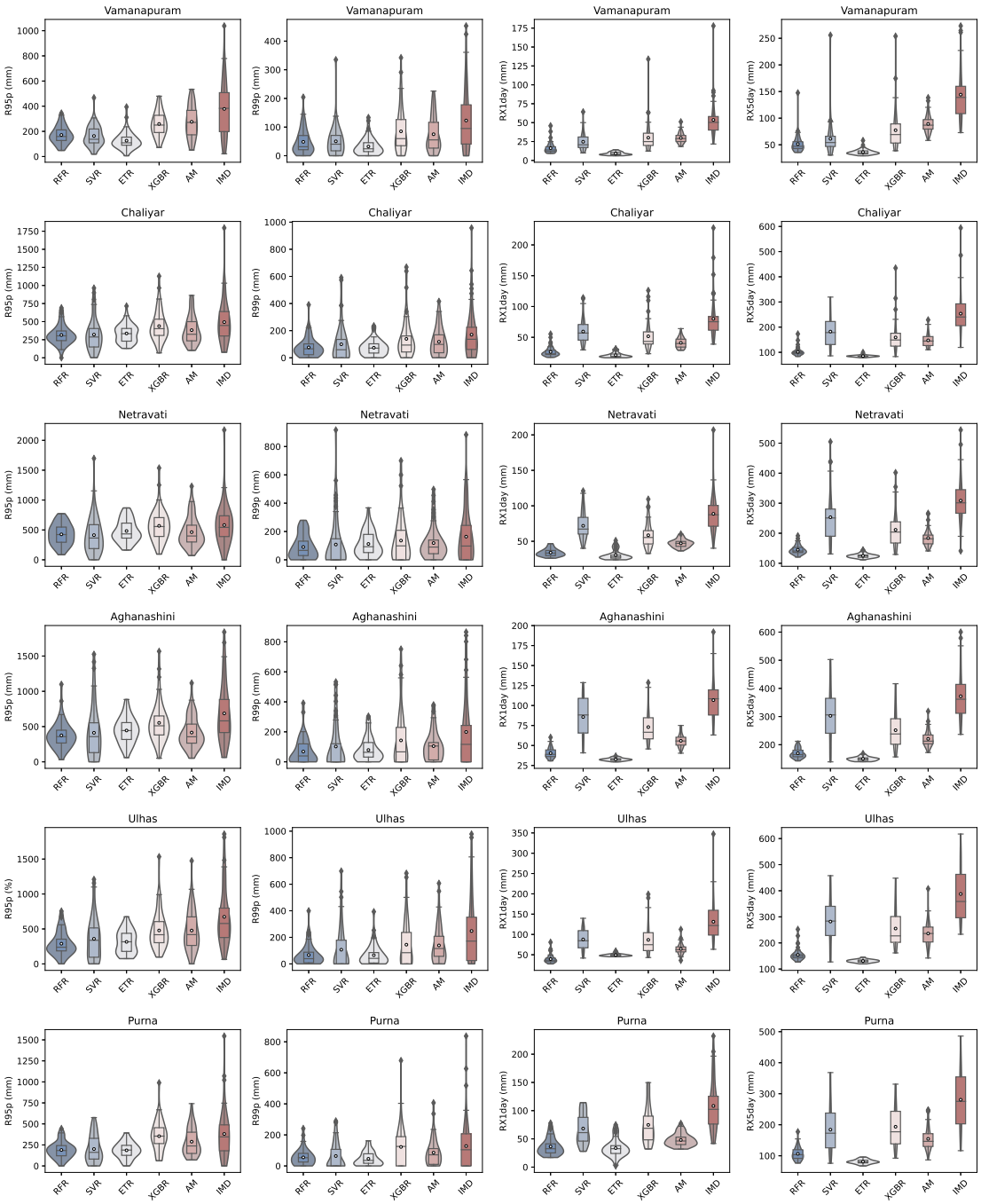

Fig. 6.7: The distribution of percentile and absolute based rainfall indices from five MME models with the observation

The duration-based indices, CDD and CWD, are poorly simulated by all the models except the SVR. A large negative bias is noted in the estimation of CDD by RFR, ETR, XGBR, and AM, and a positive bias in the SVR estimation. Whereas positive bias was noted in CWD estimation by all the MMEs in humid and dry-

sub-humid basins and negative bias in the per-humid basins. The inherent heterogeneity of the rainfall duration indices is captured using SVR MME. CDD has been overestimated approximately by 15-24 days in the southern basins, 33-43 days in the northern, -2.5 days in Netravati, and 43 days in Aghanashini. CWD

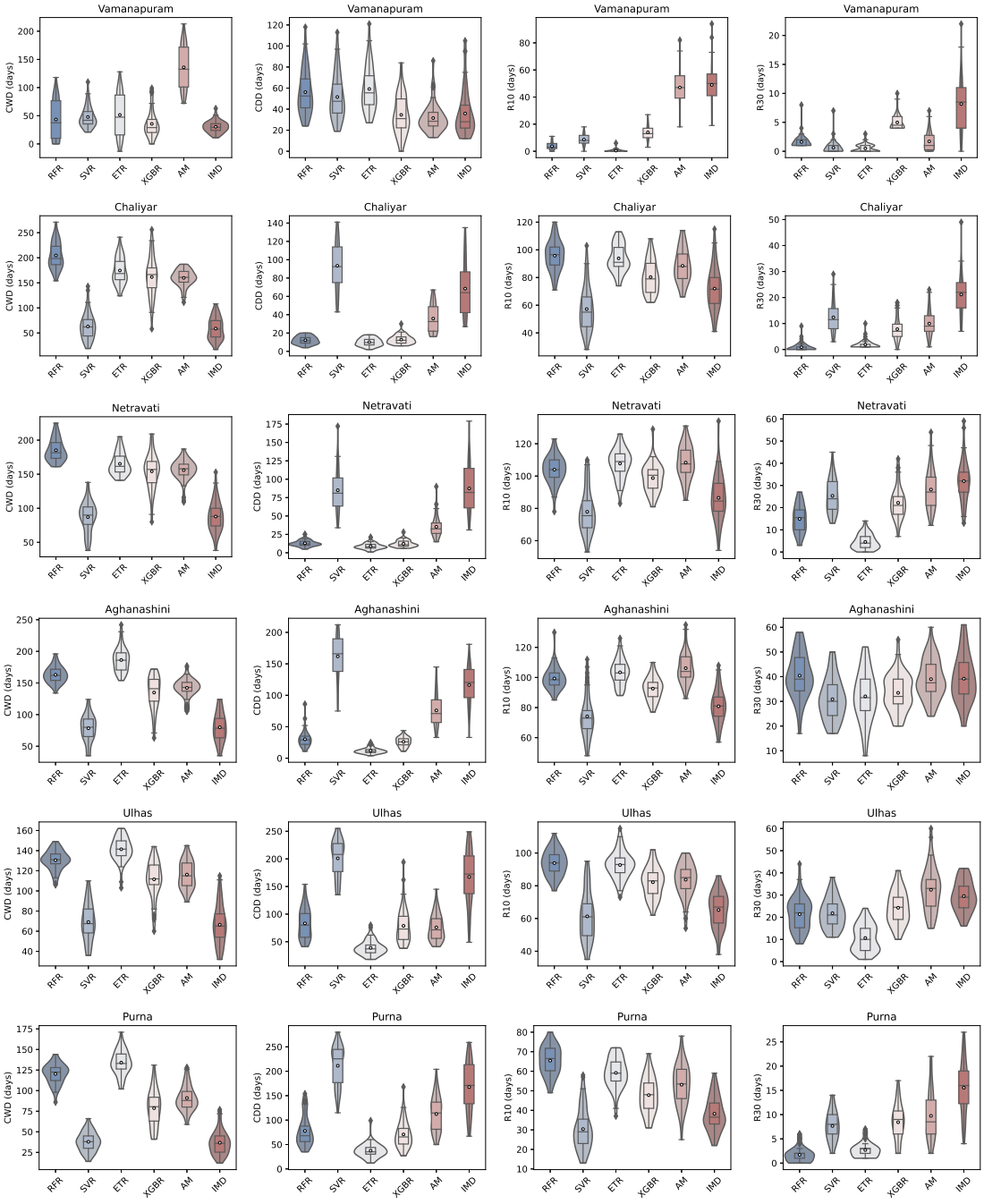

Fig. 6.8: The distribution of duration and threshold based rainfall indices from five MME models with the observation

substantially overstated by 4-17 days, 1-2.5 days, and negative bias of 1-1.5 days in central basins. The R10 and R30 days also have the nearest distribution and mean in SVR. The R10 has a negative bias of 4-8 days in the central and northern basins, with highest bias of 34 days in the Vamanapuram. R30 has a negative bias of 5-8 days. Relative to the number of days, the indices have been accurately predicted by the SVR MME.

6.3.4 Temperature Indices

The temporal variation in the temperature indices estimated from MMEs are shown in Figures 6.9, 6.10. The temperature-based indices are well simulated by all the MMEs with the nearest to observation simulation from XGBR MME. In all the MMEs, TN10p is underestimated, and TN90p is overestimated with good estimation in XGBR. A percentage bias of 1-1.7% in TN10p, and 4-6% in TN90p is noted in the central river basins. The TX10p and TX90p are accurately estimated by the XGBR, which can be noted from the bias $< 0.7\%$ in all the basins.

The intensity indices TXn, and TNn have a positive bias, TNn which represents the coldest night have a warm bias of 1-1.95^{o}C varying gradually from south to north of the Ghat. The coldest day temperature TXn is overestimated by 1-2.2^{o}C with respect to the observed temperature. Whereas the warmest day and night temperatures (TXx and TNx) have a cold bias of 0.65-1.25^{o}C in TXx and 0.65-1^{o}C in TNx.

6.3.5 Historical Trend Comparison of Indices

The trend in annual and seasonal rainfall is shown in Figure 6.11 is increasing in the Aghanashini and the northern basins, whereas it is decreasing in the other three basins. All MMEs tend to underestimate the trend relative to the trend observed in IMD, whereas the AM consistently overestimates the trend. The post-monsoon rainfall trend in MMEs are converse to the trend recorded in IMD. This is due to the overestimation of the post-monsoon rainfall by all the MMEs. The wet bias during the post-monsoon season is the most common bias observed in the CMIP

models. The past studies have noted the wet bias during post-monsoon and dry bias in pre-monsoon seasons in the CMIP6 (Ayugi *et al.*, 2021). In pre-monsoon, SVR and XGBR followed the trend direction; in winter rainfall southern basins noted an insignificant down trend and no trend in central and northern basins. The

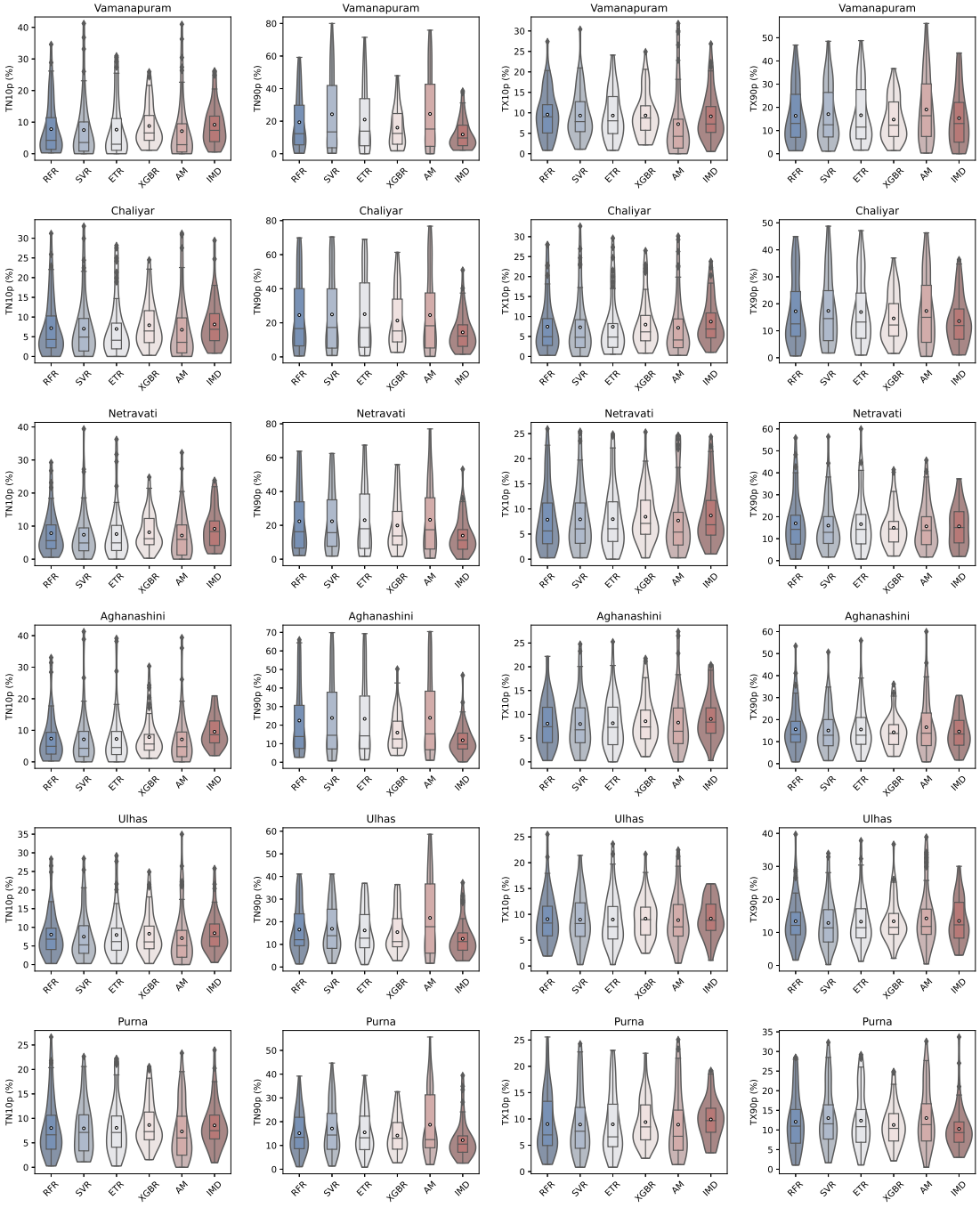

Fig. 6.9: The distribution of frequency based temperature indices from five MME models with the observation

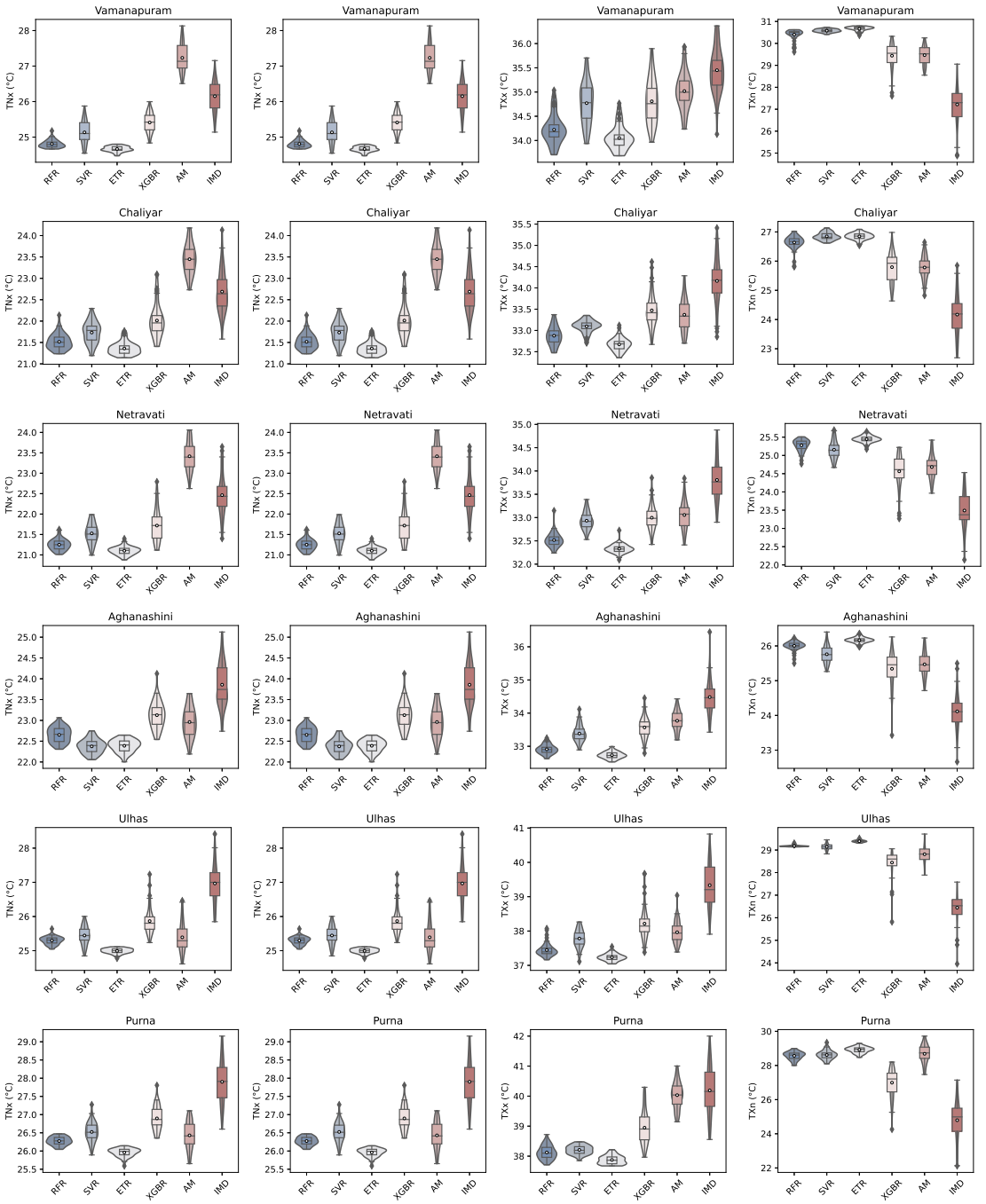

Fig. 6.10: The distribution of intensity based temperature indices from five MME models with the observation

maximum temperature (Figure 6.12) has seen an increase in all the seasons and in all the basins; all MMEs followed the trend direction but underestimated the trend magnitude, including the AM, which was over-predicted in all the scenarios. The minimum temperature (Figure 6.13) is also increasing in all the basins and all

the seasons, but the MME estimation is converse to the maximum temperature, where it over-predicts the trend compared to the IMD trend, and the maximum over-prediction is noted in the AM. The trend pre-monsoon temperature is under predicted by all the MMEs.

The trend in the indices calculated from the five MMEs and the IMD observed trend is shown in Figures 6.14. The Sen's slope was observed from the threshold-based indices, TN10p, TX10p, TN90p, TX90p, and the significance level is shown in Figure 6.14. All the MMEs have a trend in the same direction for all four indices and in all six river basins. The trend in the TN10p is decreasing; the

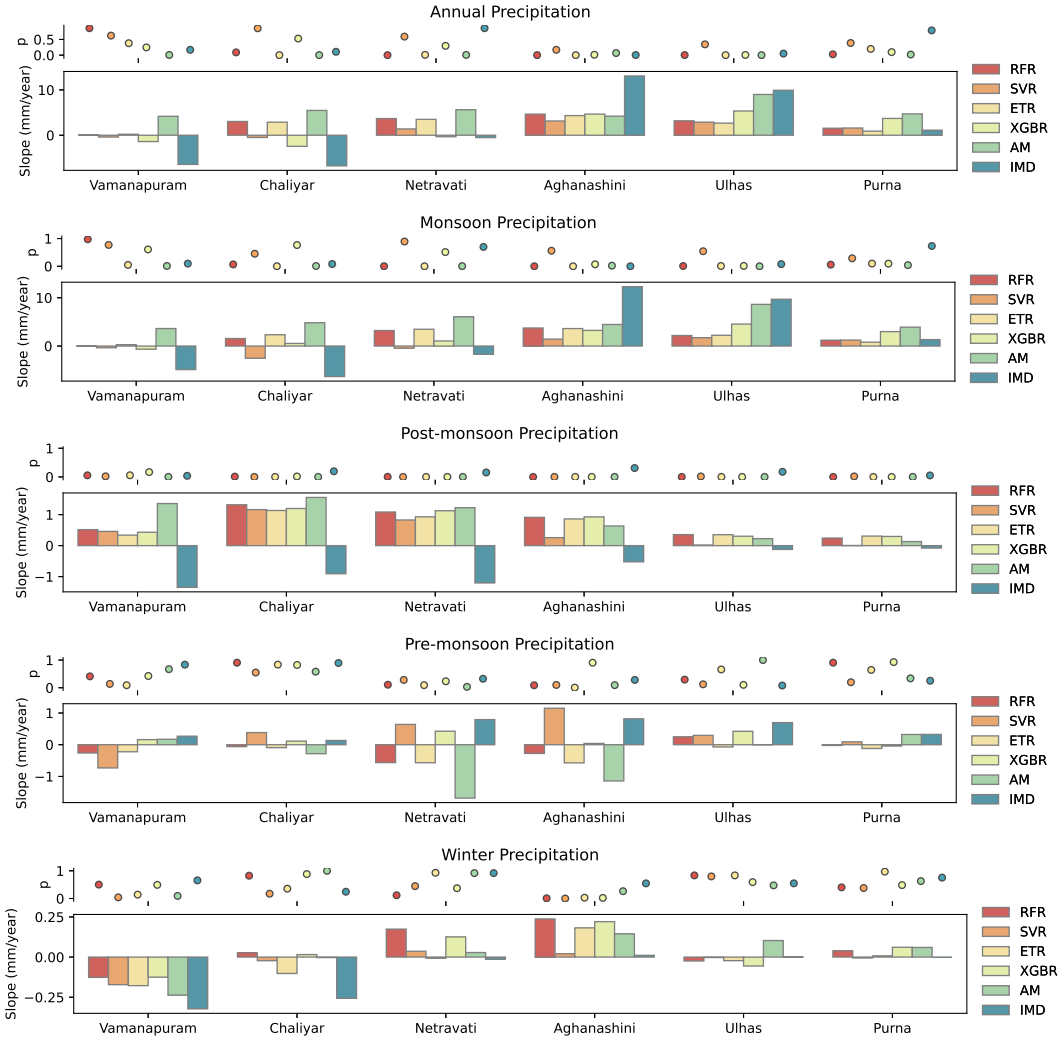

Fig. 6.11: Trend magnitude and direction in annual and seasonal rainfall estimated from MMEs and observation

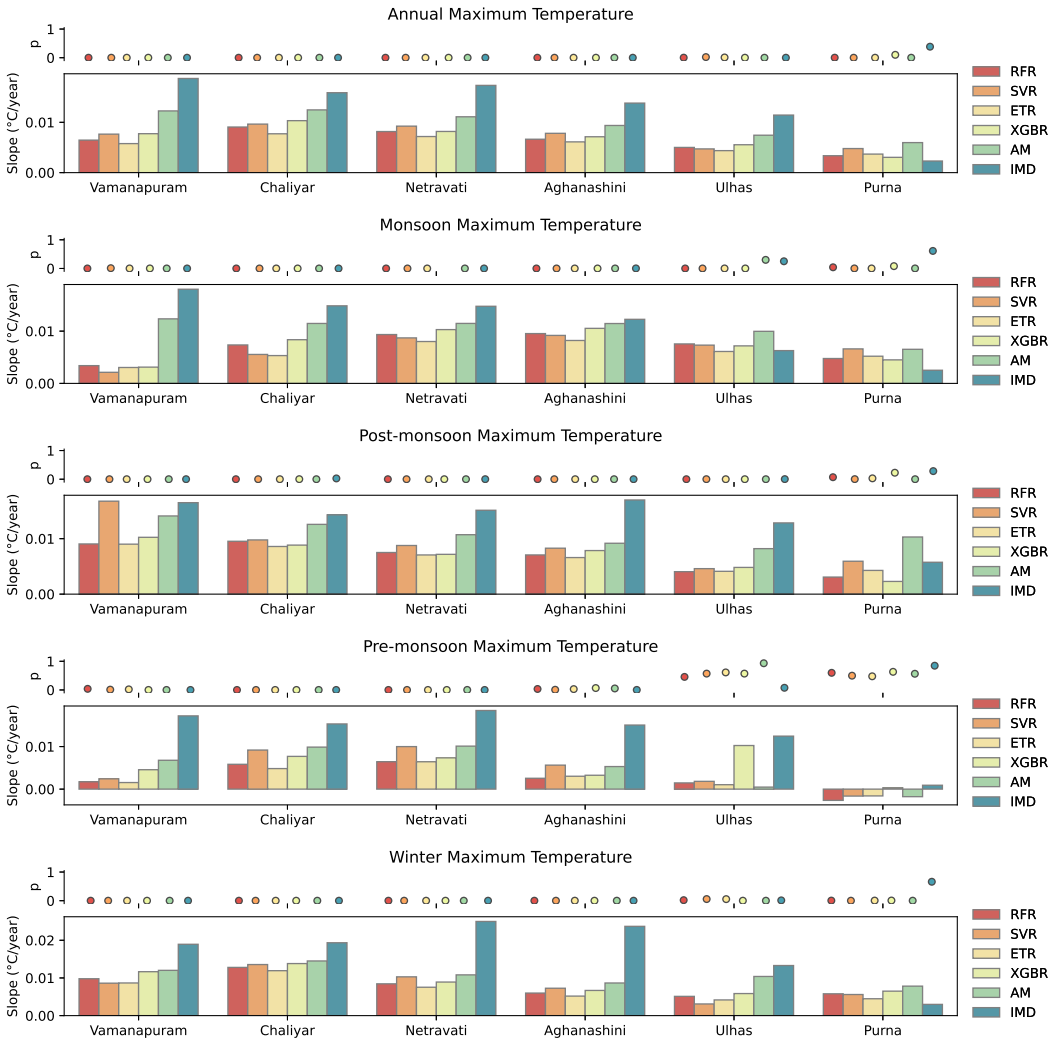

Fig. 6.12: Trend magnitude and direction in annual and seasonal maximum temperature estimated from MMEs and observation

southern basins and the northern basins have a decreasing trend at a magnitude of 0.145%/year and 0.137%/year, and the central basin Netravati has observed a trend of -0.092%/year with no significant trend in Aghanashini by the observed data. The TX10p is decreasing at a rate of 0.22%/year, 0.2%/year in southern and central basins and 0.1%/year in Ulhas, with no significant trend in the Purna basins. The reduction in the percentage of days with maximum and minimum temperature less than the 10^{th} percentile of base period days has been well simulated by all the MMEs, especially the XGBR. Whereas the percentage of days with maximum and minimum temperature more than the 90^{th} percentile of base period

days are increasing over all the basins with an insignificant increase in Aghanashini and Purna basin in the case of TN90p and in Purna river basin in TX90p. The trend in TX10p and TX90p are higher in the southern basins and are reducing towards the north. The intensity-based indices TNn, TNx, TXn, TXx are shown in Figure 6.15. Though TNn has no significant trend in the observed temperature, an insignificant upward trend is recorded in the southern and northern basins and a downward trend in the central river basins. But ETR has detected a significant declining trend in all the basins, whereas a significant increase trend is recorded by RFR, XGBR, and AM, and no significant trend in SVR over the southern

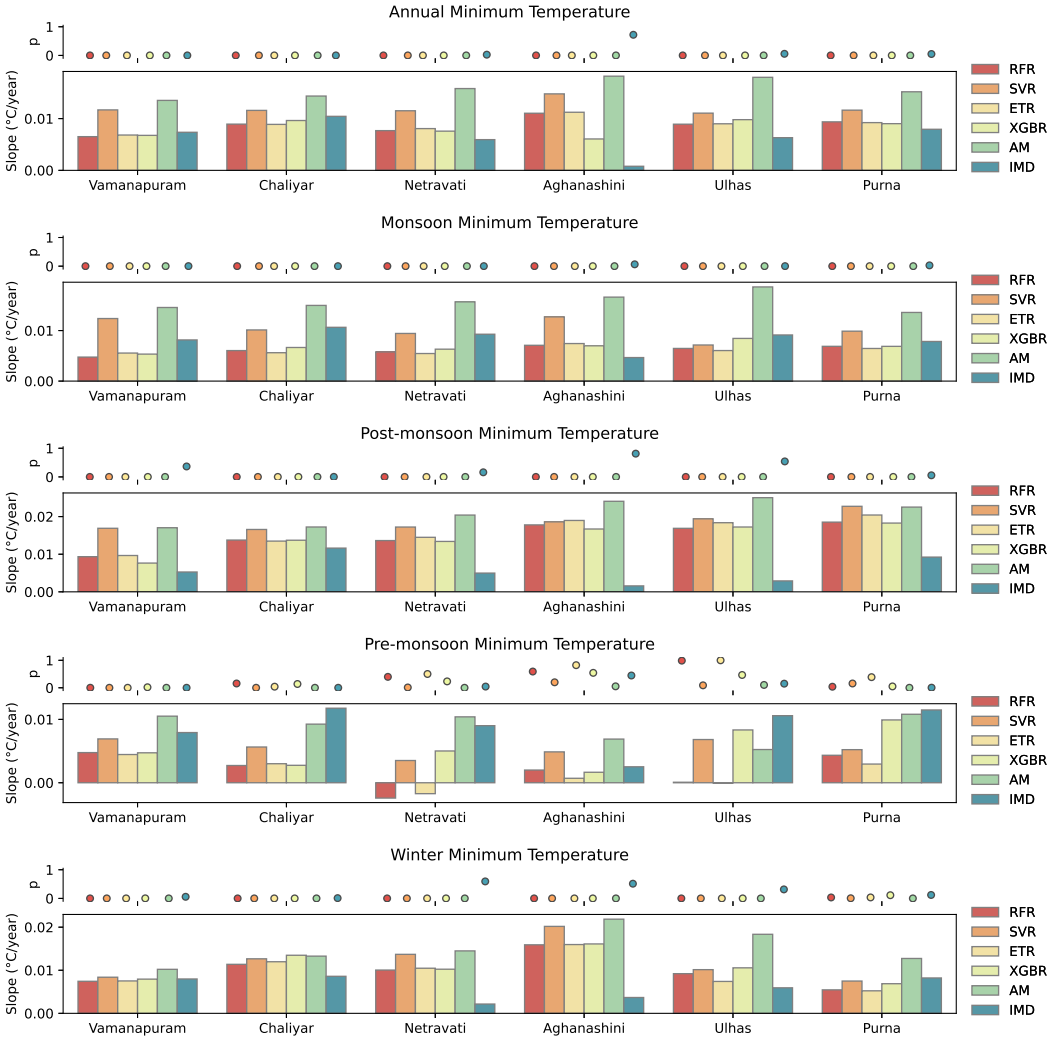

Fig. 6.13: Trend magnitude and direction in annual and seasonal minimum temperature estimated from MMEs and observation

Ghats. A significant increasing trend in TNx is recorded in the IMD over Chaliyar, and Netravati, an insignificant downward trend in Aghanashini and Ulhas, insignificant upward in Vamanapuram and Purna. A minimal difference in the trend noted in Ulhas by the MMEs when compared to the IMD trend. TXn has recorded a significant upward trend of the same magnitude in southern and central river basins, whereas the RFR, XGBR, and IMD have noticed no significant trend in Ulhas, XGBR, AM, and IMD in Purna. The trend in TXx is actively captured by the MMEs over southern basins; in central and northern basins, the RFR and XGBR have detected no significant trend but are similar to IMD in magnitude and direction.

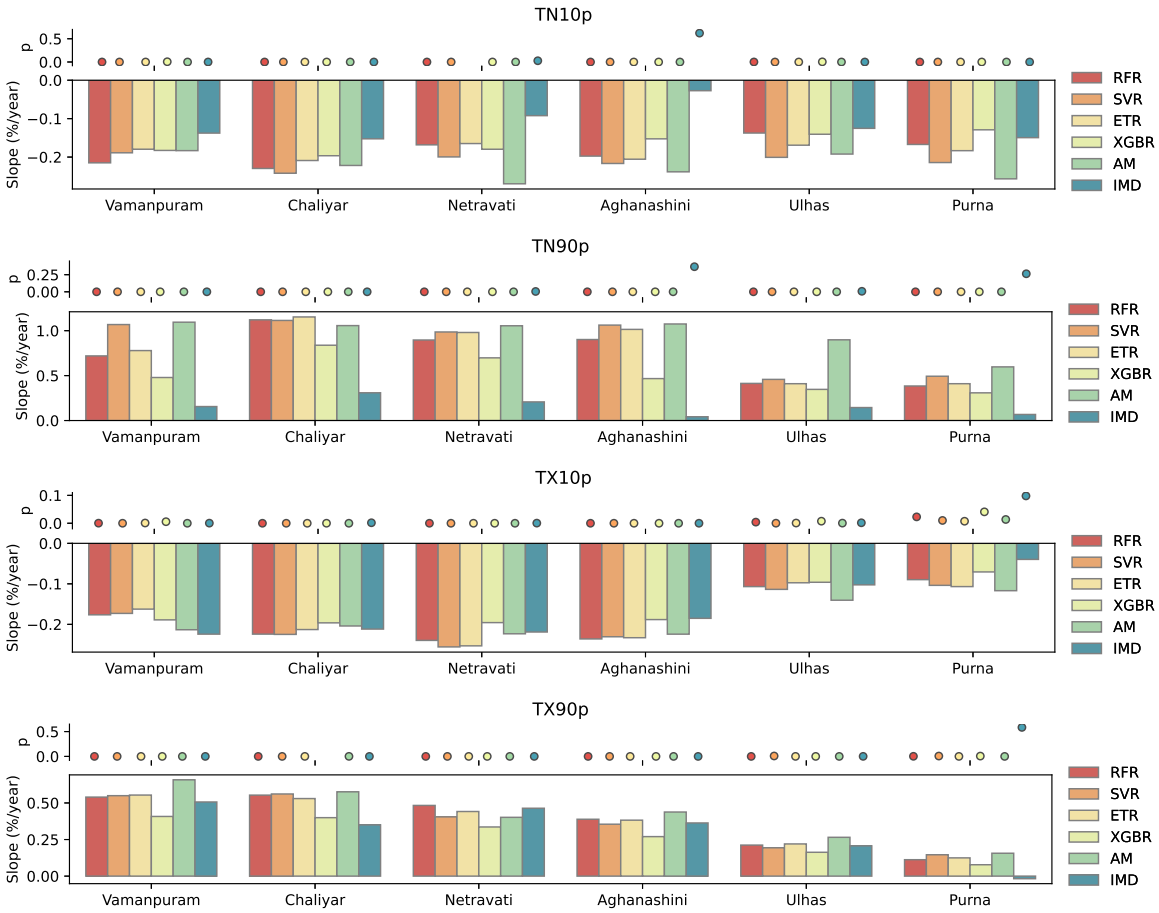

Fig. 6.14: Trend magnitude and direction in frequency based temperature indices estimated from MMEs and observation

In the case of rainfall indices, there is a huge variation in the estimated trend

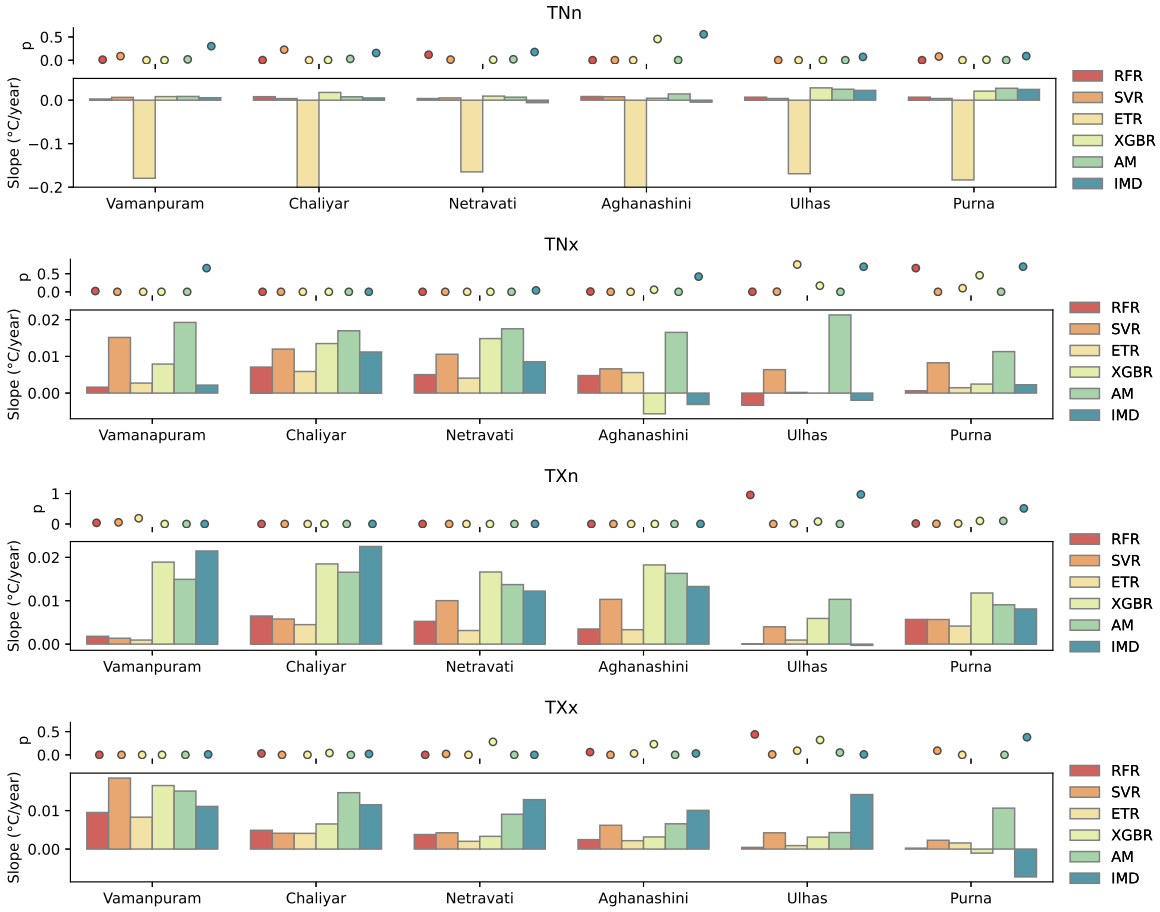

Fig. 6.15: Trend magnitude and direction in intensity based temperature indices estimated from MMEs and observation

from different MMEs. In R95p, the SVR has shown decreasing trend in all the basins; the XGBR and IMD have trend in the same direction with a higher magnitude in XGBR than IMD over the southern basins and the Netravati. In Aghanashini, the decreasing trend is recorded by XGBR, and no significant trend in other MMEs, whereas an increasing trend is recorded in the Ulhas by IMD and no significant trend by other MMEs. No significant trend was noted in R99p in IMD, XGBR, ETR, SVR, but a significant decrease is recorded by RFR and an insignificant increase by AM over Vamanapuram. In Chaliyar, Netravati, and Aghanashini, no significant trend was detected by IMD, but a significant decreasing trend is recorded by XGBR and SVR. In the northern basins, IMD has a significantly increasing trend in Ulhas and no trend in the Purna basin, the direc-

tion of the trend is captured by other MMEs with variability in magnitude.

The trend in RX1day rainfall (Figure 6.16) captured by the MMEs and the IMD varies mainly in the direction. RX1day has no significant observed trend in the southern and central basins but is significantly decreasing in the SVR and XGBR. A significant/insignificant increase in Ulhas and Purna is captured in the observed rainfall, whereas the RFR, ETR, SVR, and XGBR have not captured these trend effectively. The most considerable inconsistencies are present in the trend of percentile and absolute rainfall indices. (Avila-Diaz *et al.*, 2020; de Medeiros *et al.*, 2022) noted the similar variation in the trend of these indices. In R10, an insignificant decrease is recorded in Vamanapuram by IMD, XGBR, and RFR. In Chaliyar, IMD and MMEs have detected trends in opposite direc-

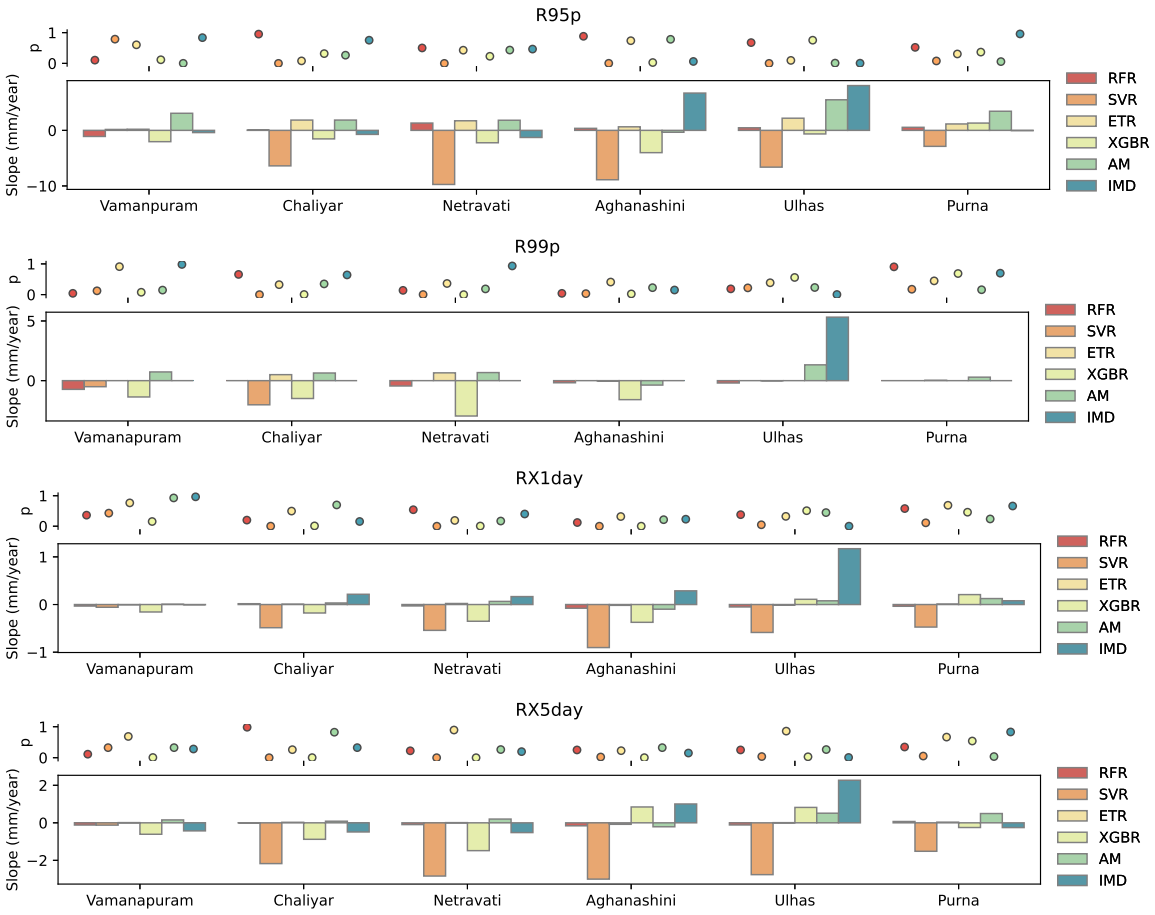

Fig. 6.16: Trend magnitude and direction in percentile and absolute rainfall indices estimated from MMEs and observation

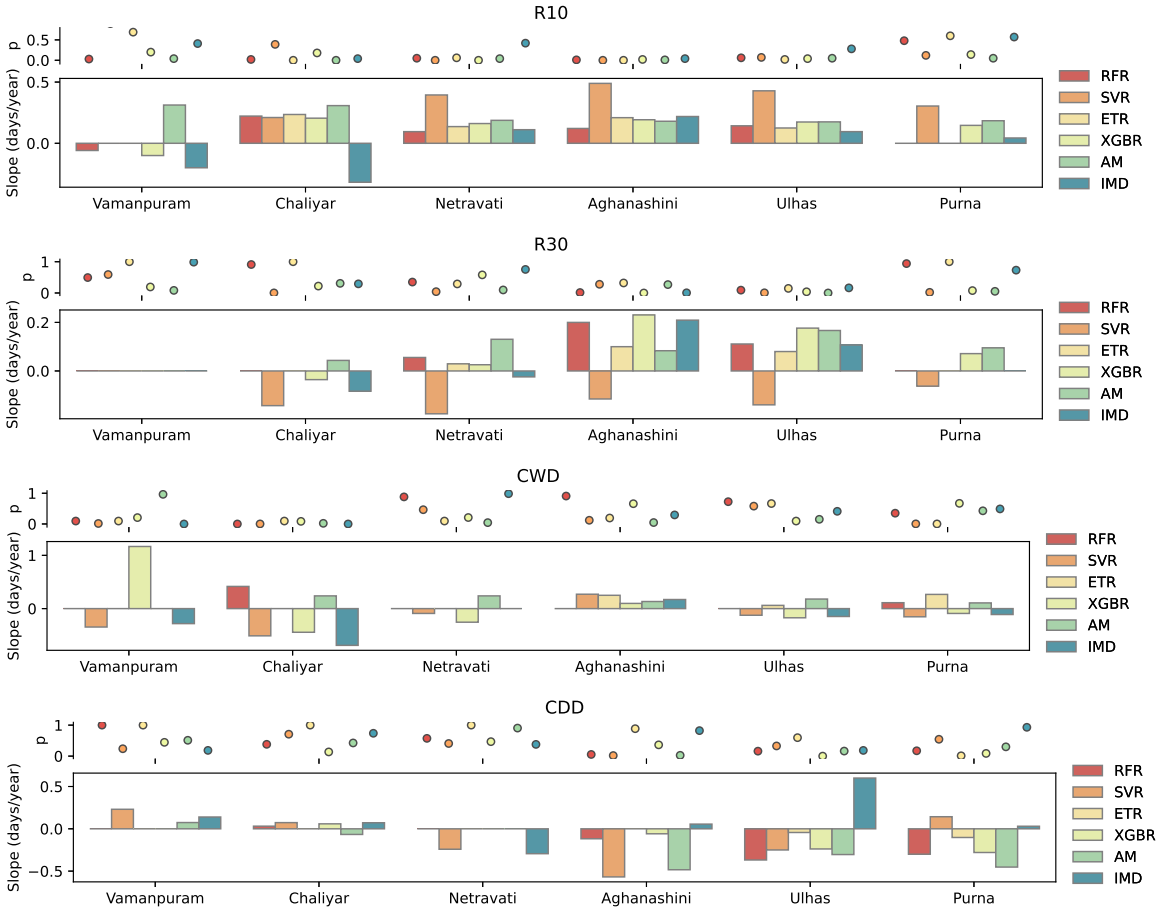

Fig. 6.17: Trend magnitude and direction in threshold and duration based rainfall indices estimated from MMEs and observation

tions, whereas the increasing trend is recorded in both central and northern basins by all the MMEs and IMD. In R30, insignificant trends following the direction of the trend observed in IMD can be noted in Figure 6.17 over all the basins except the Aghanashini, where the significant trend is recorded in both RFR, XGBR, and IMD. The decreasing trend in SVR is common in most of the indices. In duration indices, CDD insignificant increase in trend is recorded in southern basins, and a significant decrease in CWD in IMD data. Except the AM, other MMEs followed the trend with similar magnitude. The trend in CWD in southern basins and Netravati, follows the IMD trend magnitude and direction, whereas the trend observed is converse to IMD trend in other basins.

6.3.6 The Quantification of Projected Changes in Rainfall

The projected monthly anomalies in the precipitation with respect to the period 1961-1990 under SSP245 and SSP585 scenarios are shown in Figure 6.18 for the southern basin, 6.19 for central basins and 6.20 for the northern basins of the Ghat. Higher percentage anomalies are observed in the Aghanashini and northern river basins compared to the southern river basins. In Vamanapuram, positive anomalies in rainfall increase in May, August, and September, while in Chaliyar, they occur in May, June, September, and October. Notably, in Chaliyar, July

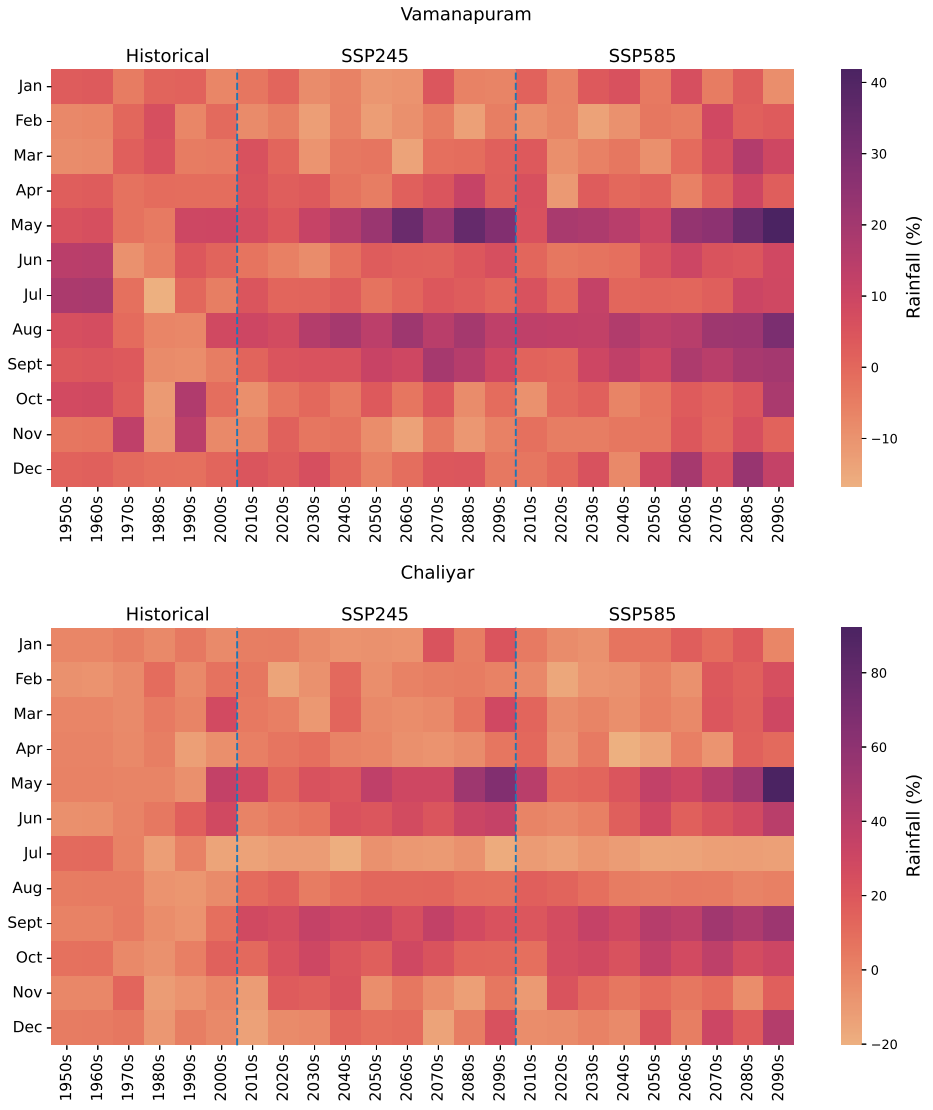

Fig. 6.18: Projected changes in monthly anomalies (%) of rainfall in southern basins

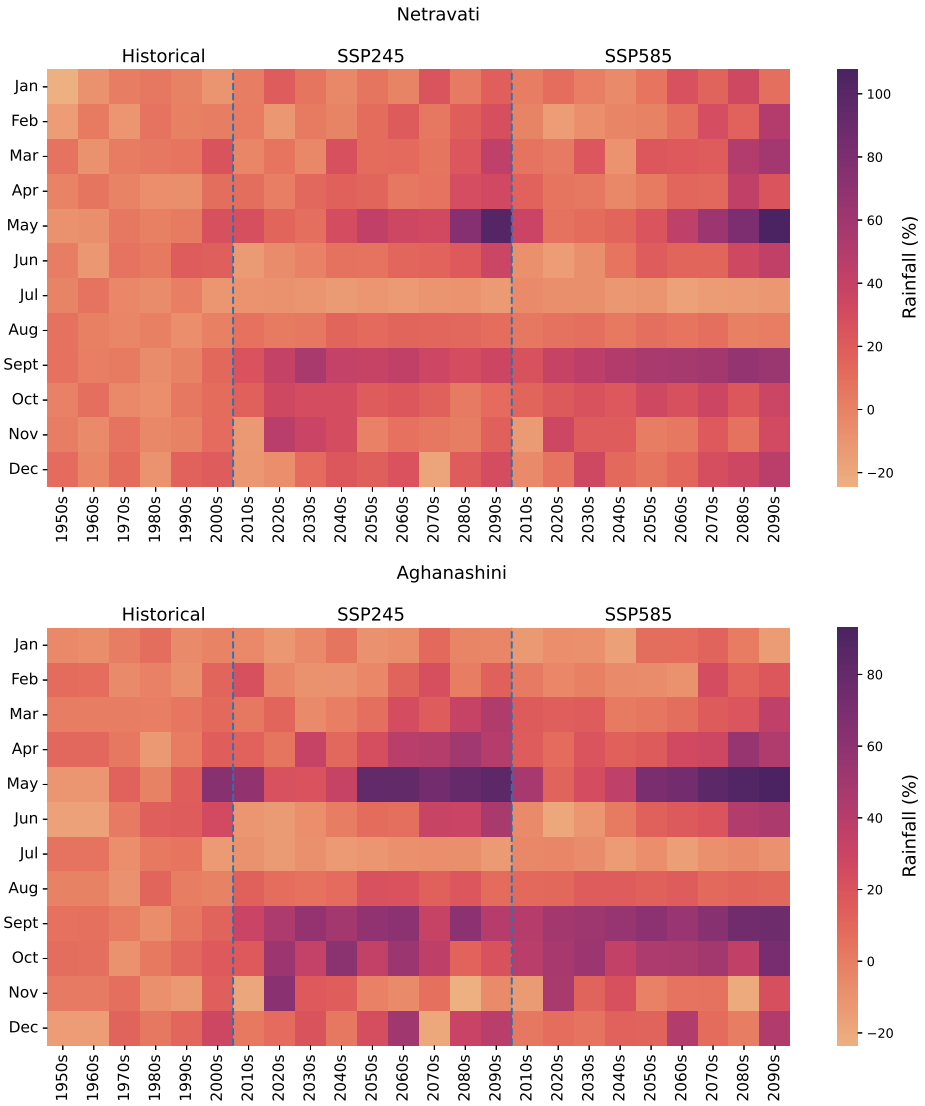

Fig. 6.19: Projected changes in monthly anomalies (%) of rainfall in central basins

rainfall, which contributes 25-30% of the annual rainfall, is projected to decrease in the future decades, with the maximum decrease observed in the SSP585 scenario. In both river basins, the pre-monsoon month of May shows an increase in rainfall ranging from 20-43% in Vamanapuram after the decade 2030 under a medium emission scenario and a decade earlier in the high emission scenario. The central river basins typically receives 25-30% of their rainfall in July and $\leq$ 10% in September. However, in the future, these basins are expected to experience a slight decrease in July rainfall and increase in September. While June rainfall shows a negative anomaly in the two decades 2020 and 2030, future projections

indicate an increase after the decade 2040s along with increased rainfall in May. The Aghanashini basin has already witnessed an increase in May rainfall, which is projected to intensify in the future decades, particularly after the 2040s, with a strong anomaly of up to 60-80% increase. Although July rainfall decreases, June and August experience higher rainfall after the decade 2040s, with a higher percentage increase observed in September and October. In the northern river Ulhas, a significant positive anomaly in rainfall of 40-120% compared to the base period is observed in September, October, and November under both emission scenarios. Currently, in the Ulhas basin, June contributes up to 15% and July contributes

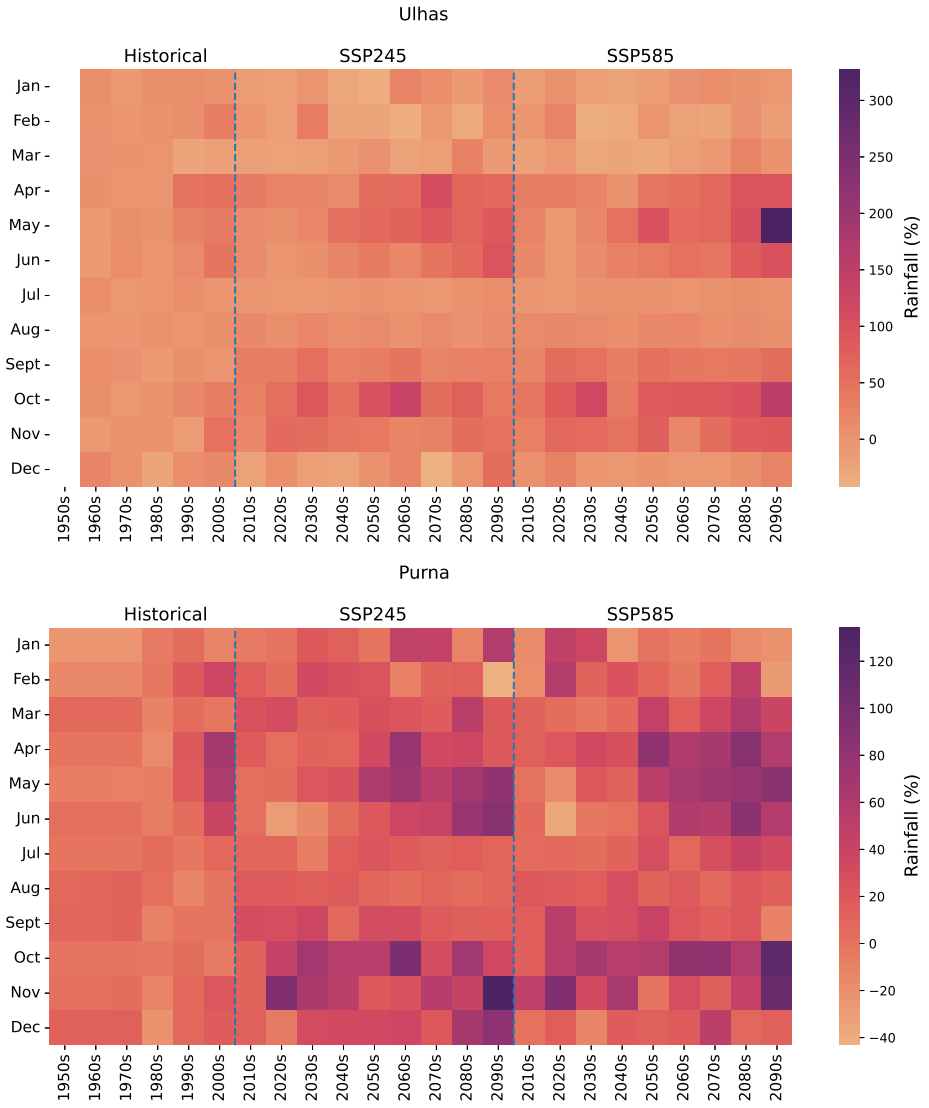

Fig. 6.20: Projected changes in monthly anomalies (%) of rainfall in northern basins

around 35-40% of the annual rainfall. However, in the near future decades, the basin is projected to experience a higher percentage of rainfall in June, while the percentage contribution decreases in July, especially after the 2030s. September and the post-monsoon months exhibit a positive anomaly greater than 30%. In the Purna basin, there has been an increase in rainfall during April, May, and June in the decade 2000s, and this increase becomes more pronounced after the mid-21st century. Similar to the Ulhas basin, the Purna basin also shows a higher percentage anomaly in October and November in both emission scenarios. The study conducted by Kumar *et al.* (2023) highlights the anticipated increase in rainfall in India in the coming decades. The observed progressive increase from March to October can be attributed to the influence of radiative forcing, which demonstrates its strength over time.

6.3.7 The Quantification of Projected Changes in Temperature

The projected monthly anomaly in the southern basin in maximum temperature, minimum temperature, and mean temperature is shown in Figures 6.21, 6.22. The temporal variation in the monthly anomaly of temperature is different in the two southern river basins located in the different climates of the WG. Figures 6.21 indicate the increase of up to 4 °C in mean temperature, and 4.3 °C, 3.5 °C in the maximum and minimum temperature by the end of the century in Vamanapuram river basin. The increase in maximum temperature is high (6 °C) in the Chaliyar basin than in the Vamanapuram basin. The magnitude of the anomaly is greater in the high-emission scenario compared to the medium-emission scenario. The gradual rise in temperature has already commenced, with the most significant increase projected to occur after the mid-century in the SSP245 scenario and after the decade 2030s in the SSP585 scenario. In the medium emission scenario, the warming increases in the basin in the month of February to May, and the month of May experiences a 2.5-3.5 °C increase which persists into the month of June in the decade 2040s. This leads to a pronounced intensification of winter temperatures and an extension of the summer season. The July and August months

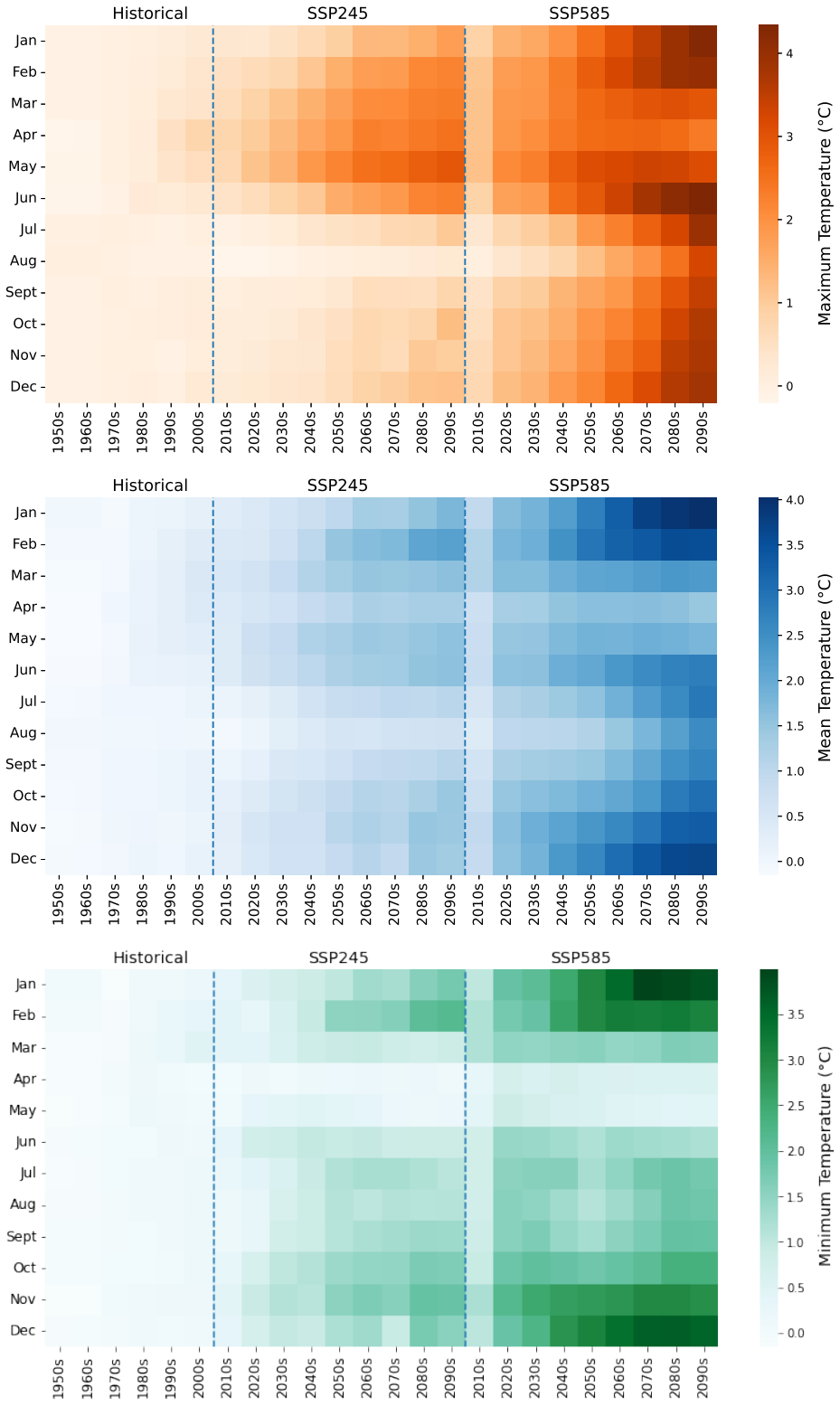

Fig. 6.21: Projected changes in monthly anomalies of maximum, mean and minimum temperature (°C) in Vamanapuram basin

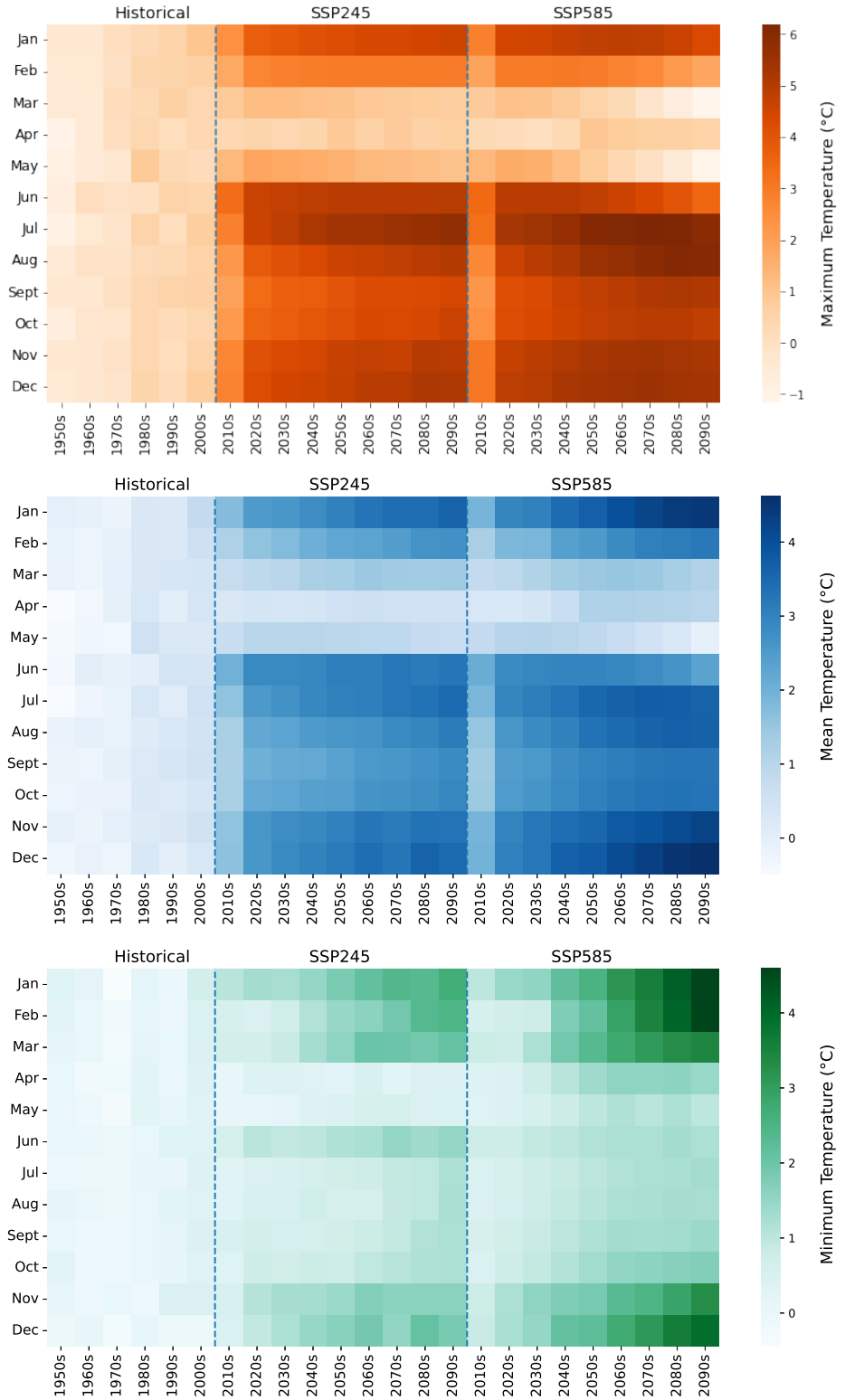

Fig. 6.22: Projected changes in monthly anomalies of maximum, mean and minimum temperature (°C) in Chaliyar basin

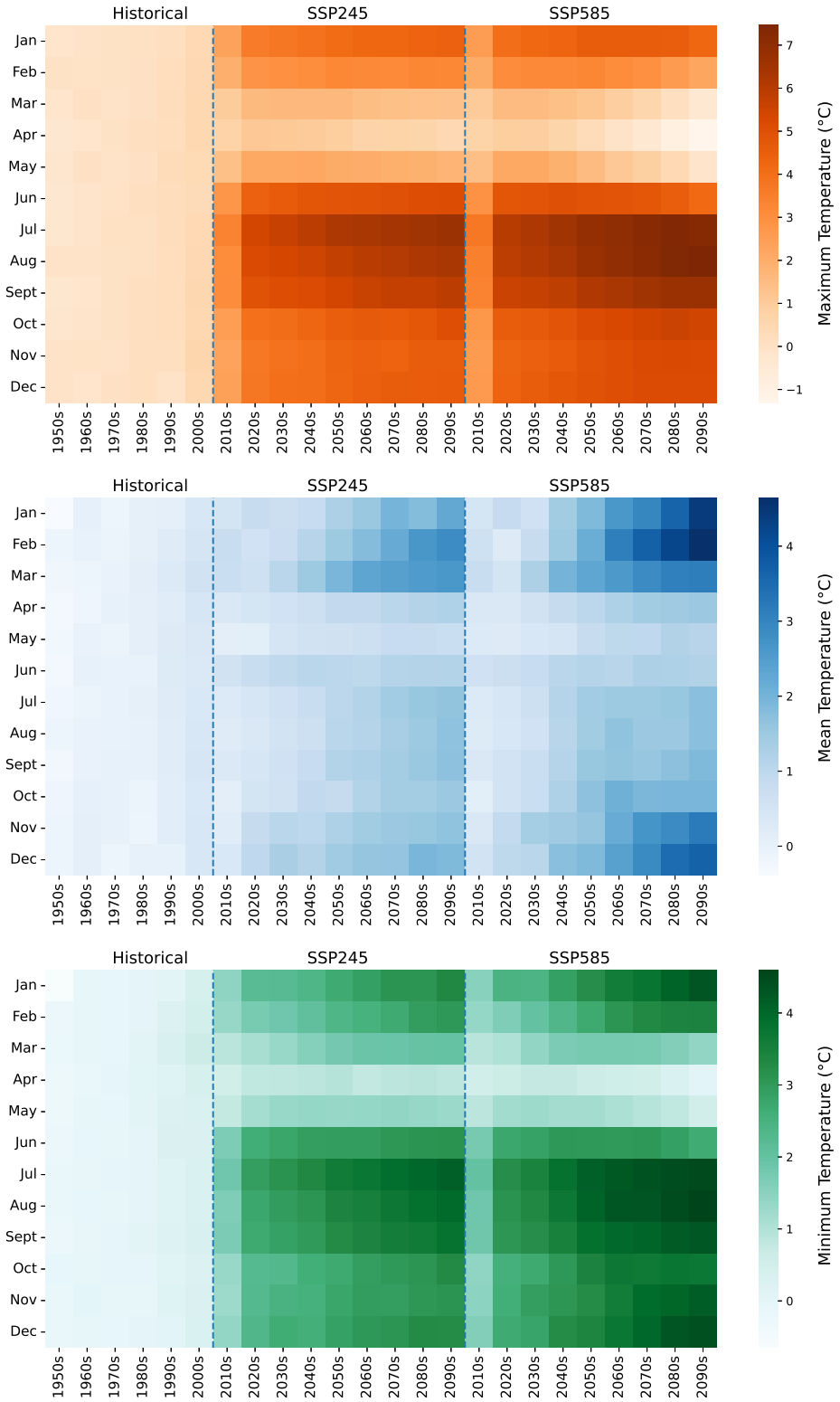

Fig. 6.23: Projected changes in monthly anomalies of maximum, mean and minimum temperature (°C) in Netravati basin

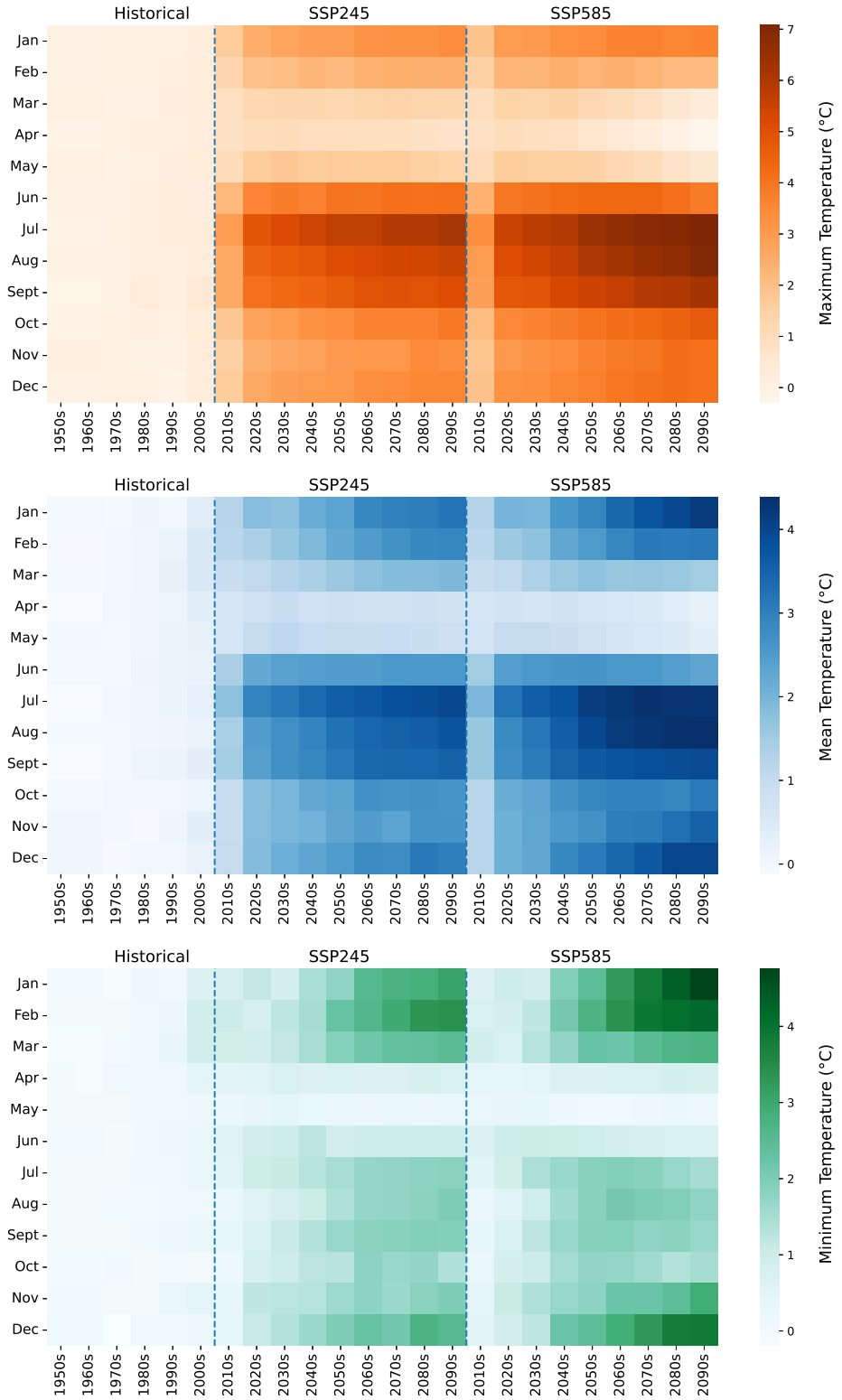

Fig. 6.24: Projected changes in monthly anomalies of maximum, mean and minimum temperature (°C) in Aghanashini basin

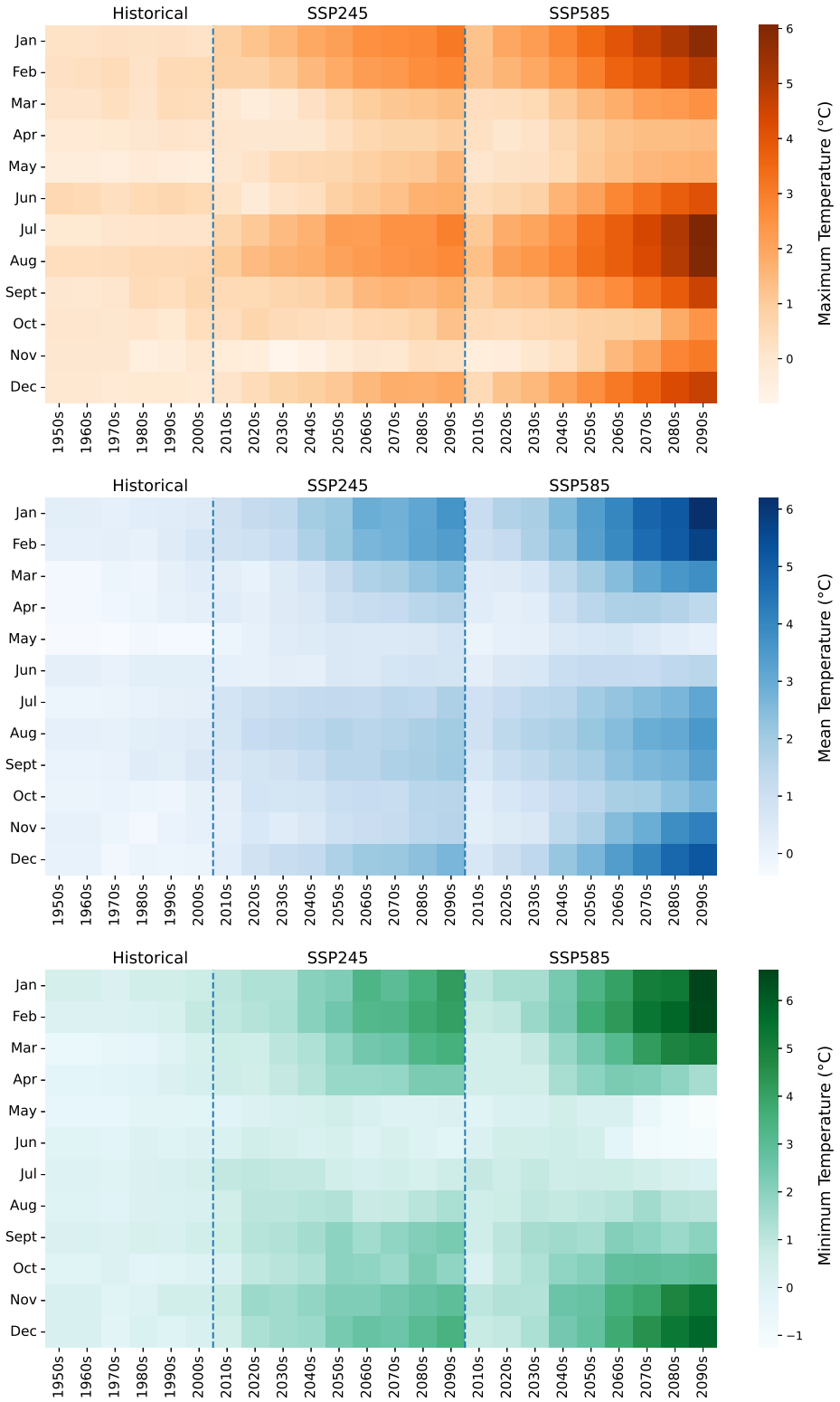

Fig. 6.25: Projected changes in monthly anomalies of maximum, mean and minimum temperature (°C) in Ulhas basin

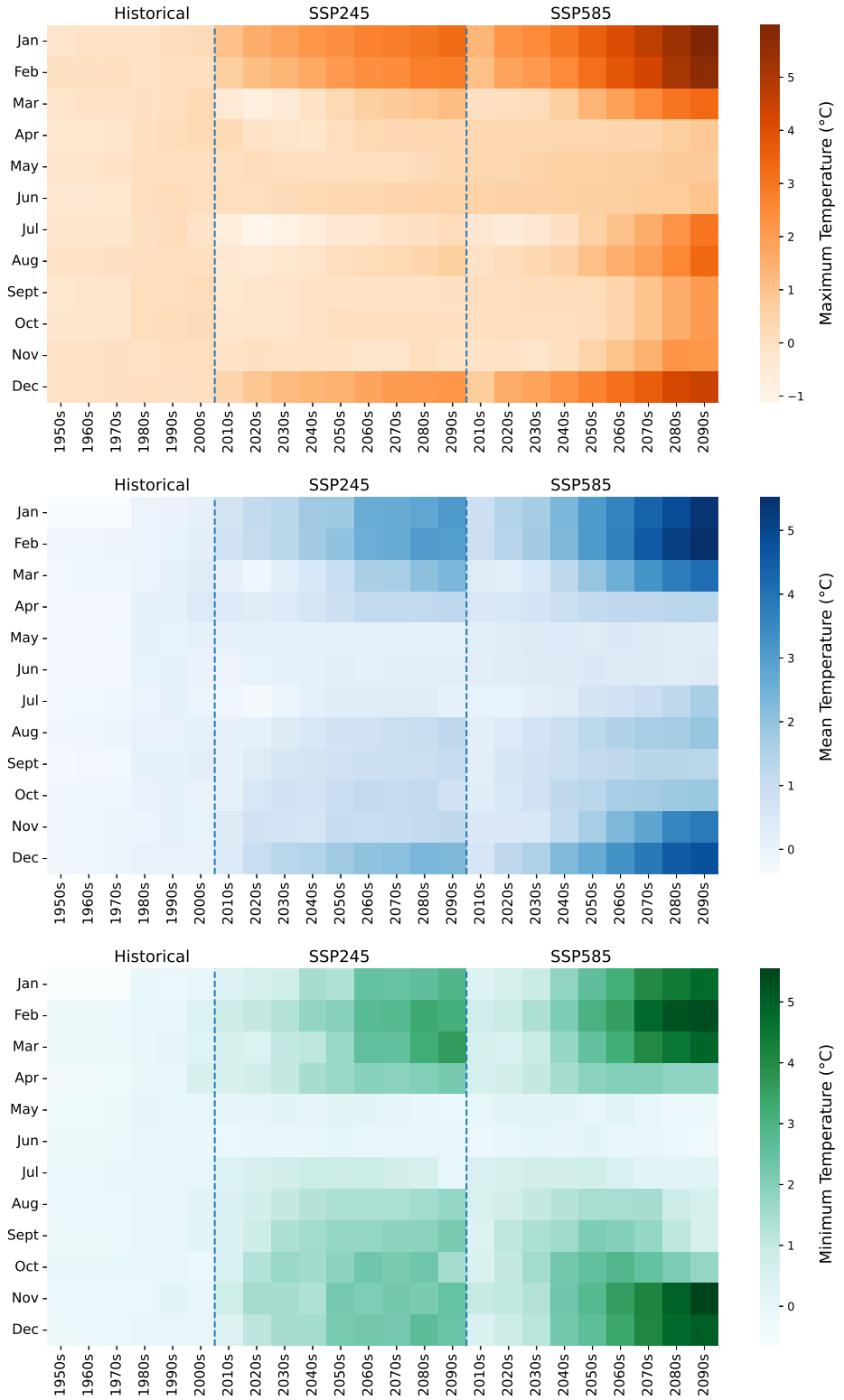

Fig. 6.26: Projected changes in monthly anomalies of maximum, mean and minimum temperature (°C) in Purna basin

experience a lower rate of increase in temperature. Whereas in the high emission scenario, the month of June emerges as the hottest month, especially after the decade 2070. In the case of minimum temperature, the rate of increase during the summer months is relatively lower compared to other months, with the anomaly being higher from October to February. In Chaliyar, higher anomaly is observed from June to January, and in both future scenarios, July shows an increase of up to 5 °C. The decrease in rainfall during the monsoon month of July in Chaliyar may be directly related to the increasing temperature during that month. The increase in minimum temperature is most pronounced in the months January, February, March, November, and December. However, in June, the rate of increase is higher in the SSP245 scenario compared to the high emission scenario, SSP585.

In the central basin Netravati, the highest increase in both maximum and minimum temperature is recorded in the monsoon months (up to 7.3 °C and 4.6 °C). The basin experience a decrease in the maximum temperature in the summer months at the end of 21st century under both scenarios. The rise in minimum temperature is highest in January and in the monsoon months; due to this, the mean temperature increases by 2-4.5 °C in the winter season after the decade 2050. Whereas, the basin Aghanashini records an increase in minimum temperature in the winter season than any other seasons after mid-century. The maximum temperature records the highest increase in the monsoon months (up to 7 °C) than the summer months, and overall the increase in mean temperature will be noted in the monsoon and winter months.

The increase in maximum and minimum temperature in the northern basins of the Ghats will be higher after mid 21st century. The mean temperature warms highly in the winter and monsoon months up to 3.5 °C (6 °C) in SSP245 (SSP585) scenario. Theminimum temperature records a higher increase during the winter season especially after 2050. The Purna basin experience a increase of 3 °C (5.5 °C) in SSP245 (SSP585) scenario in minimum temperature. The mean temperature increases over 2 °C after the decade 2050 in SSP245 and a decade earlier under SSP585 scenario. (Joshi *et al.*, 2011; Jiang *et al.*, 2016) have also predicted the

occurrence of an average 2 °C warming threshold after the decade 2040s–2060s with a delay of a decade or two in the lower emission scenarios. Wehner *et al.* (2020) showed that the warming over India is as hot as the warming shown by the emissions, i.e.,3.5 to 5.5 °C increase in mean temperature. This is evident even in the river basins located in the dense forest mountains of the Western Ghats. A study by Krishnan *et al.* (2020) suggested that unusual warming up to 4.4 °C by the end of the 21st century over India in conjunction with an increase in the number of hot days in CMIP5 high emission scenarios. The change noted in the river basins are in accordance with the previous studies in India. The higher warming in winter and monsoon months indicates that the traditional summer season is anticipated to commence earlier, prolong its duration, and intensify in terms of heat. (Kumar *et al.*, 2023) conveyed the earlier commencement of summer season in the India after the mid century. The heightened thermal conditions will exert a substantial influence on diverse domains, encompassing human and animal health, agricultural practises, ecological systems, and energy generation. Therefore, in order to quantify the rate of change in both the maximum and minimum temperatures and the rainfall over the future horizon is obtained by trend analysis methods, which are explained in the following sections.

6.3.8 Trend in Rainfall, Maximum and Minimum Temperatures

a) Southern River Basins of the Western Ghats

Figure 6.27 shows the temporal variation in rainfall and the maximum and minimum temperature in the southern river basins. The change in the mean rainfall and temperature in different seasons and their trend over the future horizon in the southern river basins are given in Table 6.2 and 6.3. The southern basins Vamanapuram and Chaliyar have seen a significant/insignificant decreasing trend in the historical rainfall in all the seasons, with a significant downward trend of 22.71 mm/decade in the pre-monsoon in Vamanapuram, 54.92 mm/decade, and 74.33 mm/decade in monsoon and annual rainfall in the Chaliyar basin. The historical maximum temperature and minimum temperature have seen a significant upward

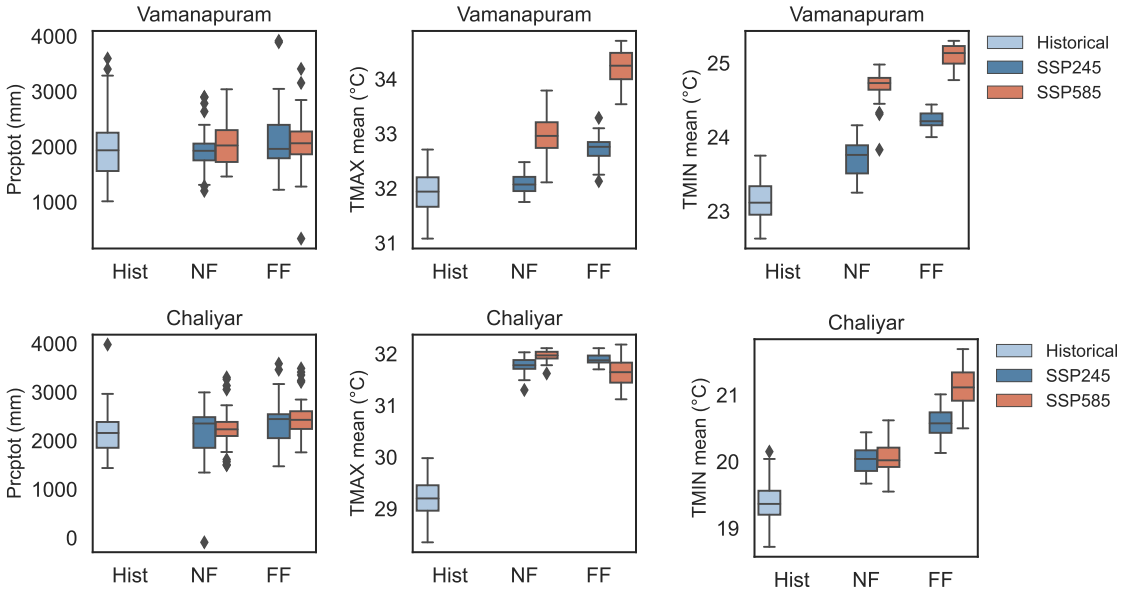

Fig. 6.27: The variation in the mean rainfall, mean maximum and minimum temperature in the historical and future horizon by MME of CMIP6 SSP245 and SSP585 scenario over the southern river basins

trend in both the basins in all the seasons with 0.07 °C/decade, 0.11 °C/decade in annual maximum temperature, 0.13 °C/decade and 0.16 °C/decade in annual minimum temperature in Chaliyar and Vamanapuram respectively. This is in accordance with the trend noted in the IMD observed rainfall and temperature (Vijay *et al.*, 2021). The minimum temperature is more susceptible to warming especially in the winter season showing a increase at a rate of 0.11 - 0.19 °C/decade.

In the near future, the basins will experience an significant(insignificant) increase in the monsoon rainfall by 8.63 mm -9.34 mm (19.26 mm -27.54 mm) per decade in Vamanapuram (Chaliyar). In other seasons and annual rainfall, Vamanapuram experience an insignificant increasing trend of 6.13 mm/decade and decreasing trend in Chaliyar by 31.05 mm/decade under medium emission scenario, and upward trend of 17.44 mm/decade, 14.92 mm/decade in high emission scenario with an insignificant decreasing trend in winter season in Vamanapuram, and pre-monsoon rainfall in Chaliyar under SSP585. The increase in the precipitation in the climate change scenario is attributed to the increase in water vapor due to the rise in CO_2 (Meehl *et al.*, 2005; Varghese *et al.*, 2020). An increase of

0.31 °C/decade in maximum temperature in the pre-monsoon temperature, 0.25 °C/decade in the minimum monsoon temperature is noted in the near future under SSP245 scenario, and an increase of 0.27 °C/decade in pre-monsoon and monsoon maximum temperature with no significant trend in the minimum temperature is noted in the later scenario with the rise in the minimum temperature in the winter season by 0.38 °C/decade in Vamanapuram. The Chaliyar basin experiences an upward trend of 0.12 °C/decade in maximum annual temperature, 0.15 °C/decade in minimum temperature. The pre-monsoon season's maximum temperature does not show a significant trend, while the maximum temperature during the monsoon season increases at a rate of 0.3 °C/decade. The winter temperature trend in the basin is more pronounced, with an increase of 0.4 °C per decade, which is twice the rate of increase in the minimum temperature during other seasons. In the future, under the SSP245 scenario, the basin is projected to sustain a rise in winter minimum temperature at a rate of 0.25 °C per decade, and under the SSP585 scenario, this increase is even higher at 0.35 °C per decade, along with increases in temperatures in other seasons. The increase in greenhouse gas concentration has higher repercussions on the daily minimum temperature than the daily maximum temperature (Easterling *et al.*, 1997; Varghese *et al.*, 2020). Therefore the minimum temperature is more susceptible to change significantly in the winter season.

After the mid-21st century, both the river basins encounters an significant increase in rainfall especially under the SSP585 scenario. The annual rainfall increases at rate of 38.57 mm/decade and 59.09 mm/decade in the Vamanapuram and Chaliyar basins respectively. The pre-monsoon (20.5($\pm$5.2) mm/decade) and monsoon rainfall (14.14 mm per decade in Vamanapuram and 32.97 mm per decade in Chaliyar) increases under the high emission scenario. Whereas, the higher rate of increase of 0.39 °C/decade (0.19 °C/decade) in the SSP585 (SSP245) is observed in the winter maximum temperature (minimum temperature) in Vamanapuram (Chaliyar). Interestingly, the decline in the pre-monsoon maximum temperature (0.15 °C/decade) under the high emission scenario is noted in the Chaliyar basin.

Though the trend decreases towards the end of the century, a 2.14(±0.28) °C increase in the maximum pre-monsoon temperature, 2.5(±0.85) °C (1.94(±0.48) °C) in the minimum winter temperature over Vamanapuram (Chaliyar).

b) Central Rivers Basins of the Western Ghats

Figure 6.28 shows the temporal variation in rainfall and the maximum and minimum temperature in the southern river basins. The change in the mean rainfall and temperature in different seasons and their trend in the historical period and in the future horizon in the central river basins are given in Tables 6.4 and 6.5. The historical precipitation has a reverse trend in the two river basins belonging to a per-humid climate. The Netravati basin has experienced an insignificant declining trend in both annual (31.10 mm/decade) and monsoon (39.01 mm/decade) and a significant declining trend of magnitude 12.96 mm/decade in the pre-monsoon season. On the other hand, the Aghanashini basin has experienced an upward trend in annual and monsoon rainfall, with an increase of 130.83 mm/decade and 122.91 mm/decade, with an insignificant downward trend in the pre-monsoon (5.22 mm/decade) season. The historical maximum temperature observed an increasing trend in the range of 0.04-0.08 °C/decade, and the minimum temperature in the range of 0.12-0.19 °C/decade in the central river basins.

Under the medium emission scenario (SSP245), annual rainfall in the river basins in the NF continues its downward trend, with the Netravati basin seeing a decrease in annual rainfall by 26.76 mm/decade and an increase in pre-monsoon rainfall by 17.47 mm/decade. Aghanashini observes an increasing trend of 5.89 mm/decade in post-monsoon and an insignificant increasing trend in annual and other seasonal rainfall. The warming trend is more severe in the near future period than in the far future, especially in the winter season. The near future is anticipated with a significant increasing trend in all the seasons except pre-monsoon maximum temperature with a higher rate of increase in the minimum winter temperature. Under the high-emission scenario, however, an increase in precipitation is noted across both basins. Netravati river basin experience a significant increase of 60.31 mm/decade and 41.46 mm/decade in the annual and monsoon rainfall,

Table 6.2: Trend analysis of rainfall and temperature in Vamanapuram river basin of Western Ghats

		Precipitation				Maximum Temperature				Minimum Temperature			
	Series	Mean (mm)	Trend	Statistic Value	Sen's Slope (mm/decade)	Mean (°C)	Trend	Statistic Value	Sen's Slope (°C/decade)	Mean (°C)	Trend	Statistic Value	Sen's Slope (°C/decade)
Historical (1951-2013)	Annual	1855	No trend	-1.37	-107.30	31.84	**Increasing**	5.44	0.11[a]	23.07	**Increasing**	3.82	0.16 [a]
	Winter	174	No trend	0.35	0.97	31.18	**Increasing**	13.54	0.11[a]	21.60	No trend	1.91	0.19[a]
	Pre-monsoon	292	**Increasing**	-2.07	-22.71[c]	33.77	**Increasing**	3.46	0.11[a]	24.21	No trend	0.91	0.14[a]
	Monsoon	851	No trend	-1.67	-78.50	31.65	**Increasing**	8.01	0.12[a]	23.66	**Increasing**	3.12	0.17[a]
	Post-monsoon	538	No trend	0.21	-7.69	30.76	**Increasing**	4.77	0.11[a]	22.83	**Increasing**	3.85	0.15[a]
Near Future (2021-2050) SSP245	Annual	1905	No trend	0.82	6.13	32.29	**Increasing**	5.72	0.18[a]	23.67	**Increasing**	7.17	0.20[a]
	Winter	186	No trend	-0.93	-2.68	31.87	**Increasing**	7.23	0.15[a]	22.30	**Increasing**	6.20	0.20[a]
	Pre-monsoon	309	No trend	0.35	2.43	34.60	**Increasing**	5.57	0.31[a]	24.49	**Increasing**	5.11	0.13[a]
	Monsoon	920	**Increasing**	2.46	8.63[b]	31.43	**Increasing**	4.41	0.12[a]	24.20	**Increasing**	6.84	0.25[a]
	Post-monsoon	489	No trend	0.41	2.24	31.25	**Increasing**	3.02	0.09[a]	23.68	**Increasing**	4.59	0.19[a]
Near Future (2021-2050) SSP585	Annual	1917	No trend	1.32	17.44	33.26	**Increasing**	6.08	0.26[a]	24.67	**Increasing**	4.88	0.11[a]
	Winter	185	No trend	-0.04	-0.22	33.00	**Increasing**	4.59	0.26[a]	23.72	**Increasing**	5.92	0.38[a]
	Pre-monsoon	308	No trend	0.69	4.67	35.46	No trend	5.21	0.27	25.10	No trend	0.40	0.01
	Monsoon	935	**Increasing**	2.24	9.34[c]	32.30	**Increasing**	6.79	0.27[a]	25.01	No trend	-0.10	-0.01
	Post-monsoon	489	No trend	0.72	4.82	32.27	**Increasing**	5.44	0.21[a]	24.86	**Increasing**	4.43	0.15[a]
Far Future (2051-2100) SSP245	Annual	1950	No trend	1.89	10.08	33.06	**Increasing**	6.24	0.14[a]	24.20	**Increasing**	3.85	0.04[a]
	Winter	183	No trend	0.90	2.12	32.75	**Increasing**	7.56	0.16[a]	23.13	**Increasing**	4.72	0.16[a]
	Pre-monsoon	332	No trend	1.62	6.46	35.66	**Increasing**	4.97	0.13[a]	24.57	**No trend**	-1.03	-0.03[b]
	Monsoon	951	No trend	0.62	2.16	32.03	**Increasing**	4.32	0.12[a]	24.69	No trend	0.03	0.00
	Post-monsoon	483	No trend	-0.30	-1.62	31.82	**Increasing**	5.19	0.14[a]	24.41	**Increasing**	3.36	0.08[a]
Far Future (2051-2100) SSP585	Annual	2031	**Increasing**	5.15	38.57[a]	34.70	**Increasing**	7.11	0.32[a]	25.11	**Increasing**	2.77	0.07[a]
	Winter	203	No trend		-0.72	34.71	**Increasing**	6.04	0.39[a]	25.03	No trend	1.92	0.10
	Pre-monsoon	338	**Increasing**	4.10	15.33[a]	36.21	No trend	0.76	0.02	25.02	No trend	-0.38	0.00
	Monsoon	975	**Increasing**	3.35	14.14[a]	34.00	**Increasing**	8.67	0.46[a]	25.12	**Increasing**	3.29	0.10[a]
	Post-monsoon	515	**Increasing**	2.59	10.50[a]	33.86	**Increasing**	9.04	0.45[a]	25.27	**Increasing**	5.22	0.09[a]

Note: Bold indicates statistically significant values. a 0.1% significance level; b 1% significance level; c 5% significance level

Table 6.3: Trend analysis of rainfall and temperature in Chaliyar River Basin of Western Ghats

		Precipitation				Maximum Temperature				Minimum Temperature			
	Series	Mean (mm)	Trend	Statistic Value	Sen's Slope (mm/decade)	Mean (°C)	Trend	Statistic Value	Sen's Slope (°C/decade)	Mean (°C)	Trend	Statistic Value	Sen's Slope (°C/decade)
Historical (1951-2013)	Annual	2185	Decreasing	-1.61	-74.33[c]	29.24	**Increasing**	5.22	0.16[a]	19.32	**Increasing**	5.50	0.13[a]
	Winter	40	No trend	-1.16	-1.96	28.95	**Increasing**	5.79	0.19[a]	17.18	**Increasing**	2.59	0.11[a]
	Pre-monsoon	223	No trend	-1.29	-12.18	32.14	**Increasing**	2.21	0.14[a]	20.72	**Increasing**	3.10	0.13[a]
	Monsoon	1586	Decreasing	-1.75	-54.92 [b]	27.71	**Increasing**	3.98	0.14[a]	20.07	**Increasing**	4.40	0.11[a]
	Post-monsoon	336	No trend	-0.13	-0.39	28.14	**Increasing**	3.76	0.15[a]	19.31	**Increasing**	4.17	0.13[a]
Near Future (2021-2050) SSP245	Annual	2423	No trend	-1.22	-11.05	32.36	**Increasing**	5.56	0.12[a]	19.96	**Increasing**	5.69	0.15[a]
	Winter	110	No trend	-0.72	-1.75	32.50	**Increasing**	5.98	0.15[a]	18.13	**Increasing**	6.74	0.25[a]
	Pre-monsoon	272	No trend	1.76	11.77	33.14	**Increasing**	-4.70	-0.07[a]	21.13	**Increasing**	4.02	0.17[a]
	Monsoon	1645	No trend	1.30	19.26	31.79	**Increasing**	5.43	0.21[a]	20.55	**Increasing**	2.94	0.07[a]
	Post-monsoon	396	No trend	0.46	5.83	32.02	**Increasing**	3.96	0.17[a]	20.03	**Increasing**	4.23	0.12[a]
Near Future (2021-2050) SSP585	Annual	2422	No trend	1.14	14.92	32.69	**Increasing**	5.05	0.06[a]	20.02	**Increasing**	4.76	0.19[a]
	Winter	108	No trend	0.90	2.31	32.88	**Increasing**	3.94	0.11[a]	18.21	**Increasing**	8.20	0.35[a]
	Pre-monsoon	263	No trend	-0.44	-2.09	32.86	**Decreasing**	-5.08	-0.08[a]	21.18	**Increasing**	4.24	0.19[a]
	Monsoon	1652	No trend	1.40	27.54	32.38	**Increasing**	5.56	0.19[a]	20.57	**Increasing**	2.13	0.07[a]
	Post-monsoon	399	No trend	1.40	11.36	32.62	**Increasing**	4.59	0.16[a]	20.11	**Increasing**	4.08	0.19[a]
Far Future (2051-2100) SSP245	Annual	2503	No trend	0.11	0.98	32.66	**Increasing**	4.35	0.04[a]	20.52	**Increasing**	8.64	0.10[a]
	Winter	118	**Increasing**	3.78	2.19[a]	32.92	**Increasing**	5.82	0.05[a]	19.12	**Increasing**	5.55	0.17[a]
	Pre-monsoon	305	**Increasing**	2.71	16.53[a]	32.64	**Increasing**	-5.30	-0.10[a]	21.58	No trend	1.66	0.03
	Monsoon	1708	No trend	-1.47	-15.50	32.43	**Increasing**	5.01	0.08[a]	20.95	**Increasing**	6.91	0.13[a]
	Post-monsoon	372	No trend	-0.64	-4.35	32.63	**Increasing**	6.36	0.09[a]	20.42	**Increasing**	3.32	0.07[a]
Far Future (2051-2100) SSP585	Annual	2556	**Increasing**	5.13	59.09 [a]	32.54	**Decreasing**	-5.95	-0.09[a]	21.09	**Increasing**	10.30	0.18[a]
	Winter	130	No trend	1.79	3.52	32.87	**Decreasing**	-4.01	-0.12[a]	20.08	**Increasing**	11.17	0.39[a]
	Pre-monsoon	321	**Increasing**	6.44	25.80[a]	32.35	**Decreasing**	-9.54	-0.10[a]	21.83	**Increasing**	5.37	0.13[a]
	Monsoon	1698	**Increasing**	7.74	32.97[a]	32.85	No trend	-1.35	-0.03	21.35	**Increasing**	3.14	0.06[a]
	Post-monsoon	408	No trend	-0.04	-0.53	33.10	No trend	-0.02	0.00	21.09	No trend		0.23

Note: Bold indicates statistically significant values. a 0.1% significance level; b 1% significance level; c 5% significance level

and an insignificant increase of 24.32 mm/decade and 35.94 mm/decade in the annual and monsoon rainfall in the Aghanashini river basin.

In the FF, as expected under the climate change scenario, both the basins have to endure an increase in rainfall. A trend magnitude of 39.45 mm/decade (SSP245) and 72.19 mm/decade (SSP585) in annual rainfall in Netravati and 115.22 mm/decade (SSP585) in annual rainfall in Aghanashini with significant/ insignificant increase in pre-monsoon/winter rainfall is noted. The basin has to endure an increase of 0.19 °C/decade in maximum monsoon temperature, 0.23 °C/decade, and 0.24 °C/decade in minimum winter and pre-monsoon temperature in the SSP245. Whereas it increases at the magnitude of 0.34 °C/decade and 0.33 °C/decade in the high emission scenario. The descending trend in the historical rainfall and ascending trend in the temperature over the Netravati river basin has been noted by (Mudbhatkal *et al.*, 2017; Jose and Dwarakish, 2022*a*; Chandu *et al.*, 2022). They have also reported a similar trend in rainfall and temperature till the mid-21st century. After the mid-21st century, the warming trends start to slow down with decreasing trends in the pre-monsoon maximum temperature and a decrease in the magnitude of the upward rise.

The SSP585 scenario shows the decreasing trend in the annual, winter, and pre-monsoon season maximum temperature with a significant increase of 0.55 °C/decade in the minimum winter temperature in Netravati. Aghanashini records a declining trend of magnitude 0.06 °C per decade in the monsoon minimum temperature. The slowing of the warming trend after the mid-21st century demonstrates the efficiency of planned initiatives for climate change reduction and adaptation under the composition of the socio-economic and radiative forcing projection. The warming in India is attributed majorly to the GHGs followed by the land use (Basha *et al.*, 2017). Several researchers have anticipated a decrease in the warming after 2050 in the low to medium emission scenarios (Basha *et al.*, 2017; Supharatid *et al.*, 2022).

c) Northern Rivers Basins of the Western Ghats

Table 6.4: Trend analysis of rainfall and temperature in Netravati River Basin of Western Ghats

		Precipitation				Maximum Temperature				Minimum Temperature			
	Series	Mean (mm)	Trend	Statistic Value	Sen's Slope (mm/decade)	Mean (°C)	Trend	Statistic Value	Sen's Slope (°C/decade)	Mean (°C)	Trend	Statistic Value	Sen's Slope (°C/decade)
Historical (1951-2013)	Annual	3209	No trend	-1.50	-31.10	28.93	**Increasing**	6.03	0.05[a]	18.88	**Increasing**	2.22	0.13[b]
	Winter	55	No trend	0.10	0.78	29.25	No trend	8.07	0.04	16.58	**Increasing**	0.53	0.17[a]
	Pre-monsoon	116	**Increasing**	-1.42	-12.96[c]	31.84	**Increasing**	3.33	0.08[a]	20.41	**Increasing**	1.40	0.14[a]
	Monsoon	2723	No trend	-0.39	-39.01	26.50	**Increasing**	3.69	0.07[b]	19.72	**Increasing**	3.39	0.13[b]
	Post-monsoon	315	No trend	0.98	2.93	28.13	**Increasing**	3.98	0.05[b]	18.83	**Increasing**	2.01	0.12[b]
Near Future (2021-2050) SSP245	Annual	3346	**Decreasing**	-2.44	-26.76[b]	32.35	**Increasing**	5.40	0.13[a]	19.56	**Increasing**	5.92	0.20[a]
	Winter	98	No trend	-0.01	-0.13	32.55	**Increasing**	10.10	0.14[a]	17.59	**Increasing**	6.45	0.23[a]
	Pre-monsoon	225	**Increasing**	3.31	17.47[a]	33.21	No trend	0.34	0.01	20.90	**Increasing**	5.14	0.24[a]
	Monsoon	2616	No trend	-1.93	-49.83	31.71	**Increasing**	5.27	0.19[a]	20.32	**Increasing**	5.92	0.17[a]
	Post-monsoon	407	No trend	-0.30	-3.03	31.92	**Increasing**	4.41	0.16[a]	19.43	**Increasing**	4.56	0.16[a]
Near Future (2021-2050) SSP585	Annual	3328	**Increasing**	2.00	60.31[c]	32.69	**Increasing**	8.18	0.10[a]	19.68	**Increasing**	5.00	0.29[a]
	Winter	99	No trend	0.73	1.41	32.96	**Increasing**	16.59	0.15[a]	17.68	**Increasing**	5.91	0.34[a]
	Pre-monsoon	217	No trend	-0.80	-4.71	33.07	**Increasing**	-3.09	-0.08[a]	20.99	**Increasing**	7.01	0.33[a]
	Monsoon	2696	**Increasing**	2.50	41.46[b]	32.25	**Increasing**	6.80	0.18[a]	20.41	**Increasing**	6.29	0.24[a]
	Post-monsoon	383	No trend	0.67	6.52	32.48	**Increasing**	5.32	0.17[a]	19.65	**Increasing**	3.84	0.25
Far Future (2051-2100) SSP245	Annual	3345	**Increasing**	3.12	39.45[a]	32.73	**Increasing**	4.45	0.04[a]	20.33	**Increasing**	6.44	0.14[a]
	Winter	110	No trend	0.61	1.89	33.04	**Increasing**	5.48	0.06[a]	18.61	**Increasing**	5.77	0.23[a]
	Pre-monsoon	275	**Increasing**	2.84	20.92[a]	32.96	**Decreasing**	-4.90	-0.05[a]	21.66	**Increasing**	5.25	0.08[a]
	Monsoon	2615	No trend	1.22	23.07	32.36	**Increasing**	6.04	0.10[a]	21.00	**Increasing**	6.54	0.13[a]
	Post-monsoon	345	No trend	-0.84	-3.86	32.56	**Increasing**	4.63	0.09[a]	20.06	**Increasing**	3.86	0.11[a]
Far Future (2051-2100) SSP585	Annual	3441	**Increasing**	3.82	72.19[a]	32.79	**Decreasing**	-2.77	-0.03[a]	21.00	**Increasing**	8.63	0.22[a]
	Winter	118	**Increasing**	3.21	6.58[a]	33.17	**Decreasing**	-3.91	-0.04[a]	19.94	**Increasing**	12.17	0.55[a]
	Pre-monsoon	289	No trend	1.98	24.54	31.85	**Decreasing**	-4.16	-0.090[a]	21.98	**Increasing**	5.45	0.13[a]
	Monsoon	2647	**Increasing**	2.93	34.31[a]	32.93	**Increasing**	2.98	0.07[a]	21.18	**Increasing**	4.94	0.05[a]
	Post-monsoon	387	No trend	0.82	6.21	33.22	**Increasing**	4.20	0.06[a]	20.90	**Increasing**	7.19	0.19[a]

Note: Bold indicates statistically significant values. a 0.1% significance level; b 1% significance level; c 5% significance level

Table 6.5: Trend analysis of rainfall and temperature in Aghanashini River Basin of Western Ghats

		Precipitation				Maximum Temperature				Minimum Temperature			
	Series	Mean (mm)	Trend	Statistic Value	Sen's Slope (mm/decade)	Mean (°C)	Trend	Statistic Value	Sen's Slope (°C/decade)	Mean (°C)	Trend	Statistic Value	Sen's Slope (°C/decade)
Historical (1951-2013)	Annual	3142	**Increasing**	2.87	167.77[a]	29.76	**Increasing**	6.12	0.05[a]	19.53	**Increasing**	3.36	0.15[a]
	Winter	91	No trend	0.60	0.11	29.97	**Increasing**	6.22	0.04[a]	16.58	**Increasing**	3.65	0.19[a]
	Pre-monsoon	47	No trend	-1.02	-6.61	32.44	**Increasing**	4.06	0.07[a]	21.28	**Increasing**	1.24	0.18[a]
	Monsoon	2665	**Increasing**	4.19	164.09[a]	27.23	**Increasing**	3.06	0.07[a]	20.84	**Increasing**	1.85	0.15[a]
	Post-monsoon	338	No trend	1.07	5.59	29.41	**Increasing**	3.16	0.07[a]	19.42	**Increasing**	0.76	0.12[a]
Near Future (2021-2050) SSP245	Annual	3230	No trend	1.14	41.75	32.35	**Increasing**	5.22	0.15[a]	20.46	**Increasing**	6.08	0.24[a]
	Winter	66	No trend	-0.35	-0.98	32.38	**Increasing**	7.20	0.17[a]	17.96	**Increasing**	3.58	0.35[a]
	Pre-monsoon	137	No trend	0.91	4.06	33.44	No trend	-0.07	0.00	21.76	**Increasing**	4.48	0.16[a]
	Monsoon	2702	No trend	0.95	24.17	31.70	**Increasing**	5.06	0.19[a]	21.80	**Increasing**	8.91	0.24[a]
	Post-monsoon	325	**Increasing**	2.29	5.89[a]	31.87	**Increasing**	4.04	0.17[a]	20.32	**Increasing**	3.75	0.21[a]
Near Future (2021-2050) SSP585	Annual	3319	No trend	0.77	24.32	32.74	**Increasing**	4.93	0.12[a]	20.54	**Increasing**	6.84	0.33[a]
	Winter	64	No trend	1.82	3.78	32.77	**Increasing**	3.34	0.12[a]	18.03	**Increasing**	6.92	0.51[a]
	Pre-monsoon	137	No trend	1.66	3.72	33.42	No trend	-1.68	-0.06	21.74	**Increasing**	5.05	0.19[a]
	Monsoon	2789	No trend	1.01	35.94	32.29	**Increasing**	6.24	0.22[a]	21.94	**Increasing**	7.23	0.34[a]
	Post-monsoon	329	No trend	-0.64	-9.04	32.46	**Increasing**	4.17	0.16[a]	20.45	**Increasing**	3.91	0.25[a]
Far Future (2051-2100) SSP245	Annual	3485	No trend	0.86	14.76	32.77	**Increasing**	3.93	0.06[a]	21.24	**Increasing**	5.87	0.09[a]
	Winter	74	No trend	-0.47	-0.33	32.85	**Increasing**	4.83	0.09[a]	19.42	**Increasing**	5.96	0.24[a]
	Pre-monsoon	199	**Increasing**	3.23	18.43[a]	33.36	no trend	-1.62	-0.03	22.17	**Increasing**	3.82	0.04[a]
	Monsoon	2933	No trend	0.45	7.65	32.38	**Increasing**	9.46	0.09[a]	22.45	**Increasing**	4.38	0.06[a]
	Post-monsoon	279	**Increasing**	-2.16	-10.75[c]	32.50	**Increasing**	4.83	0.10[a]	20.94	No trend	0.89	0.03
Far Future (2051-2100) SSP585	Annual	3546	**Increasing**	3.28	115.22[a]	33.08	No trend	0.57	0.00	21.56	**Increasing**	6.74	0.12[a]
	Winter	73	No trend	1.13	1.74	33.16	No trend	1.11	0.01	20.39	**Increasing**	6.29	0.42[a]
	Pre-monsoon	202	**Increasing**	4.33	27.36[a]	32.76	**Decreasing**	-7.36	-0.15[a]	22.21	**Increasing**	4.85	0.07[a]
	Monsoon	2956	**Increasing**	2.76	76.88[a]	33.16	**Increasing**	5.32	0.11[a]	22.45	**Decreasing**	-3.83	-0.06[a]
	Post-monsoon	315	No trend	0.63	3.60	33.23	**Increasing**	6.11	0.15[a]	21.22	**Increasing**	2.35	0.09[a]

Note: Bold indicates statistically significant values. a 0.1% significance level; b 1% significance level; c 5% significance level

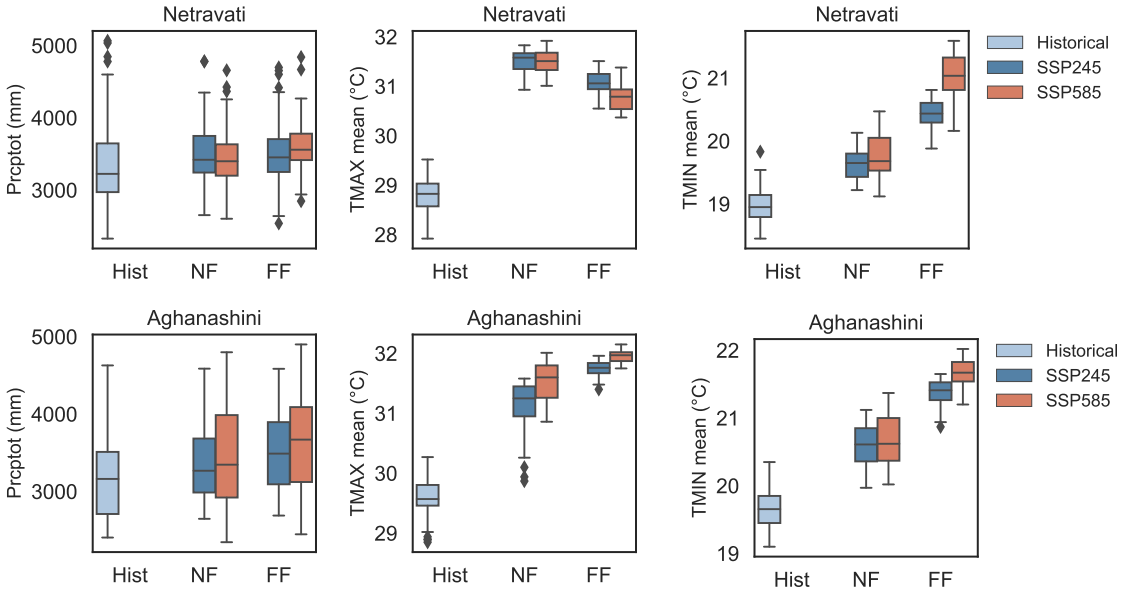

Fig. 6.28: The variation in the mean rainfall, mean maximum and minimum temperature in the historical and future horizon by MME of CMIP6 SSP245 and SSP585 scenario over the central river basins

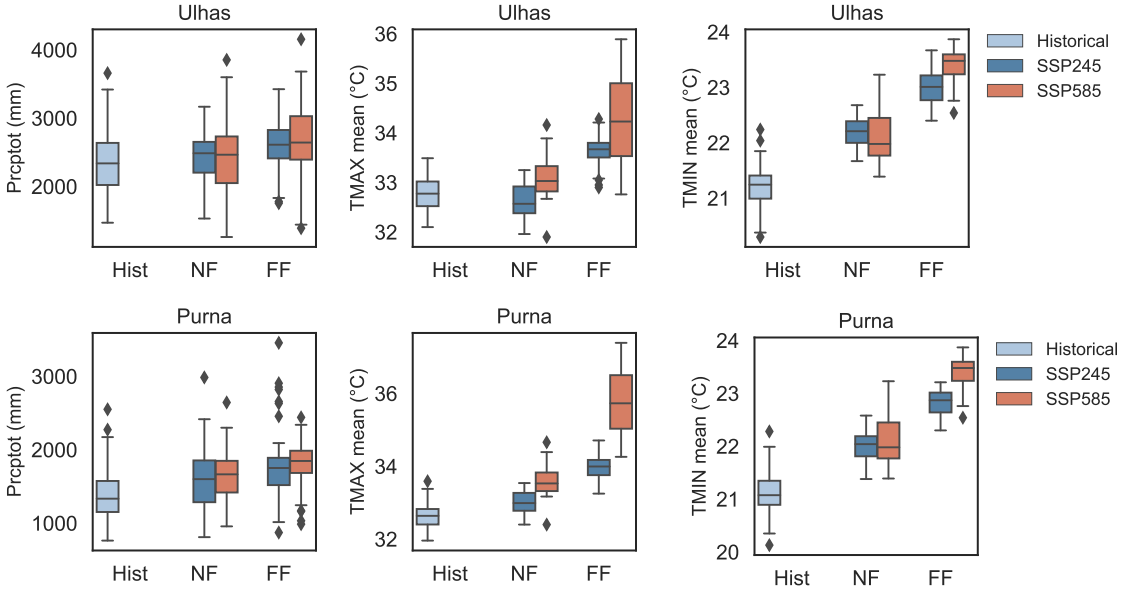

Fig. 6.29: The variation in the mean rainfall, mean maximum and minimum temperature in the historical and future horizon by MME of CMIP6 SSP245 and SSP585 scenario over the northern river basins

Table 6.6 and 6.7 describe the variation in the trend of rainfall and temperature in the historical to the future horizon. The temporal variation in the rainfall

and temperature is shown in Figure 6.29. Both the river basins has endured a insignificant increase in the historical rainfall at a rate of 99.26 mm/decade, and 13.35 mm/decade in the monsoon rainfall. The temperature had experienced a increase of 0.11°C and 0.06°C per decade. In the foreseeing decades, annual rainfall observes an insignificant increase in the trend with higher magnitude of increase in the high emission scenario. In the NF, the trend in annual maximum temperature is 0.3(±0.03)°C (0.29(±0.035)°C) and in minimum temperature is 0.31±0.05°C in Ulhas (Purna).

After the mid-21st century, both the basins have to endure an increase in rainfall under both scenarios. Over Ulhas basin, significant increase of 56.30 mm/decade and 81.77 mm/decade in the annual rainfall, with increment in the pre-monsoon rainfall at a magnitude of 9.35 mm/decade and 13.58 mm/decade, will be observed in SSP245 and SSP585, respectively. The Purna basin experience an insignificant increase in other seasons, with a significant rise of 5.28 mm/decade and 3.73 mm/decade in the pre-monsoon rainfall.

In the case of minimum temperature, the basin experience an upward trend in all the seasons at a magnitude of 0.17 °C/decade in annual temperature. The maximum trend is in the pre-monsoon season (0.1 °C in maximum temperature, 0.2 °C in minimum temperature) in the historical period, and the forthcoming year's maximum increase in temperature will be observed in the winter season. The minimum annual temperature, winter, pre-monsoon, and post-monsoon temperature, increases significantly, but the monsoon temperature declines at a rate of 0.1 °C/decade in the near future. In contrast, the maximum temperature shows an upward trend in the near future except in the post-monsoon. In the far future, the annual rainfall has no significant trend, decreasing trend in the pre-monsoon season (0.1 °C) and it's converse in the other seasons.

In the historical period and the near future, the minimum temperature in the Purna basin follows the same trend pattern as in Ulhas, with the exception of the monsoon season, where the temperature increases significantly. The maximum temperature shows a substantial increase only in the pre-monsoon and monsoon

seasons in the historical period and in all seasons except post-monsoon in the near future. In the far future, a positive trend will be recorded in the annual, winter, and monsoon seasons in maximum temperature and annual, winter, and pre-monsoon in minimum temperature. The winter season has to endure an increase of 0.26 °C in maximum temperature and pre-monsoon season (0.31 °C) in minimum temperature in the foreseeing decades. In the forthcoming years, the upper troposphere warms at a much faster rate than the lower troposphere, and this serves to stabilise the atmosphere over the WG, making it more likely to see less volatility in future precipitation than other places in India (Basha *et al.*, 2017; Varghese *et al.*, 2020). The intensified increase in the FF rainfall might be due to the extended westerly wind zone towards the southern India. Presently the WG region is dominated by the southerly wind, signifying the dominance of meridional wind. In contrast, the zonal wind is anticipated to contribute during NF, resulting in a minor south-westerly wind up to 60E. The westerly wind zone intensifies and extends to southern India during the FF resulting in the prospective increase in the rainfall (Tiwari *et al.*, 2023).

6.3.9 The Quantification of Projected Changes in Potential Evapotranspiration

Evapotranspiration is the combined loss of water from the Earth's surface due to soil evaporation, water evaporation, and plant transpiration. Potential Evapotranspiration is the amount of water that would be lost from a basin if an adequate water source were available. The projected decadal monthly changes in the PET in the six river basins are shown in Figure 6.30 to 6.32 and their trend is shown in Table 6.8 to 6.10.

a) Southern River Basins: Figure 6.30 represents the temporal variability in PET in the historical and projected decades of both medium emission and high emission scenarios. Over the southern basins, a higher percentage of the increase is noted in the Chaliyar basin; the monsoon and post-monsoon months experience an

Table 6.6: Trend analysis of rainfall and temperature in Ulhas River Basin of Western Ghats

		Precipitation				Maximum Temperature				Minimum Temperature			
	Series	Mean (mm)	Trend	Statistic Value	Sen's Slope (mm/decade)	Mean (°C)	Trend	Statistic Value	Sen's Slope (°C/decade)	Mean (°C)	Trend	Statistic Value	Sen's Slope (°C/decade)
Historical (1951-2013)	Annual	2358	**Increasing**	1.97	31.50[b]	32.97	**Increasing**	3.96	0.11[a]	20.92	**Increasing**	1.91	0.17[a]
	Winter	5	No trend	-0.60	0.00	31.66	No trend	2.54	0.05	16.40	**Increasing**	1.01	0.18[a]
	Pre-monsoon	19	**Decreasing**	-1.34	-2.04[a]	36.42	**Increasing**	2.95	0.1[a]3	22.77	**Increasing**	0.61	0.20[a]
	Monsoon	2229	No trend	1.77	27.70	30.76	**Increasing**	1.15	0.06[a]	23.93	**Increasing**	3.42	0.18[a]
	Post-monsoon	106	No trend	1.74	2.70	33.03	No trend	1.78	0.12[a]	20.60	**Increasing**	1.44	0.18[a]
Near Future (2021-2050) SSP245	Annual	2475	No trend	0.25	12.21	32.70	**Increasing**	5.82	0.27[a]	21.91	**Increasing**	5.40	0.20[a]
	Winter	33	No trend	-0.98	-2.67	32.56	**Increasing**	9.04	0.31[a]	17.83	**Increasing**	4.77	0.35[a]
	Pre-monsoon	43	**Increasing**	3.02	3.76[a]	35.09	**Increasing**	10.07	0.32[a]	23.36	**Increasing**	6.32	0.26[a]
	Monsoon	2209	No trend	-0.30	-8.23	31.56	**Increasing**	4.64	0.21[a]	24.69	No trend	1.92	0.08
	Post-monsoon	190	No trend	0.22	2.43	31.58	**Increasing**	4.09	0.23[a]	21.78	**Increasing**	2.26	0.13[b]
Near Future (2021-2050) SSP585	Annual	2562	No trend	1.50	51.80	33.47	**Increasing**	12.77	0.34[a]	21.98	**Increasing**	6.00	0.35[a]
	Winter	36	No trend	-1.87	-4.11	33.36	No trend	6.71	0.38	17.98	**Increasing**	5.30	0.51[a]
	Pre-monsoon	42	No trend	1.73	3.29	35.80	**Increasing**	4.90	0.30[a]	23.38	**Increasing**	5.57	0.41[a]
	Monsoon	2272	No trend	1.95	49.56	32.33	**Increasing**	6.52	0.35[a]	24.64	**Increasing**	3.41	0.12[a]
	Post-monsoon	212	No trend	-0.25	-2.33	32.38	**Increasing**	4.83	0.27[a]	21.92	**Increasing**	4.17	0.41[a]
Far Future (2051-2100) SSP245	Annual	2691	**Increasing**	3.83	56.30[a]	33.77	**Increasing**	6.47	0.17[a]	22.83	**Increasing**	5.65	0.17[a]
	Winter	38	No trend	0.71[a]	1.06	33.70	**Increasing**	6.39	0.19[a]	19.54	**Increasing**	6.52	0.37
	Pre-monsoon	86	**Increasing**	2.91[a]	9.35	36.22	**Increasing**	3.26	0.15[a]	24.37	**Increasing**	8.08	0.17[a]
	Monsoon	2365	**Increasing**	3.05	57.28[a]	32.60	**Increasing**	9.05	0.19[a]	24.71	No trend	1.79	0.07
	Post-monsoon	202	**Decreasing**	-2.31	-15.30[b]	32.56	**Increasing**	6.55	0.17[a]	22.70	No trend	1.77	0.10
Far Future (2051-2100) SSP585	Annual	2834	**Increasing**	3.33	81.77[a]	35.44	**Increasing**	18.76	0.46[a]	23.55	**Increasing**	7.39	0.23[a]
	Winter	37	No trend	1.25	1.63	35.60	**Increasing**	13.76	0.53[a]	21.23	**Increasing**	8.16	0.79[a]
	Pre-monsoon	86	**Increasing**	8.37	13.58[a]	37.07	**Increasing**	4.09	0.16[a]	24.53	No trend	0.64	0.03
	Monsoon	2474	No trend	1.92	45.27	34.59	**Increasing**	8.33	0.60[a]	24.55	**Decreasing**	-3.36	-0.10[a]
	Post-monsoon	237	**Increasing**	2.56	20.29[b]	34.50	**Increasing**	9.83	0.57[a]	23.89	**Increasing**	6.19	0.40[a]

Table 6.7: Trend analysis of rainfall and temperature in Purna River Basin of Western Ghats

		Precipitation				Maximum Temperature				Minimum Temperature			
	Series	Mean (mm)	Trend	Statistic Value	Sen's Slope (mm/decade)	Mean (°C)	Trend	Statistic Value	Sen's Slope (°C/decade)	Mean (°C)	Trend	Statistic Value	Sen's Slope (°C/decade)
Historical (1951-2013)	Annual	1396	No trend	0.27	-10.00	32.71	**Increasing**	0.87	0.06[a]	20.69	**Increasing**	1.97	0.08[c]
	Winter	4	No trend	-0.31	0.00	29.71	No trend	0.44	0.05	14.94	No trend	1.55	0.08
	Pre-monsoon	8	**Decreasing**	-1.95	-1.60[c]	36.45	**Increasing**	1.07	0.10[a]	23.03	No trend	1.91	0.09
	Monsoon	1337	No trend	0.34	-3.17	31.87	**Increasing**	-0.51	0.06[a]	24.76	**Increasing**	2.20	0.08[b]
	Post-monsoon	48	No trend	1.14	0.79	32.83	No trend	0.19	0.09	20.04	**Increasing**	2.89	0.11[a]
Near Future (2021-2050) SSP245	Annual	1564	No trend	0.25	4.40	31.66	**Increasing**	6.26	0.25[a]	21.66	**Increasing**	5.43	0.25[a]
	Winter	40	No trend	0.78	1.31	31.52	**Increasing**	6.06	0.26[a]	16.18	**Increasing**	4.59	0.33[a]
	Pre-monsoon	38	No trend	1.87	2.40	33.80	**Increasing**	5.49	0.37[a]	23.46	No trend		0.25
	Monsoon	1357	No trend	0.76	11.93	30.63	**Increasing**	5.06	0.20[a]	25.46	**Increasing**	6.16	0.22[a]
	Post-monsoon	129	No trend	0.21	0.82	30.70	**Increasing**	6.04	0.19[a]	21.53	**Increasing**	3.02	0.16[a]
Near Future (2021-2050) SSP585	Annual	1603	**Increasing**	4.48	63.95[a]	32.38	**Increasing**	14.62	0.32[a]	21.77	**Increasing**	6.19	0.36[a]
	Winter	38	No trend	0.18	0.22	32.21	**Increasing**	11.35	0.32[a]	16.31	**Increasing**	5.53	0.52[a]
	Pre-monsoon	36	**Increasing**	6.22	10.17	34.64[a]	No trend	6.42	0.39	23.57	**Increasing**	5.19	0.38[a]
	Monsoon	1395	**Increasing**	5.65	44.24	31.29	**Increasing**	6.18	0.29	25.51	**Increasing**	4.75	0.18
	Post-monsoon	134	**Increasing**	2.53	10.40[a]	31.37	**Increasing**	4.93	0.23[a]	21.68	**Increasing**	4.77	0.53[a]
Far Future (2051-2100) SSP245	Annual	1726	No trend	1.19	19.46	32.67	**Increasing**	6.46	0.17[a]	22.53	**Increasing**	7.07	0.12[a]
	Winter	44	No trend	-0.35	-0.50	32.51	**Increasing**	6.36	0.18[a]	17.60	**Increasing**	11.57	0.29[a]
	Pre-monsoon	60	**Increasing**	3.58	5.28	35.15[a]	**Increasing**	3.67	0.19[a]	24.42	**Increasing**	4.95	0.15[a]
	Monsoon	1494	No trend	1.19	12.26	31.49	**Increasing**	10.00	0.16[a]	25.79	No trend	-0.33	0.00
	Post-monsoon	128	No trend	-1.10	-5.05	31.50	**Increasing**	4.80	0.15[a]	22.33	No trend	1.32	0.09
Far Future (2051-2100) SSP585	Annual	1836	No trend	1.84	37.08	34.43	**Increasing**	13.59	0.54[a]	23.22	**Increasing**	5.79	0.17[a]
	Winter	38	No trend	-1.11	-1.93	34.40	**Increasing**	14.81	0.58[a]	19.24	**Increasing**	9.72	0.73[a]
	Pre-monsoon	70	**Increasing**	2.24	3.73[a]	36.87	**Increasing**	7.27[a]	0.49	24.73	**Increasing**	4.67[a]	0.13
	Monsoon	1587	No trend	1.56	48.60	33.32	**Increasing**	8.31	0.60[a]	25.53	**Decreasing**	-9.83	-0.20[a]
	Post-monsoon	141	No trend		3.85	33.16	**Increasing**	10.13	0.51[a]	23.40	**Increasing**	3.75	0.18[a]

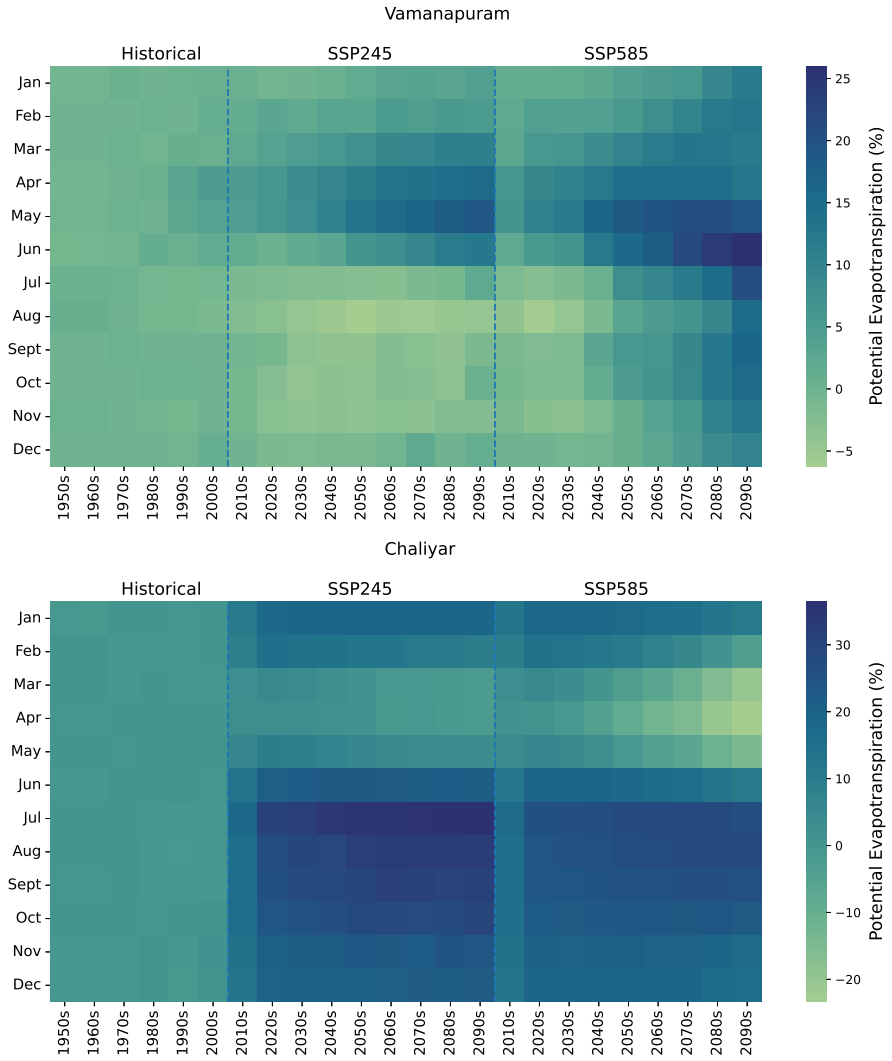

Fig. 6.30: Projected changes in Potential Evapotranspiration in southern river basins

increase of 20-35% in the future horizon. The Chaliyar basin covered with 51.70% forest area, 38% of plantation area as of year 2020, and Vamanapuram with 72% forest area, 23% plantation area. In Vamanapuram, both scenarios will note an increase of 15-24% in PET in the April, May, and June months after the decade 2050s. The PET decreases in August (up to 5%) in the medium emission scenario until the end of the century and increases after the decade 2030s in the high emission scenario. Annual and seasonal trends in the PET over the southern river basins are shown in Table 6.8. In the historical period, the PET recorded a significant increasing trend in the annual (3.10 mm/decade), winter (0.67 mm/decade), and pre-monsoon (3.33 mm/decade) seasons, with a significant down trend in

the monsoon season in Vamanapuram river basin. In the NF, the Vamanapuram basin experience an increasing trend in all the seasons under SSP245, recording a 22.32 mm/decade increase in annual PET with a significant contribution in monsoon (10.57 mm/decade) and post-monsoon (1.43 mm/decade) seasons. In the high emission scenario, the PET decreases in monsoon and post-monsoon seasons by 2.71 mm/decade and 1.10 mm/decade, increasing pre-monsoon PET by 6.98 mm/decade. The far future horizon records a significant increase in both scenarios. The magnitude of the increase is higher in the medium emission scenario (31.19 mm/decade in annual) than in the high emission scenario (13.45 mm/decade in annual PET).

The Chaliyar records a significant increase in the historical PET. In the NF, a significant increase is noted in the monsoon and post-monsoon seasons by 6.31

Table 6.8: The trend in Potential Evapotranspiration in the southern river basins

			Vamanapuram				**Chaliyar**			
		Series	Mean (mm)	Trend	Statistic value	Sen's Slope	Mean (mm)	Trend	Statistic value	Sen's Slope
Historical (1951-2013)		Annual	1631	**Increasing**	2.74[a]	3.10	1587	**Increasing**	2.67[a]	3.20
		Winter	388	**Increasing**	3.18[a]	0.67	375	**Increasing**	3.06[a]	1.24
		Pre-monsoon	462	**Increasing**	6.10[a]	3.33	482	No trend	1.16	0.66
		Monsoon	529	**Decreasing**	-2.09[b]	-0.72	496	No trend	0.36	0.14
		Post-monsoon	251	No trend	-0.58	-0.14	234	**Increasing**	2.49[a]	1.00
Near Future (2021-2050)	SSP245	Annual	1643	**Increasing**	4.98[a]	22.32	1869	**Increasing**	3.07[a]	3.84
		Winter	389	No trend	1.77	0.88	442	No trend	0.98	0.59
		Pre-monsoon	488	No trend	1.98	7.79	506	**Decreasing**	-5.05[a]	-4.41
		Monsoon	521	**Increasing**	3.72[a]	10.57	632	**Increasing**	5.22[a]	6.31
		Post-monsoon	244	**Increasing**	1.97[a]	1.43	289	**Increasing**	2.18[a]	1.48
	SSP585	Annual	1677	No trend	1.66	4.45	1887	**Decreasing**	-4.20[a]	-7.06
		Winter	394	No trend	1.11	0.80	446	**Decreasing**	-2.86[a]	-1.83
		Pre-monsoon	502	**Increasing**	4.70[a]	6.98	493	**Decreasing**	-6.66[a]	-9.94
		Monsoon	533	**Decreasing**	-4.12[a]	-2.71	651	**Increasing**	3.99[a]	3.95
		Post-monsoon	248	**Decreasing**	-2.14[a]	-1.10	296	**Increasing**	2.33[a]	0.77
Far Future (2051-2100)	SSP245	Annual	1692	**Increasing**	15.96[a]	31.19	1868	**Decreasing**	-4.18[a]	-2.50
		Winter	398	**Increasing**	6.82[a]	8.51	441	**Decreasing**	-3.17[a]	-0.78
		Pre-monsoon	518	No trend	0.53	0.51	485	**Decreasing**	-5.14[a]	-3.20
		Monsoon	531	**Increasing**	8.13[a]	15.71	647	No trend	0.97	0.56
		Post-monsoon	245	**Increasing**	7.56[a]	7.40	295	**Increasing**	2.84[a]	0.94
	SSP585	Annual	1817	**Increasing**	5.39[a]	13.45	1810	**Decreasing**	-7.84[a]	-27.30
		Winter	417	**Increasing**	2.54[a]	1.87	423	**Decreasing**	-6.00[a]	-9.60
		Pre-monsoon	527	**Increasing**	5.49[a]	4.69	433	**Decreasing**	-17.32[a]	-15.22
		Monsoon	600	**Increasing**	5.53[a]	4.79	659	**Decreasing**	-2.70[a]	-1.71
		Post-monsoon	273	**Increasing**	3.66[a]	1.75	296	**Decreasing**	-4.44[a]	-1.92

Note : Sen's slope is in mm/decade, Bold indicates statistically significant values. a 0.1% significance level; b 1% significance level; c 5% significance level

mm/decade and 3.95 mm/decade in SSP245 and SSP585, respectively. After the mid-21st century, the basin experience a decrease in PET except in the post-monsoon season in SSP245. In the SSP585 scenario, 15.22 mm/decade in pre-monsoon, 1.71 mm/decade in monsoon, 1.92 mm/decade in post-monsoon, and 9.60 mm/decade in the winter PET leads to a decreasing trend of 27.30 mm/decade annually. The higher warming in the minimum temperature compared to the maximum temperature results in a decrease in vapor pressure deficit and, consequently, a decrease in PET(Chattopadhyay and Hulme, 1997; Das *et al.*, 2022*a*).

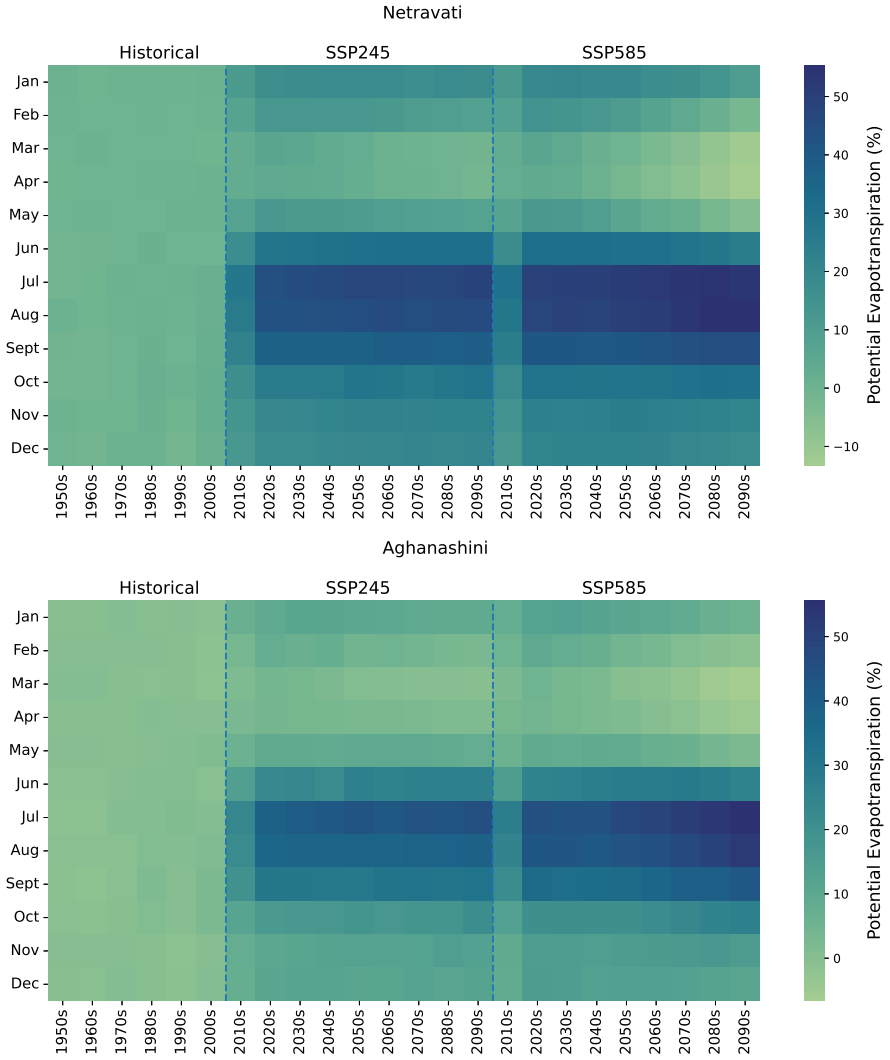

Fig. 6.31: Projected changes in Potential Evapotranspiration in central river basins

b) Central River Basins: In the central per-humid basins, the monthly

Table 6.9: The trend in Potential Evapotranspiration in the central river basins

			Netravati				Aghanashini			
		Series	Mean (mm)	Trend	Statistic value	Sen's Slope	Mean (mm)	Trend	Statistic value	Sen's Slope
Historical (1951-2013)		Annual	1556	**Increasing**	4.39[a]	4.29	1563	No trend	1.82	2.11
		Winter	380	**Increasing**	2.55[a]	0.93	384	No trend	-0.97	-0.32
		Pre-monsoon	478	No trend	1.56	0.32	477	No trend	-0.51	-0.17
		Monsoon	463	**Increasing**	3.01[a]	1.60	461	**Increasing**	2.86[a]	1.69
		Post-monsoon	236	**Increasing**	3.58[a]	1.83	240	No trend	1.70	0.75
Near Future (2021-2050)	SSP245	Annual	1877	No trend	1.16	1.18	1807	No trend	0.30	0.84
		Winter	440	No trend	0.73	0.47	422	No trend	0.29	0.27
		Pre-monsoon	511	**Decreasing**	-4.74[a]	-3.69	504	**Decreasing**	-2.19[b]	-2.28
		Monsoon	637	**Increasing**	4.90[a]	3.75	608	No trend	1.48	1.65
		Post-monsoon	288	**Increasing**	2.83[a]	0.97	273	No trend	0.84	0.64
	SSP585	Annual	1903	**Decreasing**	-3.02[a]	-5.80	1841	**Decreasing**	-3.42[a]	-5.84
		Winter	448	No trend	-0.41	-0.28	429	**Decreasing**	-3.23[a]	-2.45
		Pre-monsoon	506	**Decreasing**	-5.98[a]	-6.95	504	**Decreasing**	-3.31[a]	-4.34
		Monsoon	654	**Increasing**	1.97[a]	1.68	627	No trend	0.97	1.16
		Post-monsoon	295	No trend	0.90	0.28	281	No trend	0.30	0.17
Far Future (2051-2100)	SSP245	Annual	1872	**Decreasing**	-3.21[a]	-3.47	1808	No trend	0.85	1.18
		Winter	440	No trend		-1.36	416	**Decreasing**	-2.17[a]	-0.89
		Pre-monsoon	493	**Decreasing**	-5.10[a]	-3.28	496	**Decreasing**	-2.54[a]	-1.70
		Monsoon	646	**Increasing**	1.97[a]	1.39	618	**Increasing**	3.27[a]	1.91
		Post-monsoon	293	No trend	1.15	0.36	277	**Increasing**	2.91[a]	1.24
	SSP585	Annual	1843	**Decreasing**	-6.31[a]	-20.90	1825	**Decreasing**	-3.33[a]	-4.86
		Winter	428	**Decreasing**	-6.25[a]	-8.52	412	**Decreasing**	-11.06[a]	-4.70
		Pre-monsoon	456	**Decreasing**	-11.93[a]	-14.23	479	**Decreasing**	-11.15[a]	-8.03
		Monsoon	663	No trend	1.46	1.38	648	**Increasing**	5.94[a]	5.61
		Post-monsoon	296	No trend	-1.00	-0.34	286	**Increasing**	3.58[a]	1.65

Note : Sen's slope is in mm/decade, Bold indicates statistically significant values. a 0.1% significance level; b 1% significance level; c 5% significance level

anomaly shown in Figure 6.31 represents the higher PET increase in July, August September by 35-55% in both the river basins; the forest area contributes to 75% of land cover in Netravati and 79.50% in Aghanashini with only 2% of plantation area (14.80% in Netravati). The basins have observed an increase in the cropland by 1.67% in Netravati and 3% in Aghanashini, a span of 15 years (2005-2020). In Netravati, the PET had a significant increasing trend in the historical period by 4.29 mm/decade in annual, 3.01 mm/decade in monsoon, and 3.58 mm/decade in post-monsoon seasons (Table 6.9). The NF records a varying trend in different seasons; in pre-monsoon, PET decreases by 3.69 mm/decade in SSP245, 6.95 mm/decade in the SSP585 scenario, and it records an increasing trend in the monsoon and post-monsoon seasons. In FF, the significant decreasing trend will be recorded in all seasons except the monsoon season, where it increases significantly

(insignificantly) in SSP245 (SSP585) with a higher magnitude of decreasing trend in the higher emission scenario than the medium emission scenario. The basin Aghanashini records a decreasing trend in the winter and pre-monsoon season, with the significant increase of 1.91 mm/decade (SSP245) and 5.65 mm/decade (SSP585) in the monsoon season, 1.24 mm/decade and 1.61 mm/decade in the post monsoon season in SSP245 and SSP585 scenarios.

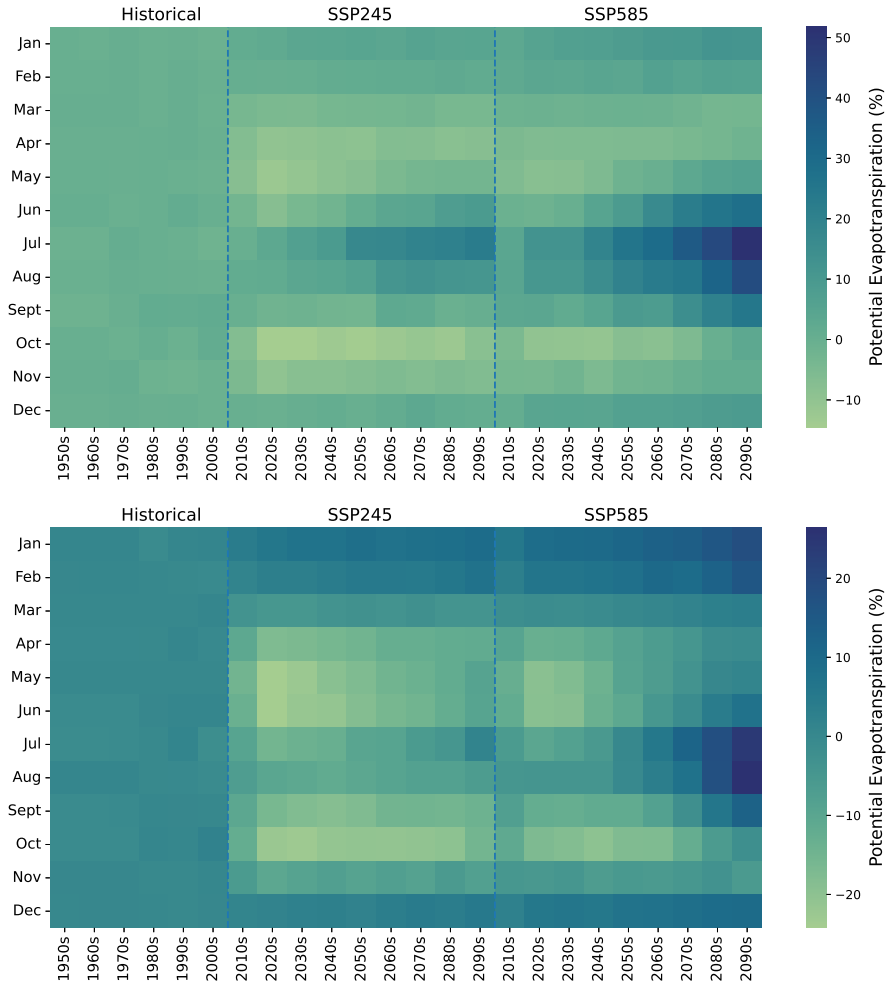

Fig. 6.32: Projected changes in Potential Evapotranspiration in northern river basins

c) Northern River Basins: The anomaly in the northern basins varies compared to others (Figure 6.32). The months July and August note an increase of up to 30-40% after the decade 2050s and a decrease of up to 15% in October. The Purna basin records a decrease of up to 35% in October month till the 2080s and

Table 6.10: The trend in Potential Evapotranspiration in the northern river basins

			Ulhas				Purna			
		Series	Mean (mm)	Trend	Statistic value	Sen's Slope	Mean (mm)	Trend	Statistic value	Sen's Slope
Historical (1951-2013)		Annual	1694	No trend	-0.18	-0.07	1658	No trend	-0.28	-0.47
		Winter	358	No trend	-0.12	-0.06	323	No trend	0.46	0.19
		Pre-monsoon	558	**Decreasing**	-2.64[a]	-1.05	550	**Decreasing**	-1.97[a]	-0.93
		Monsoon	527	No trend	0.71	0.65	548	**Increasing**	3.08[a]	0.74
		Post-monsoon	250	No trend	0.54	0.45	238	No trend	-0.60	-0.36
Near Future (2021-2050)	SSP245	Annual	1627	**Increasing**	4.43[a]	16.67	1458	**Increasing**	3.34[a]	12.21
		Winter	363	**Increasing**	2.68[a]	2.20	336	**Increasing**	3.14[a]	1.63
		Pre-monsoon	513	**Increasing**	3.12[a]	4.48	466	**Increasing**	5.45[a]	7.10
		Monsoon	528	**Increasing**	3.70[a]	7.73	458	No trend	1.09	1.64
		Post-monsoon	222	No trend	1.92	1.61	199	No trend	0.77	0.52
	SSP585	Annual	1703	**Increasing**	5.81[a]	15.66	1528	**Increasing**	23.27[a]	15.72
		Winter	375	**Increasing**	3.96[a]	2.10	345	**Increasing**	3.35[a]	1.50
		Pre-monsoon	532	No trend	1.38	1.17	488	**Increasing**	5.07[a]	6.13
		Monsoon	564	**Increasing**	4.98[a]	11.42	488	**Increasing**	4.28[a]	8.18
		Post-monsoon	232	No trend	0.22	0.25	206	No trend	-1.29	-1.01
Far Future (2051-2100)	SSP245	Annual	1701	**Increasing**	3.04[a]	9.43	1524	**Increasing**	5.32[a]	13.44
		Winter	368	No trend	0.42	0.27	341	No trend	0.87	0.42
		Pre-monsoon	531	No trend	1.29	1.33	493	**Increasing**	3.48[a]	3.79
		Monsoon	574	**Increasing**	3.63[a]	6.02	487	**Increasing**	5.45[a]	8.28
		Post-monsoon	228	**Increasing**	3.73[a]	1.90	203	**Increasing**	2.66[a]	1.46
	SSP585	Annual	1847	**Increasing**[a]	7.91	38.84	1694	**Increasing**	9.99[a]	54.08
		Winter	386	**Increasing**	4.80[a]	2.24	358	**Increasing**	5.47[a]	3.41
		Pre-monsoon	554	**Increasing**	5.39[a]	4.69	539	**Increasing**	32.90[a]	12.32
		Monsoon	661	**Increasing**	8.10[a]	26.83	579	**Increasing**	8.52[a]	32.80
		Post-monsoon	246	**Increasing**	7.11[a]	5.09	218	**Increasing**	6.68[a]	6.62

Note : Sen's slope is in mm/decade; bold indicates statistically significant values. a 0.1% significance level; b 1% significance level; c 5% significance level

in the months of May and June in the decades 2020s-2030s, which drastically increases thereafter. But the percentage of positive anomalies noted in the basins is less than in the other basins. The trend in the historical and future horizon given in Table 6.9 denotes the decreasing trend in the historical period, by 1.05 mm/decade in Ulhas and 0.93 mm/decade in Purna basins, during the pre-monsoon seasons. In contrast, both basins PET is expected to rise in the future. The NF records an increase in annual PET by 16.67 mm/decade and 15.66 mm/decade over Ulhas, 12.21 mm/decade, and 15.72 mm/decade over the Purna basins under SSP245 and SSP585 scenarios. In the FF horizon, the higher magnitude of trend is noted in the monsoon season by 6.02 mm/decade and 26.83 mm/decade in Ulhas, 8.28 mm/decade and 32.80 mm/decade in Purna under SSP245 and SSP585 scenarios. This contributes an increase of 38.84 mm/decade in annual PET in Ulhas and

54.08 mm/decade in annual PET in Purna basins.

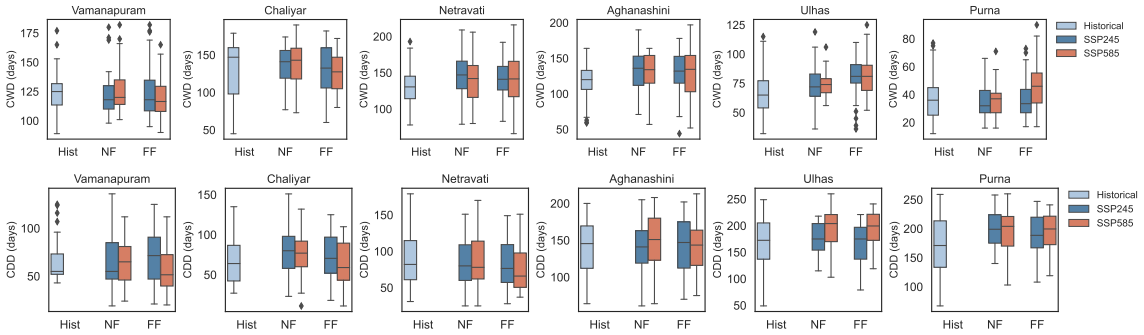

Fig. 6.33: Transition in the distribution of duration-based rainfall indices from historical to far future

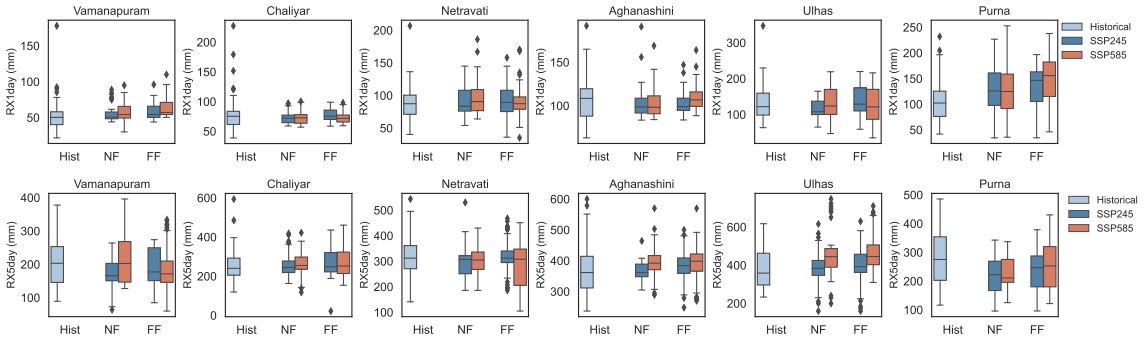

Fig. 6.34: Transition in the distribution of absolute indices of rainfall from historical to far future

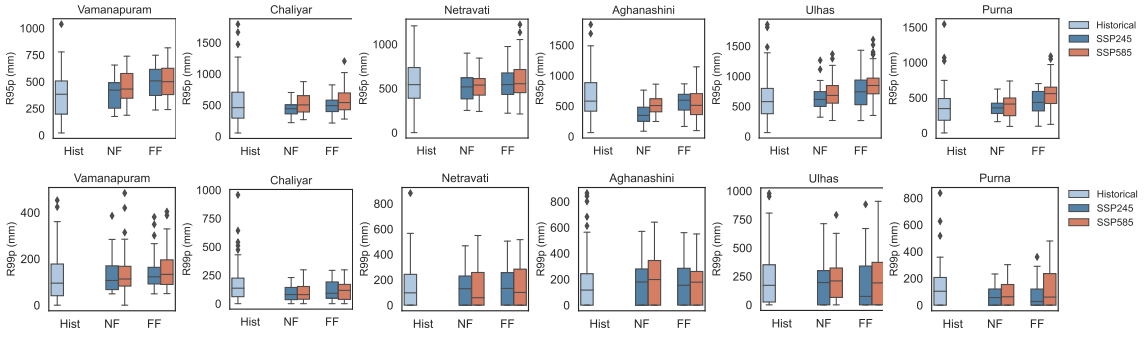

Fig. 6.35: Transition in the distribution of percentile-based rainfall indices from historical to far future

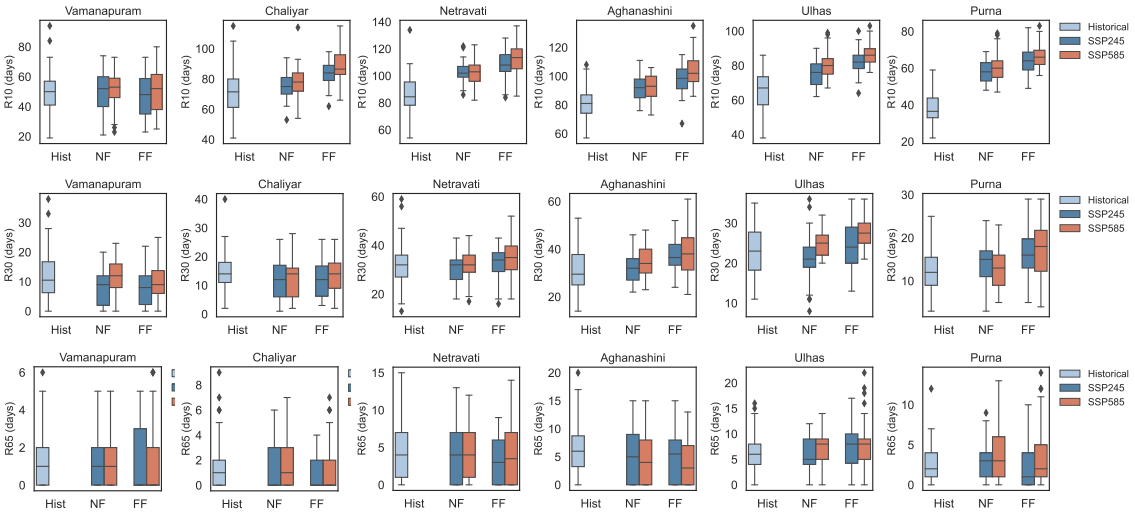

Fig. 6.36: Transition in the mean of the threshold-based rainfall indices from historical to far future

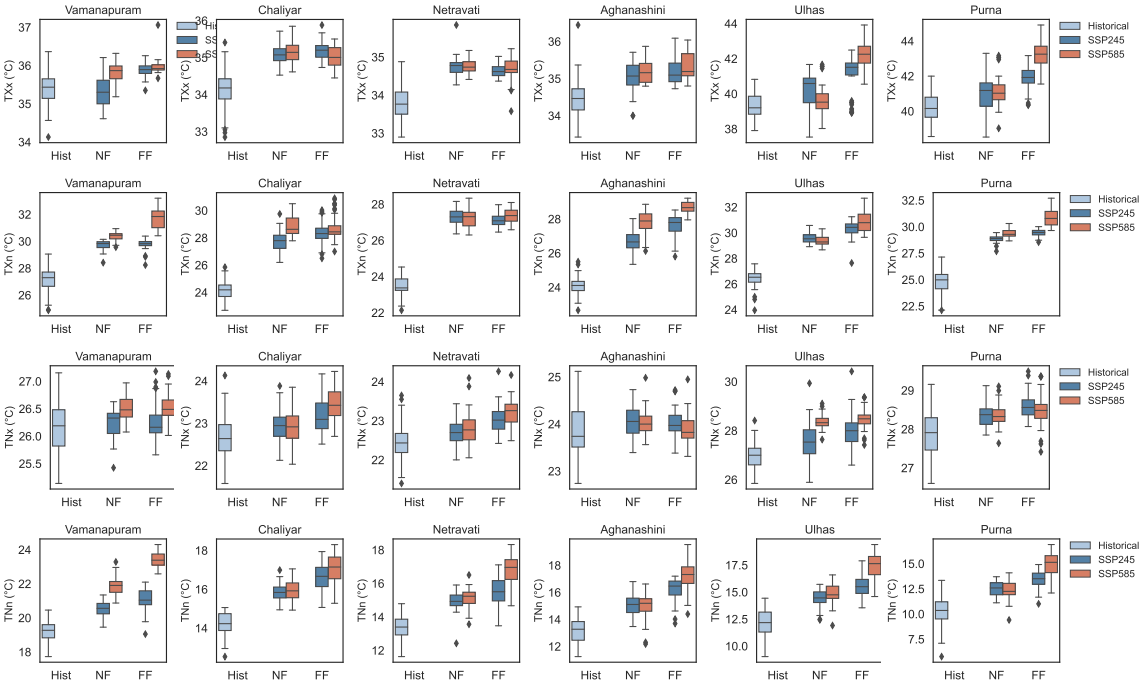

Fig. 6.37: Transition in the distribution of intensity based temperature indices from historical to far future

Table 6.11: The trend in historical and projected rainfall and temperature extreme indices in Vamanapuram basin

		Rainfall Indices				Temperature Indices			
		Indices	Trend	Statistic Value	Sen's slope	Indices	Trend	Statistic Value	Sen's slope
Historical	(1951-2013)	R10	**Decreasing**	-2.19[b]	-5.83	TNn	No trend	0.04	0.00
		R30	No trend	-1.01	-0.98	TNx	No trend	-0.90	0.00
		R65	No trend	-0.26	0.00	TXn	**Increasing**	4.44[a]	0.20
		R95p	No trend	-1.13	-40.86	TXx	**Increasing**	4.59 [a]	0.10
		R99p	No trend	-1.08	-2.83	TN10p	No trend	-1.64	-0.70
		RX1day	No trend	0.34	0.52	TX10p	**Decreasing**	-4.29 [a]	-2.80
		RX5day	**Decreasing**	-2.55[b]	-12.97	TN90p	**Increasing**	2.20 [b]	0.50
		CWD	**Decreasing**	-3.29 [a]	-3.68	TX90p	**Increasing**	5.76 [a]	4.40
		CDD	No trend	1.40	1.10	DTR	**Increasing**	2.83 [a]	0.20
Near Future (2021-2050)	**SSP245**	R10	No trend	1.48	0.83	TNn	**Increasing**	2.35 [a]	0.20
		R30	No trend	-0.13	0.00	TNx	**Increasing**	2.89 [a]	0.10
		R65	No trend	0.00	0.00	TXn	No trend	0.24	0.00
		R95p	No trend	1.63	17.2	TXx	**Increasing**	7.95 [a]	0.30
		R99p	No trend	1.11	5.20	TN10p	**Decreasing**	-8.72 [a]	-1.70
		RX1day	No trend	-0.64	-0.60	TX10p	**Decreasing**	-3.60[a]	-0.40
		RX5day	No trend	0.19	0.26	TN90p	**Increasing**	7.41[a]	11.30
		CWD	No trend	0.37	15.80	TX90p	**Increasing**	5.71[a]	10.60
		CDD	No trend	-1.35	0.00	DTR	**Decreasing**	-2.75[a]	-0.10
	SSP585	R10	No trend	1.42	1.25	TNn	No trend	0.25	0.00
		R30	**Increasing**	2.137[a]	2.00	TNx	**Increasing**	8.92[a]	0.30
		R65	No trend	0.00	0.00	TXn	**Increasing**	4.90[a]	0.10
		R95p	No trend	1.45	20.90	TXx	**Increasing**	2.89[a]	0.30
		R99p	No trend	1.35	8.30	TN10p	No trend	-0.41	0.00
		RX1day	No trend	1.95	2.80	TN90p	**Increasing**	5.21[a]	0.20
		RX5day	No trend	1.89	1.90	TX10p	No trend		0.10
		CWD	No trend	0.21	0.00	TX90p	**Decreasing**	-3.11[a]	-0.20
		CDD	No trend	0.25	0.00	DTR	**Increasing**	2.17[a]	0.60
Far Future (2051-2100)	**SSP245**	R10	No trend	-1.00	-0.20	TNn	**Increasing**	2.15[b]	0.10
		R30	No trend	1.125	0.00	TNx	No trend	-0.37	0.00
		R65	No trend	0.00	0.00	TXn	**Increasing**	2.94[b]	0.00
		R95p	No trend	-0.53	-5.1	TXx	No trend	0.00	0.00
		R99p	No trend	0.57	1.80	TN10p	No trend	-1.07	-0.10
		RX1day	No trend	0.86	0.67	TX10p	**Decreasing**	-3.30[a]	-0.50
		RX5day	No trend	0.134	0.15	TN90p	No trend	0.16	0.00
		CWD	No trend		17.22	TX90p	**Increasing**	5.42[a]	4.20
		CDD	No trend	0.08	0.00	DTR	**Increasing**	3.75[a]	0.10
	SSP585	R10	**Increasing**	4.49[a]	2.20	TNn	No trend	0.65	0.00
		R30	**Increasing**	2.04 [b]	0.00	TNx	**Increasing**	8.31 [a]	0.20
		R65	No trend	0.00	0.00	TXn	**Increasing**	2.79[a]	0.10
		R95p	**Increasing**	5.03[a]	4.80	TXx	**Increasing**	5.54 [a]	0.20
		R99p	**Increasing**	2.61[a]	11.40	TN10p	**Increasing**	2.13 [a]	0.00
		RX1day	**Increasing**	2.10	2.90	TN90p	**Increasing**	7.44 [a]	0.40
		RX5day	**Increasing**	2.87[a]	1.50	TX10p	**Decreasing**	-2.14 [a]	0.00
		CWD	No trend	-0.67	-8.50	TX90p	**Decreasing**	-2.49 [a]	0.00
		CDD	No trend	0.64	0.00	DTR	No trend	0.82	0.00

Note : Sen's slope is in unit/decade; bold indicates statistically significant values. a 0.1% significance level; b 1% significance level; c 5% significance level

Table 6.12: The trend in historical and projected rainfall and temperature extreme indices in Chaliyar basin

		Rainfall Indices				Temperature Indices			
		Indices	Trend	Statistic Value	Sen's slope	Indices	Trend	Statistic Value	Sen's slope
Historical	(1951-2013)	R10	No trend	0.26	0.22	TNn	No trend	0.95	0.10
		R30	No trend	-0.29	0.00	TNx	**Increasing**	2.76 [b]	0.10
		R65	**Decreasing**	-3.57 [a]	-0.31	TXn	**Increasing**	6.93 [a]	0.40
		R95p	No trend	-1.49	-33.44	TXx	**Increasing**	3.94[a]	0.20
		R99p	**Decreasing**	-4.65 [a]	-28.44	TN10p	**Decreasing**	-5.62[a]	-2.60
		RX1day	**Decreasing**	-2.65[a]	-15.70	TN90p	No trend	1.12	4.10
		RX5day	**Decreasing**	-3.02[a]	-5.40	TX10p	**Decreasing**	-3.57 [a]	-4.60
		CWD	**Increasing**	2.44[b]	13.80	TX90p	**Increasing**	4.63[a]	2.60
		CDD	**Increasing**	3.01[a]	5.40	DTR	No trend	0.86	0.10
Near Future (2021-2050)	**SSP245**	R10	No trend	0.95	1.60	TNn	No trend	1.31	0.10
		R30	No trend	0.05	0.00	TNx	**Increasing**	2.18[c]	0.20
		R65	No trend	-0.42	0.00	TXn	**Increasing**	2.80 [b]	0.20
		R95p	No trend	-0.49	-14.30	TXx	No trend	0.19	0.00
		R99p	No trend	-0.13	0.00	TN10p	No trend	-1.47	-0.50
		RX1day	No trend	0.53	1.00	TN90p	**Increasing**	5.59[a]	6.90
		RX5day	No trend	0.30	0.40	TX10p	**Increasing**	6.54[a]	1.70
		CWD	No trend	1.94	14.40	TX90p	**Decreasing**	-9.43[a]	-1.80
		CDD	No trend	1.22	0.80	DTR	**Decreasing**	-4.41[a]	-0.10
	SSP585	R10	**Increasing**	2.10 [b]	2.90	TNn	**Increasing**	4.05[a]	0.30
		R30	No trend	-0.01	0.00	TNx	**Increasing**	2.02[a]	0.10
		R65	No trend	0.30	0.00	TXn	**Increasing**	2.75[b]	0.10
		R95p	No trend	1.49	31.70	TXx	No trend	1.94	0.10
		R99p	No trend	0.04	0.00	TN10p	No trend	-1.10	-0.60
		RX1day	No trend	-0.76	-1.90	TN90p	**Increasing**	4.41[a]	6.50
		RX5day	No trend	1.33	1.30	TX10p	**Increasing**	4.13[a]	1.90
		CWD	No trend	1.73	5.80	TX90p	**Decreasing**	-4.89[a]	-2.00
		CDD	No trend	-0.47	0.00	DTR	**Decreasing**	-4.53[a]	-0.20
Far Future (2051-2100)	**SSP245**	R10	No trend	-0.61	-0.40	TNn	**Increasing**	2.32 [c]	0.10
		R30	No trend	-1.12	-0.20	TNx	No trend	-1.06	0.00
		R65	No trend	-0.67	0.00	TXn	No trend	0.49	0.00
		R95p	No trend	-1.25	-18.00	TXx	No trend	1.48	0.00
		R99p	No trend	-0.05	0.00	TN10p	**Decreasing**[b]	-3.03	-0.50
		RX1day	No trend	-1.04	-2.10	TN90p	**Increasing**	4.05[a]	2.20
		RX5day	**Decreasing**	-1.91[c]	-1.50	TX10p	**Increasing**	2.78[b]	0.60
		CWD	No trend	0.54	2.40	TX90p	**Decreasing**	-3.18 [a]	-0.60
		CDD	No trend	-1.92	-1.10	DTR	**Decreasing**	-4.76[a]	-0.10
	SSP585	R10	No trend	1.16	1.40	TNn	**Increasing**	3.00[b]	0.20
		R30	**Increasing**	2.68 [b]	0.50	TNx	No trend	1.74[a]	0.10
		R65	No trend	0.35	0.00	TXn	**Decreasing**	-2.53 [b]	0.00
		R95p	**Increasing**	3.01[b]	48.30	TXx	**Decreasing**	-4.28[a]	-0.10
		R99p	No trend	1.20	11.30	TN10p	**Decreasing**	-4.66[a]	-0.20
		RX1day	**Increasing**	2.00[c]	2.40	TN90p	**Increasing**	8.50[a]	2.90
		RX5day	No trend	1.58	1.50	TX10p	No trend	1.93	0.20
		CWD	No trend	-1.78	-9.60	TX90p	**Decreasing**	-2.09[c]	-0.30
		CDD	**Decreasing**	-2.55[a]	-0.70	DTR	**Decreasing**	-10.60[a]	-0.30

Note : Sen's slope is in unit/decade; bold indicates statistically significant values. a 0.1% significance level; b 1% significance level; c 5% significance level

Table 6.13: The trend in historical and projected rainfall and temperature extreme indices in Netravati basin

			Rainfall Indices				**Temperature Indices**		
		Indices	Trend	Statistic Value	Sen's slope	Indices	Trend	Statistic Value	Sen's slope
Historical	(1951-2013)	R10	No trend	0.50	0.40	TNn	No trend	-1.95	-0.10
		R30	No trend	-0.21	0.00	TNx	No trend	0.92	0.00
		R65	No trend	-1.38	0.00	TXn	**Increasing**	4.23[a]	0.20
		R95p	No trend	-1.39	-36.30	TXx	**Increasing**	4.55 [a]	0.20
		R99p	**Decreasing**	-2.81[b]	0.00	TN10p	No trend	-1.61	-0.40
		RX1day	**Decreasing**	-2.70 [b]	-6.30	TN90p	**Increasing**	2.12 [c]	1.20
		RX5day	No trend	0.26	0.30	TX10p	**Decreasing**	-5.36[a]	-2.50
		CWD	No trend	-0.93	-1.40	TX90p	**Increasing**	14.32[a]	4.40
		CDD	No trend	-1.01	-2.50	DTR	**Increasing**	4.00[a]	0.20
Near Future (2021-2050)	SSP245	R10	No trend	1.89	2.50	TNn	No trend	0.58	0.00
		R30	No trend	0.74	0.50	TNx	**Increasing**	4.26[a]	0.10
		R65	No trend	0.52	0.00	TXn	**Increasing**	3.62[a]	0.30
		R95p	No trend	1.55	29.60	TXx	No trend	1.77	0.10
		R99p	No trend	1.17	0.00	TN10p	**Decreasing**	-5.09[a]	-1.50
		RX1day	No trend	1.66	3.40	TN90p	**Increasing**	5.64[a]	8.40
		RX5day	**Increasing**	2.05[a]	2.10	TX10p	**Increasing**	5.16[a]	4.30
		CWD	No trend	0.79	3.00	TX90p	**Decreasing**	-5.44[a]	-4.10
		CDD	No trend	-0.16	0.00	DTR	**Decreasing**	-5.91[a]	-0.30
	SSP585	R10	**Increasing**	2.40 [c]	0.33	TNn	**Increasing**	2.98[b]	0.20
		R30	No trend	1.38	0.60	TNx	No trend	1.82	0.10
		R65	No trend	1.35	0.00	TXn	No trend	1.09	0.10
		R95p	No trend	1.35	25.30	TXx	No trend	1.16	0.00
		R99p	No trend	0.81	0.00	TN10p	**Decreasing**	-7.51[a]	-1.80
		RX1day	No trend	0.04	0.10	TN90p	**Increasing**	7.23[a]	11.00
		RX5day	No trend	1.48	2.20	TX10p	**Increasing**	7.40[a]	2.20
		CWD	**Increasing**	2.05[c]	11.90	TX90p	**Decreasing**	-5.91[a]	-3.30
		CDD	No trend	-0.97	-0.40	DTR	**Decreasing**	-6.33[a]	-0.40
Far Future (2051-2100)	SSP245	R10	**Increasing**	3.47[a]	1.90	TNn	**Increasing**	3.70[a]	0.30
		R30	No trend	0.36	0.00	TNx	No trend	0.40	0.00
		R65	No trend	0.00	0.00	TXn	**Increasing**	1.07[a]	0.20
		R95p	No trend	0.47	8.50	TXx	No trend	-0.55	0.00
		R99p	No trend	0.92	0.00	TN10p	**Decreasing**	-2.59[b]	-0.20
		RX1day	No trend	0.06	0.20	TN90p	**Increasing**	5.24[a]	2.30
		RX5day	No trend	0.49	0.20	TX10p	No trend	1.89	0.20
		CWD	No trend	0.55	1.70	TX90p	No trend	-1.86	-0.40
		CDD	No trend	-1.42	-0.60	DTR	**Decreasing**	-5.77[a]	-0.20
	SSP585	R10	**Increasing**	3.07[a]	2.30	TNn	**Increasing**	7.02[a]	0.40
		R30	**Increasing**	2.00[c]	1.10	TNx	**Increasing**	3.51 [a]	0.10
		R65	No trend	0.91	0.00	TXn	**Increasing**	3.65[a]	0.10
		R95p	No trend	1.73	31.30	TXx	**Decreasing**	-2.78[b]	-0.10
		R99p	No trend	1.33	0.00	TN10p	**Decreasing**	-2.98[b]	0.00
		RX1day	No trend	1.52	2.70	TN90p	**Increasing**	5.60[a]	1.80
		RX5day	No trend	0.55	0.20	TX10p	No trend	-1.55	0.00
		CWD	No trend	-0.86	-3.50	TX90p	**Decreasing**	-4.45[a]	-0.50
		CDD	No trend	-1.89	-0.60	DTR	**Decreasing**	-8.19[a]	-0.40

Note : Sen's slope is in unit/decade; bold indicates statistically significant values. a 0.1% significance level; b 1% significance level; c 5% significance level

Table 6.14: The trend in historical and projected rainfall and temperature extreme indices in Aghanashini basin

			Rainfall Indices				**Temperature Indices**		
		Indices	Trend	Statistic Value	Sen's slope	Indices	Trend	Statistic Value	Sen's slope
Historical (1951-2013)		R10	**Increasing**	2.01[c]	1.50	TNn	No trend	-1.45	-0.10
		R30	**Increasing**	3.12[a]	1.60	TNx	No trend	-1.43	-0.10
		R65	**Increasing**	2.98[b]	0.50	TXn	**Increasing**	4.41[a]	0.20
		R95p	**Increasing**	2.83[b]	53.90	TXx	**Increasing**	3.26[a]	0.10
		R99p	No trend	0.76	0.00	TN10p	No trend	0.22	0.10
		RX1day	No trend	1.58	6.20	TN90p	No trend	0.48	0.20
		RX5day	No trend	1.42	2.20	TX10p	**Decreasing**	-5.06[a]	-2.20
		CWD	**Increasing**	6.24[a]	10.30	TX90p	**Increasing**	5.64[a]	3.60
		CDD	**Increasing**	2.44[b]	6.40	DTR	**Increasing**	4.75 [a]	0.20
Near Future (2021-2050)	SSP245	R10	**Increasing**	2.36[b]	1.90	TNn	**Increasing**	2.52[b]	0.30
		R30	No trend	-0.12	0.00	TNx	No trend	1.95	0.10
		R65	No trend	1.37	0.00	TXn	No trend	0.36	0.00
		R95p	No trend	0.70	12.00	TXx	**Increasing**	2.49[c]	0.10
		R99p	No trend	1.56	0.00	TN10p	**Decreasing**	-4.14[a]	-0.90
		RX1day	No trend	0.73	1.40	TN90p	**Increasing**	5.51 [a]	8.20
		RX5day	**Increasing**	2.79[a]	1.80	TX10p	No trend	-1.60[a]	-0.10
		CWD	No trend	1.30	5.50	TX90p	No trend	1.09	0.30
		CDD	No trend	-0.85	-1.20	DTR	**Decreasing**	-2.32[c]	-0.10
	SSP585	R10	No trend	0.91	0.08	TNn	**Increasing**	4.49[a]	0.50
		R30	No trend	-0.20	0.00	TNx	No trend	1.64	0.00
		R65	No trend	-0.13	0.00	TXn	**Increasing**	5.12[a]	0.40
		R95p	No trend	-1.11	-31.40	TXx	No trend	0.67	0.00
		R99p	No trend	0.31	0.00	TN10p	**Decreasing**	-4.73[a]	-1.20
		RX1day	No trend	-1.74	-5.55	TN90p	**Increasing**	11.08[a]	8.70
		RX5day	No trend	-0.85	-0.90	TX10p	No trend	-1.89	-0.10
		CWD	No trend	-1.61	-5.20	TX90p	No trend	1.52	0.70
		CDD	No trend	-1.38	-1.80	DTR	**Decreasing**	-6.93 [a]	-0.20
Far Future (2051-2100)	SSP245	R10	No trend	0.82	0.60	TNn	**Increasing**	4.06[a]	0.20
		R30	No trend	-0.13	0.00	TNx	No trend	-1.93	0.00
		R65	No trend	1.17	0.00	TXn	**Increasing**	3.40[a]	0.20
		R95p	No trend	0.11	2.10	TXx	No trend	-1.24	0.00
		R99p	No trend	0.10	0.00	TN10p	No trend	-1.38	-0.10
		RX1day	No trend	-1.10	-1.50	TN90p	**Increasing**	3.06[a]	0.90
		RX5day	No trend	-0.16	-0.10	TX10p	No trend	0.47	0.00
		CWD	No trend	-0.36	-1.40	TX90p	No trend	-1.77	-0.60
		CDD	**Decreasing**	-2.80[a]	-2.70	DTR	**Decreasing**	-3.18[a]	0.00
	SSP585	R10	**Increasing**	3.03[a]	2.90	TNn	**Increasing**	6.12[a]	0.50
		R30	**Increasing**	3.04[a]	2.50	TNx	**Decreasing**	-2.24[c]	-0.10
		R65	No trend	0.48	0.00	TXn	No trend	-1.03	0.00
		R95p	**Increasing**	2.91[a]	78.40	TXx	No trend	1.57	0.00
		R99p	No trend	0.76	0.00	TN10p	**Decreasing**	-5.12[a]	-0.30
		RX1day	No trend	1.02	2.00	TN90p	**Increasing**	2.20[a]	0.80
		RX5day	No trend	0.97	0.80	TX10p	**Increasing**	3.41[a]	0.50
		CWD	No trend	0.23	0.90	TX90p	**Decreasing**	-7.04[a]	-2.50
		CDD	No trend	-0.56	-0.40	DTR	**Decreasing**	-7.54[a]	-0.20

Note : Sen's slope is in unit/decade; bold indicates statistically significant values. a 0.1% significance level; b 1% significance level; c 5% significance level

Table 6.15: The trend in historical and projected rainfall and temperature extreme indices in Ulhas basin

		Rainfall Indices				Temperature Indices			
		Indices	Trend	Statistic Value	Sen's slope	Indices	Trend	Statistic Value	Sen's slope
Historical	(1951-2013)	R10	No trend	0.48	0.30	TNn	No trend	0.84	0.10
		R30	No trend	0.32	0.00	TNx	No trend	-1.63	-0.10
		R65	No trend	1.64	0.50	TXn	No trend	0.46	0.00
		R95p	**Increasing**	2.48[c]	58.20	TXx	**Increasing**	2.48[b]	0.10
		R99p	**Increasing**	2.29[c]	33.50	TN10p	**Decreasing**	-2.94[a]	-0.70
		RX1day	**Increasing**	2.57[b]	17.20	TN90p	No trend	1.30	0.60
		RX5day	**Increasing**	2.62[b]	8.00	TX10p	**Decreasing**	-3.35[a]	-1.00
		CWD	No trend	-1.65	-2.50	TX90p	**Increasing**	4.16[a]	1.80
		CDD	**Increasing**	2.39[c]	10.40	DTR	**Increasing**	2.66[b]	0.10
Near Future (2021-2050)	**SSP245**	R10	No trend	0.80	0.90	TNn	**Increasing**	2.16[c]	0.30
		R30	No trend	0.00	0.00	TNx	**Increasing**	3.10[a]	0.30
		R65	No trend	-0.46	0.00	TXn	**Increasing**	3.67[a]	0.20
		R95p	No trend	0.50	7.40	TXx	**Increasing**	5.75[a]	0.20
		R99p	No trend	0.20	0.00	TN10p	No trend	0.37	0.10
		RX1day	No trend	-0.59	-2.50	TN90p	**Increasing**	4.95[a]	6.90
		RX5day	No trend	-0.88	-1.00	TX10p	**Decreasing**	-4.78[a]	-4.10
		CWD	No trend	-1.49	-4.50	TX90p	**Increasing**	5.72[a]	6.20
		CDD	No trend	0.60	2.40	DTR	No trend	1.61	0.10
	SSP585	R10	No trend	1.47	1.50	TNn	**Increasing**	3.03[b]	0.30
		R30	No trend	0.83	0.40	TNx	No trend	-0.66	0.00
		R65	No trend	0.36	0.00	TXn	**Increasing**	2.59[b]	0.20
		R95p	No trend	1.40	43.20	TXx	**Increasing**	4.26[a]	0.50
		R99p	No trend	-0.62	0.00	TN10p	**Decreasing**	-4.01[a]	-1.10
		RX1day	No trend	0.46	2.30	TN90p	**Increasing**	8.61[a]	11.30
		RX5day	No trend	0.20	0.40	TX10p	**Decreasing**	-6.16[a]	-5.00
		CWD	No trend	0.80	3.30	TX90p	**Increasing**	4.91[a]	2.90
		CDD	No trend	-0.47	-1.80	DTR	No trend	-0.88	0.00
Far Future (2051-2100)	**SSP245**	R10	No trend	0.47	0.30	TNn	**Increasing**	4.43[a]	0.30
		R30	No trend	1.25	1.10	TNx	No trend	0.81	0.00
		R65	**Increasing**	2.49[c]	0.00	TXn	**Increasing**	3.51[a]	0.20
		R95p	**Increasing**	3.73[a]	59.30	TXx	**Increasing**	4.90[a]	0.20
		R99p	**Increasing**	2.79[b]	0.00	TN10p	No trend	0.72	0.20
		RX1day	No trend	1.54	4.70	TN90p	**Increasing**	3.19[b]	2.30
		RX5day	**Increasing**	2.09[c]	2.40	TX10p	**Decreasing**	-5.48[a]	-2.70
		CWD	No trend	0.72	1.50	TX90p	**Increasing**	6.87[a]	3.50
		CDD	**Increasing**	3.21[a]	3.00	DTR	No trend	0.10	0.00
	SSP585	R10	No trend	0.35	0.00	TNn	**Increasing**	4.07[a]	0.50
		R30	No trend	1.86	0.40	TNx	**Decreasing**	-3.43[a]	-0.10
		R65	No trend	1.27	0.00	TXn	**Increasing**	9.05[a]	0.50
		R95p	**Increasing**	2.54[c]	42.30	TXx	**Increasing**	6.40[a]	0.40
		R99p	**Increasing**	2.54[c]	9.00	TN10p	No trend	1.53	0.30
		RX1day	**Increasing**	2.44[c]	8.10	TN90p	**Decreasing**	-4.34[a]	-2.40
		RX5day	**Increasing**	2.02[c]	3.10	TX10p	**Decreasing**	-7.53[a]	-4.70
		CWD	No trend	-0.39	-2.00	TX90p	**Increasing**	8.40[a]	8.70
		CDD	No trend	-1.77	-3.30	DTR	**Increasing**	7.37[a]	0.40

Note : Sen's slope is in unit/decade; bold indicates statistically significant values. a 0.1% significance level; b 1% significance level; c 5% significance level

Table 6.16: The trend in historical and projected rainfall and temperature extreme indices in Purna basin

		Rainfall Indices				Temperature Indices			
		Indices	Trend	Statistic Value	Sen's slope	Indices	Trend	Statistic Value	Sen's slope
Historical	(1951-2013)	R10	No trend	0.40	0.20	TNn	No trend	1.54	0.20
		R30	No trend	0.09	0.00	TNx	No trend	-0.65	0.00
		R65	No trend	-0.01	0.00	TXn	No trend	-0.81	-0.10
		R95p	No trend	-0.35	-4.30	TXx	No trend	-0.49	0.00
		R99p	No trend	0.40	0.00	TN10p	**Decreasing**	-2.76[a]	-1.00
		RX1day	No trend	-0.41	-2.90	TN90p	No trend	0.22	0.10
		RX5day	No trend	0.69	0.80	TX10p	No trend	-1.03	-0.30
		CWD	**Decreasing**	-2.02[c]	-1.10	TX90p	No trend	0.71	1.80
		CDD	No trend	0.63	2.00	DTR	No trend	-1.01	0.00
Near Future (2021-2050)	**SSP245**	R10	No trend	0.01	0.00	TNn	**Increasing**	2.34[c]	0.30
		R30	No trend	0.01	0.00	TNx	No trend	1.20	0.00
		R65	No trend	-0.48	0.00	TXn	No trend	1.72	0.10
		R95p	No trend	0.14	5.50	TXx	**Increasing**	10.81[a]	0.40
		R99p	**Increasing**	0.50	1.53[c]	TN10p	**Decreasing**	-3.96[a]	-1.10
		RX1day	No trend	0.16	0.80	TN90p	**Increasing**	7.61[a]	8.80
		RX5day	No trend	0.35	0.70	TX10p	**Decreasing**	-5.67[a]	-4.50
		CWD	No trend	-0.14	0.00	TX90p	**Increasing**	8.37[a]	2.70
		CDD	No trend	-1.09	-6.70	DTR	No trend	-0.03	0.00
	SSP585	R10	No trend	1.47	15.00	TNn	**Increasing**	3.03[a]	3.00
		R30	No trend	0.83	4.00	TNx	No trend	-0.66	0.00
		R65	No trend	0.36	0.00	TXn	**Increasing**	2.59[b]	0.20
		R95p	No trend	1.40	43.20	TXx	**Increasing**	4.26[a]	0.50
		R99p	No trend	-0.62	0.00	TN10p	**Decreasing**	-4.01[a]	-1.10
		RX1day	No trend	0.46	23.00	TN90p	**Increasing**	8.61[a]	11.30
		RX5day	No trend	0.20	4.00	TX10p	**Decreasing**	-6.16[a]	-5.00
		CWD	No trend	1.47	21.00	TX90p	**Increasing**	4.91[a]	2.90
		CDD	No trend	1.28	8.00	DTR	No Trend	-1.89	-0.039
Far Future (2051-2100)	**SSP245**	R10	No trend	0.39	0.40	TNn	**Increasing**	2.63[b]	0.20
		R30	No trend	1.08	0.30	TNx	No trend	1.57	0.00
		R65	No trend	1.36	0.00	TXn	**Increasing**	4.08[a]	0.10
		R95p	**Increasing**	1.35	22.20[c]	TXx	**Increasing**	4.47[a]	0.20
		R99p	**Increasing**	1.75	4.10[a]	TN10p	**Increasing**	2.08[a]	0.50
		RX1day	No trend	0.99	3.60	TN90p	**Increasing**	3.20[a]	1.40
		RX5day	No trend	1.44	1.50	TX10p	**Decreasing**	-10.23[a]	-3.10
		CWD	No trend	-0.16	0.00	TX90p	**Increasing**	4.95[a]	1.80
		CDD	No trend	-1.31	-5.00	DTR	Increasing	1.41	0.052
	SSP585	R10	No trend	0.35	0.00	TNn	**Decreasing**	-2.56[b]	-6.90
		R30	No trend	1.86	0.40	TNx	**Increasing**	12.62[a]	0.60
		R65	No trend	1.27	0.00	TXn	**Increasing**	5.82[a]	0.20
		R95p	**Increasing**	2.54[c]	42.30	TXx	**Increasing**	4.07[a]	0.50
		R99p	**Increasing**	2.54[c]	9.00	TN10p	**Decreasing**	-3.43[a]	-0.10
		RX1day	**Increasing**	2.44[c]	8.10	TN90p	**Increasing**	9.05[a]	0.50
		RX5day	**Increasing**	2.02[a]	3.10	TX10p	**Increasing**	6.40[a]	0.40
		CWD	No trend	0.44	0.90	TX90p	**Decreasing**	-7.53[a]	-4.70
		CDD	**Decreasing**	-2.56[b]	-6.90	DTR	**Decreasing**	-4.34[a]	-2.40

Note: Sen's slope is in unit/decade; bold indicates statistically significant values. a 0.1% significance level; b 1% significance level; c 5% significance level

6.3.10 The Quantification of Trend in Historical and Projected Rainfall Extreme Indices

The absolute indices, percentile indices, threshold-based indices, duration-based indices are used to characterize the extreme rainfall events over the river basins in the historical period, near future, and far future horizon. The variation in the mean rainfall indices in the future horizon with respect to the historical period is shown in Figures 6.33, 6.34, 6.35, and 6.36. The mean of duration based index CWD indicates the less mean than the historical period in the future over the southern basins. Whereas, it remains same in the central river basin and increases linearly in the northern river basins especially from NF to FF horizon. The Vamanapuram (3.68 days per decade), Netravati, Ulhas and Purna (1.1 days per decade) had endured a decreasing trend in the historical period and Chaliyar (13.67 days), Aghanashini (10.30 days) had experienced a increasing trend in CWD, with insignificant increase in CDD. In the future decades, insignificant increasing trend is noted under SSP245 in southern and central basins, whereas insignificant decreasing trend is noted in Ulhas river basin along with the decrease in CDD in future horizon. The variation in the mean over the northern basins shows an increase from historical to future period. Previous research has also pointed to the increase in CWD under the climate change scenarios (Basha *et al.*, 2017; Rai *et al.*, 2019; Varghese *et al.*, 2020; Kumar *et al.*, 2021).

The change in the mean value of the absolute indices is shown in Figure 6.34. From the mid-twentieth century to the first decade of the twenty-first century, the one-day (RX1day) highest rainfall has significantly decreased in the Chaliyar basin by 5.40 mm/decade, increased in the Ulhas basin by 17.23 mm/decade and total five-day maximum rainfall (RX5day) has decreased at Vamanapuram (12.97 mm/decade), Chaliyar (15.70 mm/decade), Netravati basins (6.31 mm/decade) and increased in the Ulhas by 7.95 mm/decade, respectively. In the future epoch, the significant/ insignificant upward trend is observed in both the SSPs with significant increase of 2.97 mm in Vamanapuram, 2.40 mm in Chaliyar, 8.10 mm in Ulhas and 4.10 mm in Purna per , decade in RX1day and 1.47 mm, 1.50 mm, 3.10

mm, 2.48 mm in the RX5day in these basins respectively.

The percentile indices (Figure 6.35) R95p rise in the southern and northern river basins from historical to far future, and in the central river basin Netravati the mean is almost same as of historical mean, and in Aghanashini the mean shows a decrease in the NF, which then increases toward the end of the 21st century. The observed increase in mean is higher in the SSP585 scenario than the SSP245 scenario. Whereas, in the extremely wet rainfall (R99p), the linear increase in mean is observed in the Vamanapuram and Aghanshini river basins. The extremely wet rainfall has decreased significantly in the Chaliyar at a rate of 28.4 mm/decade,and increased Ulhas at a magnitude of 58.20 mm/decade with insignificant declining trend in Vamanapuram river basin. The southern basins and the Netravati basin has recorded a insignificant decreasing trend in the very wet day rainfall (R95p) at a magnitude of 40.86 mm, 33.44 mm, 36.30 mm in Vamanapuram, Chaliyar and Netravati basin, and a significant increasing trend of 53.9 mm, 33.5 mm per decade in Aghanashini and Ulhas river basins. The magnitude of increase in the percentile based indices is more pronounced in the SSP585 scenario, than the SSP245 scenario. The northern river basins experience an significant increase in the R99p, and R95p, RX1day and RX5day compared to other river basins.

The threshold-based indices (Figure 6.36), R10 and R30 increase gradually in all the basins leaving no drastic variation in the far future in Vamanapuram. The increase in a mean R10 varies from 9($\pm$1.5)% in humid basins to 30(($\pm$15)% in other basins. The Aghanashini, Ulhas, and Purna will undergo a 53–58% increase in the R30 in the far future compared to the historical period. The R65 also records an increase over the northern river basins. The R10 significantly increases in the NF over Chaliyar (2.9 days), Aghanashini (1.9 days) with increase in R30 in the Vamanapuram. In the FF Netravati experience an increase in both R10 and R30 days with no significant trend in northern river basins. The aforementioned alterations observed in the northern river basins serve as a clear indication that these basins will experience severe climatic events in the forthcoming decades.

The study by Sarkar and Maity (2022) has noted an increase in the frequency of precipitation extremes monopolize over the intensity. This is particularly true in the Vamanapuram and northern part of WG. These changes might have different impacts on the environment, infrastructure, and communities.

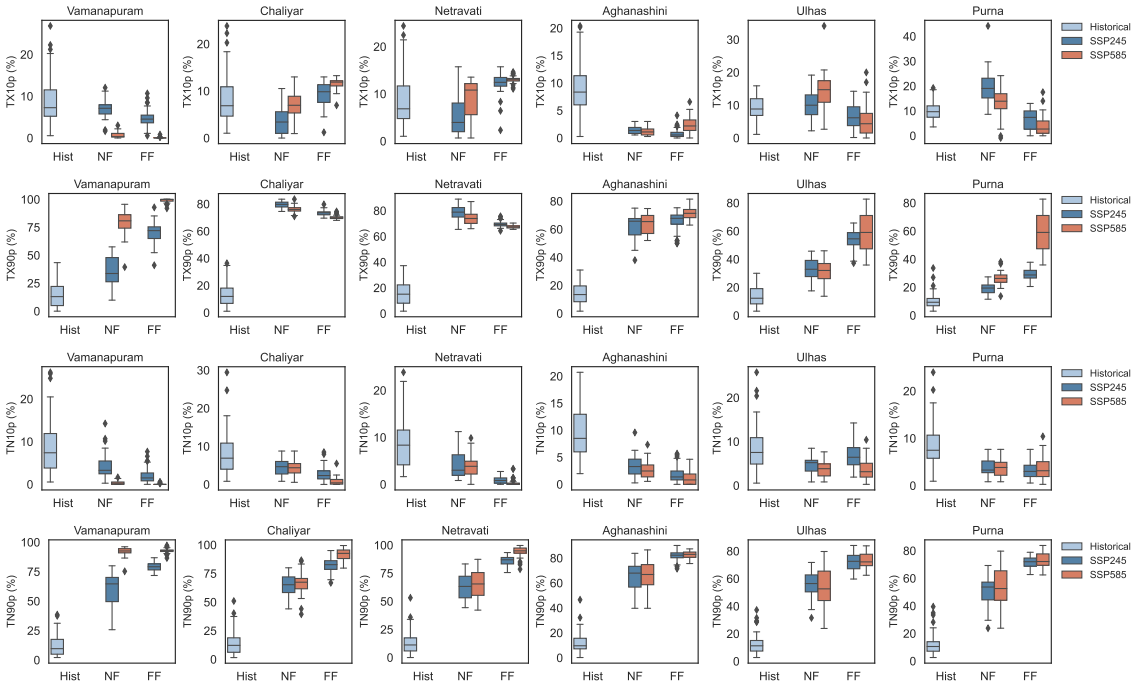

Fig. 6.38: Transition in the distribution of frequency-based temperature indices from historical to far future

6.3.11 The Quantification of Trend in Historical and Projected Temperature Extremes

The variation in the mean temperature indices in the future horizon with respect to the historical period is shown in Figures 6.37, 6.38. The annual maximum value of maximum temperature (TXx) will increase in all the basins in the NF, which remains steady/declines in the FF over the central river basins. The northern basins experience an increase in the hottest days with higher variability under the medium emission scenario. The annual minimum value of maximum temperature (TXn) exhibits a pronounced increase towards the mid 21st century in all the basins representing a decrease in the coldest days in the future with a mean

variation of approximately 4.56°C relative to the base period. The annual maximum value of minimum temperature (TNx) has a distinct variation in the basins. In the near future, the minimum temperature will intensify in all the basins. The annual minimum value of minimum temperature (TNn) discloses an increase, representing an increase in the warmest nights in the future. These have confined the variability in the maximum and minimum temperature resulting in a decrease in the di-urinal temperature. The percentile-based indices indicate the percent of warm days/nights and cool days/nights. By the end of the century, warm days and nights increase roughly by 45–65% and 45–70% in Aghanshini and northern river basins, and 45-85%, 60-80% in southern and Netravati river basins receptively. However, there will be a rapid rise in the percentage of warm nights in the near future compared to the baseline period. In Ulhas, the percentage of cool nights increases in the far future as opposed to the near future under SSP245 scenario. After the mid-century mark, the Ulhas basin endures an increase in cool nights compared to NF. The cool days (TX10p) decreases in southern and central river basins from historical to NF,which further increases in the FF. In contrary to this, increase in TX10p is noted in the Ulhas and Purna river basins, which decreases after the mid century.

In the historical period, the annual minimum value of daytime temperature (TXn) has seen an increment of 0.19°C in Vamanapuram and 0.4°C in Chaliyar basin, 0.19(±0.002) °C/decade in central basins, 0.07 °C/decade in Purna basin. The annual maximum of maximum temperature has significantly increased in all the basins ranging from 0.14(±0.04) °C/decade, 0.18(±0.02) °C/decade, 0.04(±0.01) °C/decade in southern, central and northern basins. The TNx and TNn has no significant trend in the historical period. In the near future decades, the TXn, TXn, TNx, TNn encompass a statistically significant increase in all the river basins with higher magnitude of increase in the near future under both the scenarios, with highest rate of increase in the northern river basins. The TNx decreases in the Chaliyar, Aghanshini and Ulhas river basin in the SSP585 scenario at the end of the century at a magnitude of 0.1-0.25°C. In the future, the

rate of increase in night time temperatures (TNn) will be higher than the rate of increase in daytime temperature (TXx), signifying rapid warming in night temperature than the day temperature. The percentile indices TX90p, an indicator of a warm day, has seen an increase in all the six basins at an alarming rate of 4.44%, 2.61%, 4.37%, 3.62%, 1.83%, and 1.87% from southern to northern basins. The warm night (TN90p) has significantly increased in Vamanapuram and Netravati, insignificantly in other basins with a statistically significant decrease in the cool nights (TN10p) over Chaliyar, and in the northern basins, insignificant decrease in Vamanapuram, Netravati and Aghanshini. These basins have combated the decrease in the cool days by 4.6% in Chaliyar, 2.5±0.3% over Vamanapuram, Netravati, Aghanashini, and 0.96% over Ulhas basin. With a significant increase in the warm days, the forthcoming decades have to endure a pervasive decrease in the coolest days/nights in all the basins except the Chaliyar and Netravati basins. This trend continues till the mid-21st century, thereafter the basin Vamanapuram experience an increase in the percentage of cool nights, Aghanshini (0.43%) and Purna (0.4%) in cool days. The TX90p will climb upward in the future with a higher percentage of increase in the near future; TX10p will experience an decrease in all the basins except Chaliyar and Netravati in the foreseeing decades and in far future under SSP585 in all the river basins, representing the increase in cool days. Also, the TN90p increases at an approximate average percentage of 11.4% in southern, 6.8% in central basins, 7.5% in northern basins in the near decades, which extends to the far future at a lesser magnitude of increase with reduction in the northern river basins (0.38-2.51%). Overall, these results suggest that the region will experience a high increase in the intensity, duration, and frequency of hot extremes in the forthcoming decades with the existence of increased cool days/nights and declines in hot extremes after the mid 21st century with the incline in cold extremes over the basins with respect to the base period under high emission scenario. By the end of 2100, the basins encompass an increase in cool nights over humid to per-humid basins. The decline in the trend of extreme heat days/nights and the increase in cool days/nights reduces the di-urinal tempera-

ture variability. This demonstrates the effectiveness of mitigation and adaptation measures considered in the SSP scenarios.

6.4 CONCLUSIONS

In this study an attempt has been made to obtain the ability of the top performing four ML-MMEs (RFR, SVR, ETR, and XGBR) and the AM MME in the estimation of extreme climate indices. In order to understand the simulation ability of the MMEs to capture extreme climatic events, nine precipitation indices and nine temperature-based indices, formulated by the Expert Team on Climate Change Detection and Indices have been analysed. The temperature intensity-based indices (hottest day, warmest night, coldest day, coldest night) and frequency-based indices (warm days (TX90p), warm nights (TN90p), cold days (TX10p), and cold nights (TN10p)) are used to evaluate the change in the intensity and frequency of the temperature. To evaluate the characteristics of precipitation, the absolute precipitation indices (R×1day, R×5day), percentile indices (R95p, R99p), threshold-based indices (R10, R30, R65), duration-based indices are used. Despite excellent accuracy in predicting daily/monthly rainfall, the MMEs have shown a higher variability in calculating climatic indices. The GCM models ensembled through extreme gradient boosting is capable to capture the trend, variability in time series making it useful for forecasting future extreme indices. In the coming decades, June and July rainfall will be highly inconsistent, while September rainfall in all river basins will increase in combination with an increase in May. Also, the rainfall in October and November increases in northern river basins in the future horizons. The temperature anomaly is stronger in the high-emission scenario than in the medium-emission scenario and the warming starts from November and extends upto June introducing a significantly hotter winter and the extended summer season. The increase in greenhouse gas concentration has higher repercussions on the daily minimum temperature than the daily maximum temperature, especially in the winter, leading to nearly two times the magnitude of the trend in other seasons. The basins, the mean annual tem-

perature rises by 1.2-1.79 °C over southern basins, 1.55-1.75°C over central river basins, 0.3-0.58 °C over the northern river basins by the 2050s. Which increases again by 0.6-0.72 (±0.03)°C by the end of the century over southern and central river basins and by 0.97-1.76 °C over the northern river basins. After the mid-21st century, the warming trends start to slow down with decreasing trends in the pre-monsoon maximum temperature in southern and central river basins and a decrease in the monsoon minimum temperature in the northern river basins. This perhaps demonstrates the efficiency of planned initiatives for climate reduction and adaptation under the composition of the socio-economic and radiative forcing projection. By the end of the century, warm days and nights increase roughly by 45–65% and 45–70% in Aghanshini and northern river basins, and 45-85%, 60-80% in southern and Netravati river basins receptively. However, there will be a rapid rise in the percentage of warm nights in the near future compared to the baseline period. The magnitude of increase in the percentile based rainfall indices is more pronounced in the SSP585 scenario, than the SSP245 scenario. The northern basins undergo a drastic increase in the very wet to extremely wet days rainfall and medium to very heavy rainfall with a decrease in CDD in the future. The CWD increases in the future most of the basins with a decrease in CDD. This highlights the flood risk in these basins. Overall, the basins will experience a high increase in the intensity, duration, and frequency of hot extremes in the forthcoming decades with the existence of increased cool days/nights with respect to the base period over the basins after the mid 21st century under high emission scenario. This gives an insight into the adaptation strategies that must be implemented in urban planning, infrastructure development, and agriculture.

CHAPTER 7

CLIMATE CHANGE IMPACT ON STREAMFLOW AND WATER SCARCITY RISK

7.1 BACKGROUND

The risk of water scarcity is escalating due to a rise in sectoral water demands and a decrease in basin-scale water availability caused by climate change-induced inhomogeneous temporal distribution of precipitation and decreased streamflow (Duan *et al.*, 2019). Spatiotemporal inconsistency between water availability and demand may pose a worldwide threat of water scarcity. Rapid industrialization, urbanization, population growth, a higher standard of living, and alterations in the water consumption patterns of various sectors are the anthropogenic causes of the increased water demand. India is under a water stressed condition, and the country's water demand is expected to rise by as much as 24% and 74% by 2025 and 2050 (Saleth, 2011). Further, the climate change will exacerbate the strain on freshwater systems, which are already burdened by human activities unrelated to climate change. This would occur through the modification of future water availability and usage patterns, consequently amplifying the levels of water and food stress (Döll and Zhang, 2010). To mitigate the imminent risk of severe water shortages, it is imperative for the nation to actively endorse the sustainable utilization of water resources, thereby aligning with the objectives outlined in Goal 6 of the United Nations Sustainable Development Goals. The inadequate knowledge of basin-scale hydrology, and more specifically, the causes and impacts of streamflow changes, is a significant contributor to the potential severity of water scarcity problems (Li *et al.*, 2018). The modelling and forecasting of streamflow are essential for water resource management, flood control, and hydroelectricity management. Currently, physical-based and data-driven models have been devised to forecast daily or hourly streamflow. Physical based models function by representing phys-

ical processes and boundary conditions and solving the complex mathematical equations underlying them, whereas data-driven models imitate physical norms derived from historical data to establish a functional relationship between inputs and outputs. Utilizing time-dependent mechanistic machine learning techniques, researchers have improved the accuracy of discharge modelling and captured the non-linear behaviour of basins (Masselot *et al.*, 2016). By considering different spatial scales and integrating diverse basin properties, these methods facilitate a deeper comprehension of hydrological processes and have the potential to open up new avenues in streamflow modelling (Booker and Woods, 2014; Masselot *et al.*, 2016). Long Short-Term Memory (LSTM) is a form of recurrent neural network (RNN) that has demonstrated success in modelling time-dependent and sequential data. LSTM model is particularly well-suited for capturing long-range dependencies and handling temporal dynamics in data. The model is capable of simulating hydrologic events more efficiently than the physical-based hydrological model, like the soil and Water Assessment Tool (Kim *et al.*, 2021; Song *et al.*, 2022). Therefore in this study, the projected decadal variation in the streamflow, along with the rainfall and the water risk vulnerability of the basins under the future scenario, is analysed.

7.2 METHODOLOGY

The precipitation, maximum, mean, and minimum temperature, and PET data at each basin, along with the historical streamflow data, are used as input to the LSTM model. LSTM is an extension of RNN and is highly adept at forecasting time series data. The primary distinction between RNN and LSTM is that LSTM can store long-range time dependency information and map input and output data appropriately. LSTM consists of three gates, namely the input gate, forget gate and the output gate. These gates are responsible for the network to save, forget, pay attention, or pass the information to other cells (Yamak *et al.*, 2019). Figure 7.1 depicts the architecture of an LSTM cell, an input gate (i_t), which regulates how the input x_t updates the internal state; a forget gate (f_t), and an output gate

(o_t), which controls how the internal state and new input influence the cell output ht.

$$f_t = \sigma(u_f x_t + w_f h_{\text{t-1}} + b_f) \tag{7.1}$$

$$i_t = \sigma(u_i x_t + w_i h_{\text{t-1}} + b_i) \tag{7.2}$$

$$o_t = \sigma(u_o x_t + w_o h_{\text{t-1}} + b_o) \tag{7.3}$$

$$c_{\text{et}} = tanh(w_c x_t + u_c h_{\text{t-1}} + b_c) \tag{7.4}$$

$$c_t = f_t c_{\text{t-1}} + i_t c_{\text{et}} \tag{7.5}$$

$$ht = tanh c_t \times o_t \tag{7.6}$$

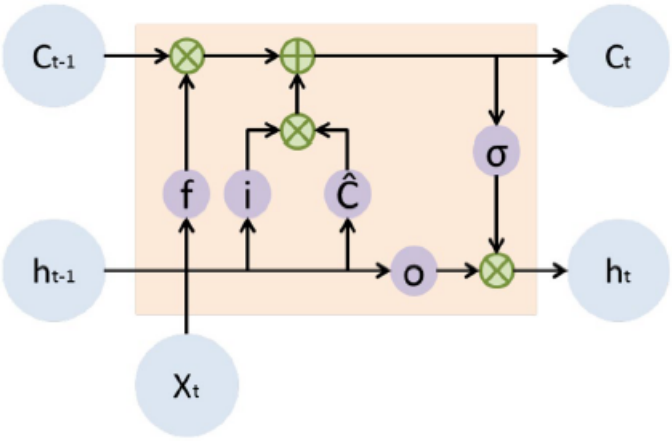

Fig. 7.1: LSTM memory cell with three gated layers

The weight matrices w_i, w_f, w_o, and w_c correspond to the input gate, forget gate, output gate, and cell gate units, respectively. While u_i, u_f, u_o, and u_c weight matrices map the hidden layer output gates, b_i, b_f, b_o, and b_c are the bias vectors of the input gate, forget gate, output gate, and cell gate units, respectively. Moreover, c_t and h_t are a memory cell and hidden state, σ and tanh

are the activation functions. The network is compiled using the Adam optimizer and mean squared error loss function; Adam, the latest version of the optimization algorithm for stochastic gradient descent, which can rapidly and accurately search for optimal machine learning values. The optimal hyper parameters have been obtained using the efficient randomized search method called Keras Tuner, developed by the Google team to search random combinations of parameters for optimized performance.

Based on the streamflow data availability Vamanapuram (1979–2013), Chaliyar (1980–2013), Netravati (1970–2013), Aghanashini (1988–2013), Ulhas (2003–2020), and Purna (1971–2013), the data is divided into training and validation of model. The long series is used to train the model, and the last eight years of data are used to validate the model's prediction. The decadal variability in the percentage of annual rainfall and the streamflow under the future scenario are evaluated for six river basins. Since granular data and sectoral water demands are not easily accessible for most river systems, baseline water demand which is the relative change in streamflow (Q) and water availability (WA), was used to conduct the water-scarcity risk assessment for the data-scarce river basins. The general water balance equation can be used to identify and model the WA using the inflow and outflow of water in an area. On sufficiently long time scales, such as decades, it is reasonable to presume that the net change in hydrologically active storage in a basin is zero. Therefore, the estimation of the WA of the basin is done using the balance between precipitation and potential evapotranspiration. The WA is the total available water that can be in the form of streamflow, soil moisture, and groundwater recharge in the basin (Tadese *et al.*, 2020; Das *et al.*, 2022*b*). Four sectors were identified as being particularly susceptible based on the relative shift in WA and Q as suggested by (Garrote *et al.*, 2018; Swain *et al.*, 2020). The criteria for potential zoning of water scarcity risk assessment are outlined below:

Zone-1 (Z1) = ($\Delta Q \geq 0$, $\Delta WA \geq 0$) = Low risk or No risk

Zone-2 (Z2) = ($\Delta Q \leq 0$, $\Delta WA \geq 0$) = Moderate risk

Zone-3 (Z3) = ($\Delta Q \geq 0$, $\Delta WA \leq 0$) = High risk

Zone-4 (Z4) = ($\Delta Q \leq 0$, $\Delta WA \leq 0$) = Extreme risk

ΔQ represents the relative change in streamflow, and ΔWA represents the relative change in water availability for the three basins. ΔQ and ΔWA lesser than zero correspond to extremely vulnerable, and greater than zero corresponds to the less vulnerable sector. Similarly, ΔQ less than zero and ΔWA greater than zero refer to moderate vulnerability. A high vulnerable zone is referred to if ΔQ is greater than zero and ΔWA is less than zero.

7.3 RESULTS AND DISCUSSION

7.3.1 Performance of LSTM Streamflow Model

The performance of the model during the calibration and validation period is shown in Table 7.1, the variation in observed and simulated streamflow during the validation period is shown in Figure 7.2, and Figure 7.3 compares the annual cycle of streamflow for the observed and simulated values during the validation period. The highest NSE and R^2 is obtained for the central river basins, and the NSE of 0.65 is obtained for the Ulhas river basin, followed by the Purna basin.

Table 7.1: Model performance for calibration and validation

	Calibration Period		Validation period	
Basin	R^2	NSE	R^2	NSE
Vamanapuram	0.83	0.79	0.75	0.74
Chaliyar	0.79	0.78	0.72	0.72
Netravati	0.86	0.85	0.85	0.84
Aghanshini	0.87	0.83	0.83	0.82
Ulhas	0.74	0.65	0.70	0.65
Purna	0.80	0.71	0.74	0.68

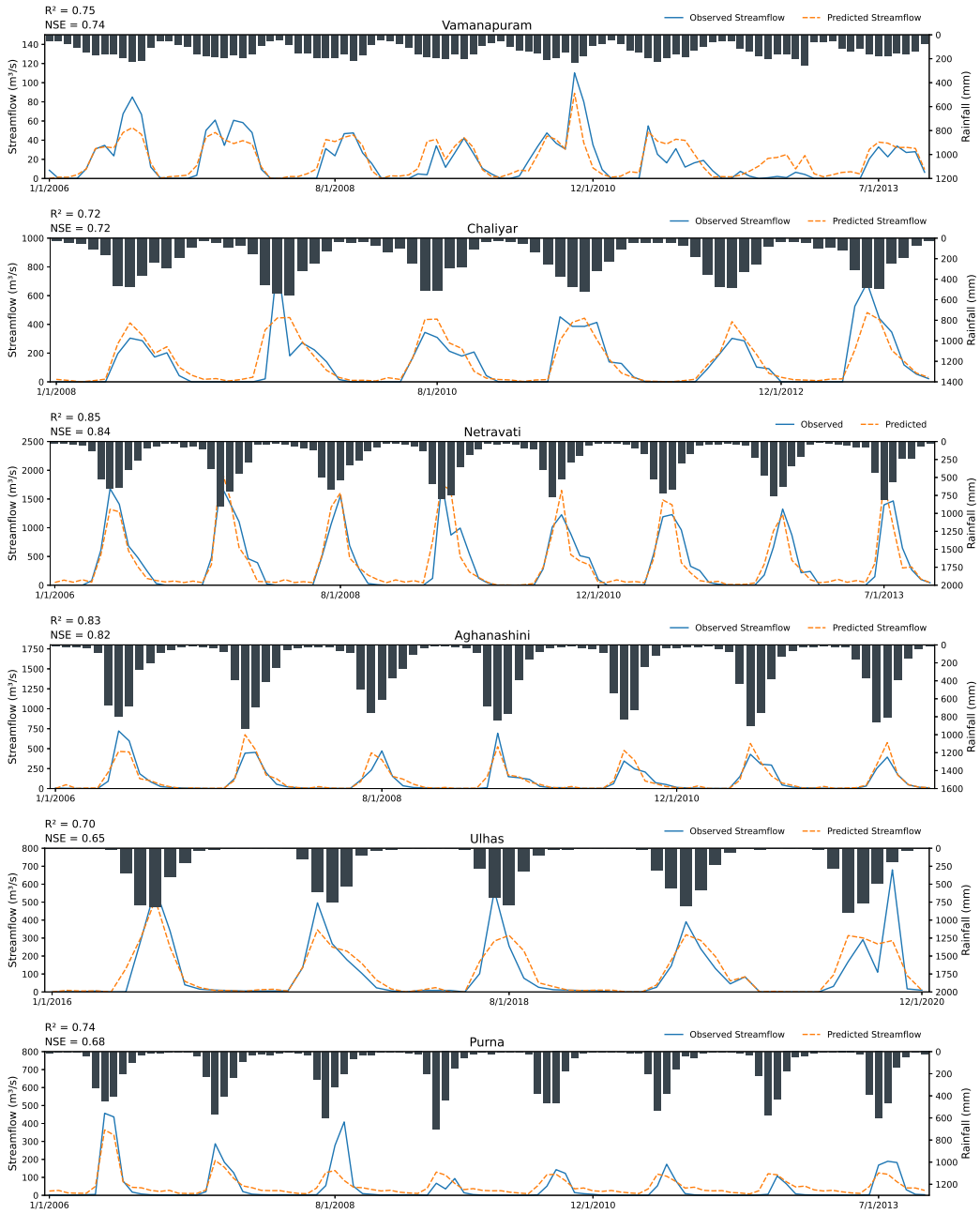

Fig. 7.2: Comparison of predicted and observed streamflow during the validation period

7.3.2 Impact of Climate Change on Streamflow

Figure 7.4 represents the expected changes in the streamflow in two-time frames under two future scenarios over the six river basins. The annual streamflow in the Vamanapuram, Aghanashini and in the northern river basins are increasing in all the future scenarios, whereas it decreases in the Chaliyar and Netravati river

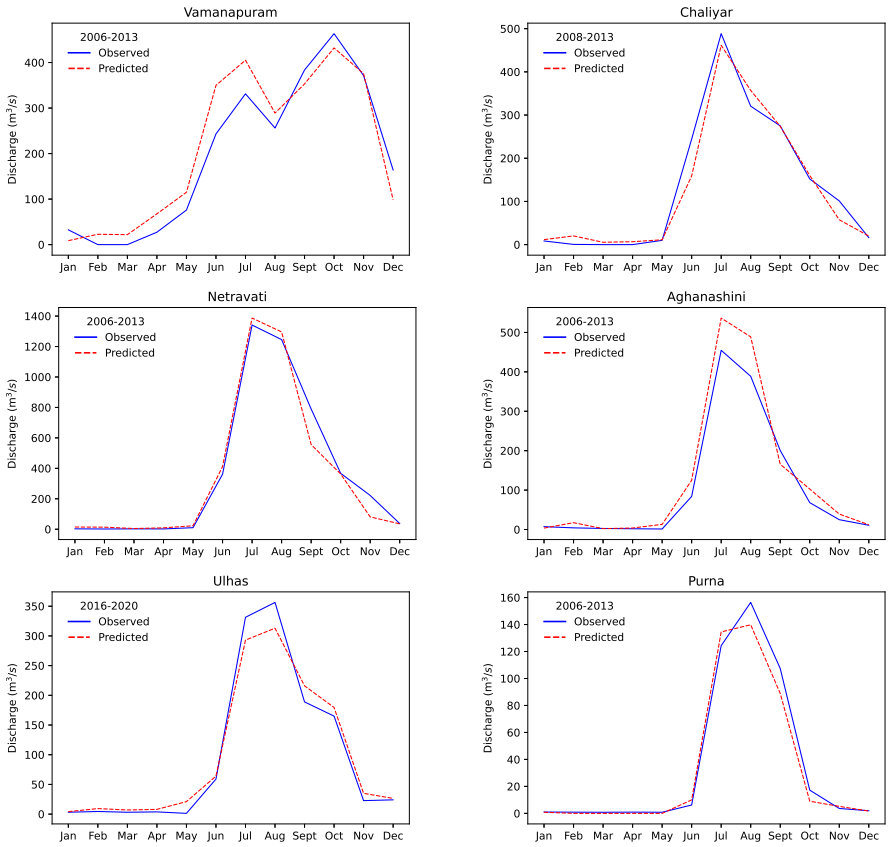

Fig. 7.3: Comparison of predicted and observed monthly streamflow during the validation period

basins. In the Vamanapuram basin an increase of 3-3.9% in mean annual rainfall, 1°C in mean annual temperature increased the annual streamflow by 6% in the near future, whereas in the far future, the annual streamflow increased by 23% with a increase of 6-11% in rainfall, 1.8°C in mean temperature. The Ulhas basin, which has a same climate (humid) but located in the northern part of the Ghat notes a increase of 11% in the annual streamflow in NF along with the increase of 0.57°C in temperature and 5-8.7% in rainfall. In the FF, the combined effect of 1.95°C in mean annual temperature, 14-20% increase in annual rainfall has shown a upward variability of 5-38% in streamflow. The basin Chaliyar and Purna highlights a converse relationship with the increase in temperature and rainfall. Chaliyar had noted a increase in mean temperature by 1.98 (2.4)°C, 10% (16%) increase in mean rainfall in the SSP245 (SSP585) scenarios, which has a negative impact on the annual streamflow, which decreases 25-40% with higher decrease in

the FF of SSP245 scenario. In Purna basin 0.87°C in NF temperature, 12-14% in rainfall resulted an increase of 20-30%, whereas the increase of 1.51°C in FF with 23-31% in rainfall has not changed the annual streamflow pattern. Over the central river basins, the decreasing streamflow of 25-30% is highlighted with a increase in temperature by 2.5°C and 4-7% in rainfall. Whereas the Aghanashini basin has shown a increase of 5-12% in rainfall, 2.2°C in mean annual temperature in the future decades experience a increase of 5-10% in streamflow. This highlights the role of regional heterogeneity on the streamflow variation. Whereas, the streamflow in the monsoon season is expected to decrease irrespective of the basin climate, and geology. However the post-monsoon streamflow increases in the northern river basins due to the increase in post-monsoon rainfall. Also, the streamflow in the winter season increases in all the basins with varied responses in the summer season.

7.3.3 Projected Transition in Streamflow Variability

Figure 7.5, 7.6 represents the decadal variation in the % of annual rainfall (primary y-axis) and % of annual streamflow (secondary y-axis) under both medium emission and high emission scenarios over the southern basins. The basin Vamanapuram received approximately 15% rainfall in June, 12.5% in July, $\leq$10% in the month of August and September, and up to 15% in October during the SW monsoon in the historical period. The streamflow contribution of 15% in the decade 1970s decreased to 10% in the July month at the beginning of the 21st century, whereas in October 12.5% in 1980 increased to 17.5% in decade 2000s, overall in the future, it can be noted that the basin receives decreased contribution of $\leq$10% rainfall in the months of June, July, August, September, and in November, and up to 15.5% in October months. Under SSP245, streamflow contributions declined in June and climbed by up to 12.5% in the subsequent months before declining again after November. While increased streamflow can be observed during the winter months, with $\leq$ 7.50% contribution in June and 11% contribution during other months, a similar distribution can be observed in the SSP585 scenario.

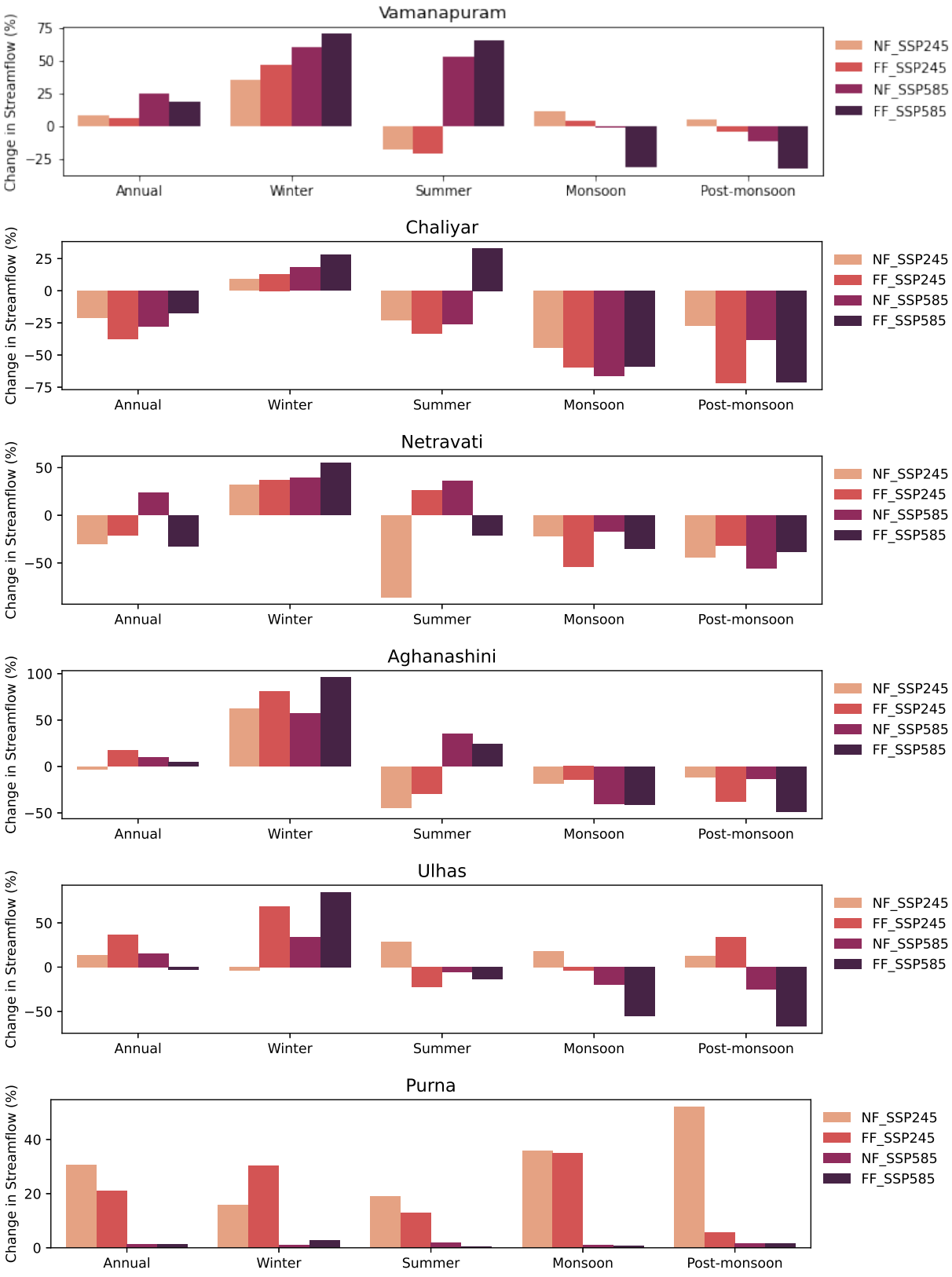

Fig. 7.4: Seasonal change in streamflow under future scenarios with respect to period 1961-1990

In the Chaliyar basin, June contribution decreased from approximately 20% to 15%, July from 25% to 20%, with increase in contribution from 10% to 15% in August and September, and no variation in the contribution in October (12%) is noted in future decades. Due to the increase in the August rainfall, the month observes peak contribution (25-30%) in the future decades, which then diminish gradually without experiencing any significant shifts in distribution in other months under SSP245. Whereas under SSP585, the streamflow distribution varies dramatically after the mid 21st century reducing the peak of the monthly contribution of the streamflow to almost equal contribution in July and August in the mid-century and further increase in June contribution is noted till the year 2070. However, after the decade 2070s, the basin observes a suppressed streamflow by up to 5-7.5% during monsoon months (July and August) and converse in the summer months (up to 10% contribution), leading to the increased availability of streamflow in the summer season.

In the Netravati river basin (Figure 7.7), the reduction in the contribution of June rainfall by 6% with respect to the historical period is noted in the decade spanning 2020-2039; thereafter, the rainfall gradually increased, eventually reaching levels similar to the historical average. Whereas the gradual decrease from 28% (the 1960s) to 20% is noted in July after mid-century, and a decrease in August from 23% to $\leq$ 20% will be experienced after 2070s; on the other hand, the September rainfall increases by about 5% in the future decades with no variation in other months. In the historical period, the streamflow contribution was higher in the month of July (up to 30%), followed by August, and decreases in September ($\leq$ 15%), which then decreases gradually. However, until the middle of the 21st century, both June and July are expected to contribute similarly to streamflow; after the mid-century, the streamflow contribution peaks during August with the significantly reduced flow during post-monsoon months. However, the hydrograph of monthly contribution changes in the last three decades of the 21st century leading to increased streamflow (contribution up to 25%) in June under both scenarios. The variation in the streamflow in the medium emission to high emission scenario

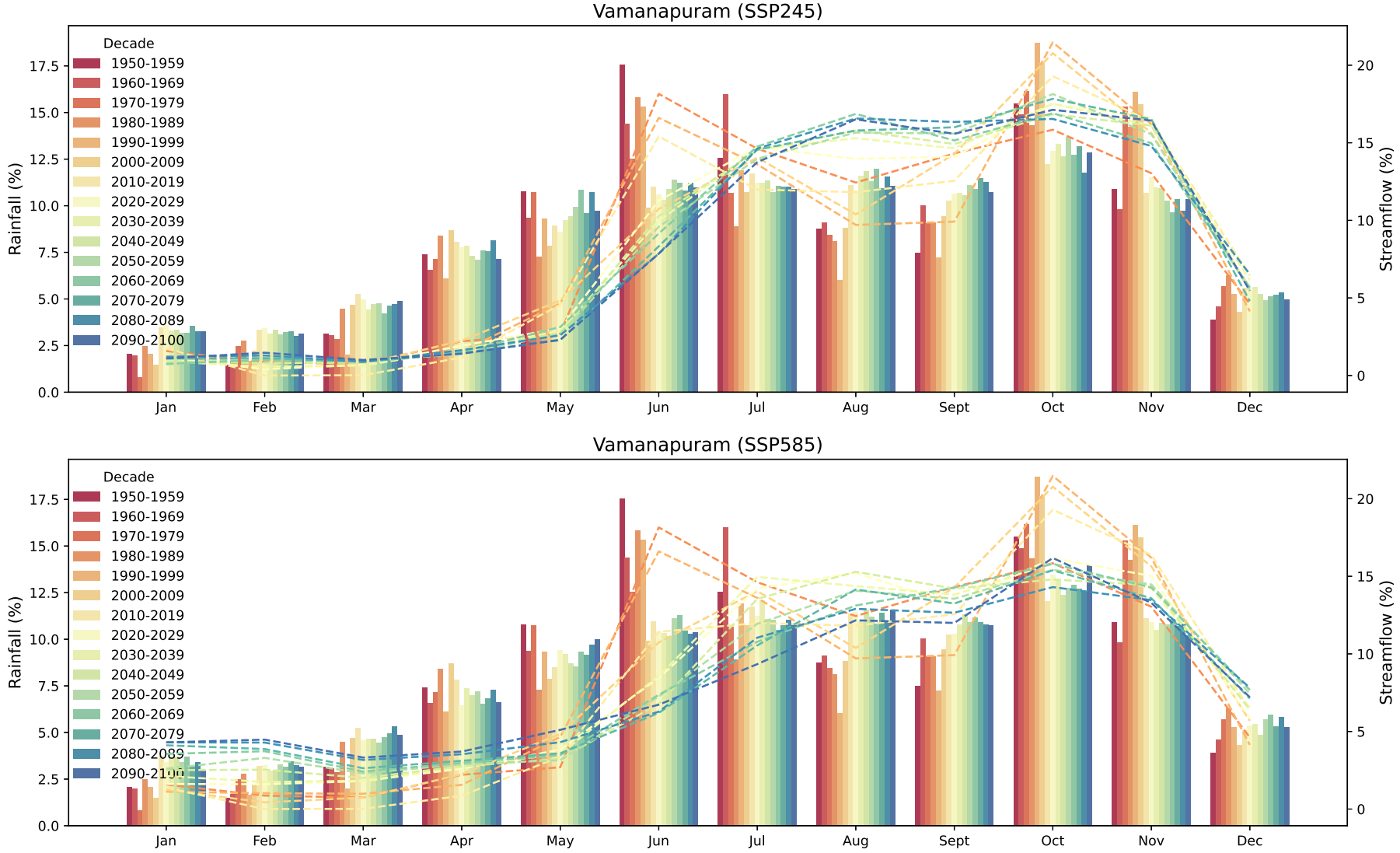

Fig. 7.5: The decadal variation in monthly precipitation and streamflow in the Vamanapuram basin under both SSP245 and SSP585 scenarios

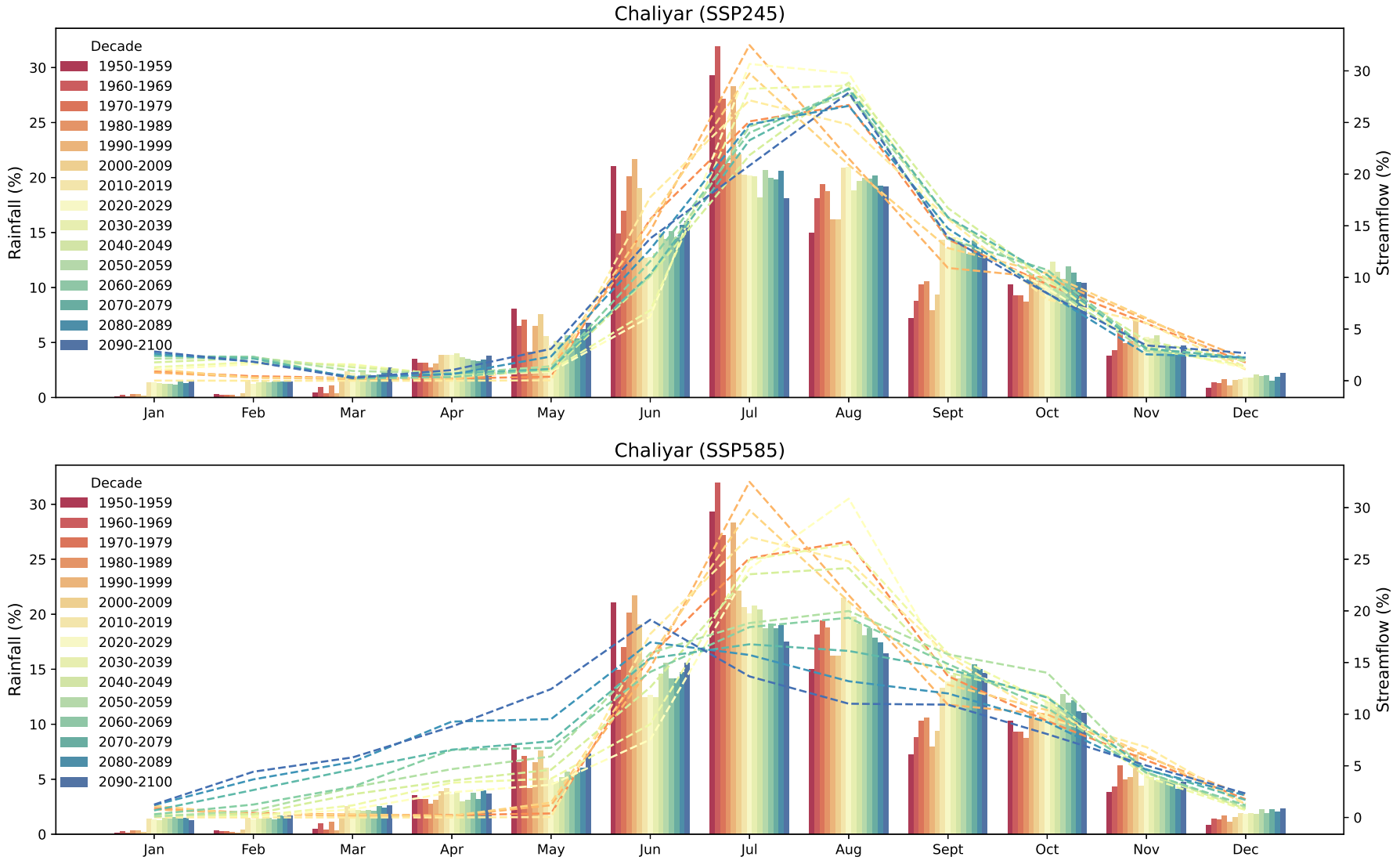

Fig. 7.6: The decadal variation in monthly precipitation and streamflow in the Chaliyar basin under both SSP245 and SSP585 scenarios

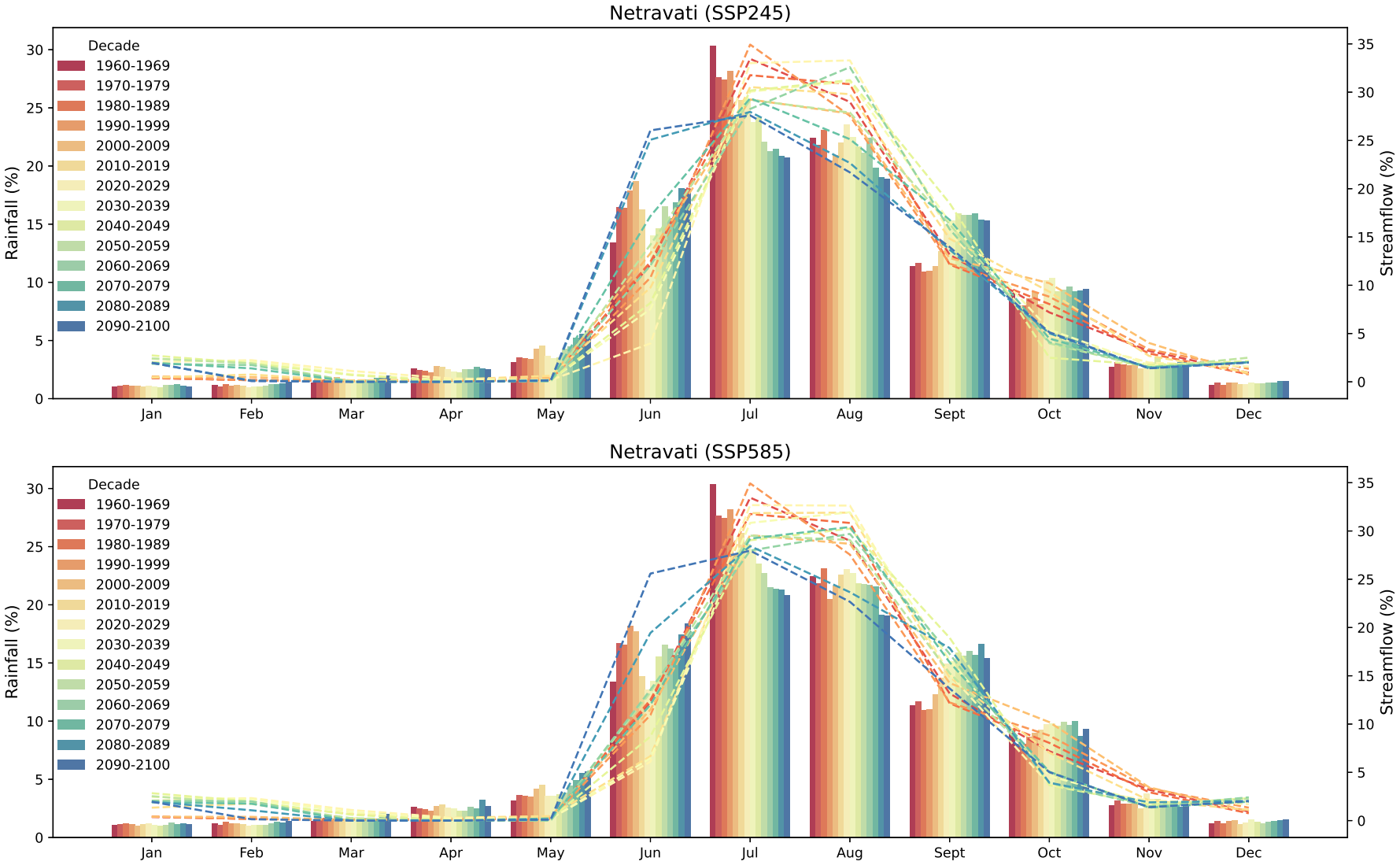

Fig. 7.7: The decadal variation in monthly precipitation and streamflow in the Netravati basin under both SSP245 and SSP585 scenarios

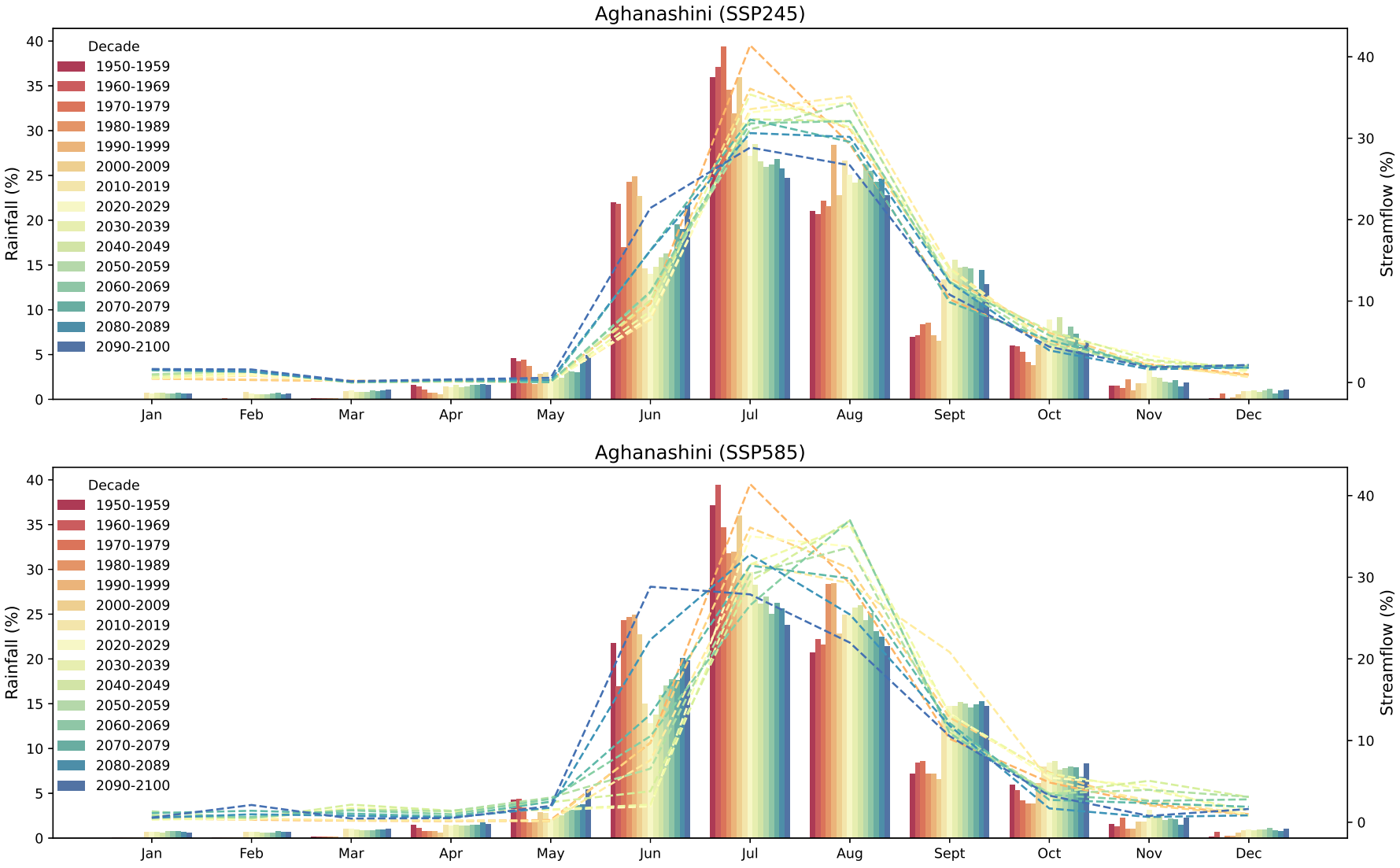

Fig. 7.8: The decadal variation in monthly precipitation and streamflow in the Aghanahini basin under both SSP245 and SSP585 scenarios

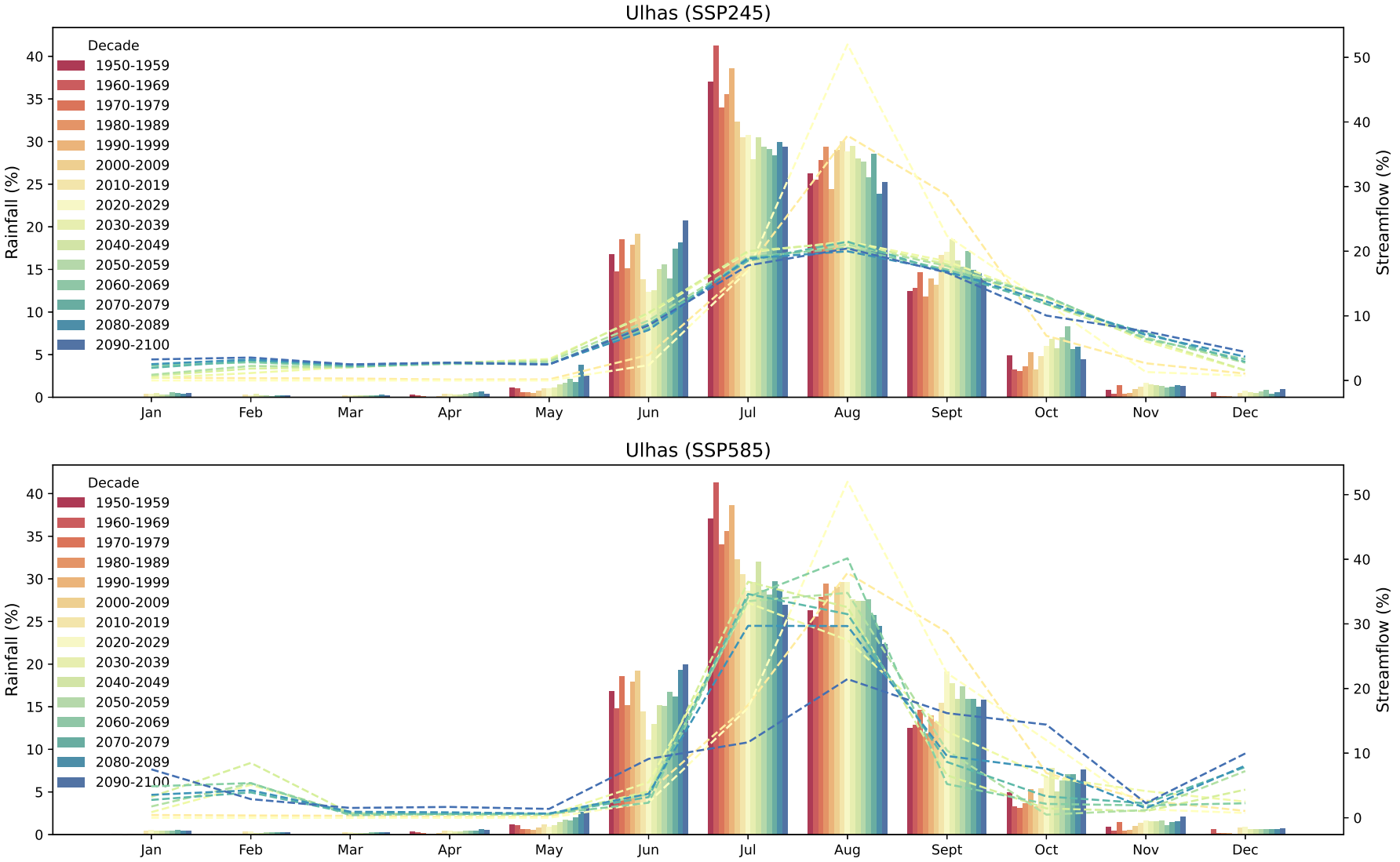

Fig. 7.9: The decadal variation in monthly precipitation and streamflow in the Ulhas basin under both SSP245 and SSP585 scenarios

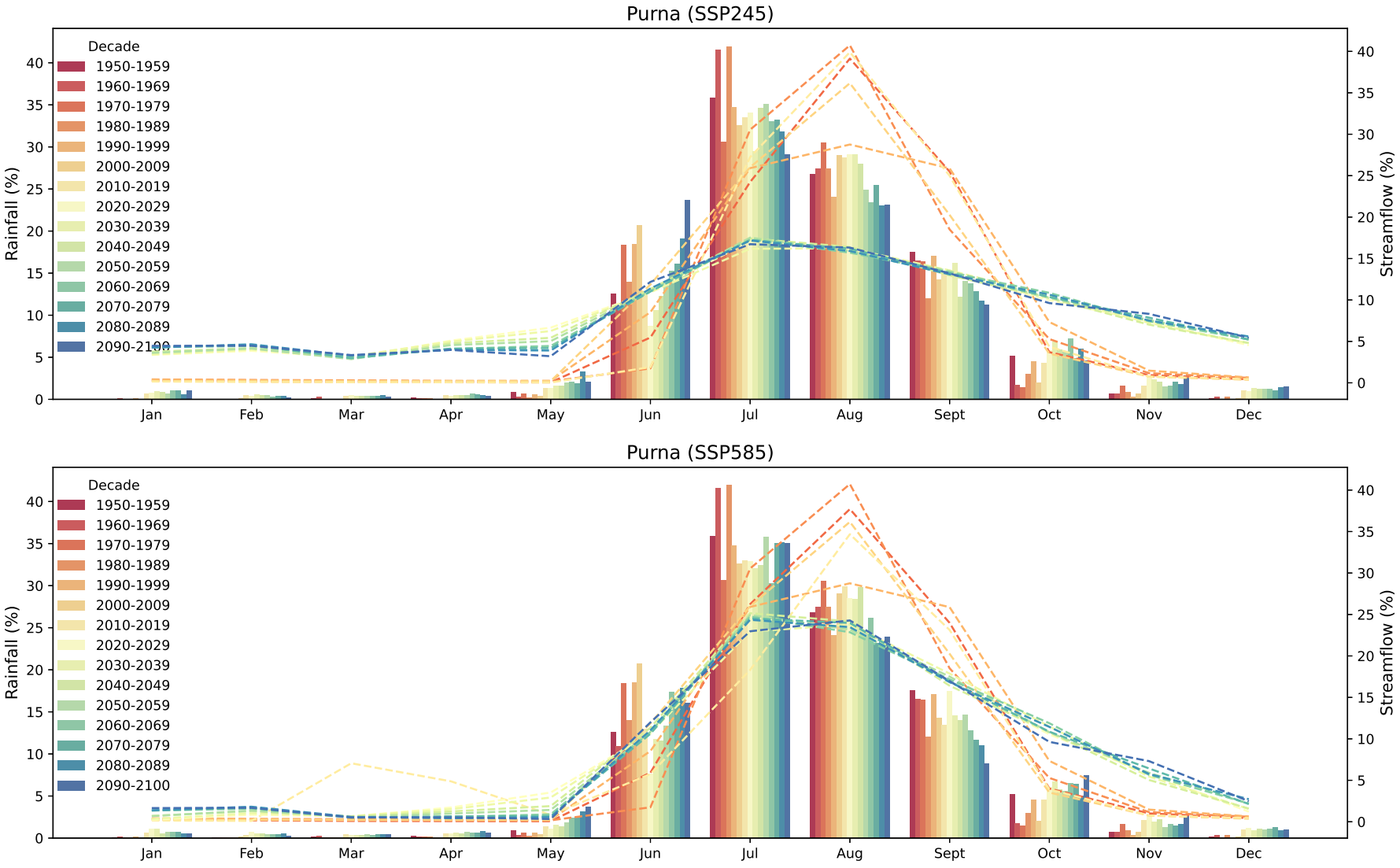

Fig. 7.10: The decadal variation in monthly precipitation and streamflow in the Purna basin under SSP245 and SSP585 scenarios

is noticeable after the decade 2070s. The streamflow distribution is similar in both the central river basins; in Aghanashini (Figure 7.8), the June rainfall contributes to 20% of total rainfall, July up to 35-40%, August up to 20%, September $\leq$ 10% in the historical period. Future decades observe a decrease in the contribution of July month rainfall by 10-12%, an increase in August by up to 3%, and September by 8% along with the increase in October. The streamflow of the basin observes 10% reduction in the month of July without any greater variation in August till the mid 21st century; in the last two decades, the streamflow varies similarly to the variation observed in the Netravati. In SSP585, the last two decades hydrograph varies significantly, with a peak in July in 2080-2089 (22%, 27% contribution in June, July), and a peak in June (30%), July (27%) in 2090-2100.

The variation in the rainfall-streamflow over the northern river basins is shown in Figures 7.9, 7.10. In the Ulhas basin, the June and July month contributes to 20% and 35-40% of rainfall in the historical period. In the NF, a decrease of 5% was noted in July, with an increase in August and September contributions. At the beginning of the 21st century, the streamflow was highest in the month of August (35-40%) with 20% contribution in July, 15-20% in September, 10% in October changed to 20-25% contribution in July, August, and September months indicating the changes in the streamflow due to the shift in the season of the years. Following the period of the 2070s, there has been a discernible increase in variability in the SSP585 scenario, specifically in relation to heightened levels of precipitation during the summer and post-monsoon seasons. The streamflow commences in the month of May and continues until November. Whereas in the Purna basin, the peak streamflow contributing months are July (up to 30%) and August (up to 40%). In the future decades, the streamflow contribution suppresses in the medium emission scenario more than in the high emission scenario with an extension in the streamflow contribution months (till December).

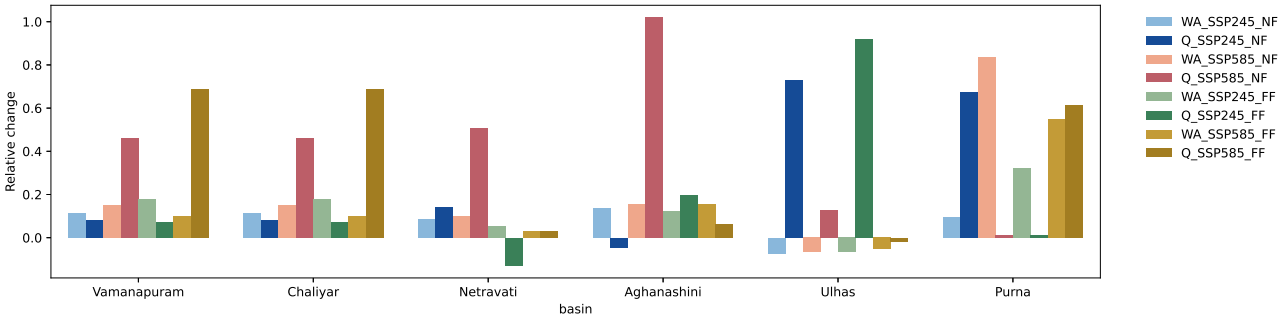

Fig. 7.11: Relative changes in streamflow and water availability in the future horizon

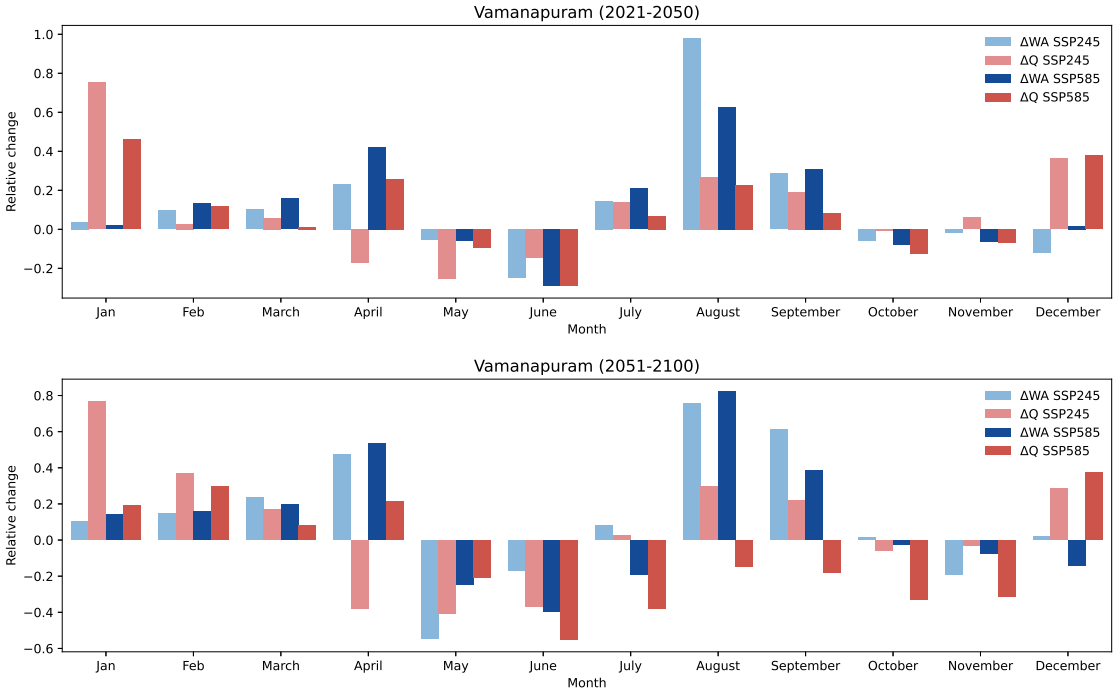

Fig. 7.12: Relative changes in monthly streamflow and water availability in the future scenario over Vamanapuram basin

7.3.4 Water Scarcity Risk Assessment of the River Basins

Figure 7.11 represents the vulnerability of the river basins to water scarcity risk in the future horizon under both medium emission and high emission scenarios. In southern river basins, in both scenarios and the two time frames, the relative change in Q and WA noted is no significant risk of water scarcity, whereas the central river basin Netravati is expected to show moderate risk in FF and Aghanashini in the NF under SSP245, with no risk in other scenarios. Though

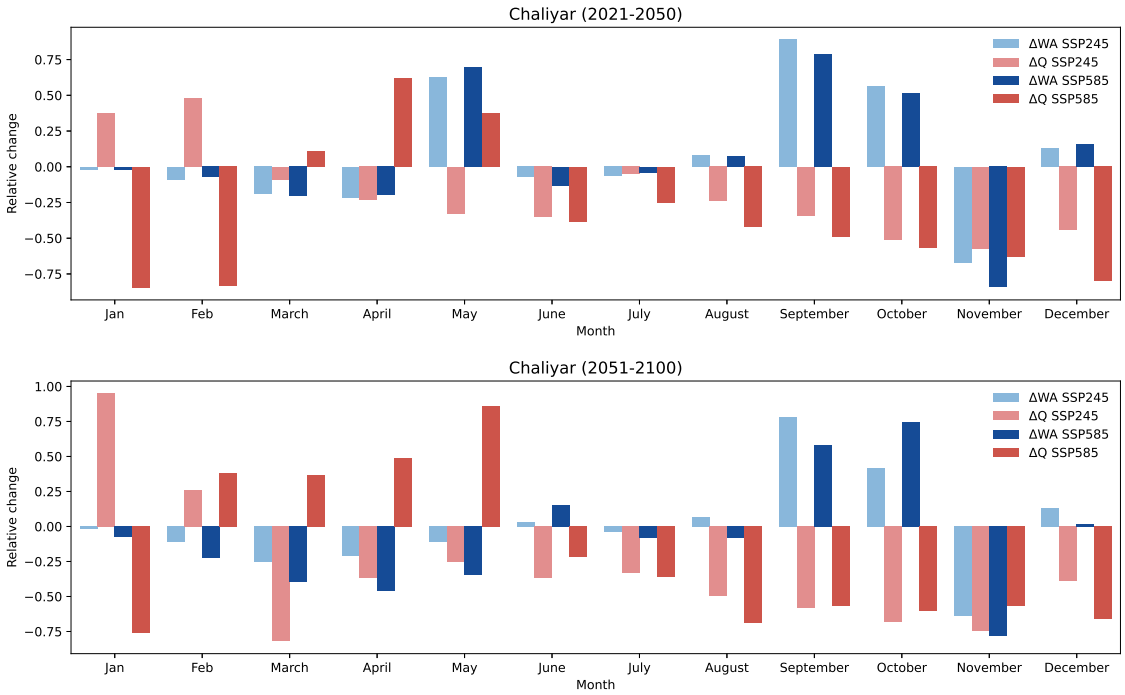

Fig. 7.13: Relative changes in monthly streamflow and water availability in the future scenario over Chaliyar basin

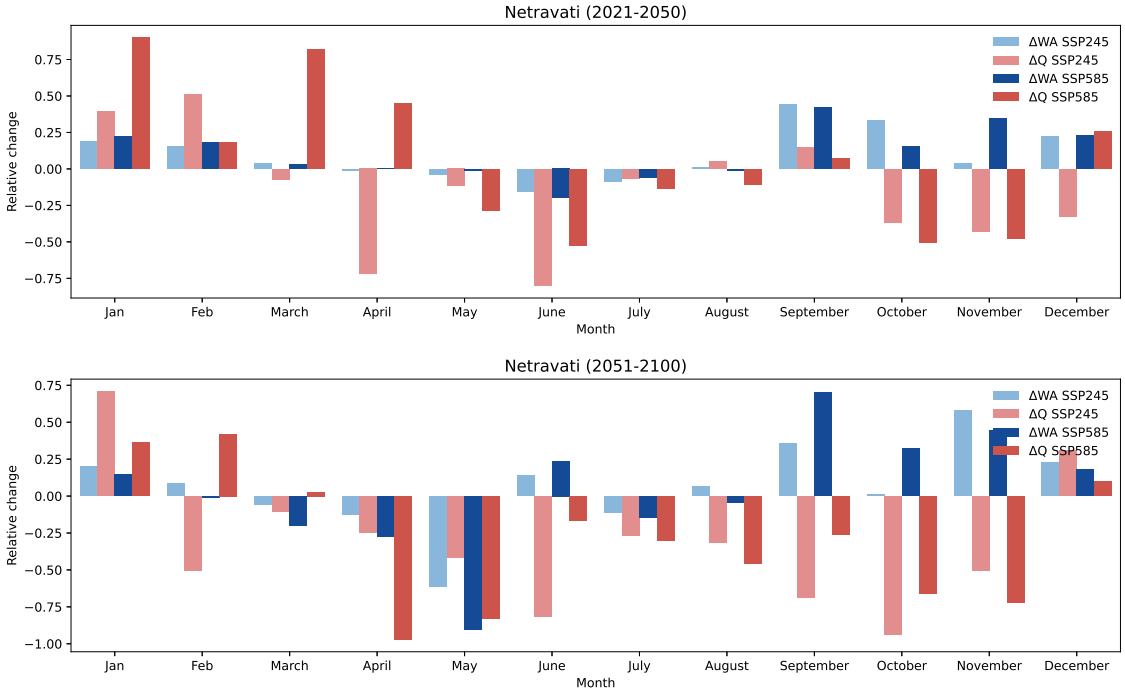

Fig. 7.14: Relative changes in monthly streamflow and water availability in the future scenario over Netravati basin

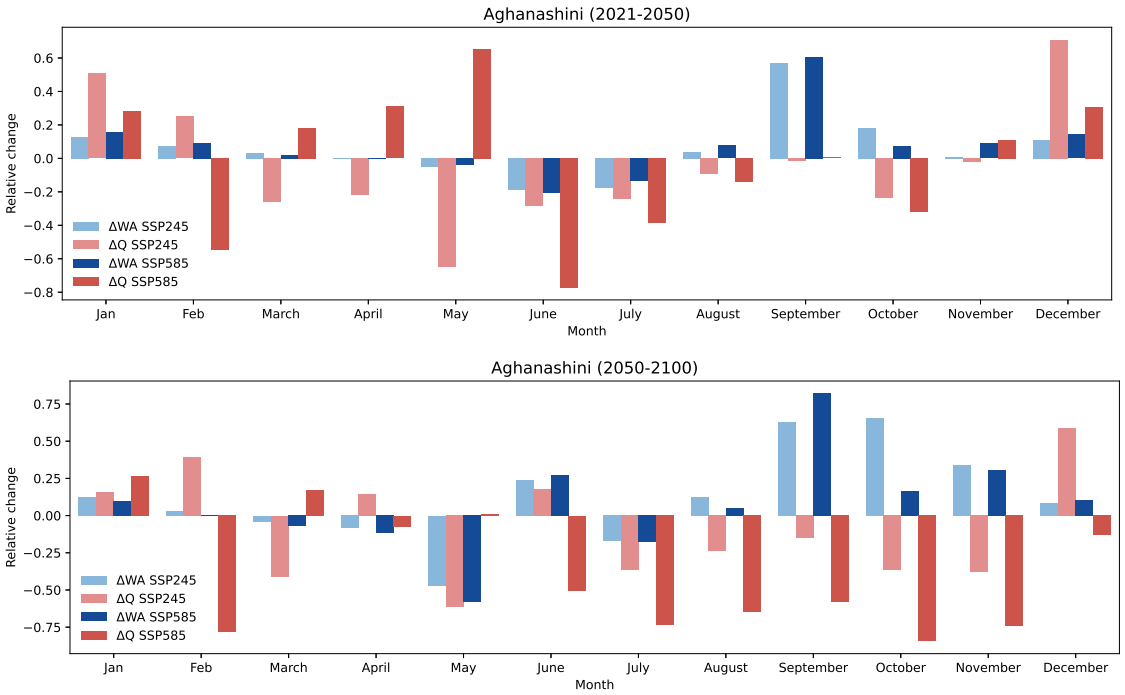

Fig. 7.15: Relative changes in monthly streamflow and water availability in the future scenario over Aghanashini basin

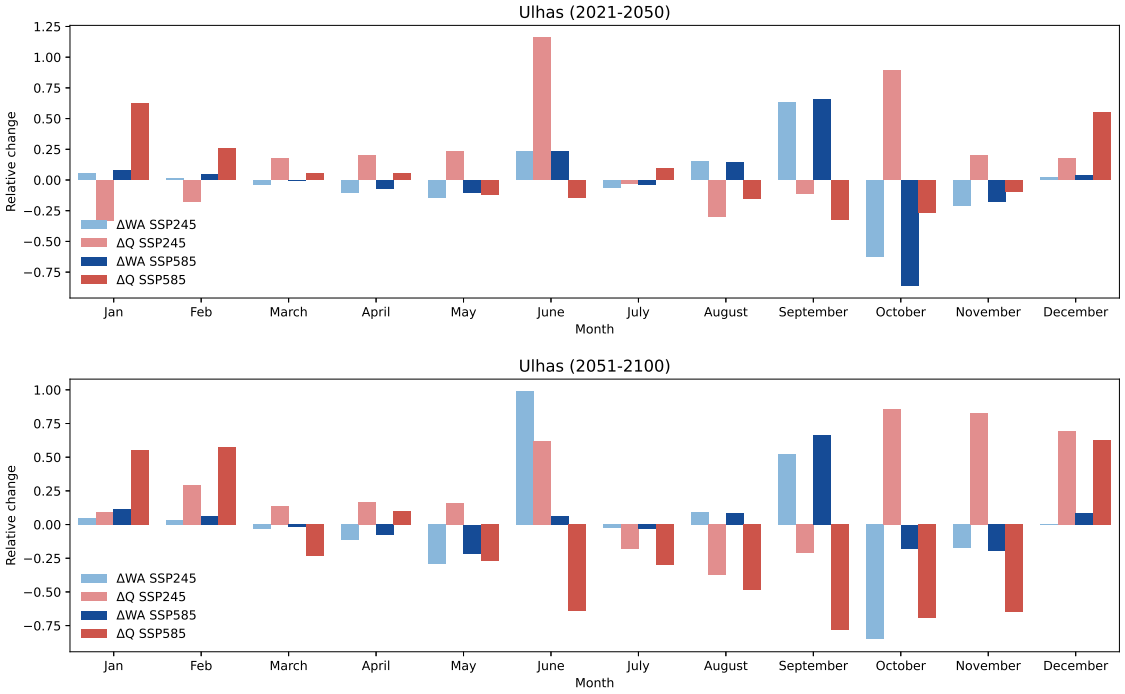

Fig. 7.16: Relative changes in monthly streamflow and water availability in the future scenario over Ulhas basin

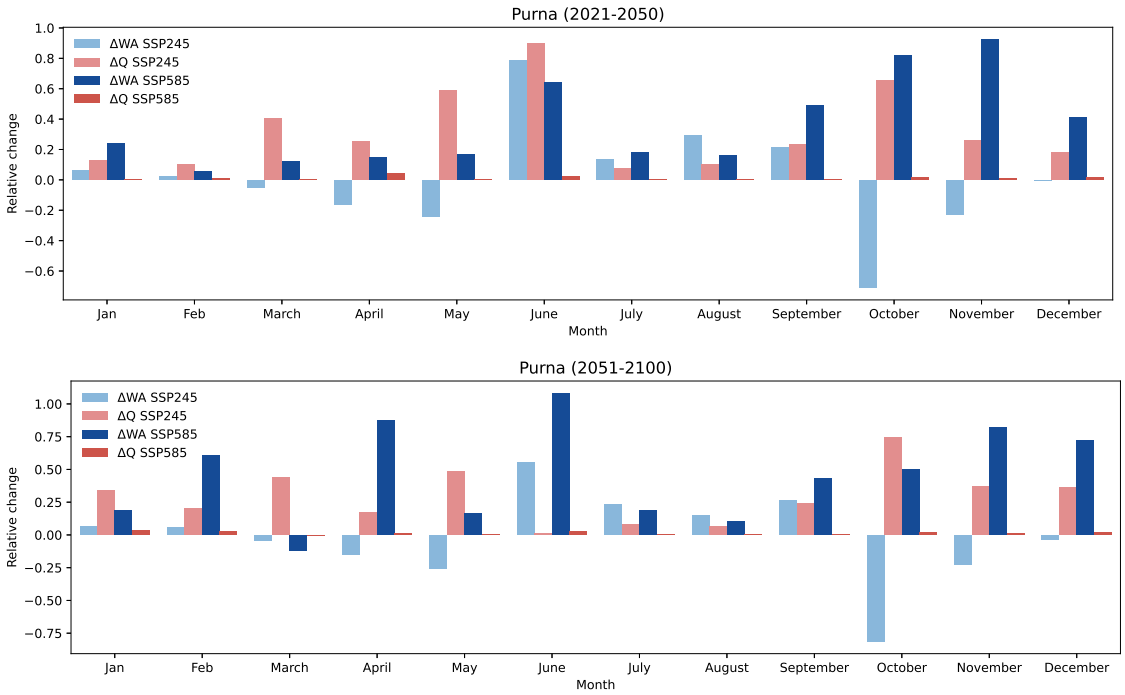

Fig. 7.17: Relative changes in monthly streamflow and water availability in the future scenario over Purna basin

the rainfall is increasing, the increase in PET along with the increasing temperature may induce a less to moderate water scarcity risk in the northern basins. The relative change in the basin scale for southern river basins are shown in Figures 7.12 to 7.17, which indicates the average monthly water scarcity risk in the two-time frames under two scenarios. May and June are highly vulnerable to water scarcity risk, followed by October and November in both scenarios. In the FF, July month is extremely vulnerable to a water crisis in the high-emission scenario due to the decrease in rainfall in July with increase in temperature and PET.

The Chaliyar, experiences a high to extreme risk of water shortage in the months of June, July, followed by November, which becomes severe in the FF. The Netravati river basin (Figure 7.14) is extremely vulnerable to water scarcity during May and June with moderate risk in other months (except January and February). Which becomes severe in the FF, with scarcity risk starts from March to May, and due to the shift in the peak streamflow from July to August further pressurize the both WA and Streamflow in the July month. The Aghanashini

(Figure 7.15) basin experiences extreme risk from May to July and moderate risk in August and September. In the FF, the highly vulnerable months start from March until July, with August to November being the moderate-risk months. Ulhas basins (Figure 7.16) experience high vulnerability in the summer months in the NF; as the June rainfall increases over the basin, low risk is noted in June, with moderate risks in other months. The Purna basin(Figure 7.17) is observed as having the least water scarcity among the six basins. The basin has low risk in the monsoon months and moderate risk in March, April, May, October, and November.

7.3.5 Discussion

The future evaluation of stream flow is conducted using a developed deep learning-based Long Short-Term Memory (LSTM) model. The optimized LSTM model has well simulated the historical streamflow of the river basin in the Western Ghats of India. The six river basins represent the different climatic conditions, and the geographical location, under the changing climate the river basins have varying response to streamflow even with the same climate of the region. It is anticipated that climate change will have a greater impact on streamflow in the southern basin Chaliyar and the central basin Netravati. Which induced a decline in the streamflow with the increase in rainfall and temperature even in the far future horizon. Despite the fact that an increase in streamflow is viewed as beneficial, high fluctuations in streamflow especially in the monsoon months are alarming for the critical changes that take place in the future decades. The prolonged summer season due to the increasing temperature might be one of the key factors in the shift in the monsoon season due to a reduction in the SW monsoon rainfall in June, and an increase in September (except for Purna). Which has increased the risk of WA in the river basins. One Billion people in India face severe water scarcity at least one month of the year (Mekonnen and Hoekstra, 2016). Whereas, the march to June will be under a high to extreme risk of water scarcity even in the WG of India. The streamflow is expected to drop in June and increase in September due to the

corresponding changes in rainfall. Also, the summer streamflow increases more in the FF horizon. The results of streamflow decrease in the monsoon and increase in the summer and winter are similar to the results stated by (Franczyk and Chang, 2009; Kim *et al.*, 2013; Sinha *et al.*, 2020). Vamanapuram, Chaliyar, and Netravati have a higher ratio of the plantation (23.10%, 38.20%, 14.82%) than the cropland (1.96%, 4.76%, 5.17%). Whereas Aghanashini, Ulhas, and Purna have more cropland (12.58%, 21.32%, and 24.38%) than the plantation (1.98%, 11.11%, 0.15%). The agricultural activities in both Kharif and Rabi seasons depend on the SW monsoon rainfall and begin in late May/early June; the delay in the June rainfall significantly affects the cropping window, heavy rainfall in the active growth period during the vegetative phase reduces the number of plants and duration of the growth period resulting in a decrease in production; whereas, the increase in temperature negatively affects the plants during the transplantation stage (Kingra *et al.*, 2018). The increase in September rainfall during the harvesting period of the crops again decreases crop productivity. In the future, May and June months will be highly vulnerable to the water scarcity risk in all the river basins, which will exacerbate in the far future, making the month of March too as vulnerable. This highlights the constant need for the water supply for irrigation throughout June in the southern and central river basins. Whereas the risk in the northern river basins is less due to the increase in June rainfall.

7.4 CONCLUSIONS

The study aimed to quantify the potential impact of climate change on streamflow and the associated risk of water scarcity, as determined by shared socioeconomic pathways. The utilisation of the Long Short Term Memory model in this research showcases its efficacy in accurately simulating streamflow patterns, particularly in challenging mountainous regions where data availability is constrained. The streamflow can be effectively modelled by incorporating the precipitation, maximum, mean, and minimum temperature, as well as the potential evapotranspiration (PET) data for each basin, in addition to the historical streamflow data.

It is anticipated that climate change will have a greater impact on streamflow especially in the Chaliyar and the Netravati river basin even in the far future horizon. The streamflow increase under the climate change scenario in the Vamanapuram, Aghanshini, Ulhas and Purna river basins under both the future scenarios. The streamflow observes a shift in the peak contributing month due to the delayed monsoon due to intensified summer season. Though the rainfall increases, the water scarcity risk increases in the future decades, the months April to June will be highly vulnerable to extreme risk of water scarcity even in the WG of India which exacerbate to April to July in the the high emission scenario of the future. Hence, the implementation of enhanced irrigation technologies, the advancement of agricultural practises on farms, and the construction of water conservation and retention structures have the potential to substantially mitigate the unmet demands and deficiencies in these basins.

CHAPTER 8

SUMMARY AND CONCLUSIONS

This chapter presents the summary and conclusions drawn from the present investigation. The four chapters (Chapter 4 to 7) in the current study addresses the five research objectives. In the first objective, the role of the mountain topographic structure on rainfall distribution and the dependence of precipitation on topo-climate (elevation, slope, Terrain Ruggedness Index (TRI), Directional Relief (DR), Relative Terrain Aspect (RTA), distance from the coast (Cd), and distance from the ridge (Rd), Land Surface Temperature (LST) and Normalised Differential Vegetation Index (NDVI), Wind speed of the WG, and its long-term spatio-temporal variation in the association is studied using the Geographically Weighted Regression. The conclusions drawn for this objective is explained in Section 8.1. In the second objective, the performance of the individual GCM models are assessed and ranked based on its performance, further the top performing GCMs are ensembled using a simple arithmetic mean and the seven machine learning based techniques. The effectiveness of these ensemble models over the diverse-climate basins of the WG of India is studied in the objective 2, the conclusions derived from this is given in Section 8.2. In the third objective, the top-performing ensemble models performance in the estimation of extreme climatic indices are evaluated for the river basins, and further in the fourth objective, the top performing ensemble model is used to project the future climatic variables (rainfall, maximum and minimum temperature, potential evapotranspiration) and the extreme indices. The future variability in these variables and their trend in the historical and future horizon is assessed under two future scenarios. The conclusions of these two objectives are explained in Section 8.3. In the last objective the streamflow is modelled by a deep-learning Long Short Term Memory (LSTM) technique and annual percentage variability in the future decades, and the water scarcity risk assessment is carried out, the conclusions derived from this study is explained in

the Section 8.4. Further, the limitations of the present study and scope for further research are also highlighted.

8.1 DEPENDABILITY OF RAINFALL TO TOPOGRAPHY AND CLIMATE

The Western Ghat mountain forest has a great spatio-temporal variation in the rainfall due to undulating mountainous terrain. The topographical zonation of the Western Ghats gives a detailed picture of the spatio-temporal variation of rainfall. The association between rainfall, elevation, slope, Terrain Ruggedness Index, aspect, directional relief, distance from the coast/ridge, wind speed, Normalized Differential Vegetation Index, and Land Surface Temperature in Western Ghats varies seasonally, indicates the influence of other seasonal parameters on the rainfall. The variation in the correlation between rainfall and other independent variables analysed by Pearson's correlation (r) at four zonations of Western Ghats are consistent over 11 decades; therefore, it does not signify any vigilant changes in rainfall variation over the decades.

The spatial variation in the rainfall is modelled using the elevation, slope, Terrain Ruggedness Index (TRI), Directional Relief, Relative Terrain Aspect, distance from the coast/ridge, Normalized Differential Vegetation Index (NDVI), Land Surface Temperature (LST) and Wind speed as independent variables using a non-parametric Geographically Weighted Regression method. The each variable has varying association with the rainfall, due to the highly complex terrain and local climatic regime of the Western Ghat. The specific conclusions drawn form this study are,

- The connection between rainfall and other variables differs significantly throughout space, with vast differences on the mountain's windward and leeward sides, as well as in the WG southern and northern regions. The topographical variables (elevation, slope, TRI, distance from the coast/ridge, Relative Terrain Aspect and Directional Relief) solely can be used as an influential predictor of rainfall in the Western Ghats of India.

- The mountain in the windward side of Karnataka has a gradually increasing slope compared to the mountains in Maharashtra and Kerala. This gradually increasing slope rises the convective activity in the mountain region by providing a large surface area to the incoming solar radiation.

- The Western Ghat has level to extremely rugged terrains. The mountain in the state of Kerala is moderate to highly rugged compared to the mountains in the state of Karnataka and Maharashtra. There is a negative association between TRI and rainfall in the moderate to highly rugged terrain of the mountain in Kerala and in Maharashtra. Therefore the terrain relief of the mountain along with the distance from the moisture source may have a predictable influence on the distribution of rainfall.

- There is a positive correlation between rainfall, LST, and NDVI in all zones during the pre-monsoon, post-monsoon, and winter seasons; the negative correlation during the monsoon is due to the fact that the vegetation cannot respond as quickly to the variation in rainfall as the rainfall varies. Additionally, rainfall exceeding certain thresholds will negatively impact plant growth.

- The association of topography with rainfall indicates that the maximum rainfall occurs at different elevation ranges depending on the steepness of the mountain on the windward side.

- This study highlights that maximum annual/monsoon rainfall varies depending upon the topographical structure of the mountain. The maximum rainfall occurs at an elevation range of 500-800 m in an isolated mountain and 800-1200 m in cascaded mountain ranges along with other variation driving factors.

- The mean rainfall is maximum at the coast than any hilly region of the mountain and is more intense on the coast of Karnataka than on the other. The influence of terrain is more enhanced in this region as this region has

intermediate rugged terrain starting from the coastline, whereas the other two coasts (Kerala and Maharashtra) have nearly level terrain, which is then followed by the rugged mountain terrain.

- The higher spillover effect in the broad mountain ranges than the isolated mountains distribute considerable rainfall near the ridge of the mountain.
- The effect of mountain ridge varies depending on the mountain topographic structure. In the cascaded mountains rainfall regains its moisture after passing around 120 km from the ridge of the mountain and gradually increases as soon as it passes the ridge of the mountain in isolated mountains.

The results obtained in this study are useful in understanding the dependency of rainfall on topographic and hydro-climatic parameters and can be used in any hydro-geological applications. The predictors of rainfall can be chosen wisely based on the correlation between variables and rainfall in further modelling of rainfall.

8.2 RANKING OF GCM MODELS AND CREATION OF MMES BY ADVANCED ML-BASED ENSEMBLE TECHNIQUES

This study evaluates the ability of 13 CMIP6 GCMs to reproduce precipitation, maximum and minimum temperature. Based on the performance metrics NRMSE, R^2, and NSE, the GCMs are ranked using an MCDM TOPSIS technique adopting an entropy-based performance indicator weighing method. The six river basins namely selected based on the different geolocation and the climate of the basins representing two river basins each in the southern (Vamanapuram, Chaliyar), central (Netravati, Aghanashini),and northern (Ulhas and Purna) region of the WG. In each basin, the top six performing models are ensembled using seven machine learning (Random Forest Regressor (RFR), Support Vector Machine (SVM), Linear Regression (LR), Adaptive Boosting Regressor (AdaBoost), Extreme Gradient Boosting Regressor (XGBR), Extra Tree Regressor (ETR) and Multi-layer Perceptron neural network (MLP)) based multi-model ensemble and the simple arithmetic mean (AM) methods and the performance are evaluated

to understand the competence of these models in emulating the characteristics of precipitation, maximum temperature, and minimum temperature is examined using the NRMSE, R^2, and NSE metrics. The following conclusions are drawn from the study.

- The top-performing GCM in the case of precipitation is EC-Earth3 in Vamanapuram and BCC-CSM2-MR in other basins. In simulating maximum temperature, MPI-ESM1-2-HR in Vamanapuram, Chaliyar, and Netravati, EC-Earth3-Veg in Aghanashini, INM-CM5-0 in Ulhas, and MPI-ESM1-2-LR in Purna. The GCM INM-CM5-0 is the best-performing GCM for minimum temperature over the five basins, except for the Purna (MPI-ESM1-2-LR).

- The simulated MME may have an erroneous distribution even with a higher NSE. Hence, a comprehensive picture of MME performance may be obtained by including a performance metric that evaluates the similarity between the probability density functions of observation and model.

- The ensemble models have been proven beneficial in river basin scale research by overcoming the constraints of bias correction methods. The XGBR and RFR have superior performance compared to other MMEs in all the basins, with poor performance by AdaBoost and SVR in MME of precipitation. The seasonal examination of simulated MME over the basins further highlights the reliability of these MME models.

- The change in the temperature in RFR, ETR, and XGBR in the NF and FF are consistent with one another, with AM showing the most dramatic change in future temperature and AdaBoost in Precipitation. The anticipated change in maximum and minimum temperature in the SSP245 and SSP585 in the future horizon corroborates the undeniable rise in temperature by all the MMEs compared to the historical mean with a two-time increase in the FF compared to those experienced during the NF epoch.

Additionally, we conclude that in regional studies involving complex and diverse mechanisms that drive precipitation, a robust testing and validation ap-

proach should be employed in developing ensembles. Though the mean and distribution of the models are in agreement with the observed data, further research on the extremes that the MMEs anticipate is necessary.

8.3 ANTICIPATED IMPACT OF CLIMATE CHANGE ON HYDRO-CLIMATE AND THE EXTREMES

In this study an attempt has been made to obtain the ability of the top performing four ML-MMEs (RFR, SVR, ETR, and XGBR) and the AM MME in the estimation of extreme climate indices. In order to understand the simulation ability of the MMEs to capture extreme climatic events, nine precipitation indices and nine temperature-based indices, formulated by the Expert Team on Climate Change Detection and Indices have been analysed. The temperature intensity-based indices (hottest day (TXx), warmest night (TNx), coldest day (TXn), coldest night (TNn) and frequency-based indices (warm days (TX90p), warm nights (TN90p), cold days (TX10p), and cold nights (TN10p)) are used to evaluate the change in the intensity and frequency of the temperature. To evaluate the characteristics of precipitation, the absolute precipitation indices (R×1day, R×5day), percentile indices (R95p, R99p), threshold-based indices (R10, R30, R65), duration-based indices (CWD, CDD) are used. The performance of the ML- MME is evaluated against the IMD daily rainfall and temperature records based on coefficient of determination and NRMSE; the Modified Mann-Kendall test, Sen's Slope estimator are used to examines the long-term trend in rainfall, maximum and minimum temperature, and associated extreme indices for all the MMEs in the historical period. Finally, based on the uncertainties assessed in the estimation of climate indices, the XGBR MME is used to assess the precipitation and temperature indices, except for the estimation of duration-based precipitation indices, where the SVR MME has been utilized. The regional variability in the monthly and annual rainfall distribution and minimum and maximum temperature, and potential evapotranspiration are actively captured in the MMEs. The regional investigation of the trend in the rainfall, maximum and minimum temperature, and the

climate extremes indices in the historical and future horizon (near future (2021-2050), far future (2051-2100)) is evaluated using SSP245 and SSP585 scenarios. The conclusions drawn from this study are,

- The precipitation indices have been estimated with higher relative bias than the temperature indices. The most considerable inconsistencies are present in the percentile and absolute precipitation indices.

- Despite excellent accuracy in predicting daily/monthly rainfall, there is still a great deal of variability in calculating climatic indices. Except for the duration-based precipitation indices, the XGBR calculated indices have been shown to be more accurate across all river basins.

- The GCM models ensembled through extreme gradient boosting may capture trend value in time series at a lesser rate of change than the observation, still making it useful for forecasting future extreme indices.

- The contribution of SW monsoon rains is approximately 95% in the northern river basins, 85% in central river basins and 70% in Chaliyar and 45% in Vamanapuram whereas the NE monsoon contributes up to 30% in Vamanapuram. In future, higher percentage of positive monthly rainfall anomalies are observed in the Aghanashini and the northern river basins than in the southern river basins.

- In the coming decades, June and July rainfall will be highly inconsistent, while September rainfall in all river basins will increase in combination with an increase in May. Also, the rainfall in October and November increases in northern river basins in the future horizons.

- The temperature anomaly is stronger in the high-emission scenario than in the medium-emission scenario. The maximum and minimum monthly temperature change in future decades is 4.3-6°C and 4-4.5°C in southern basins, 7-7.3°C and 4.6-4.8°C in central river basins and 6 °C and 5.4-6.3°C in the northern river basins. The warming starts from November and extends up

to June introducing a significantly hotter winter and the extended summer season.

- The annual mean maximum temperature and minimum temperature exhibit pronounced warming towards the end of the 21st century compared to the historical period. The mean annual temperature rises by 1.2-1.79 °C over southern basins, 1.55-1.75°C over central river basins, 0.3-0.58 °C over the northern river basins by the mid-21st century. Which increases again by 0.6-0.72 ($\pm$0.03)°C by the end of the century over southern and central river basins and by 0.97-1.76 °C over the northern river basins.

- The mean rainfall since the historical period to the far future scenario increases in all the river basins.

  a) Southern basins: Though the southern basins, which endured a decreasing trend in the historical period, may have to sustain the mixed trend in the near future under the medium emission scenario and increasing trend under the high emission scenario with an significant (insignificant) increase in the monsoon rainfall in Vamanapuram (Chaliyar).

  b) Central basins: The rainfall trend in Netravati and Aghanashini river basin is paradoxical even after having the same climate in the near future under the medium emission scenario. The central basin Netravati has endured a decrease in rainfall in the historical period and continues with the same trend in the near future decades under SSP245 with a significant increase in the pre-monsoon season. In contrast, Aghanashini has experienced an increasing trend in rainfall in the historical period and it increases eventually till the end of 21st century with a mixed trend in the post-monsoon season under the medium to high emission scenarios.

  c) Northern basins: The northern basins, Ulhas, have seen an upward trend, Purna downward trend since the mid-20th century and which will increase steadily in future decades with a significant higher rate of increase after 2050.

Though the rainfall under the climate change scenario is expected to increase in the future, the geo-climatological heterogeneity in the Western Ghats endorses a Spatio-temporal diversification in the distribution of rainfall. Past studies have featured the occurrence of substantially more intense warming in the upper troposphere than the lower troposphere warming, which tends to stabilize the atmosphere over the WG dominates the variation in the future rainfall compared to other regions in India. Additionally, the reduced moisture transport to the southern WG region is the primary cause for the decline in the future rainfall under medium emission scenario in the southern Western Ghats.

- The increase in greenhouse gas concentration has higher repercussions on the daily minimum temperature than the daily maximum temperature, especially in the winter, leading to nearly two times the magnitude of the trend compared to other seasons.

- In terms of maximum and minimum temperature, all the basins have seen an upward trend in all the seasons in the historical and near future period. After the mid-21st century, the warming trends start to slow down with decreasing trends in the pre-monsoon maximum temperature in southern and central river basins and a decrease in the monsoon minimum temperature in the northern river basins. This perhaps demonstrates the efficiency of planned initiatives for climate reduction and adaptation under the composition of the socio-economic and radiative forcing projection.

- Potential evapotranspiration has a converse relation in the southern basins, PET increases in the future horizon in Vamanapuram and decreases in the Chaliyar, and decreases in the central river basins, increases in the northern river basins with increasing trend in monsoon season in all the river basins.

- The magnitude of increase in the percentile based rainfall indices is more pronounced in the SSP585 scenario, than the SSP245 scenario. The northern river basins experience an significant increase in the R99p, and R95p,

RX1day and RX5day compared to other river basins.

- The southern basins, Vamanapuram and Chaliyar, is anticipated to have contrasting variation in the many of the rainfall indices in the forthcoming decades. The Vamanapuram basin experience higher rainfall extremes, and the Chaliyar basin experience a higher increase in the frequency of rainfall. The northern basins undergo a drastic increase in the very wet to extremely wet days rainfall and medium to very heavy rainfall with a decrease in CDD in the future. The CWD increases in the future in most of the basins with a decrease in CDD. This highlights the increased flood risk in northern basins. Also, gives an insight into the adaptation strategies that must be implemented in urban planning, infrastructure development, and agriculture.

- By the end of the century, warm days and nights increase roughly by 45–65% and 45–70% in Aghanshini and northern river basins, and 45-85%, 60-80% in southern and Netravati river basins receptively. There will be a rapid rise in the percentage of warm nights in the near future compared to the baseline period.

- The basins will experience a high increase in the intensity, duration, and frequency of hot extremes in the forthcoming decades with the existence of increased cool days/nights with respect to the base period over the basins after the mid 21st century. This demonstrates the effectiveness of mitigation and adaptation measures considered in the SSP scenario.

There is a need for immediate action on appropriate adaptation and mitigation strategies to slow the warming trend in the temperature over the regions. These findings serves as an indication of the range of anticipated changes in the magnitude of extreme maximum and minimum temperature, rainfall, and geographical pattern over the Western Ghats. This investigation can assist in comprehending the variations in the climate extremes at a regional scale of the Western Ghats of India to formulate better climate risk planning and adaptation strategies.

8.4 CLIMATE CHANGE IMPACT ON STREAMFLOW AND WATER AVAILABILITY

The precipitation, maximum, mean, minimum temperature, and potential evapotranspiration data at each basin, along with the historical streamflow data, are used as input to the Long Short Term Memory (LSTM) models. The long series is used to train the model, and the last eight years of data are used to validate the model's prediction. The decadal variability in the rainfall and the streamflow under the future scenario are evaluated for six river basins. Based on the relative change in streamflow (Q) and water availability (WA), four sectors were identified as being particularly susceptible to water scarcity. Based on the study following conclusions are drawn.

- The optimized LSTM model can be confidently used to project the streamflow using the maximum, mean, minimum temperature, potential evapotranspiration, rainfall, and historical streamflow of the river basin.
- The streamflow increase under the climate change scenario in the Vamanapuram, Aghanshini, Ulhas and Purna river basins under both the future scenarios.
- The streamflow observes a shift in the peak contributing month due to the delayed monsoon due to intensified summer season in the future decades. The streamflow decreases in the monsoon and increases in the summer and winter due to the corresponding variability in rainfall. Also, the summer streamflow increases more in the FF horizon.
- Though the rainfall increases, the water scarcity risk increases in the future decades, the months April to June will be highly vulnerable to extreme risk of water scarcity even in the WG of India which intensifies to April to July in the the high emission scenario of the future.

Hence, the implementation of enhanced irrigation technologies, the advancement of agricultural practises on farms, and the construction of water conservation

and retention structures have the potential to substantially mitigate the unmet demands and deficiencies in these basins.

8.5 OVERALL CONCLUSIONS

The Western Ghat mountain forest has a great spatio-temporal variation in the rainfall due to undulating mountainous terrain. The topographical zonation of the Western Ghats gives a detailed picture of the spatio-temporal variation of rainfall. The spatial variation in the rainfall, modelled has a varying association with the rainfall, due to the highly complex terrain and local climatic regime of the Western Ghats. The results obtained in this study are useful in understanding the dependency of rainfall on topographic and hydro-climatic parameters and can be used in any hydro-geological applications. The predictors of rainfall can be chosen wisely based on the correlation between variables and rainfall in further modelling of rainfall. Further, in the regional scale studies, even in the dense forest mountain of the Western Ghats, the GCM models ensembled through eXtreme Gradient Boosting technique has outperformed the widely used Random Forest Regression and the Support Vector Regression, thereby marking its supremacy in the performance of simulation of the climate variables irrespective of the climate condition of the region even in the dense forest mountainous basins. Also, this can be used to project the climate indices over the complex mountainous terrain of the WG.

In the future decades, the annual mean maximum temperature and minimum temperature exhibit pronounced warming towards the end of the 21st century compared to the historical period. The mean annual temperature rises by 1.2-1.79 ^{o}C over southern basins, 1.55-1.75^{o}C over central river basins, 0.3-0.58 ^{o}C over the northern river basins by the mid-21st century. Which increases again by 0.6-0.72 ($\pm$0.03)^{o}C by the end of the century over southern and central river basins and by 0.97-1.76 ^{o}C over the northern river basins. In future, the warming starts from November and extends up to June introducing a significantly hotter winter and the extended summer season in all the basins. Importantly, the increase in greenhouse

gas concentration has higher repercussions on the daily minimum temperature than the daily maximum temperature, especially in the winter, leading to nearly two times the magnitude of the trend compared to other seasons.

The rainfall will be highly inconsistent during the June and July months, while September rainfall in all river basins will increase in combination with an increase in May. Though the rainfall under the climate change scenario is expected to increase in the future, the geo-climatological heterogeneity in the Western Ghats endorses a spatio-temporal diversification in the distribution of rainfall. Past studies have featured the occurrence of substantially more intense warming in the upper troposphere than the lower troposphere warming, which tends to stabilize the atmosphere over the WG dominates the variation in the future rainfall compared to other regions in India. Additionally, the reduced moisture transport to the southern WG region is the primary cause for the decline in the future rainfall under medium emission scenario in the southern Western Ghats and vice-versa in the northern Ghats. Further, though the rainfall increases, the increase in the minimum temperature at much higher rate than the maximum temperature results in a decrease in vapour pressure deficit and, consequently, a decrease in PET. Also, the increasing CO^2 concentration with higher humidity may reduce transpiration by affecting the leaf stomata, which may counterbalance the evapotranspiration rate. Even the streamflow observes a shift in the peak contributing months due to the delayed monsoon as a result of intensified summer season in the future decades. The streamflow decreases in the monsoon and increases in the summer and winter due to the corresponding variability in rainfall. Also, the summer streamflow increases more in the FF horizon. In the future decades, a flood scenario over the northern river basin and a wast temporal variability in the drought scenario are expected especially over the southern and central river basins of the Western Ghats. To minimize the impact of the projected change and variability in rainfall and an increase in temperature and evapotranspiration on agriculture and other sectors, various site-specific adaptation measures are required in these basins. Here, the water scarcity risk increases in the future decades, the months of

April to June will be highly vulnerable to the extreme risk of water scarcity even in the WG of India, which exacerbates from April to July in the high emission scenario of the future. Hence, the implementation of enhanced irrigation technologies, the advancement of agricultural practices on farms, and the construction of water conservation and retention structures have the potential to substantially mitigate the unmet demands and deficiencies in these basins.

8.6 LIMITATIONS OF THE STUDY

- In this study we have used gauge derived product of 25 km resolution, but in order to visualize the regional rainfall variability over the complex terrain of Western Ghats,a fine resolution data is essential.
- The Uncertainty in the MMEs estimated climatic indices are analysed only for the EQM corrected GCMs. Incorporation of different bias correction methods and their impact on uncertainty has not been analysed.
- The streamflow is estimated using the deep learning based method without comparing it to the physical based hydrological models.
- The Water Scarcity risk assessment is carried out assuming the balance between the rainfall and potential evapotranspiration.

8.7 FUTURE SCOPE OF THE STUDY

- The reduction in uncertainty in the MMEs in the estimation of extreme climatic events can be analysed using advanced methods of bias correction.
- The relationship between the extreme climate events and the mountain topography can be analysed.
- The streamflow variation considering the vegetation dynamics of the region can be studied especially for the southern river basins.

REFERENCES

Aadhar, S. and V. Mishra (2020). On the projected decline in droughts over south asia in cmip6 multimodel ensemble. *Journal of Geophysical Research: Atmospheres*, 125(20), e2020JD033587.

Abbasian, M., S. Moghim, and A. Abrishamchi (2019). Performance of the General Circulation Models in Simulating Temperature and Precipitation over Iran. *Theoretical and Applied Climatology*, 135(3), 1465–1483.

Acharya, N., N. A. Shrivastava, B. Panigrahi, and U. Mohanty (2014). Development of an artificial neural network based multi-model ensemble to estimate the northeast monsoon rainfall over south peninsular india: an application of extreme learning machine. *Climate dynamics*, 43(5), 1303–1310.

Adib, M. and S. Harun (2022). Metalearning approach coupled with cmip6 multi-gcm for future monthly streamflow forecasting. *Journal of Hydrologic Engineering*, 27(6), 05022004.

Adler, R. F., G. Gu, J.-J. Wang, G. J. Huffman, S. Curtis, and D. Bolvin (2008). Relationships between Global Precipitation and Surface Temperature on Interannual and Longer Timescales (1979–2006). *Journal of Geophysical Research: Atmospheres*, 113(D22).

Adnan, R. M., Z. Liang, S. Trajkovic, M. Zounemat-Kermani, B. Li, and O. Kisi (2019). Daily streamflow prediction using optimally pruned extreme learning machine. *Journal of Hydrology*, 577, 123981.

AghaKouchak, A., F. Chiang, L. S. Huning, C. A. Love, I. Mallakpour, O. Mazdiyasni, H. Moftakhari, S. M. Papalexiou, E. Ragno, and M. Sadegh (2020). Climate Extremes and Compound Hazards in a Warming World. *Annual Review of Earth and Planetary Sciences*, 48, 519–548.

Ahmad, M., H. Y. Katman, R. A. Al-Mansob, F. Ahmad, M. Safdar, and A. C. Alguno (2022). Prediction of rockburst intensity grade in deep underground excavation using adaptive boosting classifier. *Complexity*, 2022, 1–10.

Ahmed, K., D. A. Sachindra, S. Shahid, M. C. Demirel, and E.-S. Chung (2019*a*). Selection of multi-model ensemble of general circulation models for the simulation of precipitation and maximum and minimum temperature based on spatial assessment metrics. *Hydrology and Earth System Sciences*, 23(11), 4803–4824.

Ahmed, K., D. A. Sachindra, S. Shahid, Z. Iqbal, N. Nawaz, and N. Khan (2020). Multi-model ensemble predictions of precipitation and temperature using machine learning algorithms. *Atmospheric Research*, 236, 104806.

Ahmed, K., S. Shahid, S. B. Haroon, and W. Xiao-Jun (2015). Multilayer perceptron neural network for downscaling rainfall in arid region: a case study of baluchistan, pakistan. *Journal of Earth System Science*, 124(6), 1325–1341.

Ahmed, K., S. Shahid, D. Sachindra, N. Nawaz, and E.-S. Chung (2019*b*). Fidelity Assessment of General Circulation Model Simulated Precipitation and Temperature over Pakistan using a Feature Selection Method. *Journal of hydrology*, 573, 281–298.

Akbas, A. (2023). Seasonality, persistency, regionalization, and control mechanism of extreme rainfall over complex terrain. *Theoretical and Applied Climatology*, 152(3), 981–997.

Al-Ahmadi, K. and S. Al-Ahmadi (2014). Spatiotemporal Variations in Rainfall–Topographic Relationships in Southwestern Saudi Arabia. *Arabian Journal of Geosciences*, 7(8), 3309–3324.

Alamgir, M., M. Mohsenipour, R. Homsi, X. Wang, S. Shahid, M. S. Shiru, N. E. Alias, and A. Yuzir (2019). Parametric assessment of seasonal drought risk to crop production in bangladesh. *Sustainability*, 11(5), 1442.

Alapaty, K., S. Raman, and R. Madala (1994). Simulation of Monsoon Boundary-Layer Processes using a Regional Scale Nested Grid Model. *Boundary-layer meteorology*, 67(4), 407–426.

Anil, S., V. Manikanta, and A. R. Pallakury (2021). Unravelling the influence of subjectivity on ranking of cmip6 based climate models: A case study. *International Journal of Climatology*, 41(13), 5998–6016.

Annamalai, H., K. Hamilton, and K. R. Sperber (2007). The south asian summer monsoon and its relationship with enso in the ipcc ar4 simulations. *Journal of Climate*, 20(6), 1071–1092.

Apaydin, H., H. Feizi, M. T. Sattari, M. S. Colak, S. Shamshirband, and K.-W. Chau (2020). Comparative analysis of recurrent neural network architectures for reservoir inflow forecasting. *Water*, 12(5), 1500.

Arora, M., N. Goel, and P. Singh (2005). Evaluation of temperature trends over india/evaluation de tendances de température en inde. *Hydrological sciences journal*, 50(1).

Asadollah, S. B. H. S., A. Sharafati, and S. Shahid (2022). Application of ensemble machine learning model in downscaling and projecting climate variables over different climate regions in iran. *Environmental Science and Pollution Research*, 1–20.

Avila-Diaz, A., V. Benezoli, F. Justino, R. Torres, and A. Wilson (2020). Assessing current and future trends of climate extremes across brazil based on reanalyses and earth system model projections. *Climate Dynamics*, 55(5-6), 1403–1426.

Awad, M. and R. Khanna, *Efficient learning machines: theories, concepts, and applications for engineers and system designers*. Springer nature, 2015.

Ayugi, B., J. Zhihong, H. Zhu, H. Ngoma, H. Babaousmail, K. Rizwan, and V. Dike (2021). Comparison of cmip6 and cmip5 models in simulating mean and extreme precipitation over east africa. *International Journal of Climatology*, 41(15), 6474–6496.

Babaousmail, H., B. Ayugi, A. Rajasekar, H. Zhu, C. Oduro, R. Mumo, and V. Ongoma (2022). Projection of Extreme Temperature Events over the Mediterranean and Sahara Using Bias-Corrected CMIP6 Models. *Atmosphere*, 13(5), 741.

Babar, S. and H. Ramesh (2015). Streamflow response to land use–land cover change over the nethravathi river basin, india. *Journal of Hydrologic Engineering*, 20(10), 05015002.

Barry, R. G., *Mountain Weather and Climate*. Psychology Press, 1992.

Basha, G., P. Kishore, M. V. Ratnam, A. Jayaraman, A. Agha Kouchak, T. B. Ouarda, and I. Velicogna (2017). Historical and Projected Surface Temperature over India during the 20^{th} and 21^{st} century. *Scientific reports*, 7(1), 1–10.

Basist, A., G. D. Bell, and V. Meentemeyer (1994). Statistical relationships between topography and precipitation patterns. *Journal of climate*, 7(9), 1305–1315.

Beniston, M., Climatic Change in Mountain Regions: a Review of Possible Impacts. *In Climate variability and change in high elevation regions: Past, present & future*. Springer, 2003, 5–31.

Bharti, V., C. Singh, J. Ettema, and T. Turkington (2016). Spatiotemporal characteristics of extreme rainfall events over the northwest himalaya using satellite data. *International Journal of Climatology*, 36(12), 3949–3962.

Bi, D., M. Dix, S. Marsland, S. O'farrell, A. Sullivan, R. Bodman, R. Law, I. Harman, J. Srbinovsky, H. A. Rashid, *et al.* (2020). Configuration and spin-up of access-cm2, the new generation australian community climate and earth system simulator coupled model. *Journal of Southern Hemisphere Earth Systems Science*, 70(1), 225–251.

Bizuneh, B. B., M. A. Moges, B. G. Sinshaw, and M. S. Kerebih (2021). Swat and hbv models' response to streamflow estimation in the upper blue nile basin, ethiopia. *Water-Energy Nexus*, 4, 41–53.

Böhner, J. and O. Antonić (2009). Land-Surface Parameters Specific to Topo-Climatology. *Developments in soil science*, 33, 195–226.

Booker, D. and R. Woods (2014). Comparing and combining physically-based and empirically-based approaches for estimating the hydrology of ungauged catchments. *Journal of Hydrology*, 508, 227–239.

Bookhagen, B. and D. W. Burbank (2006). Topography, relief, and trmm-derived rainfall variations along the himalaya. *Geophysical Research Letters*, 33(8).

Breiman, L. (2001). Random forests. *Machine learning*, 45(1), 5–32.

Brown, A. E., L. Zhang, T. A. McMahon, A. W. Western, and R. A. Vertessy (2005). A review of paired catchment studies for determining changes in water yield resulting from alterations in vegetation. *Journal of hydrology*, 310(1-4), 28–61.

Brunner, L., A. G. Pendergrass, F. Lehner, A. L. Merrifield, R. Lorenz, and R. Knutti (2020). Reduced global warming from cmip6 projections when weighting models by performance and independence. *Earth System Dynamics*, 11(4), 995–1012.

Brunsdon, C., A. S. Fotheringham, and M. Charlton (1999). Some Notes on Parametric Significance Tests for Geographically Weighted Regression. *Journal of regional science*, 39(3), 497–524.

Burrough, P. (2001). GIS and Geostatistics: Essential Partners for Spatial Analysis. *Environmental and ecological statistics*, 8(4), 361–377.

Buttafuoco, G. and F. Lucà (2020). Accounting for elevation and distance to the nearest coastline in geostatistical mapping of average annual precipitation. *Environmental Earth Sciences*, 79(1), 11.

Buytaert, W., R. Celleri, P. Willems, B. De Bievre, and G. Wyseure (2006). Spatial and Temporal Rainfall Variability in Mountainous areas: A case study from the south Ecuadorian Andes. *Journal of hydrology*, 329(3-4), 413–421.

Carvalho, D., S. Rafael, A. Monteiro, V. Rodrigues, M. Lopes, and A. Rocha (2022). How well have cmip3, cmip5 and cmip6 future climate projections portrayed the recently observed warming. *Scientific Reports*, 12(1), 1–7.

Chamaille-Jammes, S., H. Fritz, and F. Murindagomo (2006). Spatial Patterns of the NDVI–Rainfall Relationship at the Seasonal and Interannual Time Scales in an African Savanna. *International Journal of Remote Sensing*, 27(23), 5185–5200.

Chandu, N., T. Eldho, and A. Mondal (2022). Hydrological Impacts of Climate and Land-use Change in Western Ghats, India. *Regional Environmental Change*, 22(1), 1–15.

Chattopadhyay, N. and M. Hulme (1997). Evaporation and potential evapotranspiration in india under conditions of recent and future climate change. *Agricultural and Forest Meteorology*, 87(1), 55–73.

Chen, S.-T., P.-S. Yu, and Y.-H. Tang (2010). Statistical downscaling of daily precipitation using support vector machines and multivariate analysis. *Journal of hydrology*, 385(1-4), 13–22.

Chen, T. and C. Guestrin, Xgboost: A scalable tree boosting system. *In Proceedings of the 22nd acm sigkdd international conference on knowledge discovery and data mining*. 2016.

Cheng, M., F. Fang, T. Kinouchi, I. Navon, and C. Pain (2020). Long lead-time daily and monthly streamflow forecasting using machine learning methods. *Journal of Hydrology*, 590, 125376.

Chhetri, R., V. P. Pandey, R. Talchabhadel, and B. R. Thapa (2021). How do CMIP6 Models Project Changes in Precipitation Extremes over Seasons and Locations across the Mid Hills of Nepal? *Theoretical and Applied Climatology*, 1–18.

Cho, M.-Y. and T. T. Hoang (2017). Feature selection and parameters optimization of svm using particle swarm optimization for fault classification in power distribution systems. *Computational intelligence and neuroscience*, 2017.

Chokkavarapu, N. and V. R. Mandla (2019). Comparative study of gcms, rcms, downscaling and hydrological models: a review toward future climate change impact estimation. *SN Applied Sciences*, 1(12), 1698.

Christensen, N. S., A. W. Wood, N. Voisin, D. P. Lettenmaier, and R. N. Palmer (2004). The Effects of Climate Change on the Hydrology and Water Resources of the Colorado River basin. *Climatic change*, 62(1-3), 337–363.

Church, M. (2015). Channel Stability: Morphodynamics and the Morphology of Rivers, 281–321.

Collins, M., R. Knutti, J. Arblaster, J.-L. Dufresne, T. Fichefet, P. Friedlingstein, X. Gao, W. J. Gutowski, T. Johns, G. Krinner, *et al.*, Long-term Climate Change: Projections, Commitments and Irreversibility. *In Climate Change 2013-The Physical Science Basis: Contribution of Working Group I to the Fifth Assessment Report of the Intergovernmental Panel on Climate Change*. Cambridge University Press, 2013, 1029–1136.

Cong, R.-G. and M. Brady (2012). The Interdependence Between Rainfall and Temperature: Copula Analyses. *The Scientific World Journal*.

Cortes, C. and V. Vapnik (1995). Support-vector networks. *Machine learning*, 20(3), 273–297.

Coulibaly, P., Y. B. Dibike, and F. Anctil (2005). Downscaling precipitation and temperature with temporal neural networks. *Journal of Hydrometeorology*, 6(4), 483–496.

Crawford, J., K. Venkataraman, and J. Booth (2019). Developing climate model ensembles: A comparative case study. *Journal of hydrology*, 568, 160–173.

Daly, C., R. P. Neilson, and D. L. Phillips (1994). A statistical-Topographic Model for Mapping Climatological Precipitation over Mountainous Terrain. *Journal of Applied Meteorology and Climatology*, 33(2), 140–158.

Das, J. and U. V. Nanduri (2018). Assessment and evaluation of potential climate change impact on monsoon flows using machine learning technique over wainganga river basin, india. *Hydrological Sciences Journal*, 63(7), 1020–1046.

Das, P. (1962). Mean vertical motion and non-adiabatic heat sources over India during the monsoon. *Tellus*, 14(2), 212–220.

Das, S., P. Datta, D. Sharma, and K. Goswami (2022*a*). Trends in temperature, precipitation, potential evapotranspiration, and water availability across the teesta river basin under 1.5 and 2°c temperature rise scenarios of cmip6. *Atmosphere*, 13(6), 941.

Das, S., P. Datta, D. Sharma, and K. Goswami (2022*b*). Trends in temperature, precipitation, potential evapotranspiration, and water availability across the teesta river basin under 1.5 and 2° c temperature rise scenarios of cmip6. *Atmosphere*, 13(6), 941.

Dash, S., R. Jenamani, S. Kalsi, and S. Panda (2007). Some evidence of climate change in twentieth-century india. *Climatic change*, 85(3-4), 299–321.

Davenport, M. L. and S. E. Nicholson (1993). On the Relation Between Rainfall and the Normalized Difference Vegetation Index for Diverse Vegetation Types in East Africa. *International Journal of Remote Sensing*, 14(12), 2369–2389.

De, U. and S. Dutta (2005). West Coast Rainfall and Convective Instability. *J. Indian Geophysics Union*, 9, 71–82.

de Medeiros, F. J., C. P. de Oliveira, and A. Avila-Diaz (2022). Evaluation of extreme precipitation climate indices and their projected changes for brazil: From cmip3 to cmip6. *Weather and Climate Extremes*, 38, 100511.

DeGaetano, A. T. (2001). Spatial Grouping of United States Climate Stations using a Hybrid Clustering Approach. *International Journal of Climatology: A Journal of the Royal Meteorological Society*, 21(7), 791–807.

Dey, A., D. P. Sahoo, R. Kumar, and R. Remesan (2022). A multimodel ensemble machine learning approach for cmip6 climate model projections in an indian river basin. *International Journal of Climatology*.

Diksha, A. Kumar, and P. Lal (2022). Analysing Climatic Variability and Extremes Events in the Himalayan Regions Focusing on Mountainous Urban Agglomerations. *Geocarto International*, 1–23.

Diodato, N. (2005). The Influence of Topographic Co-Variables on the Spatial Variability of Precipitation over Small regions of Complex Terrain. *International journal of Climatology*, 25(3), 351–363.

Döll, P. and J. Zhang (2010). Impact of climate change on freshwater ecosystems: a global-scale analysis of ecologically relevant river flow alterations. *Hydrology and Earth System Sciences*, 14(5), 783–799.

Dong, N. D., K. Jayakumar, and V. Agilan (2018). Impact of Climate Change on Flood Frequency of the Trian Reservoir in Vietnam using RCMs. *Journal of Hydrologic Engineering*, 23(2), 05017032.

Döscher, R., M. Acosta, A. Alessandri, P. Anthoni, A. Arneth, T. Arsouze, T. Bergmann, R. Bernadello, S. Bousetta, L.-P. Caron, *et al.* (2021). The ec-earth3 earth system model for the climate model intercomparison project 6. *Geoscientific Model Development Discussions*, 1, 2021.

Du, L., R. Gao, P. N. Suganthan, and D. Z. Wang (2022). Bayesian optimization based dynamic ensemble for time series forecasting. *Information Sciences*, 591, 155–175.

Duan, K., P. V. Caldwell, G. Sun, S. G. McNulty, Y. Zhang, E. Shuster, B. Liu, and P. V. Bolstad (2019). Understanding the role of regional water connectivity

in mitigating climate change impacts on surface water supply stress in the united states. *Journal of Hydrology*, 570, 80–95.

Dubey, S. K., R. K. Ranjan, A. K. Misra, N. Wanjari, and S. Vishwakarma (2022). Variability of precipitation extremes and drought intensity over the Sikkim State, India, during 1950–2018. *Theoretical and Applied Climatology*, 1–14.

Easterling, D. R., B. Horton, P. D. Jones, T. C. Peterson, T. R. Karl, D. E. Parker, M. J. Salinger, V. Razuvayev, N. Plummer, P. Jamason, *et al.* (1997). Maximum and Minimum Temperature Trends for the Globe. *Science*, 277(5324), 364–367.

Elliott, R. D. and E. L. Hovind (1964). The Water Balance of Orographic Clouds. *Journal of Applied Meteorology and Climatology*, 3(3), 235–239.

Erdal, H. I. and O. Karakurt (2013). Advancing monthly streamflow prediction accuracy of cart models using ensemble learning paradigms. *Journal of Hydrology*, 477, 119–128.

Eyring, V., S. Bony, G. A. Meehl, C. A. Senior, B. Stevens, R. J. Stouffer, and K. E. Taylor (2016). Overview of the coupled model intercomparison project phase 6 (cmip6) experimental design and organization. *Geoscientific Model Development*, 9(5), 1937–1958.

Feddema, J. J. (2005). A revised Thornthwaite-type Global Climate Classification. *Physical Geography*, 26(6), 442–466.

Feidas, H., A. Karagiannidis, S. Keppas, M. Vaitis, T. Kontos, P. Zanis, D. Melas, and E. Anadranistakis (2014). Modeling and Mapping Temperature and Precipitation Climate Data in Greece using Topographical and Geographical Parameters. *Theoretical and applied climatology*, 118(1), 133–146.

Franczyk, J. and H. Chang (2009). The effects of climate change and urbanization on the runoff of the rock creek basin in the portland metropolitan area, oregon, usa. *Hydrological Processes: An International Journal*, 23(6), 805–815.

Frei, C. and C. Schär (1998). A precipitation climatology of the alps from high-resolution rain-gauge observations. *International Journal of Climatology: A Journal of the Royal Meteorological Society*, 18(8), 873–900.

Freund, Y. and R. E. Schapire (1997). A decision-theoretic generalization of on-line learning and an application to boosting. *Journal of computer and system sciences*, 55(1), 119–139.

Fu, M., T. Fan, Z. Ding, S. Q. Salih, N. Al-Ansari, and Z. M. Yaseen (2020). Deep learning data-intelligence model based on adjusted forecasting window scale: application in daily streamflow simulation. *IEEE Access*, 8, 32632–32651.

Garrote, L., A. Iglesias, and A. Granados (2018). Country-level assessment of future risk of water scarcity in europe. *Proceedings of the International Association of Hydrological Sciences*, 379, 455–462.

Gerten, D., S. Rost, W. von Bloh, and W. Lucht (2008). Causes of change in 20th century global river discharge. *Geophysical Research Letters*, 35(20).

Ghobadi, F. and D. Kang (2022). Improving long-term streamflow prediction in a poorly gauged basin using geo-spatiotemporal mesoscale data and attention-based deep learning: A comparative study. *Journal of Hydrology*, 615, 128608.

Givati, A., G. Thirel, D. Rosenfeld, and D. Paz (2019). Climate change impacts on streamflow at the upper jordan river based on an ensemble of regional climate models. *Journal of Hydrology: Regional Studies*, 21, 92–109.

Goovaerts, P. (2000). Geostatistical Approaches for Incorporating Elevation into the Spatial Interpolation of Rainfall. *Journal of hydrology*, 228(1-2), 113–129.

Gopalakrishnan, R., M. Jayaraman, G. Bala, and N. Ravindranath (2011). Climate change and indian forests. *Current Science*, 348–355.

Goswami, B. N., V. Venugopal, D. Sengupta, M. Madhusoodanan, and P. K. Xavier (2006). Increasing trend of extreme rain events over India in a warming environment. *Science*, 314(5804), 1442–1445.

Goswami, U. P., K. Bhargav, B. Hazra, and M. K. Goyal (2018). Spatiotemporal and Joint Probability Behavior of Temperature Extremes over the Himalayan Region under Changing Climate. *Theoretical and Applied Climatology*, 134(1), 477–498.

Goudarzi, F. M., A. Sarraf, and H. Ahmadi (2021). Calibration of swat and three data-driven models for monthly stream flow simulation in maharlu lake basin. *Water Supply*, 21(8), 4219–4238.

Guhathakurta, P., O. Sreejith, and P. Menon (2011). Impact of climate change on extreme rainfall events and flood risk in india. *Journal of earth system science*, 120(3), 359.

Gusain, A., S. Ghosh, and S. Karmakar (2020). Added value of cmip6 over cmip5 models in simulating indian summer monsoon rainfall. *Atmospheric Research*, 232, 104680.

Gutjahr, O., D. Putrasahan, K. Lohmann, J. H. Jungclaus, J.-S. von Storch, N. Brüggemann, H. Haak, and A. Stössel (2019). Max planck institute earth system model (mpi-esm1. 2) for the high-reresmip). *Geoscientific Model Development*, 12(7), 3241–3281.

Hargreaves, G. H. and Z. A. Samani (1985). Reference crop evapotranspiration from temperature. *Applied engineering in agriculture*, 1(2), 96–99.

Haykin, S. and N. Network (2004). A comprehensive foundation. *Neural networks*, 2(2004), 41.

Hayward, D. and R. Clarke (1996). Relationship between Rainfall, Altitude and Distance from the Sea in the Freetown Peninsula, Sierra Leone. *Hydrological sciences journal*, 41(3), 377–384.

Hengade, N. and T. Eldho (2016). Assessment of lulc and climate change on the hydrology of ashti catchment, india using vic model. *Journal of Earth System Science*, 125, 1623–1634.

Hengl, T. (2009). A Practical Guide to Geostatistical Mapping.

Hengl, T., G. B. Heuvelink, M. P. Tadić, and E. J. Pebesma (2012). Spatio-Temporal Prediction of Daily Temperatures using Time-Series of MODIS LST Images. *Theoretical and applied climatology*, 107(1-2), 265–277.

Herath, H. M. V. V., J. Chadalawada, and V. Babovic (2021). Hydrologically informed machine learning for rainfall–runoff modelling: towards distributed modelling. *Hydrology and Earth System Sciences*, 25(8), 4373–4401.

Hersbach, H., B. Bell, P. Berrisford, S. Hirahara, A. Horányi, J. Muñoz-Sabater, J. Nicolas, C. Peubey, R. Radu, D. Schepers, *et al.* (2020). The ERA5 Global Reanalysis. *Quarterly Journal of the Royal Meteorological Society*, 146(730), 1999–2049.

Hwang, C.-L., K. Yoon, C.-L. Hwang, and K. Yoon (1981). Methods for multiple attribute decision making. *Multiple attribute decision making: methods and applications a state-of-the-art survey*, 58–191.

Isabona, J., A. L. Imoize, S. Ojo, O. Karunwi, Y. Kim, C.-C. Lee, and C.-T. Li (2022). Development of a multilayer perceptron neural network for optimal predictive modeling in urban microcellular radio environments. *Applied Sciences*, 12(11), 5713.

Jain, S., V. Kumar, and M. Saharia (2013). Analysis of rainfall and temperature trends in northeast india. *International Journal of Climatology*, 33(4), 968–978.

Jemai, S., A. Kallel, B. Agoubi, and H. Abida (2022). Spatial and temporal rainfall variability and its controlling factors under an arid climate condition: case of gabes catchment, southern tunisia. *Environment, Development and Sustainability*, 1–18.

Jha, C., C. Dutt, and K. Bawa (2000). Deforestation and land use changes in western ghats, india. *Current Science*, 231–238.

Jiang, D., Y. Sui, and X. Lang (2016). Timing and associated climate change of a 2 c global warming. *International Journal of Climatology*, 36(14), 4512–4522.

Jimeno-Sáez, P., J. Senent-Aparicio, J. Pérez-Sánchez, and D. Pulido-Velazquez (2018). A comparison of swat and ann models for daily runoff simulation in different climatic zones of peninsular spain. *Water*, 10(2), 192.

Johansson, B. and D. Chen (2003). The Influence of Wind and Topography on Precipitation Distribution in Sweden: Statistical Analysis and Modelling. *International Journal of Climatology: A Journal of the Royal Meteorological Society*, 23(12), 1523–1535.

Jose, D. M. and G. Dwarakish (2022*a*). Frequency-Intensity-Distribution Bias Correction and Trend Analysis of High-Resolution CMIP6 Precipitation data over a Tropical River Basin. *Theoretical and Applied Climatology*, 1–12.

Jose, D. M. and G. S. Dwarakish (2021). Bias Correction and Trend Analysis of Temperature Data by a High-Resolution CMIP6 Model over a Tropical River Basin. *Asia-Pacific Journal of Atmospheric Sciences*, 1–19.

Jose, D. M. and G. S. Dwarakish (2022*b*). Ranking of downscaled cmip5 and cmip6 gcms at a basin scale: case study of a tropical river basin on the south west coast of india. *Arabian Journal of Geosciences*, 15(1), 120.

Jose, D. M., A. M. Vincent, and G. S. Dwarakish (2022). Improving multiple model ensemble predictions of daily precipitation and temperature through machine learning techniques. *Scientific Reports*, 12(1), 1–25.

Joshi, M., E. Hawkins, R. Sutton, J. Lowe, and D. Frame (2011). Projections of when temperature change will exceed 2 c above pre-industrial levels. *Nature Climate Change*, 1(8), 407–412.

Joshi, M. K. and A. Pandey (2011). Trend and spectral analysis of rainfall over india during 1901–2000. *Journal of Geophysical Research: Atmospheres*, 116(D6).

Jun, T., L. Munasinghe, and D. H. Rind (2015). A new metric for indian monsoon rainfall extremes. *Journal of Climate*, 28(7), 2842–2855.

Justice, C., J. Townshend, E. Vermote, E. Masuoka, R. Wolfe, N. Saleous, D. Roy, and J. Morisette (2002). An Overview of MODIS Land Data Pprocessing and Product Status. *Remote sensing of Environment*, 83(1-2), 3–15.

Kabir, S., S. Patidar, and G. Pender, Investigating capabilities of machine learning techniques in forecasting stream flow. *In Proceedings of the Institution of Civil Engineers-Water Management*volume173. Thomas Telford Ltd, 2020.

Kadkhodazadeh, M., M. Valikhan Anaraki, A. Morshed-Bozorgdel, and S. Farzin (2022). A new methodology for reference evapotranspiration prediction and uncertainty analysis under climate change conditions based on machine learning, multi criteria decision making and monte carlo methods. *Sustainability*, 14(5), 2601.

Khoi, D. N. (2016). Comparision of the hec-hms and swat hydrological models in simulating the stream flow. *Journal of Science and Technology*, 53(5A), 189–195.

Kim, J., J. Choi, C. Choi, and S. Park (2013). Impacts of changes in climate and land use/land cover under ipcc rcp scenarios on streamflow in the hoeya river basin, korea. *Science of the Total Environment*, 452, 181–195.

Kim, J. H., J. H. Sung, E.-S. Chung, S. U. Kim, M. Son, and M. S. Shiru (2021). Comparison of projection in meteorological and hydrological droughts in the cheongmicheon watershed for rcp4. 5 and ssp2-4.5. *Sustainability*, 13(4), 2066.

Kim, Y., Y. Kim, S. Hwang, and D. Kim (2022). Prospect of future water resources in the basins of chungju dam and soyang-gang dam using a physics-based distributed hydrological model and a deep-learning-based lstm model. *Journal of Korea Water Resources Association*, 55(12), 1115–1124.

Kingra, P., R. Setia, S. Kaur, S. Singh, S. P. Singh, S. Kukal, and B. Pateriya (2018). Spatio-temporal analysis of the climate impact on rice yield in north-west india. *Spatial Information Research*, 26, 381–395.

Knutti, R., R. Furrer, C. Tebaldi, J. Cermak, and G. A. Meehl (2010). Challenges in combining projections from multiple climate models. *Journal of Climate*, 23(10), 2739–2758.

Konda, G. and N. K. Vissa (2023). Evaluation of cmip6 models for simulations of surplus/deficit summer monsoon conditions over india. *Climate Dynamics*, 60(3-4), 1023–1042.

Kratzert, F., D. Klotz, C. Brenner, K. Schulz, and M. Herrnegger (2018). Rainfall–runoff modelling using long short-term memory (lstm) networks. *Hydrology and Earth System Sciences*, 22(11), 6005–6022.

Kripalani, R., A. Kulkarni, S. Sabade, and M. Khandekar (2003). Indian monsoon variability in a global warming scenario. *Natural hazards*, 29(2), 189–206.

Kripalani, R., J. Oh, A. Kulkarni, S. Sabade, and H. Chaudhari (2007). South asian summer monsoon precipitation variability: coupled climate model simulations and projections under ipcc ar4. *Theoretical and Applied Climatology*, 90(3-4), 133–159.

Krishnakumar, K., G. P. Rao, and C. Gopakumar (2009). Rainfall trends in twentieth century over kerala, india. *Atmospheric environment*, 43(11), 1940–1944.

Krishnan, R., T. Sabin, D. Ayantika, A. Kitoh, M. Sugi, H. Murakami, A. Turner, J. Slingo, and K. Rajendran (2013). Will the south asian monsoon overturning circulation stabilize any further? *Climate dynamics*, 40(1-2), 187–211.

Krishnan, R., J. Sanjay, C. Gnanaseelan, M. Mujumdar, A. Kulkarni, and S. Chakraborty, *Assessment of climate change over the Indian region: a report of the ministry of earth sciences (MOES), government of India*. Springer Nature, 2020.

Kumar, K. R., G. Pant, B. Parthasarathy, and N. Sontakke (1992). Spatial and subseasonal patterns of the long-term trends of indian summer monsoon rainfall. *International Journal of climatology*, 12(3), 257–268.

Kumar, K. R., A. Sahai, K. K. Kumar, S. Patwardhan, P. Mishra, J. Revadekar, K. Kamala, and G. Pant (2006). High-resolution climate change scenarios for india for the 21st century. *Current science*, 90(3), 334–345.

Kumar, N., M. K. Goyal, A. K. Gupta, S. Jha, J. Das, and C. A. Madramootoo (2021). Joint Behaviour of Climate Extremes across India: Past and Future. *Journal of Hydrology*, 597, 126185.

Kumar, T. L., B. Vinodhkumar, K. K. Rao, J. Chowdary, K. K. Osuri, and S. Desamsetti (2023). Insights from the bias-corrected simulations of cmip6 in india's future climate. *Global and Planetary Change*, 104137.

Kumar, V., S. K. Jain, and Y. Singh (2010). Analysis of long-term rainfall trends in india. *Hydrological Sciences Journal–Journal des Sciences Hydrologiques*, 55(4), 484–496.

Kumari, M., C. K. Singh, O. Bakimchandra, and A. Basistha (2017*a*). Geographically Weighted Regression based Quantification of Rainfall–Topography Relationship and Rainfall Gradient in Central Himalayas. *International Journal of Climatology*, 37(3), 1299–1309.

Kumari, M., C. K. Singh, A. Basistha, S. Dorji, and T. B. Tamang (2017*b*). Non-Stationary Modelling Framework for Rainfall Interpolation in Complex Terrain. *International Journal of Climatology*, 37(11), 4171–4185.

Kundu, S., D. Khare, and A. Mondal (2017). Interrelationship of rainfall, temperature and reference evapotranspiration trends and their net response to the climate change in central india. *Theoretical and Applied Climatology*, 130, 879–900.

Lal, M., G. A. Meehl, and J. M. Arblaster (2000). Simulation of indian summer monsoon rainfall and its intraseasonal variability in the ncar climate system model. *Regional Environmental Change*, 1(3-4), 163–179.

Lal, M., T. Nozawa, S. Emori, H. Harasawa, K. Takahashi, M. Kimoto, A. Abe-Ouchi, T. Nakajima, T. u. Takemura, and A. Numaguti (2001). Future climate change: Implications for indian summer monsoon and its variability. *Current science*, 1196–1207.

Lal, P., A. K. Dubey, A. Kumar, P. Kumar, and C. Dwivedi (2022). Measuring the Control of Landscape Modifications on Surface Temperature in India. *Geocarto International*, 1–18.

Lal, P., A. Shekhar, M. Gharun, and N. N. Das (2023). Spatiotemporal Evolution of Global Long-Term patterns of Soil Moisture. *Science of The Total Environment*, 161470.

Lapen, D. R. and L. W. Martz (1993). The Measurement of Two Simple Topographic Indices of Wind Sheltering-Exposure from Raster Digital Elevation Models. *Computers & Geosciences*, 19(6), 769–779.

Larcher, W., *Physiological Plant Ecology: Ecophysiology and Stress Physiology of Functional Groups*. Springer Science & Business Media, 2003.

Lee, D., G. Lee, S. Kim, and S. Jung (2020). Future runoff analysis in the mekong river basin under a climate change scenario using deep learning. *Water*, 12(6), 1556.

Legates, D. R. and G. J. McCabe Jr (1999). Evaluating the use of "goodness-of-fit" measures in hydrologic and hydroclimatic model validation. *Water resources research*, 35(1), 233–241.

Lettenmaier, D. P., D. Alsdorf, J. Dozier, G. J. Huffman, M. Pan, and E. F. Wood (2015). Inroads of Remote Sensing into Hydrologic Science during the WRR Era. *Water Resources Research*, 51(9), 7309–7342.

Li, C., L. Wang, W. Wanrui, J. Qi, Y. Linshan, Y. Zhang, W. Lei, X. Cui, and P. Wang (2018). An analytical approach to separate climate and human contributions to basin streamflow variability. *Journal of hydrology*, 559, 30–42.

Li, S., Z. Zhao, X. Miaomiao, and Y. Wang (2010). Investigating Spatial Non-Stationary and Scale-Dependent Relationships between Urban Surface Temperature and Environmental Factors using Geographically Weighted Regression. *Environmental Modelling & Software*, 25(12), 1789–1800.

Li, T., Z. Jiang, H. Le Treut, L. Li, L. Zhao, and L. Ge (2021). Machine learning to optimize climate projection over china with multi-model ensemble simulations. *Environmental Research Letters*, 16(9), 094028.

Liu, Q. and B. Cui (2011). Impacts of climate change/variability on the streamflow in the yellow river basin, china. *Ecological Modelling*, 222(2), 268–274.

Liu, Y., L. Ren, X. Yang, M. Ma, F. Yuan, and S. Jiang (2015). Effects of precipitation and potential evaporation on actual evapotranspiration over the laohahe basin, northern china. *Proceedings of the International Association of Hydrological Sciences*, 371(371), 173–179.

Lutz, A. F., H. W. ter Maat, H. Biemans, A. B. Shrestha, P. Wester, and W. W. Immerzeel (2016). Selecting representative climate models for climate change impact studies: an advanced envelope-based selection approach. *International Journal of Climatology*, 36(12), 3988–4005.

Makwana, J. J. and M. K. Tiwari (2014). Intermittent streamflow forecasting and extreme event modelling using wavelet based artificial neural networks. *Water resources management*, 28, 4857–4873.

Maraun, D. (2013). Bias correction, quantile mapping, and downscaling: Revisiting the inflation issue. *Journal of Climate*, 26(6), 2137–2143.

Masselot, P., S. Dabo-Niang, F. Chebana, and T. B. Ouarda (2016). Streamflow forecasting using functional regression. *Journal of Hydrology*, 538, 754–766.

Mauritsen, T., J. Bader, T. Becker, J. Behrens, M. Bittner, R. Brokopf, V. Brovkin, M. Claussen, T. Crueger, M. Esch, *et al.* (2019). Developments in the mpi-m earth system model version 1.2 (mpi-esm1. 2) and its response to increasing co_2. *Journal of Advances in Modeling Earth Systems*, 11(4), 998–1038.

Maxino, C., B. McAvaney, A. Pitman, and S. Perkins (2008). Ranking the ar4 climate models over the murray-darling basin using simulated maximum temperature, minimum temperature and precipitation. *International Journal of Climatology: A Journal of the Royal Meteorological Society*, 28(8), 1097–1112.

Meehl, G. A., J. M. Arblaster, and C. Tebaldi (2005). Understanding Future Patterns of Increased Precipitation Intensity in Climate Model Simulations. *Geophysical Research Letters*, 32(18).

Meehl, G. A., W. M. Washington, T. Wigley, J. M. Arblaster, and A. Dai (2003). Solar and greenhouse gas forcing and climate response in the twentieth century. *Journal of Climate*, 16(3), 426–444.

Meenu, R., S. Rehana, and P. Mujumdar (2013). Assessment of hydrologic impacts of climate change in tunga–bhadra river basin, india with hec-hms and sdsm. *Hydrological processes*, 27(11), 1572–1589.

Mekonnen, M. M. and A. Y. Hoekstra (2016). Four billion people facing severe water scarcity. *Science advances*, 2(2), e1500323.

Menon, S. and K. S. Bawa (1998). Deforestation in the tropics: reconciling disparities in estimates for india.

Minville, M., F. Brissette, and R. Leconte (2008). Uncertainty of the impact of climate change on the hydrology of a nordic watershed. *Journal of hydrology*, 358(1-2), 70–83.

Mishra, S. K., S. Sahany, P. Salunke, I.-S. Kang, and S. Jain (2018*a*). Fidelity of CMIP5 Multi-Model Mean in assessing Indian Monsoon Simulations. *Npj Climate and Atmospheric Science*, 1(1), 1–8.

Mishra, V., U. Bhatia, and A. D. Tiwari (2020). Bias-corrected climate projections for south asia from coupled model intercomparison project-6. *Scientific data*, 7(1), 1–13.

Mishra, V. and R. Lilhare (2016). Hydrologic sensitivity of indian sub-continental river basins to climate change. *Global and Planetary Change*, 139, 78–96.

Mishra, Y., T. Nakamura, M. S. Babel, S. Ninsawat, and S. Ochi (2018*b*). Impact of climate change on water resources of the bheri river basin, nepal. *Water*, 10(2), 220.

Mitra, A. (2021). A comparative study on the skill of cmip6 models to preserve daily spatial patterns of monsoon rainfall over india. *Frontiers in Climate*, 3, 654763.

Mohammadi, B., R. Moazenzadeh, K. Christian, and Z. Duan (2021). Improving streamflow simulation by combining hydrological process-driven and artificial intelligence-based models. *Environmental Science and Pollution Research*, 28, 65752–65768.

Mohan, S. and P. K. Bhaskaran (2019). Evaluation and bias correction of global climate models in the cmip5 over the indian ocean region. *Environmental monitoring and assessment*, 191, 1–14.

Mooley, D., B. Parthasarathy, N. Sontakke, and A. Munot (1981). Annual Rain-Water over India, Its Variability and Impact on the Economy. *Journal of Climatology*, 1(2), 167–186.

Mu, Q., F. A. Heinsch, M. Zhao, and S. W. Running (2007). Development of a Global Evapotranspiration Algorithm based on MODIS and Global Meteorology Data. *Remote sensing of Environment*, 111(4), 519–536.

Mudbhatkal, A. and M. Amai (2018). Regional Climate Trends and Topographic Influence over the Western Ghat catchments of India. *International Journal of Climatology*, 38(5), 2265–2279.

Mudbhatkal, A. and A. Mahesha (2018). Bias correction methods for hydrologic impact studies over india's western ghat basins. *Journal of Hydrologic Engineering*, 23(2), 05017030.

Mudbhatkal, A., R. Raikar, B. Venkatesh, and A. Mahesha (2017). Impacts of Climate Change on Varied River-Flow Regimes of Southern India. *Journal of Hydrologic Engineering*, 23, 1–13.

Mukherjee, S., S. Aadhar, D. Stone, and V. Mishra (2018). Increase in Extreme Precipitation Events under Anthropogenic Warming in India. *Weather and climate extremes*, 20, 45–53.

Muthuvel, D., B. Sivakumar, and A. Mahesha (2023). Future global concurrent droughts and their effects on maize yield. *Science of The Total Environment*, 855, 158860.

Nanditha, J., K. van der Wiel, U. Bhatia, D. Stone, F. Selton, and V. Mishra (2020). A seven-fold rise in the probability of exceeding the observed hottest summer in India in a 2^{o} C warmer world. *Environmental Research Letters*, 15(4), 044028.

Narsimlu, B., A. K. Gosain, and B. R. Chahar (2013). Assessment of future climate change impacts on water resources of upper sind river basin, india using swat model. *Water resources management*, 27, 3647–3662.

Nilawar, A. P. and M. L. Waikar (2019). Impacts of climate change on streamflow and sediment concentration under rcp 4.5 and 8.5: A case study in purna river basin, india. *Science of the total environment*, 650, 2685–2696.

Niranjan, S. and L. Nandagiri (2021). Effect of local calibration on the performance of the hargreaves reference crop evapotranspiration equation. *Journal of Water and Climate Change*, 12(6), 2654–2673.

Nischitha, V., S. Ahmed, H. Varikoden, and J. Revadekar (2014). The Impact of Seasonal Rainfall Variability on NDVI in the Tunga and Bhadra River Basins, Karnataka, India. *International Journal of Remote Sensing*, 35(23), 8025–8043.

Niyogi, D., C. Kishtawal, S. Tripathi, and R. S. Govindaraju (2010). Observational Evidence that Agricultural Intensification and Land Use Change may be reducing the Indian Summer Monsoon Rainfall. *Water Resources Research*, 46(3), 1–76.

Noori, N. and L. Kalin (2016). Coupling swat and ann models for enhanced daily streamflow prediction. *Journal of Hydrology*, 533, 141–151.

Oettli, P. and P. Camberlin (2005). Influence of Topography on Monthly Rainfall Distribution over East Africa. *Climate Research*, 28(3), 199–212.

Ojha, R., D. N. Kumar, A. Sharma, and R. Mehrotra (2014). Assessing gcm convergence for india using the variable convergence score. *Journal of Hydrologic Engineering*, 19(6), 1237–1246.

Onema, J.-M. K. and A. Taigbenu (2009). NDVI–Rainfall Relationship in the Semliki Watershed of the Equatorial Nile. *Physics and Chemistry of the Earth, Parts A/B/C*, 34(13-16), 711–721.

Ongoma, V., H. Chen, C. Gao, A. M. Nyongesa, and F. Polong (2018). Future Changes in Climate Extremes over Equatorial East Africa based on CMIP5 Multimodel Ensemble. *Natural Hazards*, 90(2), 901–920.

Organization, W. M., *Manual on estimation of probable maximum precipitation (PMP)*. World meteorological organization, 2009.

Pai, D., L. Sridhar, M. Rajeevan, O. Sreejith, N. Satbhai, and B. Mukhopadhyay (2014). Development of a New High Spatial Resolution (0.25$\times$ 0.25) Long Period (1901–2010) Daily Gridded Rainfall Data Set over India and Its Comparison with Existing Data Sets over the Region. *Mausam*, 65(1), 1–18.

Pant, M. (1978). Vertical Structure of the Planetary Boundary Layer in the West Indian Ocean during the Indian Summer Monsoon as Revealed by ISMEX Data. *J. Meteorol. Hydrol. Geophys*, 29, 189–196.

Papacharalampous, G. A. and H. Tyralis (2018). Evaluation of random forests and prophet for daily streamflow forecasting. *Advances in Geosciences*, 45, 201–208.

Parisouj, P., H. Mohebzadeh, and T. Lee (2020). Employing machine learning algorithms for streamflow prediction: a case study of four river basins with different climatic zones in the united states. *Water Resources Management*, 34, 4113–4131.

Parry, M. L., O. Canziani, J. Palutikof, P. Van der Linden, and C. Hanson, *Climate change 2007-impacts, adaptation and vulnerability: Working group II contribution to the fourth assessment report of the IPCC*volume4. Cambridge University Press, 2007.

Penman, H. and J. Monteith, Evaporation and the environment in the state and movement of water in living organisms. *In Proceedings of the Society for Experimental Biology, Symposium*, 19. 1965.

Pradhan, R. K., D. Sharma, S. Panda, S. K. Dubey, and A. Sharma (2019). Changes of precipitation regime and its indices over Rajasthan state of India: impact of climate change scenarios experiments. *Climate Dynamics*, 52(5), 3405–3420.

Prakash, S., A. K. Mitra, I. M. Momin, D. Pai, E. Rajagopal, and S. Basu (2015). Comparison of TMPA-3B42 versions 6 and 7 Precipitation Products with Gauge-Based Data over India for the Southwest Monsoon Period. *Journal of Hydrometeorology*, 16(1), 346–362.

Prasad, S. N., L. Vijayan, S. Balachandran, V. Ramachandran, and C. Verghese (1998). Conservation planning for the western ghats of kerala: I. a gis approach for location of biodiversity hot spots. *Current Science*, 211–219.

Priestley, C. H. B. and R. J. Taylor (1972). On the assessment of surface heat flux and evaporation using large-scale parameters. *Monthly weather review*, 100(2), 81–92.

Prudhomme, C. and D. W. Reed (1998). Relationships between Extreme Daily Precipitation and Topography in a Mountainous Region: a case study in Scotland. *International Journal of Climatology: A Journal of the Royal Meteorological Society*, 18(13), 1439–1453.

Puvaneswaran, K. and P. Smithson (1991). Precipitation—Elevation Relationships over Sri Lanka. *Theoretical and applied climatology*, 43(3), 113–122.

Rahimzad, M., A. Moghaddam Nia, H. Zolfonoon, J. Soltani, A. Danandeh Mehr, and H.-H. Kwon (2021). Performance comparison of an lstm-based deep learning model versus conventional machine learning algorithms for streamflow forecasting. *Water Resources Management*, 35(12), 4167–4187.

Rahman, K. U., Q. B. Pham, K. Z. Jadoon, M. Shahid, D. P. Kushwaha, Z. Duan, B. Mohammadi, K. M. Khedher, and D. T. Anh (2022). Comparison of machine learning and process-based swat model in simulating streamflow in the upper indus basin. *Applied water science*, 12(8), 178.

Rai, P., A. Choudhary, and A. Dimri (2019). Future Precipitation Extremes over India from the CORDEX-South Asia experiments. *Theoretical and Applied Climatology*, 137(3), 2961–2975.

Raj, P. and P. Azeez (2010). Changing rainfall in the palakkad plains of south india. *Atmósfera*, 23(1), 75–82.

Rajeevan, M., J. Bhate, and A. K. Jaswal (2008). Analysis of Variability and Trends of Extreme Rainfall Events over India using 104 years of Gridded Daily Rainfall Data. *Geophysical research letters*, 35(18).

Raju, K. S. and D. N. Kumar (2015). Ranking general circulation models for india using topsis. *Journal of Water and Climate Change*, 6(2), 288–299.

Raju, K. S. and D. N. Kumar (2020). Review of approaches for selection and ensembling of gcms. *Journal of Water and Climate Change*, 11(3), 577–599.

Ramachandra, T., S. Vinay, and H. Bharath (2016). Environmental flow assessment in a lotic ecosystem of central western ghats, india. *Hydrol Curr Res*, 7, 1–14.

Raman, S., B. Templeman, S. Templeman, T. Holt, A. Murthy, M. Singh, P. Agarwaal, S. Nigam, A. Prabhu, and S. Ameenullah (1990). Structure of the Indian Southwesterly Pre-monsoon and Monsoon Boundary Layers: Observations and Numerical Simulation. *Atmospheric Environment. Part A. General Topics*, 24(4), 723–734.

Rao, K. K., P. J. Reddy, and J. S. Chowdary (2023). Indian heatwaves in a future climate with varying hazard thresholds. *Environmental Research: Climate*.

Rasouli, K., W. W. Hsieh, and A. J. Cannon (2012). Daily streamflow forecasting by machine learning methods with weather and climate inputs. *Journal of Hydrology*, 414, 284–293.

Revadekar, J. and B. Preethi (2012). Statistical Analysis of the Relationship between Summer Monsoon Precipitation Extremes and Food Grain Yield over India. *International Journal of Climatology*, 32(3), 419–429.

Rezaeianzadeh, M., H. Tabari, A. Arabi Yazdi, S. Isik, and L. Kalin (2014). Flood flow forecasting using ann, anfis and regression models. *Neural Computing and Applications*, 25, 25–37.

Richards, J. F. and E. P. Flint, A century of land-use change in south and southeast asia. *In Effects of land-use change on atmospheric CO2 concentrations*. Springer, 1994, 15–66.

Riley, S. J., S. D. DeGloria, and R. Elliot (1999). Index that Quantifies Topographic Heterogeneity. *intermountain Journal of sciences*, 5(1-4), 23–27.

Roxy, M. K., S. Ghosh, A. Pathak, R. Athulya, M. Mujumdar, R. Murtugudde, P. Terray, and M. Rajeevan (2017). A threefold rise in widespread extreme rain events over central India. *Nature communications*, 8(1), 1–11.

Roy, S. S. and R. C. Balling (2004). Trends in extreme daily precipitation indices in india. *International Journal of climatology*, 24(4), 457–466.

Ruiz-Ortiz, V., J. M. GP Isidoro, H. M. Fernandez, F. M. Granja-Martins, and S. García-López (2022). Mapping the spatial variability of rainfall from a physiographic-based multilinear regression: model development and application to the southwestern iberian peninsula. *Environmental Monitoring and Assessment*, 194(10), 722.

Sachindra, D. A., K. Ahmed, M. M. Rashid, S. Shahid, and B. J. C. Perera (2018). Statistical downscaling of precipitation using machine learning techniques. *Atmospheric research*, 212, 240–258.

Sachindra, D. A., F. Huang, A. Barton, and B. J. C. Perera (2014). Statistical downscaling of general circulation model outputs to precipitation—part 2: bias-correction and future projections. *International Journal of Climatology*, 34(11), 3282–3303.

Safeeq, M. and A. Fares (2012). Hydrologic Response of a Hawaiian Watershed to Future Climate Change Scenarios. *Hydrological processes*, 26(18), 2745–2764.

Saha, A., S. C. Pal, I. Chowdhuri, A. R. M. T. Islam, R. Chakrabortty, and P. Roy (2022). Threats of soil erosion under cmip6 ssps scenarios: an integrated data mining techniques and geospatial approaches. *Geocarto International*, 1–33.

Saleth, R. M. (2011). Water scarcity and climatic change in india: the need for water demand and supply management. *Hydrological Sciences Journal*, 56(4), 671–686.

Sam, N., U. Mohanty, A. Routray, and S. Basu (2007). Variation of Coastal Atmospheric Boundary Layer Characteristics with Convective Activity Along the West Coast of India during the Arabian Sea Monsoon Experiment (ARMEX) 2002. *Natural Hazards*, 42(2), 361–378.

Sanderson, B. M., R. Knutti, and P. Caldwell (2015). Addressing interdependency in a multimodel ensemble by interpolation of model properties. *Journal of Climate*, 28(13), 5150–5170.

Sanjay Shekar, N. and D. Vinay (2021). Performance of hec-hms and swat to simulate streamflow in the sub-humid tropical hemavathi catchment. *Journal of Water and Climate Change*, 12(7), 3005–3017.

Sarkar, S. and R. Maity (2022). Future Characteristics of Extreme Precipitation Indicate the Dominance of Frequency over Intensity: A multi-Model Assessment from CMIP6 across India. *Journal of Geophysical Research: Atmospheres*, e2021JD035539.

Seland, Ø., M. Bentsen, D. Olivié, T. Toniazzo, A. Gjermundsen, L. S. Graff, J. B. Debernard, A. K. Gupta, Y.-C. He, A. Kirkevåg, *et al.* (2020). Overview of the norwegian earth system model (noresm2) and key climate response of cmip6 deck, historical, and scenario simulations. *Geoscientific Model Development*, 13(12), 6165–6200.

Sellers, S. and K. L. Ebi (2018). Climate change and health under the shared socioeconomic pathway framework. *International journal of environmental research and public health*, 15(1), 3.

Sevruk, B., Regional Dependency of Precipitation-Altitude Relationship in the Swiss Alps. *In Climatic change at high elevation sites*. Springer, 1997, 123–137.

Shafeeque, M. and Y. Luo (2021). A multi-Perspective Approach for Selecting CMIP6 scenarios to Project Climate Change Impacts on Glacio-Hydrology with a case study in Upper Indus River Basin. *Journal of Hydrology*, 599, 126466.

Sharannya, T., A. Mudbhatkal, and A. Mahesha (2018). Assessing climate change impacts on river hydrology–a case study in the western ghats of india. *Journal of Earth System Science*, 127, 1–11.

Sharannya, T., K. Venkatesh, A. Mudbhatkal, M. Dineshkumar, and A. Mahesha (2021). Effects of land use and climate change on water scarcity in rivers of the

western ghats of india. *Environmental Monitoring and Assessment*, 193(12), 820.

Sharma, A. and M. K. Goyal (2020). Assessment of the Changes in Precipitation and Temperature in Teesta River Basin in Indian Himalayan Region under Climate Change. *Atmospheric Research*, 231, 104670.

Sharma, A., D. Sharma, S. Panda, S. K. Dubey, and R. K. Pradhan (2018). Investigation of temperature and its indices under climate change scenarios over different regions of Rajasthan state in India. *Global and Planetary Change*, 161, 82–96.

Sharma, R. K., S. Kumar, D. Padmalal, and A. Roy (2023). Streamflow prediction using machine learning models in selected rivers of southern india. *International Journal of River Basin Management*, 1–27.

Shetty, S., P. Umesh, and A. Shetty (2022). Dependability of rainfall to topography and micro-climate: an observation using geographically weighted regression. *Theoretical and Applied Climatology*, 147(1), 217–237.

Shetty, S., P. Vaishnavi, P. Umesh, and A. Shetty (2021). Vertical Accuracy Assessment of Open Source Digital Elevation Models under varying Elevation and Land Cover in Western Ghats of India. *Modeling Earth Systems and Environment*.

Shiferaw, A., T. Tadesse, C. Rowe, and R. Oglesby (2018). Precipitation Extremes in Dynamically Downscaled Climate Scenarios over the Greater Horn of Africa. *Atmosphere*, 9(3), 112.

Shiru, M. S., S. Shahid, A. Dewan, E.-S. Chung, N. Alias, K. Ahmed, and Q. K. Hassan (2020). Projection of meteorological droughts in nigeria during growing seasons under climate change scenarios. *Scientific reports*, 10(1), 1–18.

Shortridge, J. E., S. D. Guikema, and B. F. Zaitchik (2016). Machine learning methods for empirical streamflow simulation: a comparison of model accuracy,

interpretability, and uncertainty in seasonal watersheds. *Hydrology and Earth System Sciences*, 20(7), 2611–2628.

Shrestha, A., M. M. Rahaman, A. Kalra, R. Jogineedi, and P. Maheshwari (2020). Climatological Drought Forecasting using Bias Corrected CMIP6 climate data: A case study for India. *Forecasting*, 2(2), 59–84.

Shrestha, D., P. Singh, and K. Nakamura (2012). Spatiotemporal variation of rainfall over the central himalayan region revealed by trmm precipitation radar. *Journal of geophysical research: atmospheres*, 117(D22).

Shrestha, M., S. C. Acharya, and P. K. Shrestha (2017). Bias correction of climate models for hydrological modelling–are simple methods still useful? *Meteorological Applications*, 24(3), 531–539.

Sijikumar, S., L. John, and K. Manjusha (2013). Sensitivity study on the role of western ghats in simulating the asian summer monsoon characteristics. *Meteorology and Atmospheric Physics*, 120, 53–60.

Simon, A. and K. Mohankumar (2004). Spatial variability and rainfall characteristics of kerala. *Journal of Earth System Science*, 113, 211–221.

Singh, D., M. Tsiang, B. Rajaratnam, and N. S. Diffenbaugh (2014). Observed changes in extreme wet and dry spells during the south asian summer monsoon season. *Nature Climate Change*, 4(6), 456–461.

Singh, D., M. Vardhan, R. Sahu, D. Chatterjee, P. Chauhan, and S. Liu (2023). Machine-learning-and deep-learning-based streamflow prediction in a hilly catchment for future scenarios using cmip6 gcm data. *Hydrology and Earth System Sciences*, 27(5), 1047–1075.

Singh, J., M. Ashfaq, C. B. Skinner, W. B. Anderson, and D. Singh (2021). Amplified Risk of Spatially Compounding Droughts during Co-occurrences of Modes of Natural Ocean Variability. *npj Climate and Atmospheric Science*, 4(1), 1–14.

Singh, P. and N. Kumar (1997). Effect of orography on precipitation in the western himalayan region. *Journal of Hydrology*, 199(1-2), 183–206.

Singh, V. and M. K. Goyal (2016). Analysis and Trends of Precipitation Lapse Rate and Extreme Indices over North Sikkim Eastern Himalayas under CMIP5ESM-2M RCPs experiments. *Atmospheric Research*, 167, 34–60.

Sinha, R. K., T. Eldho, and G. Subimal (2020). Assessing the impacts of land use/land cover and climate change on surface runoff of a humid tropical river basin in western ghats, india. *International Journal of River Basin Management*, 1–12.

Sinha, R. K., S. K. Sharma, and I. Eldho T, Climate change impacts on water balancing components for a tropical river basin, western ghats india. *In EGU General Assembly Conference Abstracts*. 2022.

Sippel, S., J. Zscheischler, M. Heimann, H. Lange, M. D. Mahecha, G. J. v. Oldenborgh, F. E. Otto, and M. Reichstein (2017). Have Precipitation Extremes and Annual Totals been Increasing in the World's Dry regions over the last 60 years? *Hydrology and Earth System Sciences*, 21(1), 441–458.

Sonali, P. and D. Nagesh Kumar (2020). Review of Recent Advances in Climate Change Detection and Attribution Studies: a Large-Scale Hydroclimatological Perspective. *Journal of Water and Climate Change*, 11(1), 1–29.

Song, Y. H., E.-S. Chung, and S. Shahid (2022). Differences in extremes and uncertainties in future runoff simulations using swat and lstm for ssp scenarios. *Science of The Total Environment*, 838, 156162.

Sreelatha, K. and P. Anand Raj (2021). Ranking of cmip5-based global climate models using standard performance metrics for telangana region in the southern part of india. *ISH Journal of Hydraulic Engineering*, 27(sup1), 556–565.

Srinivasan, V., S. Mukherji, and R. Ramamurthy (1972). Southwest Monsoon-Typical Situations over Kerala and Arabian Sea Islands. *Forecasting Manual Part III FMU Rep. No. III-3.8, India Meteorological Department, Poona-5*.

Srivastava, A., M. Rajeevan, and S. Kshirsagar (2009). Development of a high resolution daily gridded temperature data set (1969–2005) for the indian region. *Atmospheric Science Letters*, 10(4), 249–254.

Stouffer, R. J., V. Eyring, G. A. Meehl, S. Bony, C. Senior, B. Stevens, and K. Taylor (2017). Cmip5 scientific gaps and recommendations for cmip6. *Bulletin of the American Meteorological Society*, 98(1), 95–105.

Sugar, L., C. Kennedy, and D. Hoornweg (2013). Synergies between climate change adaptation and mitigation in development: Case studies of amman, jakarta, and dar es salaam. *International Journal of Climate Change Strategies and Management*.

Suman, M., R. Maity, and H. Kunstmann (2022). Precipitation of Mainland India: Copula-based bias-corrected daily CORDEX climate data for both mean and extreme values.

Supharatid, S., J. Nafung, and T. Aribarg (2022). Projected Changes in Temperature and Precipitation over Mainland Southeast Asia by CMIP6 models. *Journal of Water and Climate Change*, 13(1), 337–356.

Swain, S. S., A. Mishra, B. Sahoo, and C. Chatterjee (2020). Water scarcity-risk assessment in data-scarce river basins under decadal climate change using a hydrological modeling approach. *Journal of Hydrology*, 590, 125260.

Swart, N. C., J. N. Cole, V. V. Kharin, M. Lazare, J. F. Scinocca, N. P. Gillett, J. Anstey, V. Arora, J. R. Christian, S. Hanna, *et al.* (2019). The canadian earth system model version 5 (canesm5. 0.3). *Geoscientific Model Development*, 12(11), 4823–4873.

Tadese, M., L. Kumar, and R. Koech (2020). Long-term variability in potential evapotranspiration, water availability and drought under climate change scenarios in the awash river basin, ethiopia. *Atmosphere*, 11(9), 883.

Tan, M. L., J. Liang, N. Samat, N. W. Chan, J. M. Haywood, and K. Hodges (2021). Hydrological Extremes and Responses to Climate Change in the Kelantan River Basin, Malaysia, Based on the CMIP6 HighResMIP Experiments. *Water*, 13(11), 1472.

Tawde, S. A. and C. Singh (2015). Investigation of Orographic Features Influencing Spatial Distribution of Rainfall over the Western Ghats of India using Satellite Data. *International Journal of Climatology*, 35(9), 2280–2293.

Teutschbein, C. and J. Seibert (2012). Bias correction of regional climate model simulations for hydrological climate-change impact studies: Review and evaluation of different methods. *Journal of hydrology*, 456, 12–29.

Thapa, S., H. Li, B. Li, D. Fu, X. Shi, S. Yabo, L. Lu, H. Qi, and W. Zhang (2021). Impact of climate change on snowmelt runoff in a himalayan basin, nepal. *Environmental Monitoring and Assessment*, 193(7), 393.

Thapa, S., Z. Zhao, B. Li, L. Lu, D. Fu, X. Shi, B. Tang, and H. Qi (2020). Snowmelt-driven streamflow prediction using machine learning techniques (lstm, narx, gpr, and svr). *Water*, 12(6), 1734.

Tibangayuka, N., D. M. Mulungu, and F. Izdori (2022). Evaluating the performance of hbv, hec-hms and ann models in simulating streamflow for a data scarce high-humid tropical catchment in tanzania. *Hydrological Sciences Journal*, 67(14), 2191–2204.

Tiwari, R., A. K. Mishra, S. Rai, and L. K. Pandey (2023). Evaluation and projection of northeast monsoon precipitation over india under higher warming scenario: a multimodel assessment of cmip6. *Theoretical and Applied Climatology*, 151(1-2), 859–870.

Tokarska, K. B., M. B. Stolpe, S. Sippel, E. M. Fischer, C. J. Smith, F. Lehner, and R. Knutti (2020). Past warming trend constrains future warming in cmip6 models. *Science advances*, 6(12), eaaz9549.

Turc, L. (1961). Estimation of irrigation water requirements, potential evapotranspiration: a simple climatic formula evolved up to date. *Ann. Agron*, 12(1), 13–49.

Tyralis, H., G. Papacharalampous, and A. Langousis (2021). Super ensemble learning for daily streamflow forecasting: Large-scale demonstration and comparison with multiple machine learning algorithms. *Neural Computing and Applications*, 33(8), 3053–3068.

Varghese, S. J., S. Surendran, K. Rajendran, and A. Kitoh (2020). Future Projections of Indian Summer Monsoon under Multiple RCPs using a High-Resolution Global Climate Model multi forcing Ensemble Simulations. *Climate Dynamics*, 54(3), 1315–1328.

Venkatesh, B. and M. K. Jose (2007). Identification of Homogeneous Rainfall Regimes in Parts of Western Ghats region of Karnataka. *Journal of Earth System Science*, 116(4), 321–329.

Verma, S., R. Bhatla, N. Shahi, and R. Mall (2022). Regional modulating behavior of indian summer monsoon rainfall in context of spatio-temporal variation of drought and flood events. *Atmospheric Research*, 274, 106201.

Vijay, A., S. D. Sivan, A. Mudbhatkal, and A. Mahesha (2021). Long-term climate variability and drought characteristics in tropical region of india. *Journal of Hydrologic Engineering*, 26(4), 05021003.

Visweshwaran, R., R. Ramsankaran, T. Eldho, and M. K. Jha (2022). Hydrological impact assessment of future climate change on a complex river basin of western ghats, india. *Water*, 14(21), 3571.

Volodin, E. and A. Gritsun (2018). Simulation of observed climate changes in 1850–2014 with climate model inm-cm5. *Earth System Dynamics*, 9(4), 1235–1242.

Wan, Z. (2008). New Refinements and Validation of the MODIS Land-Surface Temperature/Emissivity Products. *Remote sensing of Environment*, 112(1), 59–74.

Wan, Z. (2014). New Refinements and Validation of the Collection-6 MODIS Land-Surface Temperature/Emissivity Product. *Remote sensing of Environment*, 140, 36–45.

Wang, B., L. Zheng, D. L. Liu, F. Ji, A. Clark, and Q. Yu (2018). Using multi-model ensembles of cmip5 global climate models to reproduce observed monthly rainfall and temperature with machine learning methods in australia. *International Journal of Climatology*, 38(13), 4891–4902.

Wang, L., R. Ranasinghe, S. Maskey, P. M. van Gelder, and J. Vrijling (2016). Comparison of empirical statistical methods for downscaling daily climate projections from cmip5 gcms: a case study of the huai river basin, china. *International journal of climatology*, 36(1), 145–164.

Wehner, M., P. Gleckler, and J. Lee (2020). Characterization of long period return values of extreme daily temperature and precipitation in the cmip6 models: Part 1, model evaluation. *Weather and Climate Extremes*, 30, 100283.

Weisse, A. K. and P. Bois (2001). Topographic Effects on Statistical Characteristics of Heavy Rainfall and Mapping in the French Alps. *Journal of Applied Meteorology*, 40(4), 720–740.

Winjum, J. K., R. K. Dixon, and P. E. Schroeder (1992). Estimating the global potential of forest and agroforest management practices to sequester carbon. *Water, Air, and Soil Pollution*, 64(1-2), 213–227.

Woo, S., G. P. Singh, J.-H. Oh, and K.-M. Lee (2019). Projection of seasonal summer precipitation over indian sub-continent with a high-resolution agcm based on the rcp scenarios. *Meteorology and Atmospheric Physics*, 131(4), 897–916.

Wu, J., X.-Y. Chen, H. Zhang, L.-D. Xiong, H. Lei, and S.-H. Deng (2019*a*). Hyperparameter optimization for machine learning models based on bayesian optimization. *Journal of Electronic Science and Technology*, 17(1), 26–40.

Wu, T., Y. Lu, Y. Fang, X. Xin, L. Li, W. Li, W. Jie, J. Zhang, Y. Liu, L. Zhang, *et al.* (2019*b*). The beijing climate center climate system model (bcc-csm): The main progress from cmip5 to cmip6. *Geoscientific Model Development*, 12(4), 1573–1600.

Wyser, K., T. v. Noije, S. Yang, J. v. Hardenberg, D. O'Donnell, and R. Döscher (2020). On the increased climate sensitivity in the ec-earth model from cmip5 to cmip6. *Geoscientific Model Development*, 13(8), 3465–3474.

Xu, L., N. Chen, X. Zhang, Z. Chen, C. Hu, and C. Wang (2019). Improving the north american multi-model ensemble (nmme) precipitation forecasts at local areas using wavelet and machine learning. *Climate dynamics*, 53(1), 601–615.

Xu, R., N. Chen, Y. Chen, and Z. Chen (2020). Downscaling and projection of multi-cmip5 precipitation using machine learning methods in the upper han river basin. *Advances in Meteorology*, 2020.

Yamak, P. T., L. Yujian, and P. K. Gadosey, A comparison between arima, lstm, and gru for time series forecasting. *In Proceedings of the 2019 2nd International Conference on Algorithms, Computing and Artificial Intelligence*. 2019.

Yang, J., Y. Xiang, J. Sun, and X. Xu (2022). Multi-model ensemble prediction of summer precipitation in china based on machine learning algorithms. *Atmosphere*, 13(9), 1424.

Yang, Q., H. Zhang, G. Wang, S. Luo, D. Chen, W. Peng, and J. Shao (2019). Dynamic runoff simulation in a changing environment: A data stream approach. *Environmental Modelling & Software*, 112, 157–165.

Yaseen, Z. M., M. F. Allawi, A. A. Yousif, O. Jaafar, F. M. Hamzah, and A. El-Shafie (2018). Non-tuned machine learning approach for hydrological time series forecasting. *Neural Computing and Applications*, 30, 1479–1491.

Yaseen, Z. M., O. Kisi, and V. Demir (2016). Enhancing long-term streamflow forecasting and predicting using periodicity data component: application of artificial intelligence. *Water resources management*, 30, 4125–4151.

Yin, J. and N. Li (2022). Ensemble learning models with a bayesian optimization algorithm for mineral prospectivity mapping. *Ore Geology Reviews*, 145, 104916.

Yu, J., W. Zheng, L. Xu, L. Zhang, G. Zhang, *et al.* (2020). A pso-xgboost model for estimating daily reference evapotranspiration in the solar greenhouse. *Intell. Autom. Soft Comput*, 26(5), 989–1003.

Yuan, L. and K. J. Forshay (2021). Enhanced streamflow prediction with swat using support vector regression for spatial calibration: A case study in the illinois river watershed, us. *Plos one*, 16(4), e0248489.

Yuan, X., C. Chen, X. Lei, Y. Yuan, and R. Muhammad Adnan (2018). Monthly runoff forecasting based on lstm–alo model. *Stochastic environmental research and risk assessment*, 32, 2199–2212.

Yue, Y., D. Yan, Q. Yue, G. Ji, and Z. Wang (2021). Future changes in precipitation and temperature over the yangtze river basin in china based on cmip6 gcms. *Atmospheric Research*, 264, 105828.

Yukimoto, S., H. Kawai, T. Koshiro, N. Oshima, K. Yoshida, S. Urakawa, H. Tsujino, M. Deushi, T. Tanaka, M. Hosaka, *et al.* (2019). The meteorological research institute earth system model version 2.0, mri-esm2. 0: Description and basic evaluation of the physical component. *Journal of the Meteorological Society of Japan. Ser. II*.

Zareian, M. J. and F. Salem (2022). Simulation of climate change effects on streamflow based on a deep learning network (case study: a semi-arid region in central iran).

Zebker, H. A. and R. M. Goldstein (1986). Topographic Mapping from Interferometric Synthetic Aperture Radar observations. *Journal of Geophysical Research: Solid Earth*, 91(B5), 4993–4999.

Zhang, G. and R. B. Smith (2018). Numerical Study of Physical Processes Controlling Summer Precipitation over the Western Ghats Region. *Journal of Climate*, 31(8), 3099–3115.

Zhang, X., L. Alexander, G. C. Hegerl, P. Jones, A. K. Tank, T. C. Peterson, B. Trewin, and F. W. Zwiers (2011). Indices for Monitoring Changes in Extremes based on Daily Temperature and Precipitation data. *Wiley Interdisciplinary Reviews: Climate Change*, 2(6), 851–870.

Zhang, X., M. A. Friedl, C. B. Schaaf, A. H. Strahler, J. C. Hodges, F. Gao, B. C. Reed, and A. Huete (2003). Monitoring Vegetation Phenology using MODIS. *Remote sensing of environment*, 84(3), 471–475.

Zhao, C., Z. Jiang, X. Sun, W. Li, and L. Li (2020). How well do climate models simulate regional atmospheric circulation over east asia? *International Journal of Climatology*, 40(1), 220–234.

Zhu, X., S.-Y. Lee, X. Wen, Z. Ji, L. Lin, Z. Wei, Z. Zheng, D. Xu, and W. Dong (2021). Extreme Climate Changes over Three Major River Basins in China as seen in CMIP5 and CMIP6. *Climate Dynamics*, 1–19.

Ziehn, T., M. A. Chamberlain, R. M. Law, A. Lenton, R. W. Bodman, M. Dix, L. Stevens, Y.-P. Wang, and J. Srbinovsky (2020). The australian earth system model: Access-esm1. 5. *Journal of Southern Hemisphere Earth Systems Science*, 70(1), 193–214.

PUBLICATIONS

- Shetty, S., Umesh, P. and Shetty, A. (2024). Multi-scenario Analysis of Hydrological Responses to Climate Change over River Basins of Western Ghats of India. ***ASCE Journal of Hydrologic Engineering*** (Revision is under review).

- Shetty, S., Umesh, P. and Shetty, A. (2023). The effectiveness of machine learning-based multi-model ensemble Predictions of CMIP6 in Western Ghats of India. ***International Journal of Climatology***.43(11), 5029-5024. https://doi.org/10.1002/joc.8131.

- Shetty, S., Umesh, P. and Shetty, A. (2023). Future transitions in climate extremes over the western Ghats of India based on CMIP6 Models. ***Environmental Monitoring and Assessment***.195(5), 578. https://doi.org/10.1007/s10661-023-11090-3

- Shetty, S., Umesh, P. and Shetty, A. (2023). Climate Indices and drought characteristics in the river catchments of Western Ghats of India. ***Acta Geophysica***. https://doi.org/10.1007/s11600-023-01054-z

- Shetty, S., Umesh, P. and Shetty, A. (2022). Dependability of rainfall to topography and micro-climate: an observation using geographically weighted regression, ***Theoretical and Applied Climatology***, 147(1), 217–237. https://doi.org/10.1007/s00704-021-03811-w

- Shetty, S.,Vaishnavi P, Umesh, P. and Shetty, A., Vertical Accuracy Assessment of Open Source Digital Elevation Models under Varying Elevation and Land Cover in Western Ghats of India, ***Modeling Earth Systems and Environment***, 8,883-895. https://doi.org/10.1007/s40808-021-01119-2

BIO **DATA**

Swathi Shetty

Born on 15/12/1993

meswathi18@gmail.com

+91 9036128601

Pushpasudha
House No 6-50
Udupi Acharya Thota
Nittur, Udupi,
Karnataka-576103

EDUCATION

2016-2018

MTech (Research) — Mangaluru, Karnataka
National Institute of Technology Karnataka Surathkal
Water Resource Engineering and Management

2011-2015

Bachelor of Engineering — Bantakal, Udupi
Shri Madhwa Vadiraja Institute of Technology and Management
Civil Engineering

WORK EXPERIENCE

2019 - March 2023

Senior Research Fellow — Mangaluru, Karnataka
National Institute of Technology Karnataka Surathkal

2015 - July 2019

Junior Research Fellow — Mangaluru, Karnataka
National Institute of Technology Karnataka Surathkal

PUBLICATIONS

International Journals - 6

International Conferences - 5